Recursive Estimation of States and Parameters in Oil Reservoir

By

Farhana Akter

A Dissertation submitted to the School of Graduate Studies in partial fulfillment of the requirements for the degree of

Doctor of Philosophy

Faculty of Engineering and Applied Science

Memorial University of Newfoundland

January 2023

St. John's Newfoundland, Canada

Abstract

A reservoir model is built with the initial guesses of reservoir parameters, which has high degree of uncertainty that may make the prediction unreliable. Appropriate assessment of the reservoir parameters' uncertainty provides dependability on the reservoir model. Among several reservoir parameters, porosity and permeability are the two key parameters that affect reserves estimation, field development, future prediction, and development of alternative oil recovery scenarios. In this regard, an extensive study is required on reservoir model to estimate dynamic states and static parameters correctly along with uncertainty assessment. However, due to the presence of large number of variables in the geophysical model, nonlinearity in the multiphase fluid flow equations and assumptions toward linearization make the reservoir model more uncertain and non-unique. Therefore, correct estimation of the unknown or poorly known states and parameters becomes very difficult. In this regard, application of ensemble Kalman filter provides realistic solution as this tool is able to deal with large scale nonlinear system. In this approach, a set of reservoir models/realizations are generated considering the reference reservoir data and data assimilation is done for all the realizations incorporating available observations. After data assimilation, a range of forecasts are generated from the updated realizations on which the uncertainty in the reservoir performance predictions is evaluated.

In this work, some key phenomena such as excitation in the reservoir due to production through injection, dynamic error in the reservoir model, non-Gaussianity effect in the water flooding case in heterogeneous reservoir, and dynamic change of parameters in asphaltic oil reservoir are investigated while estimating reservoir parameters. Investigation is conducted considering different production scenarios in reservoirs. To improve parameter estimation under these varying conditions, modifications are introduced into the traditional EnKF methodology to address these key factors.

Dynamic model error has been mostly ignored for the cases of multiphase flow in porous media for estimating parameters. Therefore, a dynamic model error along with measurement error is added in water flooding oil reservoir model. Also to capture the change happened in the reservoir due to water injection, artificial perturbation of inputs is introduced in EnKF methodology. With these modifications, about 9% improvement in history matching is observed when mismatch

between model and true system, and uncertainty in measurement are high. Next, the aspect of non-Gaussianity in state and parameter estimation is investigated in five spot oil-water reservoir by applying EnKF along with particle filter (PF). From the analysis, it is found that the performance of EnKF is comparable with PF where the non-Gaussianity is weak. However, in the presence of strong non-Gaussianity, EnKF shows four times higher error than PF. Also, the performance of particle filter is improved by incorporating "ensemble covariance" during resampling stage.

This research work includes the analysis of formation damage due to asphaltene precipitation/deposition and its impact on reservoir properties such as permeability and porosity. In this work, a modification is introduced in the pure solid model regarding explicit estimation of the asphaltene precipitation, resulting in a reduced computation time. To calculate the amount of asphaltene precipitation, the modification brings the iteration steps from five to one with a difference of 9.945% between the pure solid model and modified solid model. In addition, the simulation of wellbore region of production well in a two-dimensional oil reservoir is conducted considering four-phase black oil model. The simulation results reveal that around the wellbore, the suspended asphaltene saturation reaches to its maximum value at the bubble point pressure; the maximum reduction in permeability (8%) and porosity (9.1%) occurs around the wellbore. Finally, EnKF is applied to an asphaltic oil reservoir for estimation of reservoir parameters considering their inherent uncertainty and dynamic change due to asphaltene precipitation. Due to continued production, dynamic state change from 'pressure to saturation' of gas and asphaltene phase happens. To capture this state change, a methodology is developed while applying EnKF. History matching is done by matching the results of bottomhole flowing pressure, fluid flow rate, suspended asphaltene saturation, gas saturation obtained from the filter and model. It is found that porosity and permeability are estimated with less than 2% error.

Acknowledgements

I want to take the opportunity to thank my supervisors Dr. Syed Imtiaz, Dr. Sohrab Zendehboudi and Dr. Amer Aborig for all their generous help, support, and valuable suggestions throughout my academic voyage. They encouraged and supported me with appropriate directions, spending hours with me over various stages of the research work.

I gratefully acknowledge and thank Equinor Canada, School of Graduate Studies, Memorial University, Faculty of Engineering and Applied Science, Innovate NL, Natural Sciences and Engineering Research Council of Canada (NSERC) and Compute Canada for supporting my research work.

I would like to thank my research colleagues and friends in Memorial University who helped me through the journey with the share of their knowledge and expertise. I would like to thank the staff of Faculty of Engineering and Applied Science. I would also like to thank the Engineering Computing Service to provide me enormous assistance during my academic program at Memorial University.

I would like to express the highest gratitude to my family in St. John's and in Bangladesh, especially my husband Mohammad Mojammel Huque who supported me from the very beginning of my academic life. He supported me in all critical discussions in my research and helped me by reviewing and proof reading of my manuscripts. I also thank my siblings and relatives for their encouragement and support. Finally, I express my greatest gratitude to my sister Khadiza Akhter and dedicate this thesis to my parents.

Co-authorship Statement

I, **Farhana Akter**, hold the primary author status for all the Chapters in this thesis. However, each manuscript is co-authored by my supervisors, co-supervisors, and external research collaborators. Contributions of each of the co-authors are listed below:

1. Farhana Akter, Syed Imtiaz*, Sohrab Zendehboudi, and Kamal Hossain, "**Modified Ensemble Kalman Filter for Reservoir Parameter and State Estimation in the Presence of Model Uncertainty**" has been published in Journal of petroleum Science and Engineering. https://doi.org/10.1016/j.petrol.2020.108323

   Statement: The research was conducted by Farhana Akter as the first author. She prepared the manuscript. Other authors supervised the student, reviewed the manuscript, and provided feedback.

2. Farhana Akter, Syed Imtiaz*, Sohrab Zendehboudi, and Amer Aborig, "**Application of Particle Filter to Assess Uncertainty for Reservoir State and Parameter Estimation**". Manuscript is submitted to Journal of petroleum Science and Engineering.

   Statement: The research was conducted by Farhana Akter as the first author. She prepared the manuscript. Other authors supervised the student, reviewed the manuscript, and provided feedback.

3. Farhana Akter, Syed Imtiaz*, Sohrab Zendehboudi, and Amer Aborig, "**An Effective Approach to Implement Asphaltene Precipitation in Reservoir Simulation**" Manuscript is submitted to Journal of Fuel.

   Statement: The research was conducted by Farhana Akter as the first author. She prepared the manuscript. Other authors supervised the student, reviewed the manuscript, and provided feedback.

4. Farhana Akter, Syed Imtiaz*, Sohrab Zendehboudi, and Amer Aborig, "**Modelling and Parameter Estimation of Asphaltic Oil Reservoir with the Implementation of Ensemble Kalman Filter (EnKF)**" Manuscript is prepared for journal submission.

   Statement: The research was conducted by Farhana Akter as the first author. She prepared the manuscript. Other authors supervised the student, reviewed the manuscript, and provided feedback.

   **The manuscripts presented in this thesis is slightly different than the published version.

Table of Contents

List of Tables

List of Figures

Chapter 1 : Introduction

1.1 Background and motivation

Mathematical modelling is one of the most applied practices in reservoir engineering for production optimization and performance assessment. Considering the complexity of the reservoir model, numerical solution approach is preferable to analytical approach. Numerical model of a reservoir is built by using different dynamic and static parameters such as transmissivity, permeability, storativity, porosity, hydraulic head, and phase-saturation. These parameters are only rough estimates based on seismic and well test data such that these parameters have high degree of uncertainty. Accurate estimation of the reservoir parameters and state variables along with the degree of uncertainty is a key task in reservoir modelling for reliable production forecast. To recover the true reservoir model and bring fidelity in prediction performance, the uncertainty should be quantified.

Reservoir models are calibrated along with the uncertainty present in reservoir parameters through the process of history matching. History matching is defined as an inverse problem as the parameters are not measured directly and assessed by indirect methods. In history matching, reservoir parameters are adjusted based on the updated available measurements at individual wells to determine the representative parameters. Extensive research studies have been conducted for correct estimation of unknown or poorly known parameters with the application of ensemble-based methods. Because of computational efficiency, easy operation, and absence of adjoint code, ensemble-based methods have received increased emphasis for history matching (Shuai et al., 2016). The goal of this thesis is to use ensemble methods to estimate the states and parameters of a reservoir. In the following section, we will present a brief literature review to establish the present status of the research and the knowledge gap. Detailed review of literature is provided in each chapter.

A reservoir is a complex geological system with several governing macro and micro geophysical mechanisms. It is difficult to consider all these mechanisms in a reservoir model. Thus, often some assumptions are made and only the dominant mechanisms are included in the reservoir model. Moreover, numerical dispersion, discretization, and upscaling cause a loss in detail in terms of grid

connectivity and fluid flow. Therefore, assumptions, discretization, upscaling, uncertainties in input parameters such as rock and fluid properties, and reservoir geometry in numerical solution approach cause a prediction error to the reservoir model. Inclusion of model error while estimating reservoir parameters develops a relation between the variables in the system and thereby provides steady estimation of the parameters (Aanonsen et al., 2009). Any flowmeter inevitably has an error in its measurements. Thus, when a measured production rate is used as the reference value for history matching, the fluctuations in the measurement tools add uncertainty and mask the true state of the reservoir. As a result, modelling errors, measurement errors, and non-uniqueness of the model solution are responsible for the deviation of the reservoir model from the real situation. Exclusion of these errors in models may provide good history matching, however, will be unable to make good predictions. Literature study shows that the previous history matching studies with application of EnKF to reservoir state estimation, dynamic model error was not considered.

A reservoir is a time-varying system, due to production, fluid displacement takes place in the reservoir, and parameters change over time. Also, typically reservoir production rate is kept constant and adjusted only occasionally. Moreover, oil production through injection process involves stability distortion in the reservoir. Constant input or forcing variable creates less excitation in the system. From system identification perspective, there is a need for persistent excitation in the system to identify the system parameters. Without excitation, the system does not generate sufficient information to estimate the parameters or states accurately. The heterogeneity in reservoir model in terms of variation in static parameters such as porosity and permeability add complexity from a geological point of view and causes non-Gaussian distribution in dynamic state. The effect of geological complexity in the estimation of dynamic state variables along with parameter estimation has not been studied extensively.

In addition, for the asphaltic oil reservoir, asphaltene precipitation model plays a vital role for reservoir model development. However, the traditional precipitation model requires performing a series of repeated flash calculation for estimation of asphaltene precipitation. This requires higher computation time. While applying the asphaltene precipitation to reservoir numerical model, the flash calculation needs to be preformed at each grid block and in that case high degree of computational resources is required. In this regard, reduced computation time for asphaltene precipitation calculation is another motivation for another phase of this research work. To predict

different oil recovery circumstances under asphaltene precipitation scenario, proper estimation of porosity and permeability of an asphaltic oil reservoir is very important so that it can deal with the inherent uncertainty due to lack of data and alteration/change due to asphaltene precipitation. This study phase in this area is new and has not been investigated in the past.

These knowledge gaps motivate us to study the estimation of the reservoir parameters (porosity and permeability), and assessment of underlying uncertainty and corresponding impact in reservoir performance by applying recursive methods (Ensemble Kalman Filter and Particle Filter) with modification.

1.2 Literature Review

In reservoir management, reservoir model plays a vital role in optimization and simulation analysis. Model validation through history matching and updating model by incorporating new available information into the model provide high fidelity in the model and help in future projection. Many of the reservoir model parameters have significant uncertainties. In recent years, accurate estimation of unknown or poorly known parameters with the application of ensemble-based methods has received increased attention.

1.2.1 Implementation of Ensemble Kalman Filter (EnKF) to Oil-Water Reservoir

Ensemble Kalman Filter is increasingly being used for estimation of different model parameters because of computational efficiency, ease of operation, and absence of adjoint code. Lorentzen et al. (2001) first applied EnKF to a dynamic model for two-phase flow in a well. The model parameters including liquid hold up, gas fraction, and slip velocity, and state variables such as pressure and individual fluid flow rates were considered as the tuning parameters of the well flow model for predicting the downhole pressure behavior and amount of fluid flowing out of the well during drilling operation. Nævdal et al. (2002) utilized the EnKF tool in a simplified 2D model of North Sea field, consisting of 1931 active grid blocks with 14 producing wells and 4 gas injection wells. They estimated near-well permeability assuming porosity to be known. The reported root mean square (RMS) error between estimated and true values in the range of 0.82 - 0.97, for the initial permeability of the ensemble 1000 mD. Later, Nœvdal et al. (2005) implemented EnKF to a large-scale three phase reservoir and determined the permeability. Brouwer et al. (2004) used EnKF along with a control theory to study water flooding in heterogeneous reservoirs.

Jahanbakhshi et al. (2018) conducted their research on synthetically generated reservoir model under two phase flow to determine the impact of initial ensembles on posterior distribution of EnKF. The results showed almost zero difference between the true value and ensemble mean.

Several studies have been conducted using the PUNQ-S3 reservoir model. Gu and Oliver (2005) applied EnKF to PUNQ-S3 reservoir model under water flooding to estimate the permeability and porosity. Abdolhosseini and Khamehchi (2015) also used PUNQ-S3 model and estimated porosity and permeability by applying EnKF. In addition to permeability and porosity, other reservoir model parameters including fluid contacts (Wang et al., 2009), fluid front (Trani et al., 2013), absolute and relative permeability (Jahanbakhshi et al., 2015; Li et al., 2012), geothermal properties (Marquart et al., 2013), facies properties (Lorentzen et al., 2013), and capillary pressure (Y. Zhang et al., 2017) have been estimated using EnKF.

To deal with non-Gaussian state variables and uncertainties in parameters, several ensemble-based methods have been proposed (Abdolhosseini and Khamehchi, 2015). Parameterization and iterative filters have been used in the EnKF algorithm to correct non-Gaussian system. In parameterization strategy, three different ways are discussed in the literature; namely, posterior distribution represented as a sum of Gaussian kernels (Stordal et al., 2011), alternative state variables instead of non-Gaussian parameters, for example, use of 'water front arrival' instead of water saturation as the state variable (Chen et al., 2009), and transformation of non-Gaussian parameters to Gaussian values using cumulative distribution functions (Gu and Oliver, 2006).

Several researchers (e.g., Emerick and Reynolds, 2013; Jahanbakhshi et al., 2018; Lorentzen et al., 2005; Thulin et al., 2008) investigated the impact of initial ensemble on filter performance in the context of reservoir model. To minimize the impact of initial ensemble on the nonlinear forward model, the iterative EnKF was proposed for estimating model parameters.

Uncertainty in the model or mismatch between the model and the reservoir system has not been systematically studied for the cases of multiphase flow in porous media (Aanonsen et al., 2009). In a recent work, Jahanbakhshi et al. (2018) studied parameter estimation and uncertainty in parameters, while dynamic model error in the system was ignored. Discretization, upscaling, and input data are the common causes that are generally associated with mathematical and numerical model of a reservoir. Also, the assumptions made during model development are responsible for

model errors (Nobakht et al., 2018). Therefore, there is a need for developing methods to estimate reservoir parameters in the presence of model and reservoir mismatch.

One of the main difficulties in the estimation of the reservoir parameters is the input or the forcing variable is constant so that there is less excitation in the system. From system identification theory, it is well known that there is a need for persistent excitation in the system to identify the system parameters (Ljung, 1999). This is also valid for estimating parameters in a state estimator. Without excitation, the system does not generate sufficient information to estimate the parameters or states accurately. This leads to conduct a research work on estimation of the reservoir states and parameters in the presence of model and measurement error and by introducing a modification in the ensemble Kalman filter. Although this is a well-known problem in the control community, this issue has not been investigated with in the reservoir modeling context. We plan to deal with the estimation problem by introducing artificial perturbation to the model.

1.2.2 Estimation of Non-Gaussian States in Water Flooding Problem

When water flooding is performed in a reservoir to displace oil, the distribution of water saturation at the interface does not remain Gaussian. In addition, some of the state variables of a reservoir model (e.g., pressure, saturation, permeability, and porosity) cannot be measured directly and experience significant uncertainty (Chen et al., 2009). Since EnKF is only applicable for systems with linear relationship between state variables, model parameters, and observations; it also cannot deal with non-Gaussian probability distribution (Chen et al., 2009). These two assumptions limit the applicability of EnKF in reservoir history matching specially for the enhanced oil recovery process by water flooding, and this ultimately affects the predictability of the reservoir model. The application of particle filter (PF) in petroleum engineering is very limited as it requires a sufficiently large sample size to accurately quantify the posterior distribution. Despite having limited application, several researchers applied this to analyze different aspects of reservoir.

Yoon (2016) conducted research work regarding reservoir history matching by embedding hyper reduced model into the framework of PF and compared the results with those obtained from implementation of EnKF. Lorentzen et al. (2014) applied auxiliary PF and the transient multiphase well-flow model for automatic identification of reservoir flowrate from wellbore measurements. Later, this approach was also applied in a full-scale multiphase problem (Lorentzen et al., 2016). Liao et al. (2019) embedded a transformation adaptive stochastic collocation method into the

Markov Chain Monte Carlo (MCMC) to resolve the history matching problem with high nonlinearity. Xue et al. (2020) employed the combination of PF and PCM based surrogate model to a shale gas reservoir to predict the uncertainty in reservoir parameters such as permeability, water saturation, and thickness of shale.

While oil is produced from oil reservoir by injecting water, a bimodal water saturation distribution around the waterfront might happen. To deal this non-Gaussian water saturation distribution, both well bore flowing pressure and water saturation profile are very important dynamic states in history matching and corresponding reservoir development. Lack in water saturation profile matching around the waterfront called "water breakthrough", may affect the reliability of the reservoir model, leading to erroneous estimation of reservoir parameters. For water flooding scenario, Gaussian/non-Gaussian probability distribution function is a key factor for approximation of posterior water saturation distribution because at the waterfront, the water saturation distribution is non-Gaussian. In the previous study, PF has not been applied to oil-water reservoir for history matching considering the effect of non-Gaussianity. In addition, EnKF has limited applicability to deal with non-Gaussianity. To deal with history matching issue for non-Gaussianity systems, PF is considered a powerful tool for tracking the stochastic dynamic states. Because PF is a sequential data assimilation method that does not require model linearity and Gaussian assumption. It also provides an accurate approximation of the posterior probability distribution of the updated state variables and thereby improves the quality of history matching leading to accurate estimation reservoir parameters. Eventually, utilization of the correctly estimated reservoir parameters guides to predict production performance.

PF may suffer from the "particle impoverishment" problem during the history matching estimating the static formation properties. In the literature, different approaches are applied to overcome the problem of filter degeneracy in PF application. One of the approaches is implementation of unweighted variance of the ensemble to spread the ensemble. This approach was applied in land surface model by Qin et al. (2009) and in soil hydrology model by Montzka et al. (2011) and Manoli et al.(2015) . Yan et al. (2015) and H. Zhang et al.(2017) applied a method based on Markov Chain Monte Carlo (MCMC) in land surface model for state and parameter estimation for generation of new particles.

For the reservoir case, unlike the state variables, parameters do not have any dynamic model. Moreover, in the reservoir case, parameters such as permeability and porosity are associated with high uncertainty. Therefore, for accurate estimation of these parameters, participation of higher number of particles in resampling step is essential. From the literature, it is found that generation of new particles or spreading the ensemble after data assimilation plays a vital role in estimating unknown parameters. Considering this crucial part, this work introduces an approach to increase new particle generation.

1.2.3 Asphaltene Precipitation Model

In the literature, various models have been found regarding modelling of asphaltene precipitation such as solubility model, solid model, colloidal model, and micellization model. In the models, the asphaltene phase is treated in different way. All these different views about asphaltene in crude oil and asphaltene precipitation have combined to define the phase diagram of asphaltene precipitation and asphaltene solubility.

Solubility model is based on the Flory-Huggins theory where crude oil is split into vapor and liquid phases. In this model, vapor-liquid equilibrium calculation is performed using Soave Redlich-Kwong (SRK) equation of state (EoS). Later, the liquid phase is divided into oil rich solvent phase and asphalt phase. The amount of asphaltene precipitation is calculated from the liquid phase based on the assumption that the precipitated asphaltene does not change the vapor/liquid equilibrium (Hirschberg et al., 1984; Pan and Firoozabadi, 2000; Wang and Civan, 2001). Statistical Associating Fluid Theory (SAFT) EOS is also widely used as it takes the influence of association and non-spherical chain of molecules into consideration (Mohebbinia et al., 2017). Considering modelling of asphaltene precipitation by the SAFT theory, Perturbed-Chain SAFT (PC-SAFT) has exhibited a successful performance for calculating asphaltene precipitation (Alimohammadi et al., 2019).

In the solid model, asphaltene is treated as a single component in the solid phase and it requires calculating some empirical parameters. The empirical parameters are determined by tuning through matching the experimental data. The amount of asphaltene precipitation is calculated by equating the fugacity of asphaltene in solid and liquid phases (Nghiem and Coombe, 1997; Qin et al., 2000). The colloidal solution model considers asphaltene as solid particles in a colloidal suspension stabilized by adsorbed resins on asphaltene surface (Correra and Donaggio, 2000;

Leontaritis and Mansoori, 1987). In thermodynamic micellization model, the asphaltene molecules are assumed to form a micelle core and the resin molecules adsorb onto the core surface to stabilize the micelle. The principle of the minimization of the Gibbs free energy is used to determine the micelle structure and concentration (Pan and Firoozabadi, 2000, 1998).

Apart from the methods mentioned above, researchers also have been used scaling equations for rapid estimation of asphaltene precipitation. However, associated nonlinearity in scaling equation for asphaltene precipitation calculation requires tuning of the input parameters such as pressure, molecular weight, API gravity of the crude oil, and dilution ratio. In this regard, application of smart technology tries to eliminate the limitations regarding applicability of scaling equation. Sayyad Amin et al. (2017) used a predictive tool named as response surface methodology (RSM) for rapid estimation of asphaltene precipitation accurately. The research work was based on finding important factors that have major impacts on asphaltene precipitation and corresponding interaction effects between factors found from parametric sensitivity analysis. Ahmadi (2011) proposed imperialist competitive algorithm (ICA) for optimizing weights of feed forward neural network model for asphaltene precipitation prediction. Ahmadi and Shadizadeh (2012) conducted a research work on Northern Persian Gulf Oil Field for asphaltene precipitation. In their work, a model was developed based on feed forward ANN, and the model was optimized by particle swarm optimization (PSO) to predict asphaltene precipitation. Similar approach was also employed by Zendehboudi et al. (2014) to investigate the impact of parameters such as temperature, pressure, dilution ration, and composition on asphaltene precipitation for the case of with and without CO_2 injection. Chamkalani et al.(2014) developed scaling equation in terms of temperature, molecular weight, and dilution ratio, and proposed methodology using least square support vector machines/regression (LSSVM/LSSVR) to perform nonlinear modeling. Menshad et al.(2008) determined onset of asphaltene precipitation by applying scaling equation as a function of pressure linked with genetic algorithm (GA). Sayyad Amin et al.(2010) implemented Bayesian Belief Network (BBN) as an ANN tool to analyze the impact of input parameters such as dilution ratio, reservoir pressure and molecular weight on asphaltene precipitation estimated by following scaling theory.

In asphaltene precipitation calculation, stability criteria are ensured by the thermodynamic equilibrium between all phases at each pressure. This thermodynamic equilibrium determines

whether asphaltene will precipitate or not. At each pressure, once the equilibrium is established, the amount of precipitated asphaltene is calculated and the calculation will continue for the next pressure. However, to reach this equilibrium condition, it requires repeated flash calculation and stability check at each pressure. This approach leads to consumption of more time and makes the entire calculation very slow. Furthermore, for reservoir simulation, the reservoir is split into many grid blocks, and the calculations are performed for individual grids. This increases computation time and requires more computational resources. Considering the importance of computational time, this thesis work introduces a modification in the flash calculation so that the amount of asphaltene can be calculated explicitly at each pressure drop.

1.2.4 Implementation of EnKF to Asphaltic Oil Reservoir

Oil production from the reservoir causes a change in reservoir pressure, temperature, oil composition and thereby reservoir equilibrium which eventually leads to asphaltene precipitation. Asphaltene precipitation and consequently deposition on the rock surface is defined as serious threat to formation damage, wellbore plugging, and production facilities (Andersen and Speight, 1999; Bland et al., 2006). Researchers have proposed various models to predict asphaltene precipitation behaviors such as solubility model, solid model, colloidal model, and micellization model. Moreover, other predictive approaches (tools) and/or intelligent techniques such as artificial neural network (ANN) linked with particle swarm optimization (PSO) and genetic algorithm, support vector machine, response surface methodology, and Bayesian Belief Network.

Besides developing asphaltene precipitation model, Darabi et al. (2014) investigated the impact of gas flooding on the dynamics of asphaltene precipitation and deposition. Qin et al.(2000) studied the effect of asphaltene precipitation on reservoir flow behavior. Tabzar et al.(2018) investigated the influence of asphaltene precipitation on fluid flow rate, porosity, and permeability in saturated and under saturated oil reservoirs. Fallahnejad and Kharrat (2015) developed a fully implicit compositional simulator for modeling asphaltene deposition during natural depletion, and predicted formation damage in terms of porosity and permeability reduction. Almehaideb (2004) developed a new single-well model considering four-component (asphaltene–oil–gas–water) to simulate asphaltene precipitation, deposition, and plugging of oil wells during primary production with the resulting effect on well productivity.

Two important parameters of a reservoir model are porosity and permeability. In fact, they are roughly estimated from seismic and well test data representing only small portion of the reservoir. Therefore, these parameters contain high degree of uncertainty. Moreover, because of oil production, reservoir pressure changes and leads to asphaltene precipitation. Later, this precipitated asphaltene is deposited on the rock surface; therefore, a reduction occurs in porosity and permeability. As a result, asphaltene precipitation makes a dynamic change in these two important parameters with respect to reservoir pressure change. Therefore, proper assessment of asphaltene precipitation based on correct estimation of porosity and permeability appears to be necessary for the reliability of the reservoir model and accurate future projection.

In the previous studies, the focus has been on the development of asphaltene precipitation model and corresponding its impact on the reservoir production and field development. However, current estimation of porosity and permeability for asphaltic oil reservoir is not found in the literature. This leads to application of EnKF to asphaltic oil reservoir for history matching and parameter estimation. While applying EnKF, a methodology is developed to address the change of dynamic state for the gas and asphaltene phases.

This thesis aims to fulfill the knowledge gaps highlighted above. The detailed goals and expected outcomes are presented in the next section.

1.3 Objectives

This research focuses on the estimation of important reservoir parameters such as permeability, porosity and corresponding uncertainty of the oil reservoir considering several factors such as dynamic model error, measurement error, perturbation of input or forcing variables, non-Gaussianity in dynamic state variables, avoiding particle collapse and providing guidelines for application of ensemble-based methods to asphaltic oil reservoir. In addition, this thesis investigates the modification of the asphaltene precipitation model with an aim to reduce computational time. The main tasks to attain the goals are given below:

Task 1: History matching and parameter estimation study using ensemble Kalman filter (EnKF) in the presence of dynamic model error. The model is also adapted for lack of excitation (i.e., constant input) in the system.

Task 2: Investigation of the impact of non-Gaussian probability distribution in dynamic state estimation in case of water flooding problem in heterogeneous oil reservoirs.

Task 3: Modification of the asphaltene precipitation model to lower computational time while incorporating the model during reservoir simulation.

Task 4: Application of EnKF to asphaltic oil reservoir for parameter estimation and uncertainty assessment.

1.4 Research Tools and Expected Outcomes

The core research objectives, investigation tools, case studies, and expected outcomes are listed in **Table 1-1.**

Table 1-1: Research Tools and Expected Outcomes.

Core Objectives	**Features**	**Description**
1. Estimation of the reservoir states and parameters in presence of dynamic model and measurement error and capturing the excitation in the system happened due to 'oil production by water injection'.	Tools Used	• MATLAB for 2D oil reservoir model development. • EnKF implementation for history matching.
	Case Study	Water flooding in 2D oil-water reservoir.
	Expected Outcome	Porosity and permeability estimation and their uncertainty assessment.
2. Estimation of the reservoir states and parameters considering non-Gaussianity in the dynamic states and introduction of an approach in resample stage in PF to avoid particle impoverishment.	Tools Used	• MATLAB for 2D reservoir model development. • PF and EnKF implementation for history matching
	Case Study	Water flooding in five spot 2D oil-water reservoir.
	Expected Outcome	Porosity and permeability estimation and their uncertainty assessment.
3. Modification of the solid model for asphaltene precipitation calculation to minimize the execution time and enable recursive estimation.	Tools Used	• MATLAB for 2D oil reservoir model development.
	Case Study	An asphaltic oil reservoir producing oil through primary recovery process.
	Expected Outcome	Explicit estimation of the amount of precipitated asphaltene at each time step.
4. Estimation of states and parameters of the asphaltic oil reservoir including the effect of asphaltene precipitation on rock surface.	Tools Used	• MATLAB for 2D oil reservoir model development. • EnKF implementation for history matching.
	Case Study	An asphaltic oil reservoir producing oil through primary recovery process
	Expected Outcome	Porosity and permeability estimation considering the impact of asphaltene precipitation.

1.5 Organization of Thesis

The thesis is written in a manuscript format. One published journal article and three journal manuscripts are included in the thesis. A co-authorship statement is provided at the beginning of the thesis. Overall organization of the thesis is shown in **Figure 1-1**.

A brief overview of each chapter is described below-

Chapter 1 of the thesis describes the motivations and objectives of the research. This chapter also includes a brief review of the related previous studies.

Chapter 2 describes about the history matching of a 2D oil-water reservoir model and corresponding estimation of the reservoir parameters (porosity and permeability) along with uncertainty quantification. The investigation is conducted to adapt the estimator for lack of excitation in the system.

Chapter 3 presents an investigation on the impact of non-Gaussianity in estimating dynamic state such as water saturation in 2D oil-water reservoir while producing oil by secondary recovery process, i.e., water injection with the implementation of particle filter.

Chapter 4 presents a thorough discussion on the pure solid model for asphaltene precipitation in asphaltic oil reservoir and introduction of a modification in performing flash calculation in pure solid model aiming to minimize the execution time for asphaltene precipitation calculation. In addition, reservoir simulation of a 2D asphaltic oil reservoir is conducted to investigate the effect of asphaltene precipitation on rock properties (porosity and permeability).

Chapter 5 focuses on the estimation of reservoir parameters (porosity and permeability) of a 2D asphaltic oil reservoir by applying ensemble Kalman filter (EnKF), considering the impact of asphaltene precipitation on the reservoir characteristics.

Chapter 6 presents the conclusions of the study and the possible scopes for future work.

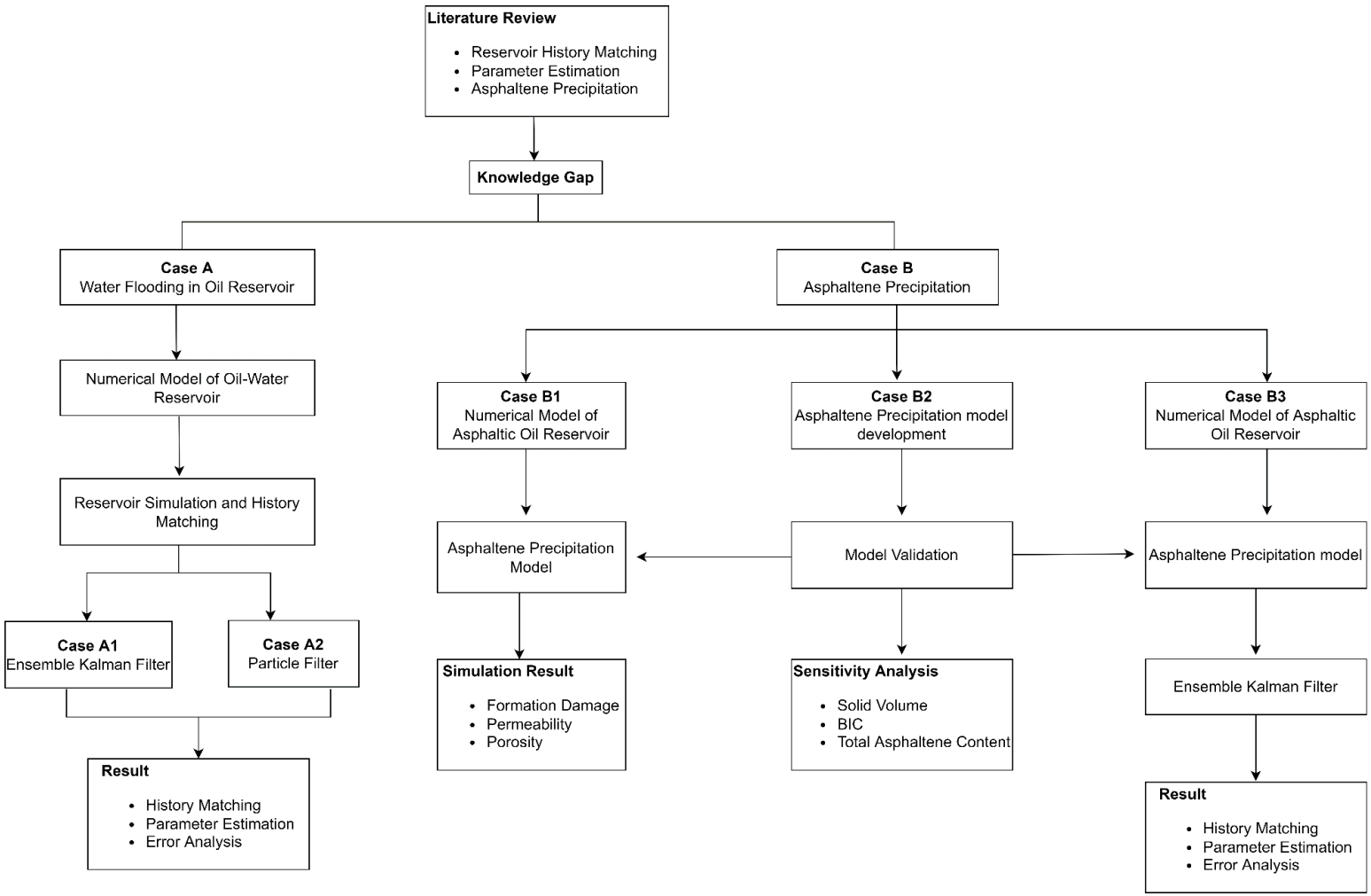

Figure 1-1: Organization of the Thesis

References

1. Aanonsen, S.I., Nœvdal, G., Oliver, D.S., Reynolds, A.C., Vallès, B., 2009. The ensemble Kalman filter in reservoir engineering-A Review. SPE J. 14, 393–412. https://doi.org/10.2118/117274-PA
2. Abdolhosseini, H., Khamehchi, E., 2015. History matching using traditional and finite size ensemble Kalman filter. J. Nat. Gas Sci. Eng. 27, 1748–1757. https://doi.org/10.1016/j.jngse.2015.10.041
3. Ahmadi, M.A., 2011. Prediction of asphaltene precipitation using artificial neural network optimized by imperialist competitive algorithm. J. Pet. Explor. Prod. Technol. 1, 99–106. https://doi.org/10.1007/s13202-011-0013-7
4. Ahmadi, M.A., Shadizadeh, S.R., 2012. New approach for prediction of asphaltene precipitation due to natural depletion by using evolutionary algorithm concept. Fuel 102, 716–723. https://doi.org/10.1016/j.fuel.2012.05.050
5. Alimohammadi, S., Zendehboudi, S., James, L., 2019. A comprehensive review of asphaltene deposition in petroleum reservoirs: Theory, challenges, and tips. Fuel 252, 753–791. https://doi.org/10.1016/j.fuel.2019.03.016
6. Almehaideb, R.A., 2004. Asphaltene precipitation and deposition in the near wellbore region: A modeling approach. J. Pet. Sci. Eng. 42, 157–170. https://doi.org/10.1016/j.petrol.2003.12.008
7. Andersen, S.I., Speight, J.G., 1999. Thermodynamic models for asphaltene solubility and precipitation. J. Pet. Sci. Eng. 22, 53–66. https://doi.org/10.1016/S0920-4105(98)00057-6
8. Bland, R., Mullen, G., Gonzalez, Y., Harvey, F., Pless, M., Hughes, B., 2006. HP/HT Drilling Fluid Challenges, in: IADC/SPE Asia Pacific Drilling Technology Conference and Exhibition. Bangkok, Thailand.
9. Brouwer, D.R., Nævdal, G., Jansen, J.D., Vefring, E.H., 2004. Improved reservoir management through optimal control and continuous model updating, in: Proceedings - SPE Annual Technical Conference and Exhibition. pp. 1551–1561. https://doi.org/10.2523/90149-ms
10. Chamkalani, A., Zendehboudi, S., Bahadori, A., Kharrat, R., Chamkalani, R., James, L., Chatzis, I., 2014. Integration of LSSVM technique with PSO to determine asphaltene

deposition. J. Pet. Sci. Eng. 124, 243–253. https://doi.org/10.1016/j.petrol.2014.10.001

11. Chen, Y., Oliver, D.S., Zhang, D., 2009. Data assimilation for nonlinear problems by ensemble Kalman filter with reparameterization. J. Pet. Sci. Eng. 66, 1–14. https://doi.org/10.1016/j.petrol.2008.12.002
12. Correra, S., Donaggio, F., 2000. OCCAM: Onset-constrained colloidal asphaltene model, in: SPE International Symposium on Asphaltene Deposition Is a Well Known Problem in Oil Formation Damage. https://doi.org/10.2118/58724-ms
13. Darabi, H., Shirdel, M., Kalaei, M.H., Sepehrnoori, K., 2014. Aspects of modeling asphaltene deposition in a compositional coupled wellbore/reservoir simulator, in: SPE Improved Oil Recovery Symposium. p. SPE-169121-MS. https://doi.org/10.2118/169121-MS
14. Emerick, A.A., Reynolds, A.C., 2013. Investigation of the sampling performance of ensemble-based methods with a simple reservoir model. Comput. Geosci. 17, 325–350. https://doi.org/10.1007/s10596-012-9333-z
15. Fallahnejad, G., Kharrat, R., 2015. Fully implicit compositional simulator for modeling of asphaltene deposition during natural depletion. Fluid Phase Equilib. 398, 15–25. https://doi.org/10.1016/j.fluid.2015.03.045
16. Gu, Y., Oliver, D.S., 2006. The ensemble Kalman filter for continuous updating of reservoir simulation models. J. Energy Resour. Technol. Trans. ASME 128, 79–87. https://doi.org/10.1115/1.2134735
17. Gu, Y., Oliver, D.S., 2005. History matching of the PUNQ-S3 reservoir model using the ensemble Kalman filter. SPE J. 10, 217–224. https://doi.org/10.2118/89942-PA
18. Hirschberg, A., DeJong, L.N.J., Schipper, B.A., Meijer, J.G., 1984. Influence of temperature and pressure on asphaltene flocculation. Soc. Pet. Eng. J. 24, 283–293. https://doi.org/10.2118/11202-PA
19. Jahanbakhshi, S., Pishvaie, M.R., Boozarjomehry, R.B., 2018. Impact of initial ensembles on posterior distribution of ensemble-based assimilation methods. J. Pet. Sci. Eng. 171, 82–98. https://doi.org/10.1016/j.petrol.2018.07.022
20. Jahanbakhshi, S., Pishvaie, M.R., Boozarjomehry, R.B., 2015. Joint estimation of absolute and relative permeabilities using ensemble-based Kalman filter. J. Nat. Gas Sci. Eng. 26, 1232–1245. https://doi.org/10.1016/j.jngse.2015.08.029

21. Leontaritis, K.J., Mansoori, G.A., 1987. Asphaltene flocculation during oil production and processing: a thermodynamic colloidal model., in: SPE International Symposium on Oilfield Chemistry. pp. 149–158. https://doi.org/10.2523/16258-ms
22. Li, H., Chen, S., Yang, D., Tontiwachwuthikul, P., 2012. Estimation of relative permeability by assisted history matching using the ensemble-kalman-filter method. J. Can. Pet. Technol. 51, 205–214. https://doi.org/10.2118/156027-PA
23. Liao, Q., Zeng, L., Chang, H., Zhang, D., 2019. Efficient history matching using the markov-chain monte carlo method by means of the transformed adaptive stochastic collocation method. SPE J. 24, 1468–1489. https://doi.org/10.2118/194488-PA
24. Ljung, L., 1998. System Identification, PRENTICE HALL PTR. https://doi.org/10.1007/978-1-4612-1768-8_11
25. Lorentzen, R.J., Fjelde, K.K., Frøyen, J., Lage, A.C.V.M., Nævdal, G., Vefring, E.H., 2001. Underbalanced and low-head drilling operations: real time interpretation of measured data and operational support, in: SPE Annual Technical Conference and Exhibition. pp. 591–602. https://doi.org/10.2523/71384-ms
26. Lorentzen, R.J., Nævdal, G., Vallès, B., Berg, A.M., Grimstad, A.A., 2005. Analysis of the ensemble kalman filter for estimation of permeability and porosity in reservoir models, in: SPE Annual Technical Conference and Exhibition. pp. 2695–2704. https://doi.org/10.2523/96375-ms
27. Lorentzen, R.J., Ncevdal, G., Shafieirad, A., 2013. Estimating facies fields by use of the ensemble kalman filter and distance functions-applied to shallow-marine environments. SPE J. 18, 146–158. https://doi.org/10.2118/143031-pa
28. Lorentzen, R.J., Stordal, A.S., Luo, X., Nævdal, G., 2016. Estimation of production rates by use of transient well-flow modeling and the auxiliary particle filter: Full-scale applications. SPE Prod. Oper. 31, 163–175. https://doi.org/10.2118/176033-PA
29. Lorentzen, R.J., Stordal, A.S., Luo, X., Nævdal, G., 2014. Estimation of production rates by use of transient well-flow modeling and the auxiliary particle filter: Full-scale applications. SPE Prod. Oper. 31, 163–175. https://doi.org/10.2118/176033-PA
30. Manoli, G., Rossi, M., Pasetto, D., Deiana, R., Ferraris, S., Cassiani, G., Putti, M., 2015. An iterative particle filter approach for coupled hydro-geophysical inversion of a controlled infiltration experiment. J. Comput. Phys. 283, 37–51.

https://doi.org/https://doi.org/10.1016/j.jcp.2014.11.035

31. Marquart, G., Vogt, C., Klein, C., Widera, A., 2013. Estimation of geothermal reservoir properties using the ensemble Kalman filter. Energy Procedia 40, 117–126. https://doi.org/10.1016/j.egypro.2013.08.015
32. Menshad, A.K., Mofidi, A.M., Shariatpanahi, F., Edalat, M., 2008. Developing of scaling equation with function of pressure to determine onset of asphaltene precipitation. J. Japan Pet. Inst. 51, 102–106. https://doi.org/10.1627/jpi.51.102
33. Mohebbinia, S., Sepehrnoori, K., Johns, R.T., Kazemi Nia Korrani, A., 2017. Simulation of asphaltene precipitation during gas injection using PC-SAFT EOS. J. Pet. Sci. Eng. 158, 693–706. https://doi.org/10.1016/j.petrol.2017.09.008
34. Montzka, C., Moradkhani, H., Weihermüller, L., Franssen, H.-J.H., Canty, M., Vereecken, H., 2011. Hydraulic parameter estimation by remotely-sensed top soil moisture observations with the particle filter. J. Hydrol. 399, 410–421. https://doi.org/https://doi.org/10.1016/j.jhydrol.2011.01.020
35. Nævdal, G., Mannseth, T., Vefring, E.H., 2002. Near-well reservoir monitoring through ensemble Kalman filter, in: SPE Symposium on Improved Oil Recovery. pp. 959–967. https://doi.org/10.2523/75235-ms
36. Nghiem, L.X., Coombe, D.A., 1997. Modeling asphaltene precipitation during primary depletion. SPE J. 2, 170–176. https://doi.org/10.2118/36106-pa
37. Nobakht, B.N.K., Christie, M., Demyanov, V., 2018. Model selection for error generalization in history matching, in: EAGE Conference and Exhibition. pp. 11–14. https://doi.org/10.2118/190778-ms
38. Nœvdal, G., Johnsen, L.M., Aanonsen, S.I., Vefring, E.H., 2005. Reservoir monitoring and continuous model updating using ensemble Kalman Filter. SPE Repr. Ser. 66–74. https://doi.org/10.2523/84372-ms
39. Pan, H., Firoozabadi, A., 2000. Thermodynamic micellization model for asphaltene precipitation from reservoir crudes at high pressures and temperatures. SPE Prod. Facil. 15, 58–65. https://doi.org/10.2118/60842-PA
40. Pan, H., Firoozabadi, A., 1998. Thermodynamic micellization model for asphaltene aggregation and precipitation in petroleum fluids. SPE Prod. Facil. 13, 118–125. https://doi.org/10.2118/36741-pa

41. Qin, J., Liang, S., Yang, K., Kaihotsu, I., Liu, R., Koike, T., 2009. Simultaneous estimation of both soil moisture and model parameters using particle filtering method through the assimilation of microwave signal. J. Geophys. Res. Atmos. 114. https://doi.org/https://doi.org/10.1029/2008JD011358
42. Qin, X., Wang, P., Sepehrnoori, K., Pope, G.A., 2000. Modeling asphaltene precipitation in reservoir simulation. Ind. Eng. Chem. Res. 39, 2644–2654. https://doi.org/10.1021/ie990781g
43. Sayyad Amin, J., Alamdari, A., Mehranbod, N., Ayatollahi, S., Nikooee, E., 2010. Prediction of asphaltene precipitation: Learning from data at different conditions. Energy and Fuels 24, 4046–4053. https://doi.org/10.1021/ef100106r
44. Sayyad Amin, J., Nikkhah, S., Zendehboudi, S., 2017. A new experimental and modeling strategy to determine asphaltene precipitation in crude oil. Chem. Eng. Res. Des. 128, 162–173. https://doi.org/10.1016/j.cherd.2017.09.035
45. Stordal, A.S., Karlsen, H.A., Nævdal, G., Skaug, H.J., Vallès, B., 2011. Bridging the ensemble Kalman filter and particle filters: The adaptive Gaussian mixture filter. Comput. Geosci. 15, 293–305. https://doi.org/10.1007/s10596-010-9207-1
46. Tabzar, A., Fathinasab, M., Salehi, A., Bahrami, B., Mohammadi, A.H., 2018. Multiphase flow modeling of asphaltene precipitation and deposition. Oil Gas Sci. Technol. – Rev. d'IFP Energies Nouv. 73, 51. https://doi.org/10.2516/ogst/2018039
47. Thulin, K., Nævdal, G., Skaug, H.J., Aanonsen, S.I., 2011. Quantifying Monte Carlo uncertainty in the ensemble Kalman filter. SPE J. https://doi.org/10.3997/2214-4609.20146415
48. Trani, M., Arts, R., Leeuwenburgh, O., 2012. Seismic history matching of fluid fronts using the ensemble Kalman filter. SPE J. 18, 159–171. https://doi.org/10.2118/163043-PA
49. Wang, S., Civan, F., 2001. Productivity decline of vertical and horizontal wells by asphaltene deposition in petroleum reservoirs, in: SPE International Symposium on Oilfield Chemistry. pp. 145–160. https://doi.org/10.2118/64991-ms
50. Wang, Y., Li, G., Reynolds, A.C., 2009. Estimation of depths of fluid contacts by history matching using iterative ensemble kalman smoothers, in: SPE Reservoir Simulation Symposium. pp. 750–766. https://doi.org/10.2118/119056-ms
51. Xue, L., Liu, Y., Nan, T., Liu, Q., Jiang, X., 2020. An efficient automatic history matching

method through the probabilistic collocation based particle filter for shale gas reservoir. J. Pet. Sci. Eng. 190, 107086. https://doi.org/10.1016/j.petrol.2020.107086

52. Yan, H., DeChant, C.M., Moradkhani, H., 2015. Improving Soil Moisture Profile Prediction With the Particle Filter-Markov Chain Monte Carlo Method. IEEE Trans. Geosci. Remote Sens. 53, 6134–6147. https://doi.org/10.1109/TGRS.2015.2432067
53. Yoon, S., 2016. Ensemble-based reservoir history matching using hyper-reduced-order models. Massachusetts Institute of Technology.
54. Zendehboudi, S., Shafiei, A., Bahadori, A., James, L.A., Elkamel, A., Lohi, A., 2014. Asphaltene precipitation and deposition in oil reservoirs - Technical aspects, experimental and hybrid neural network predictive tools. Chem. Eng. Res. Des. 92, 857–875. https://doi.org/10.1016/j.cherd.2013.08.001
55. Zhang, H., Hendricks Franssen, H.-J., Han, X., Vrugt, J.A., Vereecken, H., 2017. State and parameter estimation of two land surface models using the ensemble Kalman filter and the particle filter. Hydrol. Earth Syst. Sci. 21, 4927–4958. https://doi.org/10.5194/hess-21-4927-2017
56. Zhang, Y., Yang, D., Li, H., Patil, S., 2017. Simultaneous estimation of relative permeability and capillary pressure for PUNQ-S3 model with a damped iterative ensemble Kalman Filter technique. SPE J. 971–984. https://doi.org/10.2118/177846-ms

Chapter 2 : Modified Ensemble Kalman Filter for Reservoir Parameter and State Estimation in the Presence of Model Uncertainty

Preface

This chapter addresses an objective of this dissertation as outlined in Section 2.1 which is to estimate the dynamic states and static parameters of the reservoir under model and system mismatch as well as uncertainty in the measured signals. The methodology presented in this chapter aims to improve history matching by introducing modifications in EnKF and thereby estimate reservoir parameters with more accuracy, as presented in Section 2.2 and Section 2.4.

I (Farhana Akter) have contributed to Conceptualization, Methodology, Formal Analysis, Investigation, Writing - Original Draft, and Writing - Review & Editing of this work, while Dr. Syed Imtiaz contributed to Conceptualization, Methodology, Formal Analysis, Writing - Review & Editing, Supervision; Dr. Sohrab Zendehboudi contributed to Writing - Review & Editing, and Supervision; Dr. Kamal Hossain contributed to Writing - Review & Editing. A version of this chapter has been published in the Journal of Petroleum Science and Engineering. https://doi.org/10.1016/j.petrol.2020.108323, Volume 199, April 2021.

Abstract

Ensemble Kalman filter (EnKF) is widely used in reservoir modelling for on-line history matching. Typically, it is assumed that structurally the model is an accurate representation of the reservoir and uncertainty exists only in the parameters. This paper focuses on estimating reservoir static parameters (i.e., porosity and permeability) and dynamic states using EnKF in the presence of mismatch between the reservoir and the model. An in-depth investigation of the application challenges of EnKF is reported. Two modifications are introduced for joint state-parameter estimation: i) addition of error to the model to represent the mismatch between the predictive model and real system, and ii) introduction of a tuning parameter called ‘forcing data’ to the perturbation variable for dealing with a noisy system. A benchmark problem defined as ‘tank series model’ is designed for the verification of the EnKF algorithm. Using the simplified model

mathematical formulation of state estimation combined with parameter calibration is presented systematically. Later, similar approach is applied to a nonlinear two-dimensional reservoir under water flooding operation. To assess the performance in history matching, a sensitivity analysis is conducted. It was observed that due to forcing data perturbation, about 13.6 % and 9% improvement is possible in history matching of the tank and reservoir cases respectively when model mismatch and uncertainty in measurement are high.

Keywords: EnKF; Reservoir Model; Tank Model; History Matching; Parameter Estimation; Forcing Data.

2.1 Introduction

A typical reservoir model contains several parameters that are difficult to measure/determine, leading to uncertainties in model prediction. Validation of reservoir model through history matching and updating the model by incorporating new available information is important to maintain high fidelity in model prediction. Kalman filter (KF) was originally developed for dynamic control systems (Kalman, 1960). Since then, different versions of Kalman filter such as extended Kalman filter (EKF) and unscented Kalman filter (UKF) have been proposed and used in several other areas such as weather forecasting, oceanography, and hydrology (Gu and Oliver, 2005). Evensen (1994) first proposed EnKF where he showed the improvement of the EKF algorithm by accurate estimation of state covariance matrix. Computational efficiency, ease of operation, and absence of adjoint code make EnKF suitable for estimation of different model parameters and is increasingly being used in commercial reservoir simulators(Shuai et al., 2016).

In petroleum industry, Lorentzen et al.(2001)first applied EnKF to a dynamic model for two-phase flow in a well. The model parameters such as liquid hold up, gas fraction, and slip velocity, and state variables such as pressure and individual fluid flow rates were considered as tuning parameters of the well flow model for predicting the downhole pressure behavior and amount of fluid flowing out of the well during drilling operation. Nævdal et al. (2002) utilized the EnKF tool in a simplified 2D model of North Sea field, having 1931 active grid blocks with 14 producing wells and 4 gas injection wells. They estimated the static parameter (e.g., permeability) near well assuming porosity to be known. They found that the RMS error between estimated and true values varies between 0.82 and 0.97, assuming the initial mean of the permeability of the ensemble

1000mD. Later, Nœvdal et al.(2005) implemented EnKF to a large-scale three phase reservoir and determined the permeability. Brouwer et al.(2004) used EnKF along with a control theory to study water flooding into heterogeneous reservoirs. Jahanbakhshi et al. (2018) conducted their research on synthetically generated reservoir model under two phase flow to determine the impact of initial ensembles on posterior distribution of EnKF. The results showed almost zero difference between the true value and ensemble mean.

Several studies have been conducted using the PUNQ-S3 reservoir model. For instance, Gu and Oliver (2005) applied EnKF to PUNQ-S3 reservoir model under water flooding to estimate the permeability and porosity. The estimated porosity varies from 0.17 to 0.3 with layers against true mean value of 0.3. Also for permeability estimation, one layer reflected true mean value of 148 mD, but other layers showed increasing deviation from the true values. Abdolhosseini and Khamehchi (2015) also used PUNQ-S3 model and estimated porosity and permeability by applying EnKF. They showed the result in terms of RMSE values change from initial to final condition for parameters estimation. The RMSE changes from 0.0842 to 0.0376 for porosity, from 2.7417 to 0.8684 for vertical permeability and from 3.5994 to 1.1842 for vertical and horizontal permeability. Liu and Oliver (2005) employed the EnKF to predict the location and distribution of geologic facies in terms of porosity and permeability, as well as history matching. Wen and Chen (2005) applied the EnKF to a 2D reservoir of 50 × 50 ×1 grids with the dimension of 20 ft ×20 ft×2 ft to examine the influence of ensemble size on model updating. Skjervheim et al.(2007) first presented the application of EnKF to North Sea Field case using 4D seismic data (time lapse seismic data).

In addition to permeability and porosity, other reservoir model parameters including fluid contacts (Wang et al., 2009), fluid front (Trani et al., 2012), absolute and relative permeability (Jahanbakhshi et al., 2015; Li et al., 2012), geothermal properties(Marquart et al., 2013), facies properties (Lorentzen et al., 2013), and capillary pressure (Zhang et al., 2017) have been estimated using EnKF.

Bimodal probability distribution function for water saturation at front region, and facies distribution in complex reservoir are the non-Gaussian model parameters that cannot be dealt with standard EnKF analysis as the result exceeds the physical possible limit(Gu and Oliver, 2006). Despite a wide range of applications of EnKF reported in the literature, several limitations have

been identified for the EnKF applications in reservoir modeling: i) Gaussian model parameters, ii) finite size of ensemble, and iii) inappropriate initial ensembles(Jung et al., 2018).

Several ensemble-based methods have been proposed to deal with non-Gaussian state variables and uncertainties in parameters (Abdolhosseini and Khamehchi, 2015). Parameterization and iterative filters have been used in the EnKF algorithm to correct non-Gaussian system. In parameterization strategy, three different ways are discussed in the literature; namely, posterior distribution represented as a sum of Gaussian kernels (Stordal et al., 2011), alternative state variables instead of non-Gaussian parameters, for example, use of 'water front arrival' instead of water saturation as the state variable(Chen et al., 2009), and transformation of non-Gaussian parameters to Gaussian values using cumulative distribution functions (Gu and Oliver, 2006).

Researchers such as (Emerick and Reynolds, 2013; Jahanbakhshi et al., 2018; Lorentzen et al., 2005; Thulin et al., 2011) investigated the impact of initial ensemble on filter performance in the context of reservoir model. To minimize the impact of initial ensemble on the nonlinear forward model, the iterative EnKF was proposed for estimating model parameters.

Uncertainty in the model or mismatch between the model and the reservoir has not been rigorously studied for the cases of multiphase flow in porous media (Aanonsen et al., 2009). In a recent work, (Jahanbakhshi et al., 2018) studied parameter estimation and uncertainty in parameters while dynamic model error in the system has been mostly ignored by the reservoir modelling community. Discretization, upscaling, and input are the common model errors that are generally associated with mathematical and numerical model of a reservoir. Also, the assumptions made during model development are responsible for model errors (Nobakht et al., 2018).

Noise in measurement is one of the factors for the deviation of the reservoir model from the true state. In addition, consideration of constant input or forcing variable creates less excitation in the system. Due to these reasons, state estimators are unable to estimate state accurately. As such, models could provide good history matching, but would be unable to make good prediction.

The key focus of this research is to estimate the dynamic states and static parameters of the reservoir under model and system mismatch as well as uncertainty in the measured signals. Rough estimates of the key parameters such as permeability and porosity are available and associated with uncertainty. Several modifications have been proposed to the EnKF including exciting the system

with randomly varying input signals for better estimation of the system parameters. In addition, a synthetic tank series model is created to develop guidelines for tuning of the reservoir model. The tank series model resembles a reservoir system in many ways. The fluid level in the tank is equivalent to pressure in a reservoir, and cross-sectional area of the pipe joining two adjacent tanks are being like reservoir permeability. Followed by this, the proposed methodology is applied to a reservoir case.

The article is organized as follows: theory and formulation on EnKF is presented in **Section 2.2**. Detail discussion regarding tuning parameter is also discussed in this section by providing a flowchart for combined state and parameter estimation. **Section 2.3** presents the case studies of the two different cases where mathematical formulation of benchmark 'tank series model' system and synthetic 2D reservoir under water flooding operation are shown. Methodology is presented in **Section 2.4**. **Section 2.5** discusses case wise results including history matching and parameter estimation for both tank series model and reservoir model in the light of model error and forcing data perturbation. Finally, **Section 2.6** represents the conclusions.

2.2 Theory and Formulation of Ensemble Kalman Filter

In this section we provide the theoretical background of EnKF and introduction of the tuning parameter for improving EnKF estimation.

2.2.1 Ensemble Kalman Filter

EnKF is a Monte Carlo method used for data assimilation. With this technique, an ensemble of state variables of a system is generated from prior information and the system is updated through sequential data assimilation. The methodology comprises of two steps such as forecast step and update step. In the forecast step, state variables are projected forward in time. The estimated values of the states are corrected in the update step by considering the most recent observations.

Forecast step: The state variables are predicted as follows:

$$x^{i-}{}_{t+1} = f(x^{i+}{}_{t}, u_t) + Q^{i}{}_{t}, \quad Q^{i}{}_{t} \sim N(0, \Sigma_t^m) \tag{2-1}$$

Here, x is the augmented state vector, containing both states and parameters that need to be estimated.

Ensemble mean of the state variables, $\bar{x}_{t+1} = \frac{1}{N}\sum_{i=1}^{N} x^{i-}{}_{t+1}$

Estimated measurement, $\hat{y}^i{}_{t+1} = h(x^{i-}{}_{t+1}, u_t)$ (2-2)

Ensemble mean of estimated measurement, $\bar{y}_{t+1} = \frac{1}{N}\sum_{i=1}^{N} \hat{y}^i{}_{t+1}$

Update step: The Kalman gain is calculated by the following equation:

$$K_{t+1} = \Sigma_{t+1}^{xy}\left[\Sigma_{t+1}^{yy} + R_{t+1}\right]^{-1}, R_{t+1} \sim N\left(0, \Sigma_{t+1}^{y}\right) \quad (2\text{-}3)$$

where Σ_{t+1}^{yy} is the forecast error covariance matrix of the prediction, and Σ_{t+1}^{xy} is the cross covariance between the state variables and predicted output. They are defined as follows:

$$\Sigma_{t+1}^{yy} = \left(\hat{y}^i{}_{t+1} - \bar{y}_{t+1}\right)\left(\hat{y}^i{}_{t+1} - \bar{y}_{t+1}\right)^T \quad and \quad \Sigma_{t+1}^{xy} = \left(\hat{y}^i{}_{t+1} - \bar{y}_{t+1}\right)\left(x^{i-}{}_{t+1} - \bar{x}_{t+1}\right)^T$$

Perturbed production data

$$y^i{}_{t+1} = y_{t+1} + \eta^i{}_{t+1};\ \ \eta^i{}_{t+1} \sim N\left(0, \Sigma_{t+1}^{y}\right) \quad (2\text{-}4)$$

The state is updated as follows:

$$x^{i+}{}_{t+1} = x^{i-}{}_{t+1} + K_{t+1}\left(y^i{}_{t+1} - \hat{y}^i{}_{t+1}\right) \quad (2\text{-}5)$$

2.2.2 Tuning Parameter Introduction

Reservoir models are generated based on the prior geological knowledge/data such as seismic and well test data. Transmissivity, porosity, permeability, relative permeability, and fluid contact are the reservoir's primary parameters utilized for reservoir model generation. These parameters are only approximate estimates based on seismic and well test data, as these parameters have high degree of uncertainty associated with them. In addition, the measured output variables (e.g., saturation and pressure) also have noise adding uncertainty to the estimation problem. These uncertainties are responsible for the deviation of the generated reservoir model from the true model. Furthermore, due to production, fluid displacement takes place in the reservoir, and this causes a change in the reservoir parameters over time.

One of the main difficulties in the estimation of the reservoir parameters is the input or the forcing variable is constant, as such there is less excitation in the system. From system identification, it is well known, there is a need for persistent excitation in the system to identify the system parameters (Ljung, 1998). This is also true for the parameter's estimation in a state estimator. Without excitation, the system does not generate sufficient information to estimate the parameters or states accurately. In order to circumvent this problem, Sorooshian and Dracup (1980) suggested

perturbing the input with a small random noise, which can improve the estimation. The noises are stochastic and assumed to be Gaussian with variances as the tuning parameter. After adding the random noise, the perturbed input is given as follows:

Perturbed Input, $u^i{}_t = u_t + \zeta^i{}_t \;\; ; \;\; \zeta^i{}_t \sim N(0, \Sigma_t^u)$ (2-6)

Accordingly, the forecast equation (Eq. 2-1) changes as follows

$x^{i-}{}_{t+1} = f(x^{i+}{}_t, u^i{}_t) + Q^i{}_t$, (2-7)

Like the update equation (Eq. 2-4), observation perturbation generated by adding noise is expressed below:

Perturbed output, $y^i{}_{t+1} = y_{t+1} + \eta^i{}_{t+1}; \;\; \eta^i{}_{t+1} \sim N\left(0, \Sigma_{t+1}^y\right)$ (2-8)

In Eq. (2-6) and Eq. (2-8), the variances $(\Sigma_t^u, \Sigma_{t+1}^y)$ are proportional to the magnitude of input (forcing data) and output (observation data). The variances can be defined as follows:

$\Sigma_t^u = R_u \times u_t$ and $\Sigma_{t+1}^y = R_y \times y_{t+1}$

Where $R_u$and R_y introduce the proportionality factor and they are used as the tuning parameters.

2.2.3 Performance Measure

The tuning parameters R_u and R_y play an important role in generating meaningful ensemble spread and drive the state of the ensemble model to the true state. Based on the procedure outlined by Anderson (2001), the time averaged root mean square error (RMSE) or R_T and the mean RMSE or R_N of the ensemble are calculated by the following relationships:

$$R_T = \frac{1}{T}\sum_{t=1}^{T}\sqrt{\left[\left(\frac{1}{N}\sum_{i=1}^{N}\hat{y}^i{}_t\right) - y^i{}_t\right]^2} \quad (2\text{-}9)$$

$$R_N = \frac{1}{N}\sum_{i=1}^{N}\sqrt{\frac{1}{T}\sum_{t=1}^{T}\left(\hat{y}^i{}_t - y^i{}_t\right)^2} \quad (2\text{-}10)$$

The expected RMSE ratio $(E(R_a))$ is defined as $\sqrt{\frac{N+1}{2N}}$. To calculate this ratio, it is assumed that actual observation is statistically indistinguishable from '*N*' ensemble members. Here, *N* stands for the ensemble size and *T* refers to the total time. The normalized RMSE ratio (NRR) can be

determined as $NRR = \frac{R_T/R_N}{E(R_a)}$. The value of NRR dictates the spread of ensemble and the expected value of NRR is determined by tuning R_u and R_y. The implemented methodology is outlined in **Figure 2-1.**

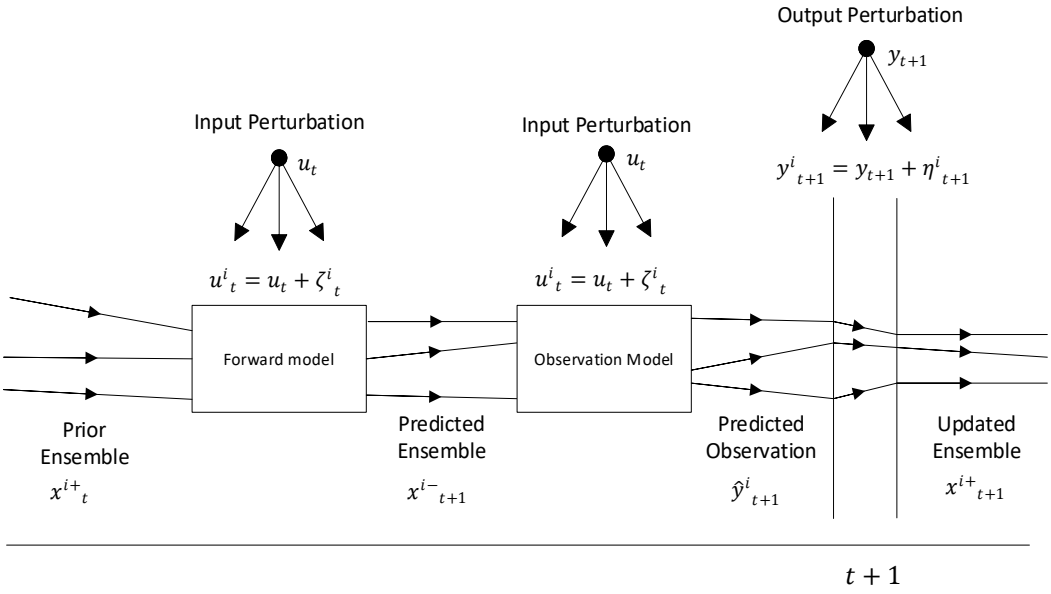

Figure 2-1: Graphical Representation of the Methodology

Model parameters are estimated by matching the simulated observations with the measurement history. For better data assimilation, the tuning parameters are tuned in the range of 2 to 10 standard deviation of the proposed forcing data. The range of the values are taken based on the literature (Moradkhani et al., 2005). In the work, the range of observation tuning parameter is 5%–25% and input tuning parameter is 10%. These variations have been taken with an aim of decreasing trend of RMSE and corresponding stabilized NRR trend. RMSE has been calculated between the ensemble mean and true model.

2.3 Case Study

The proposed method is applied to two different cases: (i) tank series model, and (ii) homogeneous oil reservoir under water flooding. The mathematical formulation of the EnKF with respect to the two models are described in this section.

2.3.1 Tank Series Model

The tank series model is a series of four cylindrical tanks connected by narrow pipelines. A schematic configuration of a tank series model is shown in **Figure 2-2**. Fluid (water) comes through a pipeline with a controlled input flow rate (q_{in}). Each tank is connected by an orifice with a diameter of a. The fluid flows from one tank to another through the pipes. We also assume that the input flow rate (q_{in}) and fluid level (h_4) of Tank-4 are measured at each time-step.

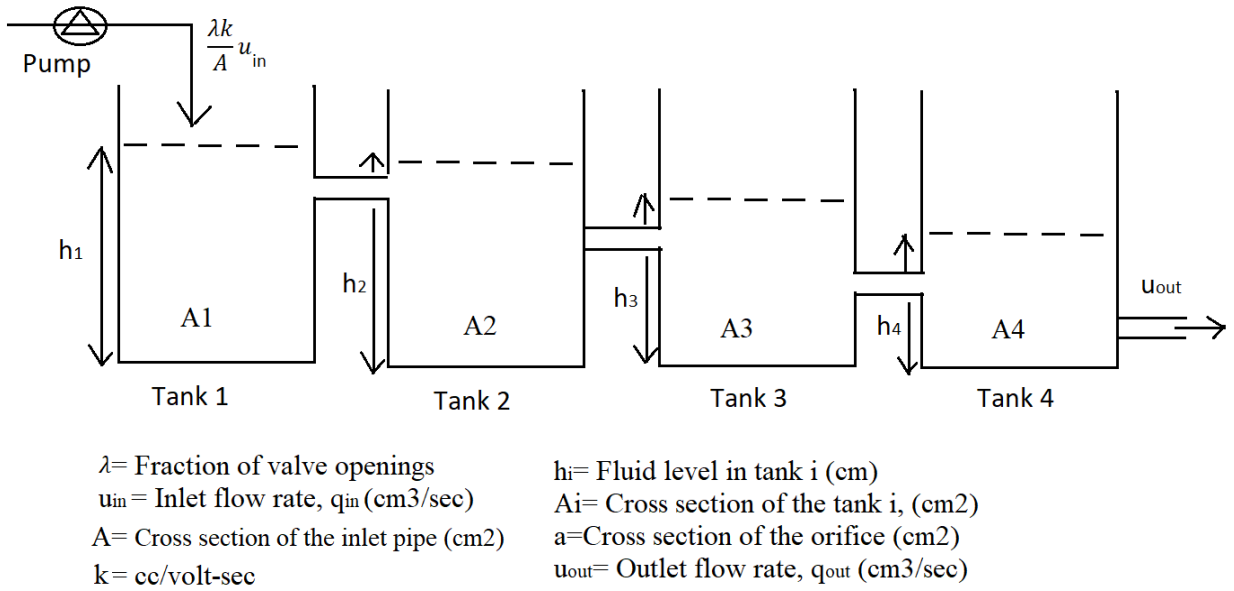

Figure 2-2: Schematic Representation of the Tank Model.

Mathematical formulation: The following dynamic equations are obtained from mass balance for each of the tank:

Tank-1: $\frac{dh_1}{dt} = \frac{\lambda k}{A} u - \frac{a_1}{A}\sqrt{2gh_1}$ (2-11)

Tank-2: $\frac{dh_2}{dt} = \frac{a_1}{A}\sqrt{2gh_1} - \frac{a_2}{A}\sqrt{2gh_2}$ (2-12)

Tank-3: $\frac{dh_3}{dt} = \frac{a_2}{A}\sqrt{2gh_2} - \frac{a_3}{A}\sqrt{2gh_3}$ (2-13)

Tank-4: $\frac{dh_4}{dt} = \frac{a_3}{A}\sqrt{2gh_3} - \frac{a_4}{A}\sqrt{2gh_4}$ (2-14)

In the Eq. from (2-11) to (2-14), the fluid level (h) in each tank is the dynamic state and the nozzle area (a) is considered as the static parameter. A uniform (same) area is assumed for all the nozzles (e.g., $a_1=a_2=a_3=a_4=a$).

State space representation for EnKF application: The tank model is represented by the state space form and subsequently discretized by following finite difference method. The state vector is replaced by the augmented vector that contains the dynamic states (h) and static parameter (a).

The state equation in the matrix form is expressed as follows:

$$x_{t+1}=\begin{bmatrix}h_{1_{t+1}}\\h_{2_{t+1}}\\h_{3_{t+1}}\\h_{4_{t+1}}\\a_{t+1}\end{bmatrix}=\begin{bmatrix}1-T_1 & 0 & 0 & 0 & -S_1\\ T_1 & 1-T_2 & 0 & 0 & S_1-S_2\\ 0 & T_2 & 1-T_3 & 0 & S_2-S_3\\ 0 & 0 & T_3 & 1-T_4 & S_3-S_4\\ 0 & 0 & 0 & 0 & 1\end{bmatrix}*\begin{bmatrix}h_{1_t}\\h_{2_t}\\h_{3_t}\\h_{4_t}\\a_t\end{bmatrix}+\begin{bmatrix}\frac{\lambda k}{A}*\Delta t\\0\\0\\0\\0\end{bmatrix}*[u_t]+Q_t \qquad (2\text{-}15)$$

Here, model error is defined as $Q_t \sim N(0,\Sigma_t^m)$

$$T_1=\frac{\sqrt{g}}{\sqrt{2}A}\frac{a_o}{h_{1o}}\Delta t \quad T_2=\frac{\sqrt{g}}{\sqrt{2}A}\frac{a_o}{h_{1o}}\Delta t \quad T_3=\frac{\sqrt{g}}{\sqrt{2}A}\frac{a_o}{h_{3o}}\Delta t \quad T_4=\frac{\sqrt{g}}{\sqrt{2}A}\frac{a_o}{h_{4o}}\Delta t \quad S_1=\frac{\sqrt{2g}}{A}\sqrt{h_{1o}}\Delta t;$$

$$S_2=\frac{a_o\sqrt{2g}}{A}\left(\sqrt{h_{1o}}-\sqrt{h_{2o}}\right)\Delta t \quad S_3=\frac{a_o\sqrt{2g}}{A}\left(\sqrt{h_{2o}}-\sqrt{h_{3o}}\right)\Delta t \quad S_4=\frac{a_o\sqrt{2g}}{A}\left(\sqrt{h_{3o}}-\sqrt{h_{4o}}\right)\Delta t$$

The output equation defines the relationship between the input vector and the state vector of the system that can be represented by the following expression:

$$y_{t+1}=[\,0\quad 0\quad 0\quad 1\quad 0][x_{t+1}]+R_{t+1} \qquad (2\text{-}16)$$

where measurement error is defined as $R_{t+1} \sim N(0,\Sigma_{t+1}^y)$

Once the model has been expressed in the state space form, implementation of the model is straight forward for this simple system. The implementation of the EnKF is given in details for the reservoir model in the next section.

2.3.2 Reservoir Model

A synthetic 2D homogeneous reservoir model of 10 × 10 × 1 grids with the dimension of 100 ft ×100 ft ×100 ft is generated as shown in **Figure 2-3**. No flow boundary condition is considered for all sides of the reservoir. The reservoir's initial pressure is 1000 psi. There is one water injection well in grid block (5, 1) and one production well in grid block (5,10) in the reservoir. Production

rate is set at 500 ft^3/d with a minimum bottomhole pressure of 500 psi. Injection rate is maintained at 500 ft^3/d with a maximum bottom hole pressure limit of 2000 psi.

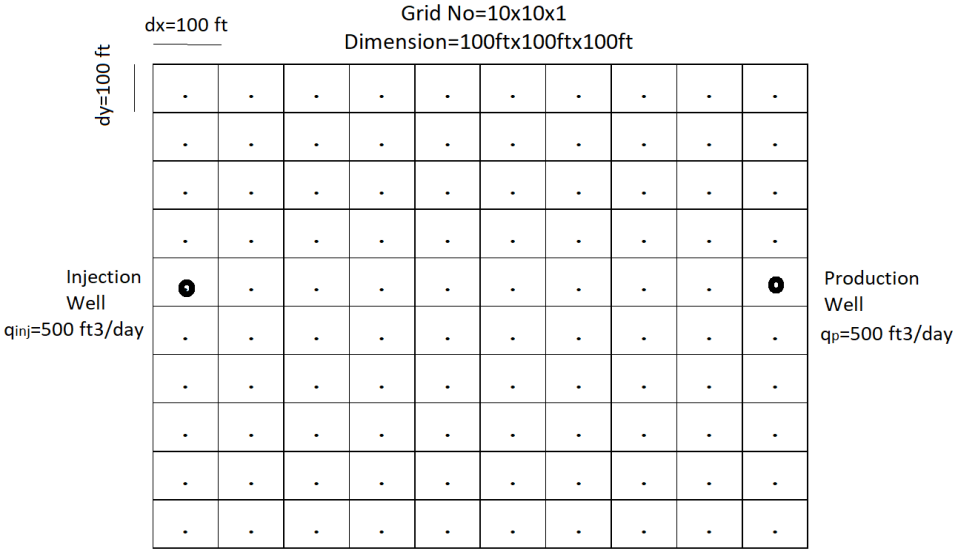

Figure 2-3: Schematic Representation of the 2D Reservoir

Parameterization and mathematical formulation: In this analysis, two static parameters, porosity and permeability are estimated along with the dynamic states (pressure and water saturation). Therefore, the augmented state vector consists of two static vectors (e.g., porosity and permeability), and two dynamic vectors namely water saturation and pressure. The discretized partial differential equation of two phase (oil and water) reservoir is given below:

For water phase:

$$V\left[\emptyset S_w(c_w+c_r)\frac{\partial p}{\partial t}+\emptyset\frac{\partial s_w}{\partial t}\right]_{i,j}-(T_w)_{i-\frac{1}{2},j}p_{i-1,j}-(T_w)_{i,j-\frac{1}{2}}p_{i,j-1}$$
$$+\left[(T_w)_{i-\frac{1}{2},j}+(T_w)_{i,j-\frac{1}{2}}+(T_w)_{i+\frac{1}{2},j}+(T_w)_{i,j+\frac{1}{2}}\right]p_{i,j}-(T_w)_{i+\frac{1}{2},j}p_{i+1,j}-(T_w)_{i,j+\frac{1}{2}}p_{i,j+1}=[q_w]_{i,j}$$
$$=[f_w q_p]_{i,j} \qquad (2\text{-}17)$$

For oil phase:

$$V\left[\emptyset S_o(c_o+c_r)\frac{\partial p}{\partial t}-\emptyset\frac{\partial s_w}{\partial t}\right]_{i,j}-(T_o)_{i-\frac{1}{2},j}p_{i-1,j}-(T_o)_{i,j-\frac{1}{2}}p_{i,j-1}$$
$$+\left[(T_o)_{i-\frac{1}{2},j}+(T_o)_{i,j-\frac{1}{2}}+(T_o)_{i+\frac{1}{2},j}+(T_o)_{i,j+\frac{1}{2}}\right]p_{i,j}-(T_o)_{i+\frac{1}{2},j}p_{i+1,j}-(T_o)_{i,j+\frac{1}{2}}p_{i,j+1}=[q_o]_{i,j}$$
$$=[f_o q_p]_{i,j} \qquad (2\text{-}18)$$

Where $T_{i-1/2,j}=\frac{\Delta x}{\Delta y}\frac{h}{\mu}k_{i-1/2,j}$; $T_{i,j-1/2}=\frac{\Delta y}{\Delta x}\frac{h}{\mu}k_{i,j-1/2}$; $S_w+S_o=1$; $f_w=\frac{k_{rw}}{k_{rw}+k_{ro}\frac{\mu_w}{\mu_o}}=1-f_o$

The state- space formulation is presented below:

$$\begin{bmatrix} \begin{bmatrix} V_{wp} & V_{ws} \\ V_{op} & V_{os} \end{bmatrix} & \begin{bmatrix} 0 & 0 \\ 0 & 0 \end{bmatrix} \\ \begin{bmatrix} 0 & 0 \\ 0 & 0 \end{bmatrix} & \begin{bmatrix} 1 & 0 \\ 0 & 1 \end{bmatrix} \end{bmatrix} \times \begin{bmatrix} \frac{dp}{dt} \\ \frac{dS_w}{dt} \\ \frac{dk}{dt} \\ \frac{d\emptyset}{dt} \end{bmatrix} + \begin{bmatrix} \begin{bmatrix} T_w & 0 \\ T_o & 0 \end{bmatrix} & \begin{bmatrix} 0 & 0 \\ 0 & 0 \end{bmatrix} \\ \begin{bmatrix} 0 & 0 \\ 0 & 0 \end{bmatrix} & \begin{bmatrix} 0 & 0 \\ 0 & 0 \end{bmatrix} \end{bmatrix} \times \begin{bmatrix} p \\ \frac{S_w}{k} \\ \emptyset \end{bmatrix} = \begin{bmatrix} q_w \\ \frac{q_o}{0} \\ 0 \end{bmatrix} + \begin{bmatrix} F_w \\ \frac{F_o}{0} \\ 0 \end{bmatrix} [q_p] \quad (2\text{-}19)$$

Here,

$p = [p_{i,j-1} \quad \dots \quad p_{i-1,j} \quad p_{i,j} \quad p_{i+1,j} \quad \cdots \quad p_{i,j+1}]$; $\mathrm{S_w} = \left[\mathrm{S_{w_{i,j-1}}} \quad \dots \quad \mathrm{S_{w_{i-1,j}}} \quad \mathrm{S_{w_{i,j}}} \quad \mathrm{S_{w_{i+1,j}}} \quad \dots \quad \mathrm{S_{w_{i,j+1}}}\right]$

$k = [k_{i,j-1} \quad \dots\dots \quad k_{i-1,j} \quad k_{i,j} \quad k_{i+1,j} \quad \dots\dots \quad k_{i,j+1}]$; $\emptyset = [\emptyset_{i,j-1} \quad \dots\dots \quad \emptyset_{i-1,j} \quad \emptyset_{i,j} \quad \emptyset_{i+1,j} \quad \dots\dots \quad \emptyset_{i,j+1}]$

$V_{wp} = V(c_w + c_r)[0 \quad \dots \quad \emptyset_{i,j} \times (S_w)_{i,j} \quad 0 \quad \dots \quad 0]$; $V_{op} = V(c_o + c_r)[0 \quad \dots \quad \emptyset_{i,j} \times (1 - S_w)_{i,j} \quad 0 \quad \dots \quad 0]$

$V_{ws} = V[0 \quad \dots \quad \emptyset_{i,j} \quad 0 \quad \dots \quad 0]$; $V_{os} = -V[0 \quad \dots \quad \emptyset_{i,j} \quad 0 \quad \dots \quad 0]$; $\quad V = \Delta x \times \Delta y \times h$

$T_w = \left[-(T_w)_{i,j-\frac{1}{2}} \quad \dots \quad -(T_w)_{i-\frac{1}{2},j} \quad \left((T_w)_{i,j-\frac{1}{2}} + (T_w)_{i-\frac{1}{2},j} + (T_w)_{i+\frac{1}{2},j} + (T_w)_{i,j+\frac{1}{2}}\right) \quad -(T_w)_{i+\frac{1}{2},j} \quad \dots \quad -(T_w)_{i,j+\frac{1}{2}}\right]$

$T_o = \left[-(T_o)_{i,j-\frac{1}{2}} \quad \dots \quad -(T_o)_{i-\frac{1}{2},j} \quad \left((T_o)_{i,j-\frac{1}{2}} + (T_o)_{i-\frac{1}{2},j} + (T_o)_{i+\frac{1}{2},j} + (T_o)_{i,j+\frac{1}{2}}\right) \quad -(T_o)_{i+\frac{1}{2},j} \quad \dots \quad -(T_o)_{i,j+\frac{1}{2}}\right]$

$q_w = [\dots \quad (q_w)_{i,j} \quad \dots]$, $\quad F_w = [\dots \quad (f_w)_{i,j} \quad \dots]$, $\quad q_o = [\dots \quad (q_o)_{i,j} \quad \dots]$, $\quad F_o = [\dots \quad (f_o)_{i,j} \quad \dots]$

After simplification, Eq. (2-19) can be rewritten as follows:

$$\begin{bmatrix} p \\ \frac{S_w}{k} \\ \emptyset \end{bmatrix}_{t+1} = A_t \begin{bmatrix} p \\ \frac{S_w}{k} \\ \emptyset \end{bmatrix}_t + B_t \begin{bmatrix} q_{inj_t} \\ -q_{p_t} \end{bmatrix} + Q_t \; ; \quad Q_t \sim N(0, \Sigma_t^m) \quad (2\text{-}20)$$

In Eq. (2-20), $\mathrm{q_{inj}}$ and $\mathrm{q_p}$ are the two input parameters.

The injection flow rate of injection well (5,1) is related to the reservoir and fluid properties and process condition as follows:

$$q_{inj_t} = \left(\frac{2 \times \pi \times k \times h \times 6.33 \times 10^{-3}}{B_w \left[log \frac{r_e}{r_w} + S \right]} \left[\frac{k_{ro}}{\mu_o} + \frac{k_{rw}}{\mu_w} \right] \right)_t \left[p_{inj_{t+1}} - p_{5,1_{t+1}} \right] = J_{inj_t} \left[p_{inj_{t+1}} - p_{5,1_{t+1}} \right] \quad (2\text{-}21)$$

$$p_{inj}{}_{t+1} = \left(J_{inj}{}_{t}\right)^{-1} q_{inj}{}_{t} + p_{5,1}{}_{t+1;} \quad where\, J_{inj}{}_{t} = \left(\frac{2\times\pi\times k\times h\times 6.33\times 10^{-3}}{B_w\left[log\frac{r_e}{r_w}+S\right]}\left[\frac{k_{ro}}{\mu_o}+\frac{k_{rw}}{\mu_w}\right]\right)_t ;$$

The corresponding equation for production well (5,10) to show the flow rate in terms of other parameters (e.g., fluid and reservoir characteristics) is given below:

$$q_{p_t} = \left(\frac{2\times\pi\times k\times h\times 6.33\times 10^{-3}}{\left[log\frac{r_e}{r_w}+S\right]}\left[\frac{k_{ro}}{B_o\,\mu_o}+\frac{k_{rw}}{B_w\,\mu_w}\right]\right)_t \left[p_{5,10}{}_{t+1} - p_{prod}{}_{t+1}\right] = J_{p_t}\left[p_{5,10}{}_{t+1} - p_{prod}{}_{t+1}\right] \quad (2\text{-}22)$$

$$p_{prod}{}_{t+1} = p_{5,10}{}_{t+1} - \left(J_{p_t}\right)^{-1} q_{p_t}; where\, J_{p_t} = \left(\frac{2\times\pi\times k\times h\times 6.33\times 10^{-3}}{\left[log\frac{r_e}{r_w}+S\right]}\left[\frac{k_{ro}}{B_o\,\mu_o}+\frac{k_{rw}}{B_w\,\mu_w}\right]\right)_t ;$$

The state-space form of the well's flow rate equation can be rewritten as follows:

$$\begin{bmatrix} P_{inj} \\ P_{prod} \end{bmatrix}_{t+1} = \left[\begin{bmatrix} 1 & 0 \\ 0 & 1 \end{bmatrix} \begin{bmatrix} 0 & 0 \\ 0 & 0 \end{bmatrix}\right] \begin{bmatrix} p \\ \frac{S_w}{k} \\ \emptyset \end{bmatrix}_{t+1} + \begin{bmatrix} \left(J_{inj}{}_{t}\right)^{-1} & 0 \\ 0 & \left(J_{p_t}\right)^{-1} \end{bmatrix} \begin{bmatrix} q_{inj} \\ -q_p \end{bmatrix}_t + R_{t+1}, \quad R_{t+1} \sim N(0, \Sigma_{t+1}^{y}) \qquad (2\text{-}23)$$

Steps of EnKF for the Reservoir Model:

1. Forecast of the states through forward model

$$\begin{bmatrix} p \\ \frac{S_w}{k} \\ \emptyset \end{bmatrix}_{t+1}^{i-} = A_t \begin{bmatrix} p \\ \frac{S_w}{k} \\ \emptyset \end{bmatrix}_t^{i+} + B_t \begin{bmatrix} q_{inj} \\ -q_p \end{bmatrix}_t^{i} + {Q_t}^{i}; \quad {Q_t}^{i} \sim N(0, \Sigma_t^{m}) \qquad (2\text{-}24)$$

Forcing data perturbation, $\begin{bmatrix} q_{inj} \\ -q_p \end{bmatrix}_t^{i} = \begin{bmatrix} q_{inj} \\ -q_p \end{bmatrix}_t + {\zeta^t}_i \;\; ; \;\; {\zeta^t}_i \sim N(0, \Sigma_t^{u}) \qquad (2\text{-}25)$

Ensemble mean of the state variables, $\begin{bmatrix} \overline{p} \\ \frac{S_w}{k} \\ \emptyset \end{bmatrix}_{t+1} = \frac{1}{N}\sum_{i=1}^{N} \begin{bmatrix} p \\ \frac{S_w}{k} \\ \emptyset \end{bmatrix}_{t+1}^{i-} \qquad (2\text{-}26$

2. Prediction of the measurement

$$\begin{bmatrix} \overline{P}_{inj} \\ P_{prod} \end{bmatrix}_{t+1} = \left[\begin{bmatrix} 1 & 0 \\ 0 & 1 \end{bmatrix} \begin{bmatrix} 0 & 0 \\ 0 & 0 \end{bmatrix}\right] \begin{bmatrix} p \\ \frac{S_w}{k} \\ \emptyset \end{bmatrix}_{t+1}^{i-} + \begin{bmatrix} \left(J_{inj}{}_{t}\right)^{-1} & 0 \\ 0 & \left(J_{p_t}\right)^{-1} \end{bmatrix} \begin{bmatrix} q_{inj} \\ -q_p \end{bmatrix}_t^{i} \qquad (2\text{-}27)$$

Ensemble mean of prediction, $\begin{bmatrix} \overline{P}_{inj} \\ P_{prod} \end{bmatrix}_{t+1} = \frac{1}{N}\sum_{i=1}^{N} \begin{bmatrix} \hat{P}_{inj} \\ P_{prod} \end{bmatrix}_{t+1}^{i} \qquad (2\text{-}28)$

Here, Σ_{t+1}^{yy} , Σ_{t+1}^{xy} are the forecast error covariance matrix of the prediction and cross covariance of the state variables and prediction. They are defined as follows:

$$\Sigma_{t+1}^{yy} = \left(\begin{bmatrix} \hat{P}_{inj} \\ P_{prod} \end{bmatrix}^{i}_{t+1} - \begin{bmatrix} \overline{P}_{inj} \\ P_{prod} \end{bmatrix}_{t+1} \right) \left(\begin{bmatrix} \hat{P}_{inj} \\ P_{prod} \end{bmatrix}^{i}_{t+1} - \begin{bmatrix} \overline{P}_{inj} \\ P_{prod} \end{bmatrix}_{t+1} \right)^{T} \tag{2-29}$$

$$\sum_{t+1}^{xy} = \left(\begin{bmatrix} \hat{P}_{inj} \\ P_{prod} \end{bmatrix}^{i}_{t+1} - \begin{bmatrix} \overline{P}_{inj} \\ P_{prod} \end{bmatrix}_{t+1} \right) \left(\begin{bmatrix} p \\ \frac{S_w}{k} \\ \emptyset \end{bmatrix}^{i-}_{t+1} - \begin{bmatrix} \overline{p} \\ \frac{S_w}{k} \\ \emptyset \end{bmatrix}_{t+1} \right)^{T} \tag{2-30}$$

Perturbed production data, $\begin{bmatrix} P_{inj} \\ P_{prod} \end{bmatrix}^{i}_{t+1} = \begin{bmatrix} P_{inj} \\ P_{prod} \end{bmatrix}_{t+1} + \eta^{i}{}_{t+1};\ \eta^{i}{}_{t+1} \sim N\left(0, \Sigma_{t+1}^{y}\right)$ (2-31)

Kalman gain calculation, $K_{t+1} = \sum_{t+1}^{xy} \left[\sum_{t+1}^{yy} + R_{t+1} \right]^{-1}, R_{t+1} \sim N\left(0, \Sigma_{t+1}^{y}\right)$ (2-32)

The state is updated as follows:

$$\begin{bmatrix} p \\ \frac{S_w}{k} \\ \emptyset \end{bmatrix}^{i+}_{t+1} = \begin{bmatrix} p \\ \frac{S_w}{k} \\ \emptyset \end{bmatrix}^{i-}_{t+1} + K_{t+1} \left(\begin{bmatrix} P_{inj} \\ P_{prod} \end{bmatrix}^{i}_{t+1} - \begin{bmatrix} \hat{P}_{inj} \\ P_{prod} \end{bmatrix}^{i}_{t+1} \right) \tag{2-33}$$

Observability test: Global observability establishment for linear systems is well defined. Applying the same method to the nonlinear case does not satisfy the observability criteria for estimating parameters, especially for large scale nonlinear systems such as reservoir. Considering this challenge, based on the theorem of local observability, the following approach/steps can guarantee the identifiability of the parameters:

- Spanning initial ensemble in a smaller space that is more likely to lie within the locally observable region (between the injection and production wells).
- Adding more measurements which means adding more wells in the reservoir.
- Excitation of the input system so that the input can make more states distinguishable.

2.4 Methodology

The flowchart using EnKF with forcing data perturbation is presented in **Figure 2-4**. This section illustrates the combined state estimation of the dynamic system where both parameter (permeability and porosity) vectors are augmented with state (pressure and saturation) into a single state vector. In this flowchart, the input variables and corresponding equations are specific to the reservoir model.

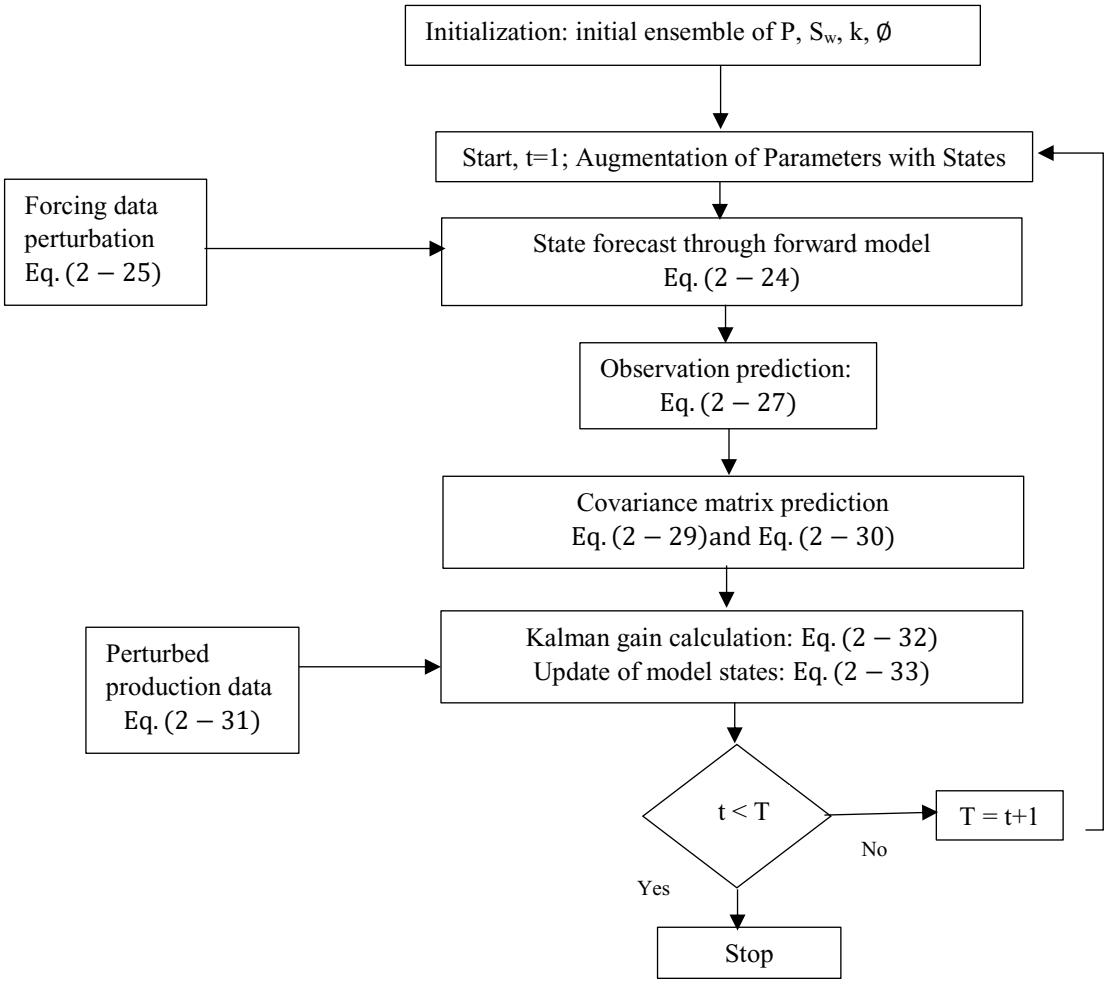

Figure 2-4: State-Parameter Estimation Flowchart Using Ensemble Kalman Filter

2.5 Results and Discussion

This section presents the results from the two case studies. The ensemble Kalman filter (EnKF) was tested for mismatch between the model and the system. The mismatch was characterized as random Gaussian noise. Accordingly, the effect of the proposed tuning strategy was tested on the parameter and state estimation.

2.5.1 Tank Series Model

The tank series model is described in **Section 2.3.1**. The required data for the analysis/investigation conducted in this study are listed in **Table 2-1**. The simulation was run for 1000-time steps.

Table 2-1: Characteristics and Data for Tank Model

Parameter Name	**Tank-1**	**Tank-2**	**Tank-3**	**Tank-4**
Fluid level, h (cm)	25	20	10	10
Tank area, A (cm^2)	25	20	25	20
Orifice diameter, a (cm^2)	0.07	0.07	0.07	0.07
Gravity acceleration, g (cm/sec^2)	981			
Opening of the valve at the input (λ)	0.7			
Base value for orifice area, a_{io} (cm^2)	0.07			
Fluid density (gm/cm^3)	1			
Fluid viscosity (cp)	1			

2.5.1.1 History Matching and State Estimation

Random model error with standard deviation of 0.1 and random measurement error with standard deviation of 0.03 were added to simulate the system model mismatch. For this case, the ensembles size was 30.

We assumed that only tank 4 level is the measured state, all other tank levels are unmeasured states. **Figure 2-5** (a to d) compares the estimated states with the actual tank levels. As expected, the estimated level and the measured level of tank 4 show the best match as it was the measured signal. Levels of Tank 1, Tank 2, and Tank 3 are purely estimates, as such it is noticed that spread in the ensemble estimates is greater compared to Tank 1. However, the average of the ensembles (dark blue line) is closer to the actual states (red line). The initial mismatch (the first 200 sec of

the simulation) between the estimate and actual value shows some discrepancy. This is because of the burn-in period of the EnKF and a common phenomenon for any recursive filter.

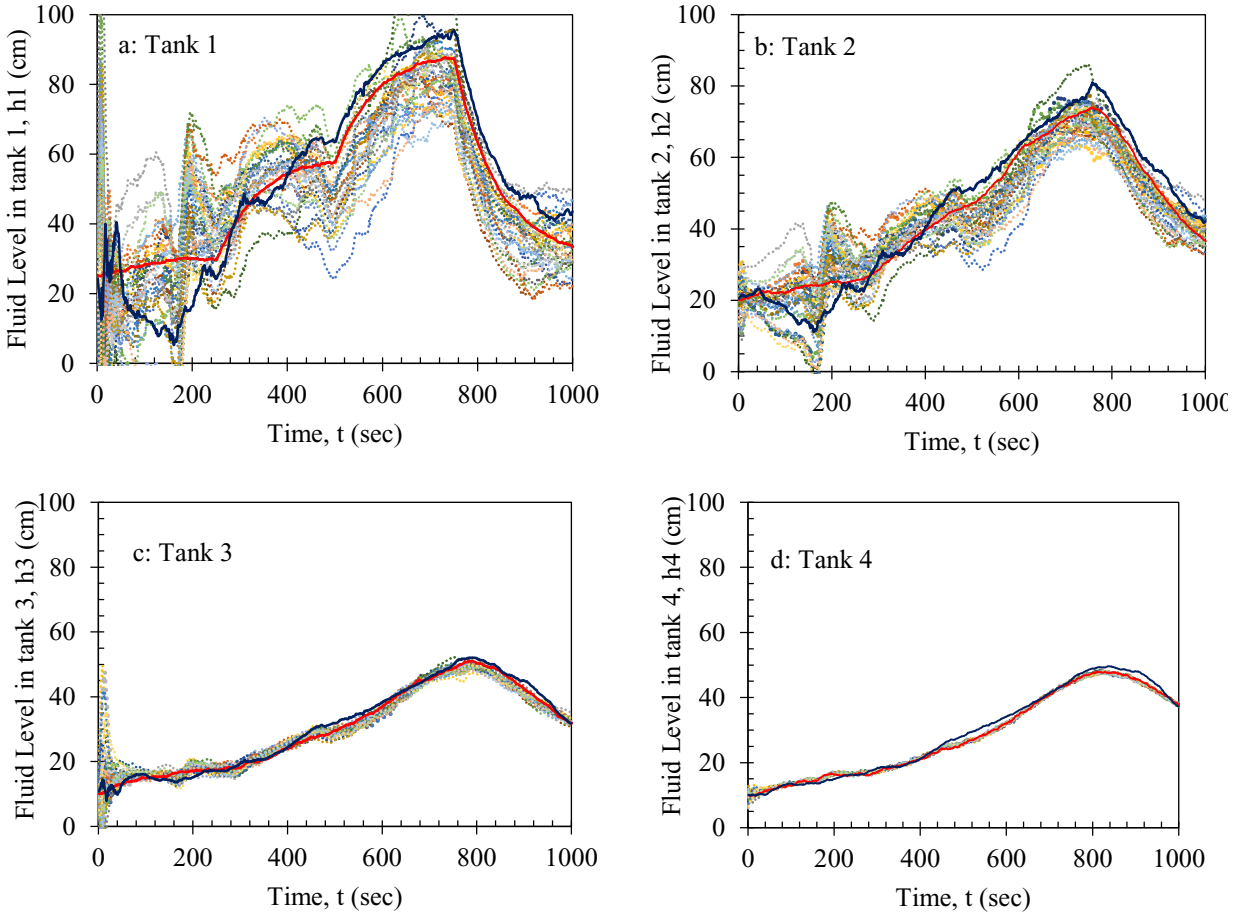

Figure 2-5: History Matching for Tank 1, 2, 3 and 4

Figure 2-6 presents the estimation performance of parameter (orifice area, *a*) using the EnKF method. Figure 2-6 shows the difference between the estimated parameter and the actual parameter (i.e., $\hat{a}_i = a_i - a_{io}$). After a short burn-in period of less than 100s, the parameter is converged to the true value.

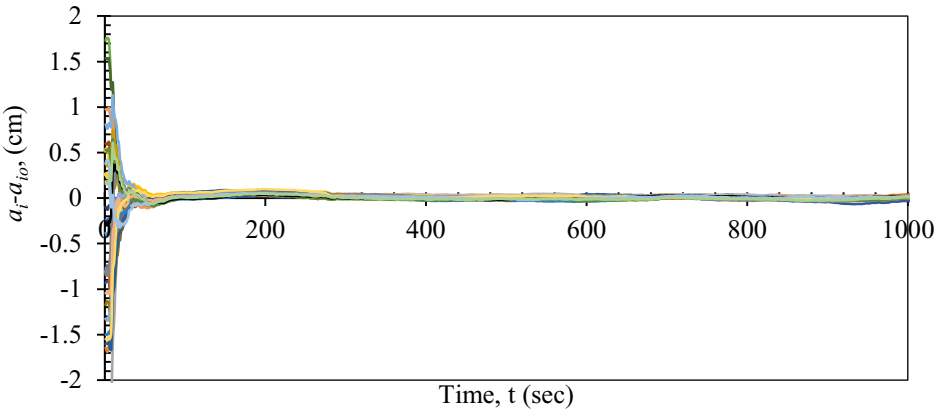

Figure 2-6: Estimation of Parameter, Orifice Area (a).

2.5.1.2 Effect of Tuning on Parameter Estimation

The focus of this study is to improve the estimation performance using perturbation in the input or forcing variables. We created different scenarios to demonstrate the impact of tuning on the state and parameter estimation. NRR values were calculated for the different tuning scenarios to guide with the selection of tuning parameters.

Effect of tuning parameter (R_u) on history matching is demonstrated in **Figure 2-7** for two values of R_y, one for low measurement noise and the other for high measurement noise (e.g., 0.01 and 0.2). In each case, R_u is tuned for each ensemble number to check the effect of tuning (parameter) on the ensemble size.

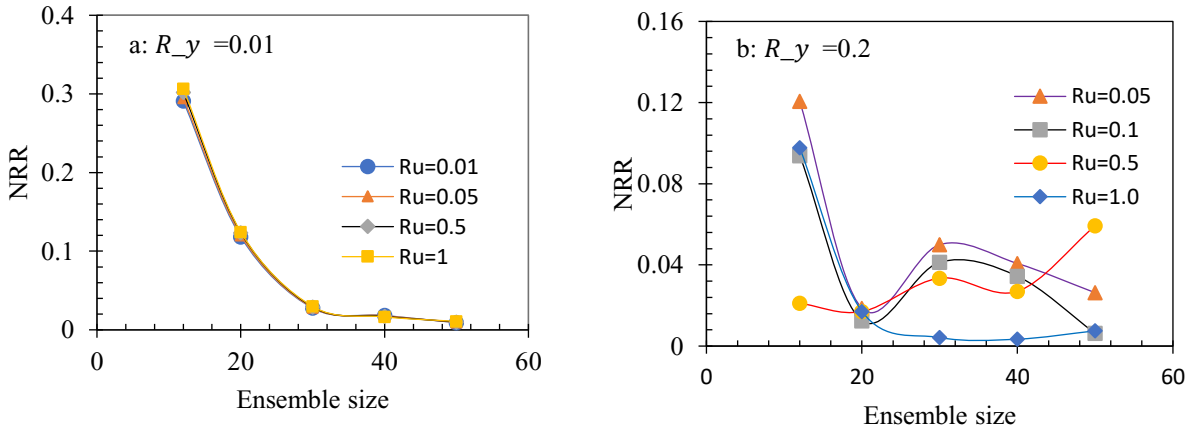

Figure 2-7: Impact of the Tuning Parameter (R_y) on History Matching and Ensemble Size; a) Low Value of R_y, and b) High Value of R_y.

According to **Figure 2-7a**, for the low value of $R_y = 0.01$, almost the same NRR was found for all R_u and for all ensemble size. Hence, variation of R_u does not have an impact on the stability. Steady value of NRR between 30 and 50 ensemble size indicates that ensemble size in this range will provide the stable result. However, when R_y is increased to 0.2, impact of R_u on the history matching can be noticed clearly in **Figure 2-7b**. Variation of R_u affects the relationship between the NRR and number of ensembles. **Figure 2-7b** demonstrates that $R_u = 1$ provides a steady NRR behaviour and contributes to a better history matching.

Figure 2-8 shows the estimation of the states and parameter for low noise case (R_y=*0.01*) where no perturbation in the input parameter was introduced. It is found that with a large enough ensemble size (~50 ensembles) without perturbation, better estimation can be attained.

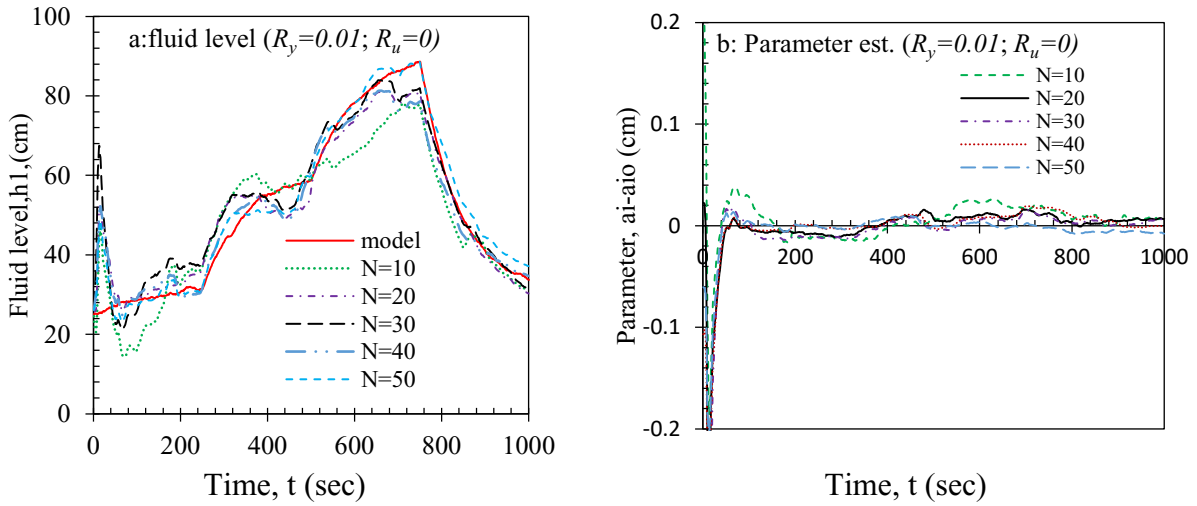

Figure 2-8: Impact of Ensemble Size on the State (panel a) and Parameter Estimation (panel b).

Effect of R_u tuning parameter on fluid level and parameter estimation is presented in **Figure 2-9** for the high value of R_y =0.2. To show the effect of tuning of $R_u$on history matching, ensemble size 10 is chosen. From **Figure 2-9a**, at $R_u = 10$, the difference between model and filter is very low. From **Figure 2-9b**, the convergence is steady throughout the run time. The error analysis corresponding to fluid level and parameter estimation is shown quantitatively in **Figure 2-10**.

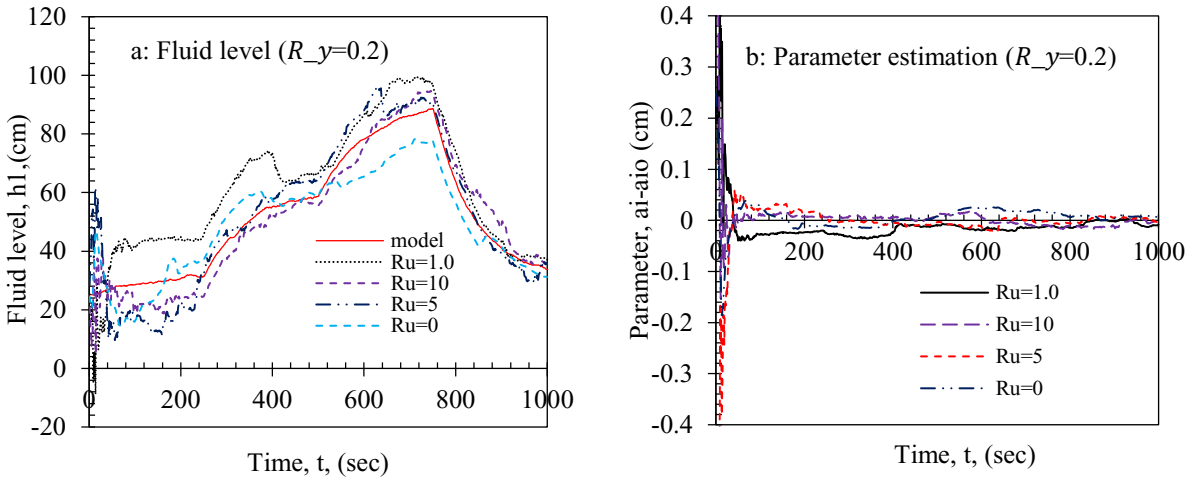

Figure 2-9: Impact of *R_u* and *R_y* on History Matching for Tank 1

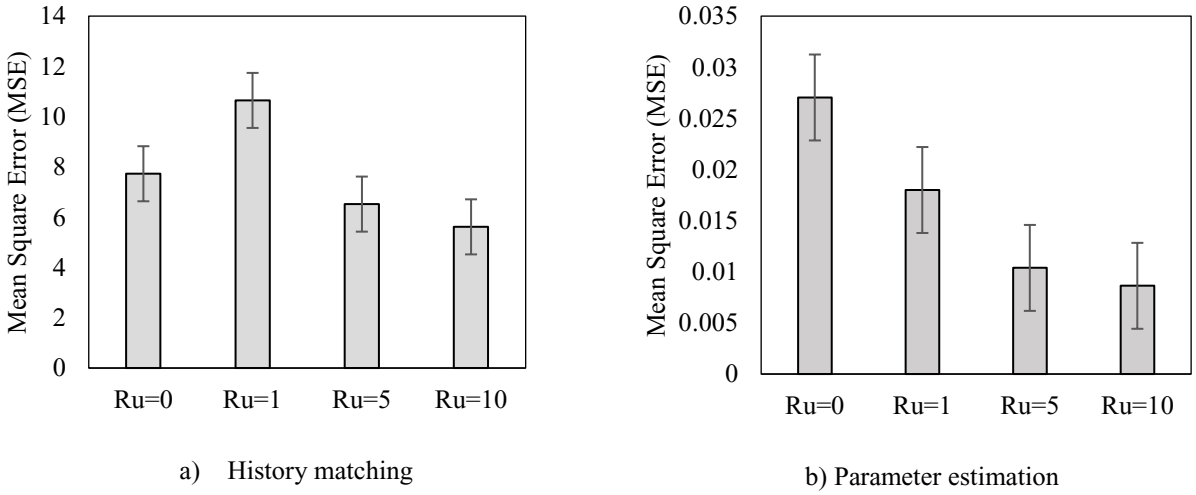

Figure 2-10: Error Analysis for the Tank Case (Tank 1).

In **Figure 2-10a**, R_u=0 indicates the case without tuning and the corresponding MSE is 7.72; the magnitude of MSE for R_u=10 is about 5.5. This error analysis reveals that tuning of R_u has a positive impact on history matching.

2.5.2 Reservoir Model Case

In this study, the oil reservoir under water flooding operation is analyzed. The reservoir is assumed to be homogeneous in terms of rock and fluid properties (as shown in **Figure 2-3**). The wells are constrained by constant production and injection rates. Hence, the adjusted parameters are the bottomhole pressure of injection and production wells. The data are recorded each day from the starting day of production.

The mean values of porosity and permeability are 0.2 and 100 mD with a standard deviation of 0.03 and 10.0, respectively, for all grid blocks. The permeability values in x and y directions are assumed to be uniform and equal. For relative permeability calculation, Corey's model is followed with an exponent of 3. Other assumptions include only two incompressible fluids (water and oil) are present, constant compressibility, no gravity effect, and negligible capillary pressure. **Table 2-2** lists the required data for the reservoir.

Table 2-2: Reservoir Fluid and Rock Properties (Zafari, 2005)

Parameter name	**Value**	**Parameter name**	**Value**
Initial water saturation, (%)	0.2	Water formation volume factor	1
Residual oil saturation, (%)	0.2	Oil formation volume factor	1.05
Rock compressibility, (psi^{-1})	4×10^{-6}	Water viscosity, (cp)	1
Water compressibility, (psi^{-1})	1×10^{-5}	Oil viscosity, (cp)	1.1
Oil compressibility, (psi^{-1})	1×10^{-5}	Reservoir Temperature, (^{o}F)	100

2.5.2.1 History Matching and State Estimation

For this part, the filter is run for 1000 days from the first day of the production. For analyzing the physical phenomena happened in this reservoir, 1000 days of production time is enough. The total number of ensembles is 50. A random model error is added with standard deviation for pressure 0.03 and water saturation 0.001. In addition, random measurement error is included with standard deviation of 0.03.

The outcomes of the EnKF for the two wells are depicted in **Figure 2-11**. The small difference between the model and filter shows good matching. The pressure declining trend as in **Figure 2-11a** and the pressure rising trend as in **Figure 2-11b** reveal that water break through did not

happen until day1000. In the history matching section, all the red color lines represent the trend obtained from the model and other lines are the estimates for different ensemble size. The estimates are averages of the realizations due to the ensembles.

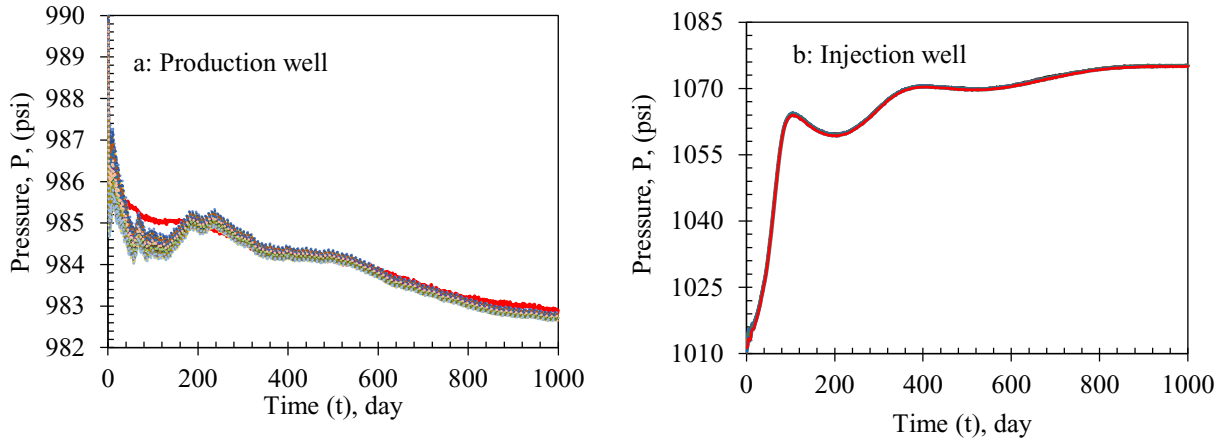

Figure 2-11: Bottomhole Pressure at the Production and Injection Well.

For simplification, a grid block between the injection well and production well (5, 5) is selected as the representative grid block to show the estimated result. **Figure 2-12** (a & b) presents the estimated dynamic states (P and S_w) for the corresponding grid block after 1000-time steps of simulation.

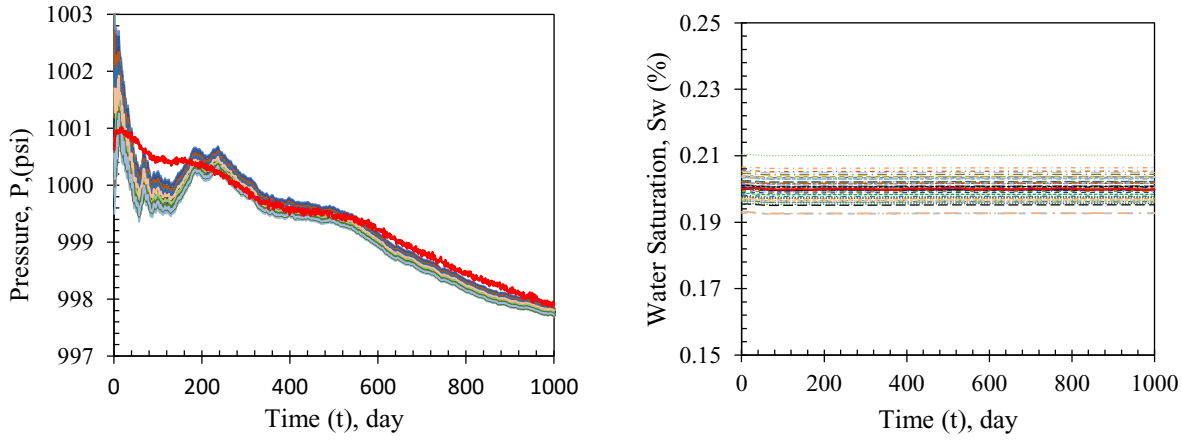

a) Bottomhole pressure at grid (5, 5). **b)** Water saturation at grid (5, 5).

Figure 2-12: Bottomhole Pressure and Water Saturation at Grid Block (5,5).

After the history matching, static parameters (e.g., k and ϕ) are estimated for each block. Here, only for grid block (5, 5) is shown in **Figure 2-13**.

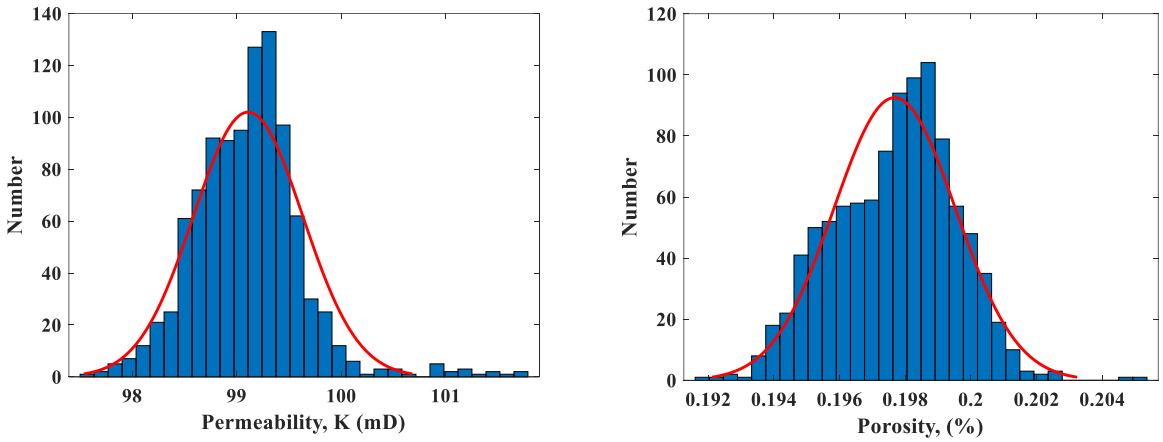

c)Permeability estimation d)Porosity estimation

Figure 2-13: State and Parameter Estimation after 1000-Time Steps of Simulation.

In **Figure 2-13**, the mean value represents the estimated value of the parameters. The estimated values seem close to the real values after 1000-time steps of production.

2.5.2.2 Effect of Tuning on Parameter Estimation

Like tank series model, three different scenarios were generated to show the impact of tuning on the state and parameter estimation. Corresponding NRR values were also calculated for the different tuning scenarios for selection of tuning parameters. In this section, the scenarios are discussed with a focus on the cell (5, 5).

Figure 2-14 represents the effect of R_u tuning for different values of R_y. For low measurement noise $R_y = 0.01$ and for high measurement noise $R_y = 0.2$ were selected. In each case, $R_u$is tuned for each ensemble size to check the effect of tuning parameter on the ensemble size. Figure 2 14a reveals that when uncertainty in the observed data is low (R_y=0.01), the NRR remains steady, and it is almost the same for all R_u and all ensemble sizes. Therefore, the change of R_u does not have a significant influence on stability. Steady value of NRR between 20 and 50 ensemble size indicates that ensemble size in this range will provide the stable result.

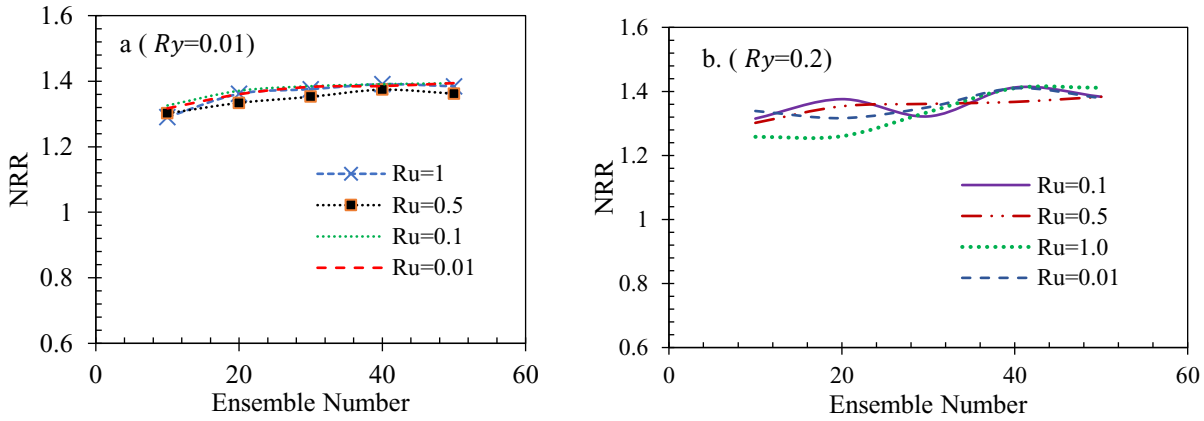

Figure 2-14: Impact of the Tuning Parameter (R_y) on History Matching and Ensemble Size; a) Low Value of R_y, and b) High Value of R_y.

However, when the value of R_y is increased to 0.2, impact of R_u on the history matching can be noticed clearly in **Figure 2-14b**. It shows that $R_u = 0.5$ provides stable value of NRR and contributes to better history matching.

Figure 2-15 shows the pressure profile of cell (5, 5) for different ensemble sizes for low noise case (R_y=*0.01*) where no perturbation in the input parameter was introduced. From **Figure 2-15**, it is concluded that ensemble size of 40 and 50 show better pressure matching with the model.

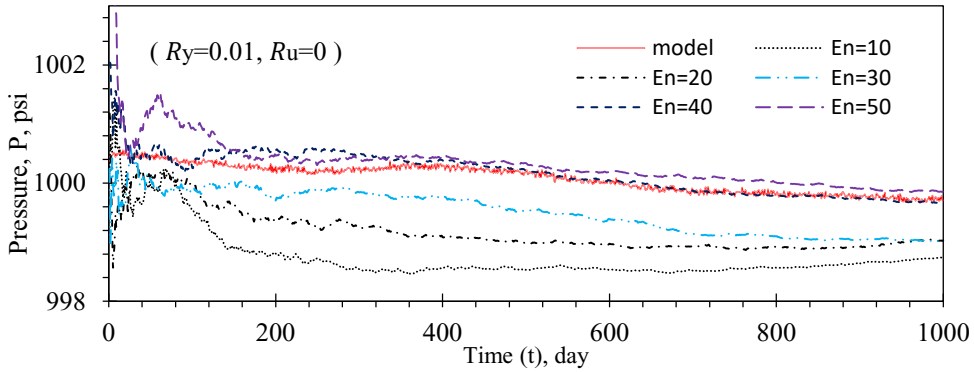

Figure 2-15: Pressure Profile of the Cell (5,5) for Various Ensemble Sizes.

Impact of $R_u$tuning parameter on pressure estimation for the cell (5,5) is presented in **Figure 2-16** for high value of $R_y = 0.2$. To show the effect of $R_u$tuning on pressure matching, an ensemble size of 20 is chosen.

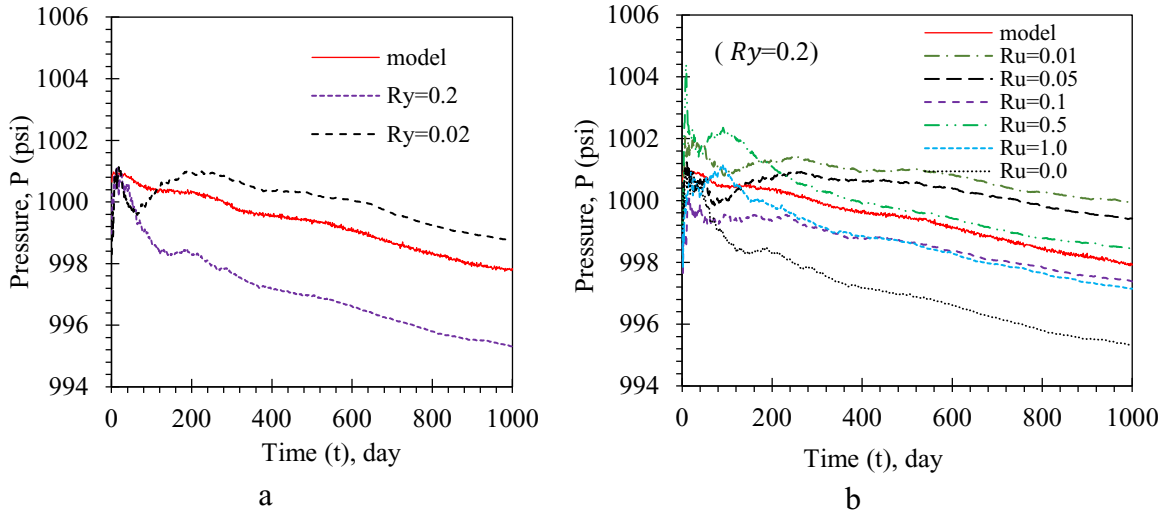

Figure 2-16: Influence of High Value of R_y and the Corresponding Ensemble Size on Pressure.

Figure 2-16a represents the pressure profile for three different cases. It is found that for low value of R_y, deviation from the model is less compared to high value of R_y. **Figure 2-16b** displays the impact of tuning of R_u for high value of R_y and shows that $R_u = 0.5$ provides better estimation. Corresponding error analysis based on these results is presented in **Figure 2-17**.

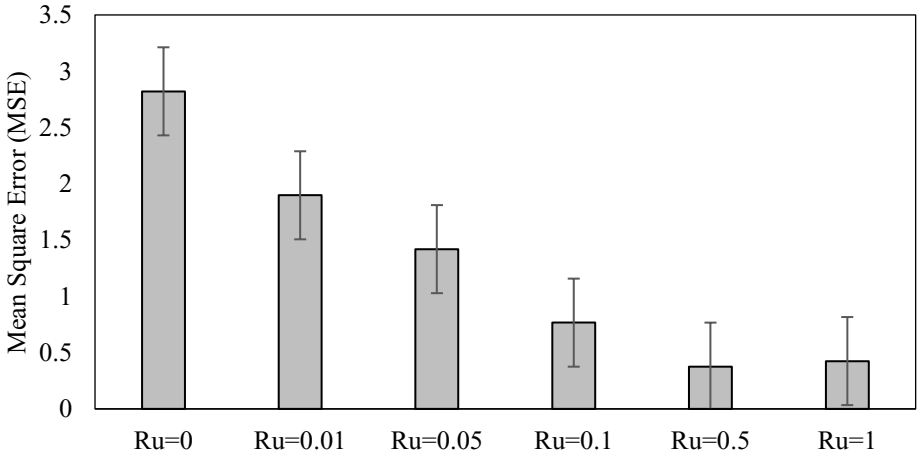

Figure 2-17: Error Analysis in History Matching for Reservoir Case.

In **Figure 2-17**, for no tuning case where R_u=0, the magnitude of MSE is 2.82, while for $R_u = 0.5$ the numerical value of MSE is about 0.53. This decrease in the MSE represents a significant improvement in the history matching and tuning of R_u has a positive impact on history matching.

2.6 Conclusions

In this study we focused on the effect of model error and measurement noise on history matching of reservoir states and parameters. Subsequently, we proposed tuning methods to improve the performance of EnKF in the presence of model error. For the reservoir, two static parameters (porosity and permeability) were estimated adaptively, together with other dynamic states (i.e., pressures at the internal nodes). In addition to the reservoir system, an equivalent benchmark tank series system was developed. The tank system was used to develop the initial understanding of the tuning of EnKF in the presence of model error.

Forcing data perturbation was considered as a tuning parameter. This research shows the effect of forcing data tuning on history matching along with ensemble size. It is found that the tuning factor has an influence on history matching. During history matching, around 13.6 % and 9% improvement is noticed for the four-tank and the reservoir cases respectively for the low ensemble size when the uncertainty in the model and measurement are high.

Comparing between the estimation problem in tank and reservoir case, it can be concluded that as the number of states and unknown parameters increases, the ensemble size needs to be increased significantly to get better performance in history matching.

For the reservoir case study, assumptions such as no capillary pressure, incompressible fluid, isotropic permeability, and no gravity forces were considered to reduce the nonlinearity. This study can be extended to more realistic cases such as heterogeneous and fractured reservoirs and/or reservoirs under different production strategies.

Acknowledgements

The financial support of the Memorial University, Equinor Canada, Innovate NL, and the Natural Sciences and Engineering Research Council of Canada (NSERC) is acknowledged.

Nomenclatures

Symbols: Tank Model

A	Tank area in cm^2
h	Fluid level in the tank in cm
u	Fluid velocity cm/sec
μ	Viscosity of the fluid in cp
a	Orifice dia in cm
g	Acceleration of gravity, cm/sec^2

Symbols: Reservoir Model

ϕ	Porosity (%)
k	Absolute permeability in mD
k_{rw}	Relative permeability to water
k_{ro}	Relative permeability to oil
P	Reservoir pressure, psi
P_{wf}	Bottom hole flowing pressure, psi
C_w	Water compressibility in psi^{-1}
C_o	Oil compressibility in psi^{-1}
C_r	Rock compressibility in psi^{-1}
S_w	Water saturation (%)
S_o	Oil saturation (%)
V	Bulk volume in ft3
Δx	Grid dimension in x direction in ft
Δy	Grid dimension in y direction in ft
h	Thickness of the reservoir in ft
r_w	Wellbore radius in ft
r_e	distance between reservoir outer boundary to wellbore in ft
μ_w	Water viscosity in cp

μ_o	Oil viscosity in cp
B_w	Formation volume factor of water res.ft^3/std.ft^3
B_o	Formation volume factor of oil res.ft^3/std.ft^3
q_{inj}	Injection rate in ft^3/day
q_p	Production rate in ft^3/day
f_w	Water fraction

Superscripts

t	Time step index
i	Ensemble member index in algorithm
i, j	Grid number index in the reservoir model

References

1. Aanonsen, S.I., Nœvdal, G., Oliver, D.S., Reynolds, A.C., Vallès, B., 2009. The ensemble Kalman filter in reservoir engineering-A Review. SPE J. 14, 393–412. https://doi.org/10.2118/117274-PA
2. Abdolhosseini, H., Khamehchi, E., 2015. History matching using traditional and finite size ensemble Kalman filter. J. Nat. Gas Sci. Eng. 27, 1748–1757. https://doi.org/10.1016/j.jngse.2015.10.041
3. Anderson, J.L., 2001. An Ensemble Adjustment Kalman Filter for Data Assimilation. Mon. Weather Rev. 129, 2884–2903. https://doi.org/10.1175/1520-0493(2001)129<2884:AEAKFF>2.0.CO;2
4. Brouwer, D.R., Nævdal, G., Jansen, J.D., Vefring, E.H., 2004. Improved reservoir management through optimal control and continuous model updating, in: Proceedings - SPE Annual Technical Conference and Exhibition. pp. 1551–1561. https://doi.org/10.2523/90149-ms
5. Chen, Y., Oliver, D.S., Zhang, D., 2009. Data assimilation for nonlinear problems by ensemble Kalman filter with reparameterization. J. Pet. Sci. Eng. 66, 1–14. https://doi.org/10.1016/j.petrol.2008.12.002

6. Emerick, A.A., Reynolds, A.C., 2013. Investigation of the sampling performance of ensemble-based methods with a simple reservoir model. Comput. Geosci. 17, 325–350. https://doi.org/10.1007/s10596-012-9333-z
7. Evensen, G., 1994. Sequential data assimilation with a nonlinear quasi-geostrophic model using Monte Carlo methods to forecast error statistics. J. Geophys. Res. https://doi.org/10.1029/94JC00572
8. Gu, Y., Oliver, D.S., 2006. The ensemble Kalman filter for continuous updating of reservoir simulation models. J. Energy Resour. Technol. Trans. ASME 128, 79–87. https://doi.org/10.1115/1.2134735
9. Gu, Y., Oliver, D.S., 2005. History matching of the PUNQ-S3 reservoir model using the ensemble Kalman filter. SPE J. 10, 217–224. https://doi.org/10.2118/89942-PA
10. Jahanbakhshi, S., Pishvaie, M.R., Boozarjomehry, R.B., 2018. Impact of initial ensembles on posterior distribution of ensemble-based assimilation methods. J. Pet. Sci. Eng. 171, 82–98. https://doi.org/10.1016/j.petrol.2018.07.022
11. Jahanbakhshi, S., Pishvaie, M.R., Boozarjomehry, R.B., 2015. Joint estimation of absolute and relative permeabilities using ensemble-based Kalman filter. J. Nat. Gas Sci. Eng. 26, 1232–1245. https://doi.org/10.1016/j.jngse.2015.08.029
12. Jung, S., Lee, K., Park, C., Choe, J., 2018. Ensemble-based data assimilation in reservoir characterization: a review. Energies 11. https://doi.org/10.3390/en11020445
13. Kalman, R.E., 1960. A new approach to linear filtering and prediction problems. J. Basic Eng. 82, 35–45. https://doi.org/10.1115/1.3662552
14. Li, H., Chen, S., Yang, D., Tontiwachwuthikul, P., 2012. Estimation of relative permeability by assisted history matching using the ensemble-kalman-filter method. J. Can. Pet. Technol. 51, 205–214. https://doi.org/10.2118/156027-PA
15. Liu, N., Oliver, D.S., 2005. Critical evaluation of the ensemble Kalman filter on history matching of geologic facies, in: Reservoir Simulation and Symposium. pp. 470–477. https://doi.org/10.2118/92867-pa
16. Ljung, L., 1998. System Identification, PRENTICE HALL PTR. https://doi.org/10.1007/978-1-4612-1768-8_11
17. Lorentzen, R.J., Fjelde, K.K., Frøyen, J., Lage, A.C.V.M., Nævdal, G., Vefring, E.H., 2001. Underbalanced and low-head drilling operations: real time interpretation of

measured data and operational support, in: SPE Annual Technical Conference and Exhibition. pp. 591–602. https://doi.org/10.2523/71384-ms

18. Lorentzen, R.J., Nævdal, G., Vallès, B., Berg, A.M., Grimstad, A.A., 2005. Analysis of the ensemble kalman filter for estimation of permeability and porosity in reservoir models, in: SPE Annual Technical Conference and Exhibition. pp. 2695–2704. https://doi.org/10.2523/96375-ms
19. Lorentzen, R.J., Ncevdal, G., Shafieirad, A., 2013. Estimating facies fields by use of the ensemble kalman filter and distance functions-applied to shallow-marine environments. SPE J. 18, 146–158. https://doi.org/10.2118/143031-pa
20. Marquart, G., Vogt, C., Klein, C., Widera, A., 2013. Estimation of geothermal reservoir properties using the ensemble Kalman filter. Energy Procedia 40, 117–126. https://doi.org/10.1016/j.egypro.2013.08.015
21. Moradkhani, H., Sorooshian, S., Gupta, H. V., Houser, P.R., 2005. Dual state–parameter estimation of hydrological models using ensemble Kalman filter. Adv. Water Resour. 28, 135–147. https://doi.org/10.1016/j.advwatres.2004.09.002
22. Nævdal, G., Mannseth, T., Vefring, E.H., 2002. Near-well reservoir monitoring through ensemble Kalman filter, in: SPE Symposium on Improved Oil Recovery. pp. 959–967. https://doi.org/10.2523/75235-ms
23. Nobakht, B.N.K., Christie, M., Demyanov, V., 2018. Model selection for error generalization in history matching, in: EAGE Conference and Exhibition. pp. 11–14. https://doi.org/10.2118/190778-ms
24. Nœvdal, G., Johnsen, L.M., Aanonsen, S.I., Vefring, E.H., 2005. Reservoir monitoring and continuous model updating using ensemble Kalman Filter. SPE Repr. Ser. 66–74. https://doi.org/10.2523/84372-ms
25. Shuai, Y., White, C., Sun, T., Feng, Y., 2016. A gathered EnKF for continuous reservoir model updating. J. Pet. Sci. Eng. 139, 205–218. https://doi.org/10.1016/j.petrol.2016.01.005
26. Skjervheim, J.A., Evensen, G., Aanonsen, S.I., Ruud, B.O., Johansen, T.A., 2007. Incorporating 4D seismic data in reservoir simulation models using ensemble Kalman filter. SPE J. 12, 282–292. https://doi.org/10.2118/95789-PA
27. Sorooshian, S., Dracup, J.A., 1980. Stochastic parameter estimation procedures for

hydrologie rainfall-runoff models: Correlated and heteroscedastic error cases. Water Resour. Res. 16, 430–442. https://doi.org/10.1029/WR016i002p00430

28. Stordal, A.S., Karlsen, H.A., Nævdal, G., Skaug, H.J., Vallès, B., 2011. Bridging the ensemble Kalman filter and particle filters: The adaptive Gaussian mixture filter. Comput. Geosci. 15, 293–305. https://doi.org/10.1007/s10596-010-9207-1
29. Thulin, K., Nævdal, G., Skaug, H.J., Aanonsen, S.I., 2011. Quantifying Monte Carlo uncertainty in the ensemble Kalman filter. SPE J. https://doi.org/10.3997/2214-4609.20146415
30. Trani, M., Arts, R., Leeuwenburgh, O., 2012. Seismic history matching of fluid fronts using the ensemble Kalman filter. SPE J. 18, 159–171. https://doi.org/10.2118/163043-PA
31. Wang, Y., Li, G., Reynolds, A.C., 2009. Estimation of depths of fluid contacts by history matching using iterative ensemble kalman smoothers, in: SPE Reservoir Simulation Symposium. pp. 750–766. https://doi.org/10.2118/119056-ms
32. Wen, X.-H., Chen, W.H., 2005. Real-time reservoir model updating using ensemble Kalman filter, in: SPE Reservoir Simulation Symposium. Society of Petroleum Engineers, pp. 167–180. https://doi.org/10.2523/92991-MS
33. Zhang, Y., Yang, D., Li, H., Patil, S., 2017. Simultaneous estimation of relative permeability and capillary pressure for PUNQ-S3 model with a damped iterative ensemble Kalman Filter technique. SPE J. 971–984. https://doi.org/10.2118/177846-ms
34. Zafari, M., 2005. Assessing the uncertainty in reservoir description and performance predictis with the ensemble Kalman filter. SPE Annual Technical Conference and Exhibition. https://doi.org/10.2118/95750-MS

Chapter 3 : Application of Particle Filter to Assess Uncertainty for Reservoir State and Parameter Estimation

Preface

This chapter addresses an objective of this dissertation as outlined in Section 3.1 which is to investigate the aspect of non-Gaussianity in state and parameter estimation in five spot oil-water reservoir by applying EnKF along with particle filter (PF). Also, a work has been done on the performance of particle filter improvement by incorporating "ensemble covariance" during resampling stage. The methodology presented in this chapter aims to improve history matching by addressing the non-Gaussianity, as presented in Section 3.2 and Section 3.4.

I (Farhana Akter) have contributed to Conceptualization, Methodology, Formal Analysis, Investigation, Writing - Original Draft, and Writing - Review & Editing of this work, while Dr. Syed Imtiaz contributed to Conceptualization, Methodology, Formal Analysis, Writing - Review & Editing, Supervision; Dr. Sohrab Zendehboudi contributed to Writing - Review & Editing, and Supervision; Dr. Amer Aborig contributed to Writing - Review & Editing. A version of this chapter has been submitted in the Journal of Petroleum Science and Engineering.

Abstract

For water flooding in an oil reservoir, a bimodal water saturation distribution around the waterfront leads to subsequent non-Gaussian distribution of water saturation. Nonlinear relationship between the state variables and model parameters, the non-Gaussian probability distribution of water saturation near shock front limits the applicability of the methods that are based on Gaussianity; this causes poor history matching. Therefore, one potential concern is to ensure the realistic update of water saturation during history matching at any phase of production from oil reservoirs.

This work employs particle filter (PF) to water flooding reservoir for data assimilation, considering the effect of "non-Gaussianity" in water saturation distribution around the shock front. This chapter investigates the performance of the PF in updating state variables, particularly water saturation and efficiency to approximation of posterior probability distribution. In addition to that while applying PF, particle perturbation has been done by applying "ensemble covariance" in

resampling stage aiming to diverse particles and thereby avoid particle collapse; this approach is investigated in terms of number of particles' participation in resampling and corresponding reservoir parameters estimation. The methodology is presented stepwise considering a two-dimensional (2D) five-spot water flood problem followed by one-dimensional (1D) case. After updating state variables, the approximation of the forward model is done using the solution of Buckley-Leverett equation with the application of PF and ensemble Kalman filter (EnKF). The results obtained from PF are compared with the result obtained from EnKF with respect to pressure and water saturation matching, and approximation of posterior probability distribution. The result shows that the performance of EnKF is competent with PF where the non-Gaussianity is weak but in presence of strong non-Gaussianity, the error is four times higher in case of EnKF. Regarding particle diversity, it is found that higher number of particles are participated in resampling stage when particle perturbation has been done by applying "ensemble covariance" compared to Gaussian based "randomization".

Keywords: Particle filter; Water flooding; Non-Gaussian; Water saturation; Kalman filter; State estimation

3.1 Introduction

An oil and gas reservoir are a highly nonlinear and non-Gaussian system. The system contains different sources of nonlinearity such as saturation dependent relative permeability, source term, and pressure dependent fluid properties (Jansen, 2013). When water flooding is performed in a reservoir to displace oil, at the oil-water interface, water saturation is higher behind the waterfront and lower ahead of the waterfront which results in a bimodal water saturation distribution. Therefore, the distribution of water saturation at the interface does not remain Gaussian. In addition, some of the state variables of a reservoir model (e.g., pressure, saturation, permeability, and porosity) cannot be measured directly and experience significant uncertainty (Chen et al., 2009).

Considering the above issues, accurate estimation of state variables in the reservoir model is a key concern for ensuring good history matching and prediction. Ensemble Kalman filter (EnKF) has been used widely for real time reservoir data assimilation. However, EnKF is only applicable for

systems with linear relationship between state variables, model parameters, and observations; it also cannot deal with non-Gaussian probability distribution (Chen et al., 2009). These two assumptions limit the applicability of EnKF in reservoir history matching specially for the enhanced oil recovery process through water flooding, and this ultimately affects the predictability of the reservoir model.

In previous studies, different modifications have been introduced into EnKF to address the nonlinearity or the non-Gaussian distribution of state variables. One of the modification is parameterization of the state variables. Gu and Oliver (2005) suggested normal score transform while applying EnKF for data assimilation. Zhou et al. (2011) and Schniger et al. (2012) applied the same methodology. Upon using this filter, water saturation transformed into normal distribution, and this transformation resulted in improved history matching. However, at later stage of the history matching, this filter generated unrealistic saturation values at the front. Chen et al. (2009) replaced the non-Gaussian variable "saturation" by Gaussian variable "shock arrival time" in the state vector for the use of EnKF in the water flooding problem. Later, saturation values were computed from the curve of arrival time to saturation. Gu and Oliver (2006) applied the similar correction strategy in EnKF by replacing the saturation by position of the shock front in the state vector. For 1D case, the impressive improvement was achieved, but for 2D or 3D cases, the results were not satisfactory. Another modifications in EnKF are updating by multiple point statistics (Li et al., 2015), combination of EnKF and multidimensional scaling (Tavakoli et al., 2014) and indicator based data assimilation (Kumar and Srinivasan, 2019) where individual component of the state vector will be updated preserving non-Gaussianity.

For water flooding scenario, Gaussian/non-Gaussian probability distribution function plays a vital role for approximation of posterior water saturation distribution. In the literature, it is mentioned that non-Gaussian distribution of initial ensemble of the model state and nonlinear dynamic reservoir model are considered as the two sources for causing non-Gaussianity. Violation of any of the considerations may lead to erroneous results. In addition, the heterogeneity in terms of variation in static parameters such as porosity and permeability add further complexity from geological point of view. This will make a big difference between the forecasted results and actual observations. Particle filter (PF) is a sequential data assimilation method that does not require model linearity and Gaussian assumption. Therefore, PF is considered as a powerful tool for

tracking the stochastic dynamic states by providing the accurate approximation of the posterior probability distribution of the updated state variables. However, the application of PF in petroleum engineering systems is very much limited.

Yoon (2016) conducted research work regarding reservoir history matching by embedding hyper reduced model into the framework of PF and compared the results obtained from implementation of EnKF. In the research, it was found that under the same framework, the performance of PF is better in terms of computational cost and history matching. Lorentzen et al. (2014) applied auxiliary PF and the transient multiphase well-flow model for automatic identification of reservoir flowrate from wellbore measurements. For this case, auxiliary PF was possible to capture detail variation (sudden jump and smooth transition) in the flow rate. Later, this approach was also applied in a full scale multiphase problem (Lorentzen et al., 2016). In this case, total volume of produced flow rate was measured with high accuracy; however, individual flow rate estimation was associated with higher uncertainty. Liao et al. (2019) embedded a transformation adaptive stochastic collocation method into the Markov Chain Monte Carlo (MCMC) to resolve the history matching problem with high nonlinearity. Xue et al. (2020) employed the combination of PF and PCM based surrogate model to a shale gas reservoir to predict the uncertainty in reservoir parameters such as permeability, water saturation, and thickness of shale. Their conclusion is that long term history and higher number of particles' participation ensure better history matching and corresponding estimation of reservoir parameters.

From the previous study, it is found that to deal with history matching problem with high nonlinearity and non-Gaussianity, performance of particle filter is quite promising, and application of particle filter is very limited. Since oil production through water injection is the secondary approach; also, water saturation profile matching plays a dynamic role for estimating uncertain reservoir parameters. Considering the potential advantages, PF is used for the case of water flooding in a heterogeneous oil reservoir, and its capability and usefulness for data assimilation are investigated. For the application of the PF to the reservoir case, the reservoir fluid flow equations are discretized and formulated in state space form. In addition, sources of nonlinearity in the flow equations are presented, emphasizing the robustness of PF for water flooding case. This work demonstrates the development of non-Gaussianity in state variables and its impact on the history matching and parameter estimation while applying Gaussian distribution-based methods

such as EnKF. Then, considering the presence of non-Gaussianity, the performance of PF is investigated and compared with EnKF. In this work, a heterogeneous reservoir is considered instead of a homogeneous reservoir to assess the robustness of the PF in terms of history matching, and state and parameter estimation.

Filter degeneracy is a common problem in PF application. Due to this, with time a smaller number of particles participate in resampling. Like the state variables (pressure-saturation), parameters (porosity-permeability) do not have any dynamic model. Moreover, in reservoir case, parameters are associated with high uncertainty. Therefore, for accurate estimation of these parameters, participation of higher number of particles in resampling step is essential. In the literature, different approaches are applied to increase the particle diversity. One of the approaches is implementation of unweighted variance of the ensemble to spread the ensemble. This approach was applied in land surface model by Qin et al.(2009) and in soil hydrology model by Montzka et al.(2011), and Manoli et al. (2015). Later, Yan et al. (2015) and H. Zhang et al. (2017) applied a method based on Markov Chain Monte Carlo (MCMC) in the land surface model for state and parameter estimation for generation of new particles. From the literature, it is found that generation of new particles or spreading the ensemble after data assimilation plays a vital role in estimating unknown parameters. Considering this crucial part, this work introduces an approach regarding particle perturbation in resampling step. In this method, the particles are diversified by calculating the covariance from the updated ensemble obtained from the model and introducing it into resampling step. Since all particles are considered in covariance calculation, covariance contains both observed and unobserved information and thereby particle degeneracy can be avoided. For new particle generation, the proposed line of work is compared with the general approach called "randomization" with respect to participation of particle number and parameter estimation.

The rest of the paper is organized as follows: Theory, mathematical formulation, and corresponding flowchart of PF are presented in **Section 3.2**. **Section 3.3** presents formulation of the reservoir fluid flow equations in the state space form. A five spot 2D reservoir case is considered. **Section 3.4** includes the flowchart of the methodology regarding application of PF to reservoir case. **Section 3.5** shows results and discussion where illustrative reservoir cases are demonstrated. This section starts with a 1D case, and the corresponding results are discussed. Later, a 2D five spot water flood case is studied. At the end of this section, a discussion on

introduction of ensemble covariance in resampling is provided. **Section 3.6** summarizes the main conclusions of this study.

3.2 Theory and Formulation of Particle Filter

Particle filter (PF) is a sequential Monte Carlo approach, and it can handle non-Gaussian distribution that propagates through nonlinear model. The dynamic state space formulation of nonlinear non-Gaussian system (Imtiaz et al., 2006) is given below:

System equation: $x_{t+1} = f(x_t, u_t) + w_t$ (3-1)

Measurement equation: $y_{t+1} = h(x_{t+1}) + v_{t+1}$ (3-2)

Here, x_t is the state vector at time step t; $f(.)$ introduces the nonlinear function for reservoir simulation model with system noise w_t; y_t represents the measurement vector at time step *t*; and $h(.)$ denotes the measurement function with measurement noise v_t. In this method, both system and measurement disturbances are not necessarily assumed to be Gaussian (Imtiaz et al., 2006).

Figure 3-1 describes the graphical representation of data assimilation with the application of PF. This method involves three stages of operation such as prediction, update, and resampling. At each time step, current states *(x_t)* are estimated through data assimilation using available observations *($y_{1:t-1}$),* and posterior probability density function (pdf) $p(x_t|y_{1:t})$ is generated through prediction and update stages. Posterior pdf is approximated by a set of weighted particles where particle weights are selected based on the importance of sampling after normalization.

The prior distribution of the state vector at *t ($P(x_t|y_{1:t-1})$)* is as follows:

$$P(x_t|y_{1:t-1}) = \int P(x_t|x_{t-1})P(x_{t-1}|y_{1:t-1})dx_{t-1} = \sum_{i=1}^{N} \omega_{t-1}^{i}\delta(x_t - x_t^i) \quad (3\text{-}3)$$

The posterior distribution of the state vector at *t ($P(x_t|y_{1:t})$)* is given below:

$$P(x_t|y_{1:t}) = \frac{P(y_t|x_t)P(x_t|y_{1:t-1})}{P(y_t|y_{1:t-1})} \quad (3\text{-}4)$$

The updated particle weight (ω_t^i) is obtained as follows:

$$\omega_t^i = \frac{\omega_{t-1}^i P(y_t|x_t^i)}{\sum_{i=1}^N \omega_{t-1}^i P(y_t|x_t^i)} \tag{3-5}$$

The likelihood function ($P(y_t|x_t^i)$) is given below:

$$P(y_t|x_t^i) = \frac{1}{(2\pi)^{1/2}|R_{t+1}|^{1/2}} \times exp\left[-\frac{1}{2v_t}(h(x_t^i) - y_t)^T(h(x_t^i) - y_t)\right] \tag{3-6}$$

The updated posterior distribution ($P(x_t|y_{1:t})$) is expressed below:

$$P(x_t|y_{1:t}) = \sum_{i=1}^{N} \omega_t^i \delta(x_t - x_t^i) \tag{3-7}$$

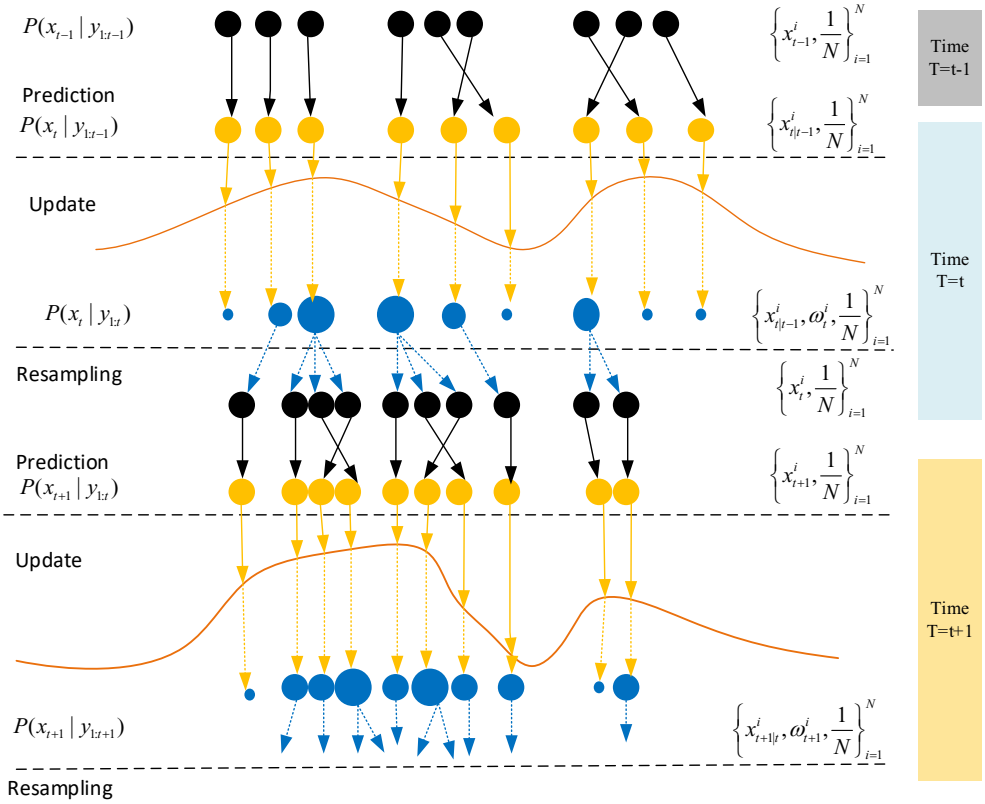

Figure 3-1: Graphical Representation of Particle Filter

This methodology is applied to the reservoir case for history matching, prediction, and parameters estimation. The following section/subsection describes the formulation of the state space model for the reservoir and corresponding methodology.

3.3 Reservoir Model

A synthetic two-dimensional (2D) reservoir model of 10 × 10 × 1 grids with the dimension of 100 ft ×100 ft ×50 ft is generated as shown in **Figure 3-2**. The initial pressure is 1000 psi. One injection well is in grid block (5, 5) and four production wells in grid blocks (2, 2), (2, 9), (9, 2), and (9, 9) in the reservoir. Production rate is set at 1000 ft^3/d in each well with a minimum bottomhole pressure of 500 psi. Injection rate is maintained at 4000 ft^3/d with a maximum bottom hole pressure limit of 2000 psi. For this case, a random permeability field is generated assuming Gaussian distribution with a mean value of 100 mD and a standard deviation of 50. The simulation is run for 1000 days.

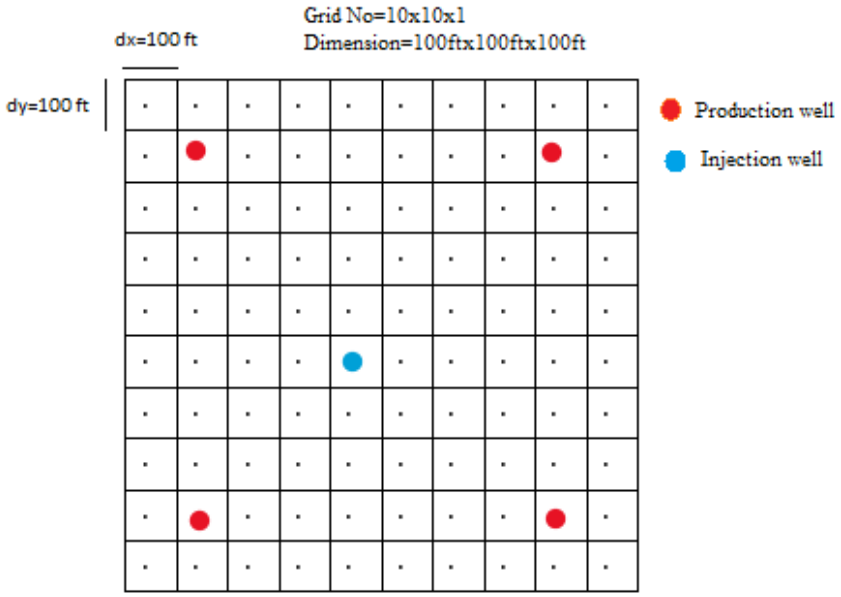

Figure 3-2: Two-Dimensional Oil-Water Reservoir

3.3.1 Two Phase Flow Equations

This section lists (and describes) the governing equations for two-phase (oil-water) flow. The simultaneous solution method is formulated in the state space form to calculate the dynamic state (P_o and S_w). The formulation is done in terms of surface condition using fluid formation volume factor. The impact of capillary pressure and gravity is neglected. The partial differential equation for each phase can be expressed as follows (Jansen, 2013):

Water phase:

$$\nabla.\left(\alpha\rho_w\vec{V}_w\right)+\alpha\frac{\delta(\rho_w\emptyset S_w)}{\delta t}-\alpha\rho_w q_w'''=0 \quad (3\text{-}8)$$

$$\vec{V}_w=-\frac{k_{rw}}{\mu_w}\vec{K}(\nabla\rho_w-\rho_w g\nabla d) \quad (3\text{-}9)$$

Oil phase:

$$\nabla.\left(\alpha\rho_o\vec{V}_o\right)+\alpha\frac{\delta(\rho_o\emptyset S_o)}{\delta t}-\alpha\rho_o q_o'''=0 \quad (3\text{-}10)$$

$$\vec{V}_o=-\frac{k_{ro}}{\mu_o}\vec{K}(\nabla\rho_o-\rho_o g\nabla d) \quad (3\text{-}11)$$

Here, $\vec{K}=\begin{bmatrix}k_x & 0\\ 0 & k_y\end{bmatrix}$ $\nabla.\triangleq\begin{bmatrix}\delta. & \delta.\\ \delta x & \delta y\end{bmatrix}^T$

Well model:

$$p=p_{wf}-\frac{\mu q}{2\pi kh}ln\left(\frac{r}{r_{well}}\right) \quad (3\text{-}12)$$

The sources of nonlinearity are given below:

1. Saturation and pressure dependent relative permeability *(k_r)* (Jansen, 2013), as introduced below.

$$k_{rw}=k_{rw}^0S^{n_w} \quad (3\text{-}13)$$

$$k_{ro}=k_{ro}^0(1-S)^{n_o} \quad (3\text{-}14)$$

$$S\triangleq\frac{S_w-S_{wc}}{1-S_{or}-S_{wc}},0\le S\le 1 \quad (3\text{-}15)$$

2. Source term (flow rate) in the production well: This term is called the saturation dependent mobility *(λ)* as defined below.

$$q_w = f_w q_t = \frac{\lambda_w}{\lambda_o + \lambda_w} q_t \quad (3\text{-}16)$$

$$\lambda_w = \frac{k \times k_{rw}}{\mu_w} \quad (3\text{-}17)$$

$$q_o = f_o q_t = \frac{\lambda_o}{\lambda_o + \lambda_w} q_t \quad (3\text{-}18)$$

$$\lambda_o = \frac{k \times k_{ro}}{\mu_o} \quad (3\text{-}19)$$

3.3.2 Parameterization and Mathematical Formulation

In this analysis, the state vector consists of two static vectors (e.g., porosity and permeability), and two dynamic vectors namely water saturation and pressure. The discretized partial differential equations of two-phase (oil and water) in the reservoir are given below (Jansen, 2013):

Water phase:

$$V\left[\emptyset S_w(c_w + c_r)\frac{\partial p}{\partial t} + \emptyset\frac{\partial s_w}{\partial t}\right]_{i,j} - (T_w)_{i-\frac{1}{2},j} p_{i-1,j} - (T_w)_{i,j-\frac{1}{2}} p_{i,j-1} + \left[(T_w)_{i-\frac{1}{2},j} + (T_w)_{i,j-\frac{1}{2}} + (T_w)_{i+\frac{1}{2},j} + (T_w)_{i,j+\frac{1}{2}}\right] p_{i,j} - (T_w)_{i+\frac{1}{2},j} p_{i+1,j} - (T_w)_{i,j+\frac{1}{2}} p_{i,j+1} = [q_w]_{i,j} = [f_w q_p]_{i,j} \quad (3\text{-}20)$$

Oil phase:

$$V\left[\emptyset S_o(c_o + c_r)\frac{\partial p}{\partial t} - \emptyset\frac{\partial s_w}{\partial t}\right]_{i,j} - (T_o)_{i-\frac{1}{2},j} p_{i-1,j} - (T_o)_{i,j-\frac{1}{2}} p_{i,j-1} + \left[(T_o)_{i-\frac{1}{2},j} + (T_o)_{i,j-\frac{1}{2}} + (T_o)_{i+\frac{1}{2},j} + (T_o)_{i,j+\frac{1}{2}}\right] p_{i,j} - (T_o)_{i+\frac{1}{2},j} p_{i+1,j} - (T_o)_{i,j+\frac{1}{2}} p_{i,j+1} = [q_o]_{i,j} = [f_o q_p]_{i,j} \quad (3\text{-}21)$$

where,

$$T_{i-1/2,j} = \frac{\Delta x}{\Delta y}\frac{h}{\mu} k_{i-1/2,j}\,; \quad T_{i,j-1/2} = \frac{\Delta y}{\Delta x}\frac{h}{\mu} k_{i,j-1/2}; \quad S_w + S_o = 1; \quad f_w = \frac{k_{rw}}{k_{rw} + k_{ro}\frac{\mu_w}{\mu_o}} = 1 - f_o$$

The general state- space formulation is presented below:

$$\begin{bmatrix} \begin{bmatrix} V_{wp} & V_{ws} \\ V_{op} & V_{os} \end{bmatrix} & \begin{bmatrix} 0 & 0 \\ 0 & 0 \end{bmatrix} \\ \begin{bmatrix} 0 & 0 \\ 0 & 0 \end{bmatrix} & \begin{bmatrix} 1 & 0 \\ 0 & 1 \end{bmatrix} \end{bmatrix} \times \begin{bmatrix} \frac{dp}{dt} \\ \frac{dS_w}{dt} \\ \frac{dk}{dt} \\ \frac{d\emptyset}{dt} \end{bmatrix} + \begin{bmatrix} \begin{bmatrix} T_w & 0 \\ T_o & 0 \end{bmatrix} & \begin{bmatrix} 0 & 0 \\ 0 & 0 \end{bmatrix} \\ \begin{bmatrix} 0 & 0 \\ 0 & 0 \end{bmatrix} & \begin{bmatrix} 0 & 0 \\ 0 & 0 \end{bmatrix} \end{bmatrix} \times \begin{bmatrix} p \\ \frac{S_w}{k} \\ \emptyset \end{bmatrix} = \begin{bmatrix} q_w \\ \frac{q_o}{0} \\ 0 \end{bmatrix} + \begin{bmatrix} F_w \\ \frac{F_o}{0} \\ 0 \end{bmatrix} [q_p] \quad (3\text{-}22)$$

Here,

$p = [p_{i,j-1} \quad \dots \quad p_{i-1,j} \quad p_{i,j} \quad p_{i+1,j} \quad \dots \quad p_{i,j+1}]$; $S_w = [S_{w_{i,j-1}} \quad \dots \quad S_{w_{i-1,j}} \quad S_{w_{i,j}} \quad S_{w_{i+1,j}} \quad \dots \quad S_{w_{i,j+1}}]$

$k = [k_{i,j-1} \quad \dots\dots \quad k_{i-1,j} \quad k_{i,j} \quad k_{i+1,j} \quad \dots\dots \quad k_{i,j+1}]$; $\emptyset = [\emptyset_{i,j-1} \quad \dots\dots \quad \emptyset_{i-1,j} \quad \emptyset_{i,j} \quad \emptyset_{i+1,j} \quad \dots\dots \quad \emptyset_{i,j+1}]$

$V_{wp} = V(c_w + c_r)[0 \quad \dots \quad \emptyset_{i,j} \times (S_w)_{i,j} \quad 0 \quad \dots \quad 0]$; $V_{op} = V(c_o + c_r)[0 \quad \dots \quad \emptyset_{i,j} \times (1 - S_w)_{i,j} \quad 0 \quad \dots \quad 0]$

$V_{ws} = V[0 \quad \dots \quad \emptyset_{i,j} \quad 0 \quad \dots \quad 0]$; $V_{os} = -V[0 \quad \dots \quad \emptyset_{i,j} \quad 0 \quad \dots \quad 0]$; $\quad V = \Delta x \times \Delta y \times h$

$T_w = \left[-(T_w)_{i,j-\frac{1}{2}} \quad \dots \quad -(T_w)_{i-\frac{1}{2},j} \quad \left((T_w)_{i,j-\frac{1}{2}} + (T_w)_{i-\frac{1}{2},j} + (T_w)_{i+\frac{1}{2},j} + (T_w)_{i,j+\frac{1}{2}}\right) \quad -(T_w)_{i+\frac{1}{2},j} \quad \dots \quad -(T_w)_{i,j+\frac{1}{2}}\right]$

$T_o = \left[-(T_o)_{i,j-\frac{1}{2}} \quad \dots \quad -(T_o)_{i-\frac{1}{2},j} \quad \left((T_o)_{i,j-\frac{1}{2}} + (T_o)_{i-\frac{1}{2},j} + (T_o)_{i+\frac{1}{2},j} + (T_o)_{i,j+\frac{1}{2}}\right) \quad -(T_o)_{i+\frac{1}{2},j} \quad \dots \quad -(T_o)_{i,j+\frac{1}{2}}\right]$

$q_w = [\dots \quad (q_w)_{i,j} \quad \dots]$, $\quad F_w = [\dots \quad (f_w)_{i,j} \quad \dots]$, $\quad q_o = [\dots \quad (q_o)_{i,j} \quad \dots]$, $\quad F_o = [\dots \quad (f_o)_{i,j} \quad \dots]$

After simplification, Eq. (3-22) can be rewritten as follows:

$$\begin{bmatrix} p \\ \frac{S_w}{k} \\ \emptyset \end{bmatrix}_{t+1} = A_t \begin{bmatrix} p \\ \frac{S_w}{k} \\ \emptyset \end{bmatrix}_t + B_t \begin{bmatrix} -q_{p1} \\ -q_{p2} \\ q_{inj} \\ -q_{p3} \\ -q_{p4} \end{bmatrix}_t + Q_t \; ; \quad Q_t \sim N(0, \Sigma_t^m) \quad (3\text{-}23)$$

In Eq. (3-23), $q_{inj}, q_{p1}, q_{p2}, \; q_{p3}, \;$ and q_{p4} are the five input parameters. The injection flow rate of injection wells (5, 5) is related to the reservoir and fluid properties and process condition as follows:

$$q_{inj_t} = \left(\frac{2 \times \pi \times k \times h \times 6.33 \times 10^{-3}}{B_w \left[log \frac{r_e}{r_w} + S \right]} \left[\frac{k_{ro}}{\mu_o} + \frac{k_{rw}}{\mu_w} \right] \right)_t \left[p_{inj_{t+1}} - p_{5,5_{t+1}} \right] = J_{i_t} \left[p_{inj_{t+1}} - p_{5,5_{t+1}} \right] \quad (3\text{-}24)$$

$$p_{inj_{t+1}} = \left(J_{i_t} \right)^{-1} q_{inj_t} + p_{5,5_{t+1;}} \quad where\ J_{i_t} = \left(\frac{2 \times \pi \times k \times h \times 6.33 \times 10^{-3}}{B_w \left[log \frac{r_e}{r_w} + S \right]} \left[\frac{k_{ro}}{\mu_o} + \frac{k_{rw}}{\mu_w} \right] \right)_t ;$$

The corresponding equation for production well *(i, j)* to show the flow rate in terms of other parameters (e.g., fluid and reservoir characteristics) is given below:

$$q_{p_t} = \left(\frac{2 \times \pi \times k \times h \times 6.33 \times 10^{-3}}{\left[log \frac{r_e}{r_w} + S \right]} \left[\frac{k_{ro}}{B_o \mu_o} + \frac{k_{rw}}{B_w \mu_w} \right] \right)_t \left[p_{i,j_{t+1}} - p_{prod_{t+1}} \right] = J_{p_t} \left[p_{i,j_{t+1}} - p_{prod_{t+1}} \right] \quad (3\text{-}25)$$

$$p_{prod_{t+1}} = p_{i,j_{t+1}} - \left(J_{p_t} \right)^{-1} q_{p_t}; where\ J_{p_t} = \left(\frac{2 \times \pi \times k \times h \times 6.33 \times 10^{-3}}{\left[log \frac{r_e}{r_w} + S \right]} \left[\frac{k_{ro}}{B_o \mu_o} + \frac{k_{rw}}{B_w \mu_w} \right] \right)_t ;$$

Eq. (3-25) is applicable for four production-well grid blocks (i,j) = *(2,2), (2,9), (9,2),* and *(9,9).*

The state-space form of the well's flow rate equation can be rewritten as follows:

$$\begin{bmatrix} p_{prod1} \\ p_{prod2} \\ p_{inj} \\ p_{prod3} \\ p_{prod4} \end{bmatrix}_{t+1} = \left[\begin{bmatrix} 1 & 0 & 0 & 0 & 0 \\ 0 & 1 & 0 & 0 & 0 \\ 0 & 0 & 1 & 0 & 0 \\ 0 & 0 & 0 & 1 & 0 \\ 0 & 0 & 0 & 1 & 1 \end{bmatrix} \begin{bmatrix} 0 & 0 & 0 & 0 & 0 \\ 0 & 0 & 0 & 0 & 0 \\ 0 & 0 & 0 & 0 & 0 \\ 0 & 0 & 0 & 0 & 0 \\ 0 & 0 & 0 & 0 & 0 \end{bmatrix} \right] \begin{bmatrix} p \\ \frac{S_w}{k} \\ \emptyset \end{bmatrix}_{t+1} + \begin{bmatrix} \left(J_{p_t} \right)^{-1} & 0 & 0 & 0 & 0 \\ 0 & \left(J_{p_t} \right)^{-1} & 0 & 0 & 0 \\ 0 & 0 & \left(J_{i_t} \right)^{-1} & 0 & 0 \\ 0 & 0 & 0 & \left(J_{p_t} \right)^{-1} & 0 \\ 0 & 0 & 0 & 0 & \left(J_{p_t} \right)^{-1} \end{bmatrix} \begin{bmatrix} -q_{p1} \\ -q_{p2} \\ q_{inj} \\ -q_{p3} \\ -q_{p4} \end{bmatrix}_t + R_{t+1}, \quad R_{t+1} \sim N\left(0, \Sigma_{t+1}^{y}\right) \quad (3\text{-}26)$$

3.3.3 Steps of Particle Filter (PF) for the Reservoir Model

1. Initialization step: Particles $x_t^i \{where\ i = 1, \dots \dots \dots \dots N_p\}$ are generated from an assumed initial state distribution x_0 associated with uniform weight, $w_t^i = {}^1/_{N_p}$ for sample size N_p.
2. Prediction step: Prediction of state variable through forward model is done as follows:

$$\begin{bmatrix} p \\ \frac{S_w}{k} \\ \emptyset \end{bmatrix}_{t+1}^{i} = A_t \begin{bmatrix} p \\ \frac{S_w}{k} \\ \emptyset \end{bmatrix}_t^{i} + B_t \begin{bmatrix} -q_{p1} \\ -q_{p2} \\ q_{inj} \\ -q_{p3} \\ -q_{p4} \end{bmatrix}_t^{i} + {w_t}^i; \quad {w_t}^i \sim N(0, Q_t) \quad (3\text{-}27)$$

Prediction of the measurements is given below:

$$\begin{bmatrix} p_{prod1} \\ p_{prod2} \\ p_{inj} \\ p_{prod3} \\ p_{prod4} \end{bmatrix}_{t+1} = \left[\begin{bmatrix} 1 & 0 & 0 & 0 & 0 \\ 0 & 1 & 0 & 0 & 0 \\ 0 & 0 & 1 & 0 & 0 \\ 0 & 0 & 0 & 1 & 0 \\ 0 & 0 & 0 & 0 & 1 \end{bmatrix} \begin{bmatrix} 0 & 0 & 0 & 0 & 0 \\ 0 & 0 & 0 & 0 & 0 \\ 0 & 0 & 0 & 0 & 0 \\ 0 & 0 & 0 & 0 & 0 \\ 0 & 0 & 0 & 0 & 0 \end{bmatrix}\right] \begin{bmatrix} p \\ \frac{S_w}{k} \\ \emptyset \end{bmatrix}_{t+1} + \begin{bmatrix} \left(J_{p_t}\right)^{-1} & 0 & 0 & 0 & 0 \\ 0 & \left(J_{p_t}\right)^{-1} & 0 & 0 & 0 \\ 0 & 0 & \left(J_{i_t}\right)^{-1} & 0 & 0 \\ 0 & 0 & 0 & \left(J_{p_t}\right)^{-1} & 0 \\ 0 & 0 & 0 & 0 & \left(J_{p_t}\right)^{-1} \end{bmatrix} \begin{bmatrix} -q_{p1} \\ -q_{p2} \\ q_{inj} \\ -q_{p3} \\ -q_{p4} \end{bmatrix}_t + R_{t+1}, \quad R_{t+1} \sim N\left(0, \Sigma_{t+1}^{y}\right) \quad (3\text{-}28)$$

3. Likelihood estimation is obtained as follows:

$$L\begin{pmatrix} p_{prod1} & p^{\,i} \\ p_{prod2} & \\ p_{inj} & |\frac{S_w}{k} \\ p_{prod3} & \\ p_{prod4}{}_{t+1} & \emptyset\ {}_{t+1} \end{pmatrix} = \frac{1}{(2\pi)^{1/2}|R_{t+1}|^{1/2}} \times exp\left(-\frac{1}{2R_{t+1}}\left\{\begin{bmatrix} p_{prod1}{}^{i} & p_{prod1} \\ p_{prod2} & p_{prod2} \\ p_{inj} & -\ p_{inj} \\ p_{prod3} & p_{prod3} \\ p_{prod4}{}_{t+1} & p_{prod4}{}_{t+1} \end{bmatrix} \times \begin{bmatrix} p_{prod1}{}^{i} & p_{prod1} \\ p_{prod2} & p_{prod2} \\ p_{inj} & -\ p_{inj} \\ p_{prod3} & p_{prod3} \\ p_{prod4}{}_{t+1} & p_{prod4}{}_{t+1} \end{bmatrix}^{T}\right\}\right) \quad (3\text{-}29)$$

4. The particle weight is updated as follows:

$$w_{t+1}^{i} = \frac{w_t^i \times L\begin{pmatrix} p_{prod1} & p^{\,i} \\ p_{prod2} & \\ p_{inj} & |\frac{S_w}{k} \\ p_{prod3} & \\ p_{prod4}{}_{t+1} & \emptyset\ {}_{t+1} \end{pmatrix}}{\sum_{i=1}^{N_p} w_t^i\, L\begin{pmatrix} p_{prod1} & p^{\,i} \\ p_{prod2} & \\ p_{inj} & |\frac{S_w}{k} \\ p_{prod3} & \\ p_{prod4}{}_{t+1} & \emptyset\ {}_{t+1} \end{pmatrix}} \quad (3\text{-}30)$$

5. Resampling includes the following steps:

Cumulative sum of the weights, $c^i = \sum_{i=1}^{N_p} w_{t+1}^i$ (3-31)

a. Generation of uniform distribution, $u^i \sim u(0, {}^1/_{N_p})$

b. Compare c^i with w^i

c. Update the uniform distribution, $u^i = u^{i-1} + \frac{1}{N_p}$

d. A random particle $\begin{bmatrix} p \\ \frac{S_w}{k} \\ \emptyset \end{bmatrix}_{t+1}^{\ i}$ with weight w_{t+1}^{i} is mapped into new indexed particle $\begin{bmatrix} p \\ \frac{S_w}{k} \\ \emptyset \end{bmatrix}_{t+1}^{\ j}$ with weight $\frac{1}{N_p}$.

6. Perturbation of the particle: At each time step, particles with high likelihood are preferred for the next time step state estimation. Therefore, after several iterations, the maximum

particles are associated with low importance weight and are ignored for further calculation. With time, a small number of particles with high weight are used repeatedly, causing loss of particle diversity. This situation is called "particle impoverishment". In this condition, parameters with uncertainty cannot be properly estimated. To improve the particle diversity, perturbation of the particle should be done. For particle perturbation, additional steps can be added to the updated particle in each time step, as shown below:

$$\begin{bmatrix} p \\ \frac{S_w}{k} \\ \emptyset \end{bmatrix}_{t+1}^{i} = \begin{bmatrix} p \\ \frac{S_w}{k} \\ \emptyset \end{bmatrix}_{t}^{i} + d_i \; ; \qquad d_i \sim N(0, n_t) \tag{3-32}$$

The covariance n_t can be determined from the updated state and parameter before resampling takes place. In this case, n_t is determined through ensemble covariance calculation as outlined in the procedure below.

a. Calculate the mean of the updated state vector

$$\begin{bmatrix} \overline{p} \\ \frac{S_w}{k} \\ \emptyset \end{bmatrix}_{t+1} = \sum_{i=1}^{N_p} w_{t+1}^{i} \begin{bmatrix} p \\ \frac{S_w}{k} \\ \emptyset \end{bmatrix}_{t+1}^{i} \tag{3-33}$$

b. Compute the ensemble covariance

$$Ensemble\ covariance = r \times \left\{ \sum_{i=1}^{N_p} w_{t+1}^{i} \begin{bmatrix} p & \overline{p} \\ \frac{S_w}{k} & -\frac{S_w}{k} \\ \emptyset & \emptyset \end{bmatrix}_{t+1}^{i} \times \begin{bmatrix} p & \overline{p} \\ \frac{S_w}{k} & -\frac{S_w}{k} \\ \emptyset & \emptyset \end{bmatrix}_{t+1}^{T} \right\} \tag{3-34}$$

Here, "r" refers to the tuning factor.

3.4 Methodology

The methodology regarding PF is presented in **Figure 3-3**. The flowchart is used for combined state estimation of the dynamic system where both parameter (permeability and porosity) vectors are augmented with state (pressure-saturation) into a single state vector. Perturbation of particle using ensemble covariance (outlined in step 6 in section 3.3.3) is embedded. In this flow chart, the input variables and corresponding equations are specific to the reservoir model. In addition, the methodology outlined by Akter et al.(2021) is followed.

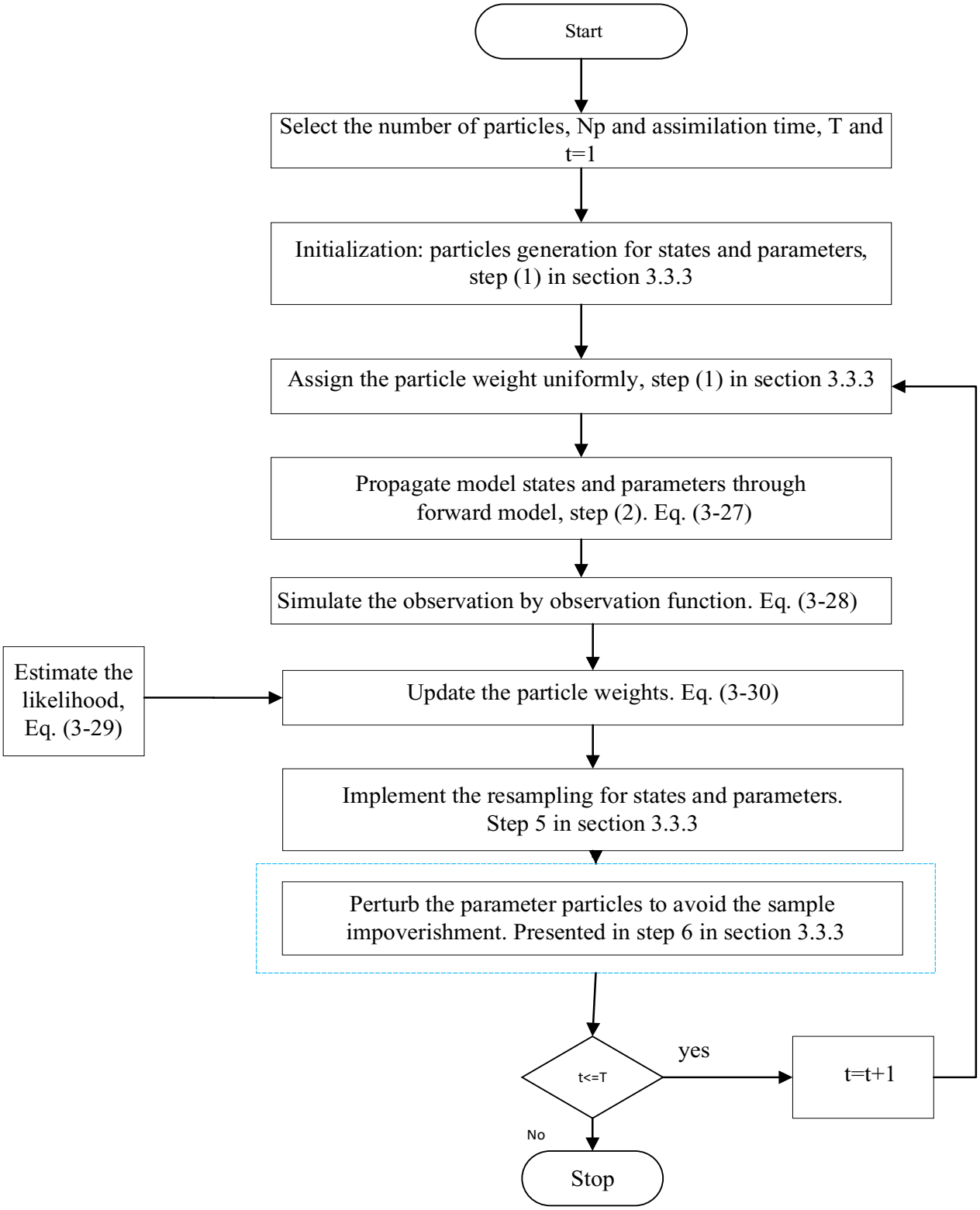

Figure 3-3: Particle Filter Flowchart for Water Flooding Reservoir Case

3.5 Results and Discussion

3.5.1 Reservoir Simulation

In this study, the oil reservoir under water flooding operation is analyzed, where synthetic reservoirs for 1D and 2D cases are generated.

The reservoir is discretized into several grids and the wells (injection and production) are constrained by constant rates. Hence, the adjusted parameters are the bottomhole pressures. The production and pressure data are recorded each day from the starting day of production. The porosity is generated assuming the mean value of porosity is 0.4 with a standard deviation of 0.03. To calculate relative permeability, the Corey's model is used with an exponent of three (3). Other assumptions include no flow boundary condition for all sides of the reservoir; only two incompressible fluids (water and oil) are present; constant compressibility; no gravity effect; and negligible capillary pressure. **Table 3-1** shows the key data for the reservoir.

Table 3-1: Reservoir Fluid and Rock Properties (Zafari, 2005)

Parameter, (unit)	**Value**	**Parameter, (unit)**	**Value**
Initial water saturation, (%)	0.2	Oil formation volume factor	1.05
Residual oil saturation, (%)	0.2	Water viscosity, (cp)	1
Rock compressibility, (psi^{-1})	4×10^{-6}	Oil viscosity, (cp)	1.1
Water compressibility, (psi^{-1})	1×10^{-5}	Reservoir temperature, (^{o}F)	100
Oil compressibility, (psi^{-1})	1×10^{-5}		

3.5.2 Case Study

3.5.2.1 One-dimensional reservoir

In 1D case, Buckley-Leverett equation is solved numerically to obtain the behavior/trend of water saturation for all realizations. 100 realizations are used for this analysis.

The 1D reservoir consists of 10 × 1 grids with the dimension of 10 ft ×10 ft, as shown in **Figure 3-4a.** The height of each grid is 10 ft. The reservoir's initial pressure is 1000 psi. The injection and production wells are in grid blocks (1, 1) and (1, 10) in the reservoir, respectively. Production rate is set at 410 ft^3/d with a minimum bottomhole pressure of 500 psi. Injection rate is maintained at 410 ft^3/d with a maximum bottom hole pressure limit of 1500 psi. It is assumed that water saturation is sensitive to porosity but not sensitive to permeability; therefore, a heterogeneous reservoir is generated by considering a random distribution of porosity, and the absolute

permeability is set to a constant value of 100 mD for all grids. **Figure 3-4b** represents the initial ensemble of porosity along with model porosity (red line). For simplification, water saturation of the reservoir is assumed to be uniform, equal to 0.2.

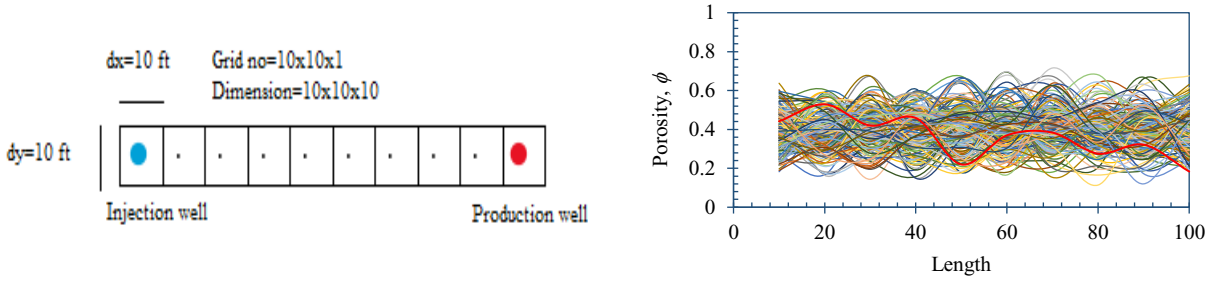

a) Reservoir with grid dimension and well location

b) Initial ensemble of porosity

Figure 3-4: A Schematic of 1D Reservoir

Initially, EnKF is applied for the analysis of non-Gaussianity in water saturation profile with respect to length.

Figure *3-5* shows the water saturation profile for 100 realizations at four different time steps such as 10, 50, 80, and 100 days. The thick red line represents the reservoir saturation profile.

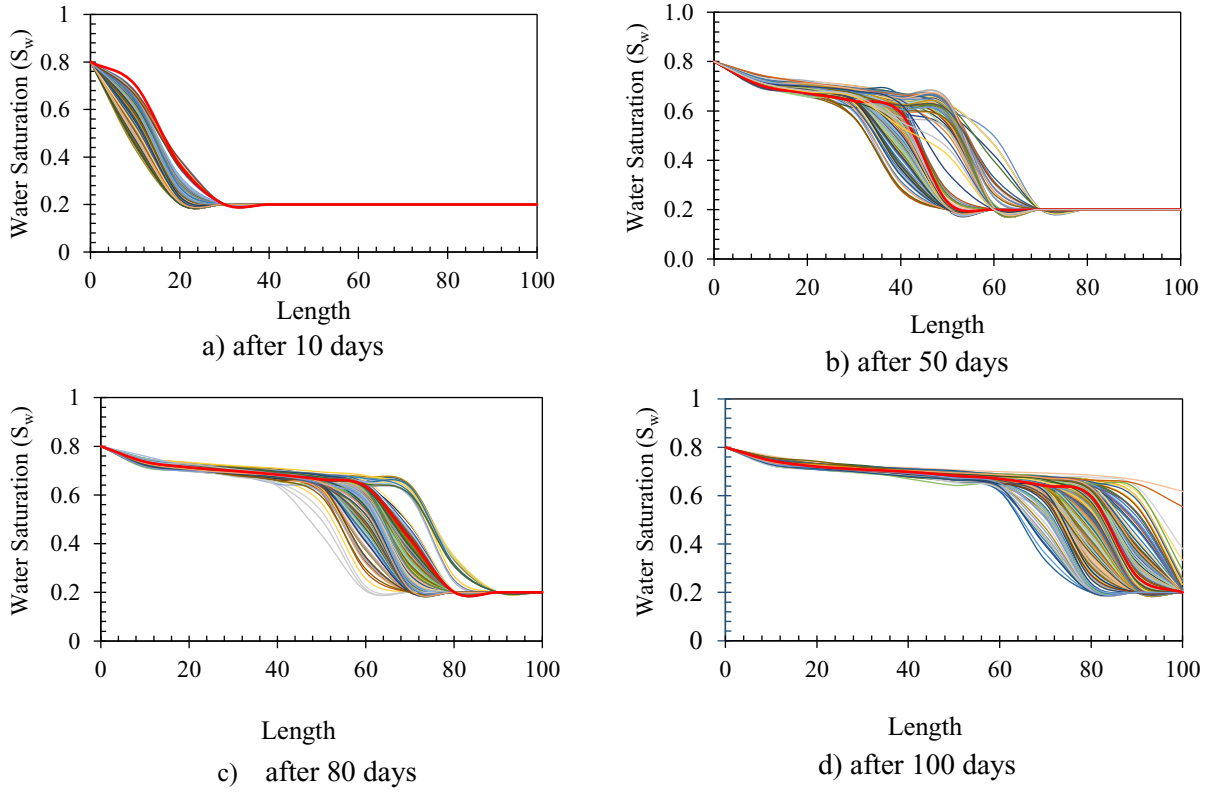

a) after 10 days

b) after 50 days

c) after 80 days

d) after 100 days

Figure 3-5: Water Saturation Obtained from EnKF and Model (Red Line) at Different Times

According to

Figure *3-5*a, after 10 days of operation, water flooding approaches up to the length of x=20 ft. At this point, the model waterfront stays ahead of most of the predicted realizations. This happens as the model porosity in the inlet is higher than most of the realizations (see **Figure 3-4b**). After 50, 80, and 100 days, waterfront of some realizations stays ahead of the model waterfront. This creates a unique situation called non-Gaussianity in terms of water saturation distribution. For explanation purpose, the time step of 50 days is taken as an example (see

Figure *3-5*b). In

Figure *3-5*b, the model waterfront is found at the length of x=50 ft. A region of high and low water saturation is observed between x=30 ft and x=60 ft. It is seen from

Figure *3-5*b that grid 2 (x=20 ft) is completely flooded representing high water saturation distribution, while grid 5 (x=50 ft) is in mixed condition with low and high-water saturation distribution. A graphical representation of this situation is presented in

Figure *3-6* where water the saturation distributions for grid blocks 2 and 5 are shown.

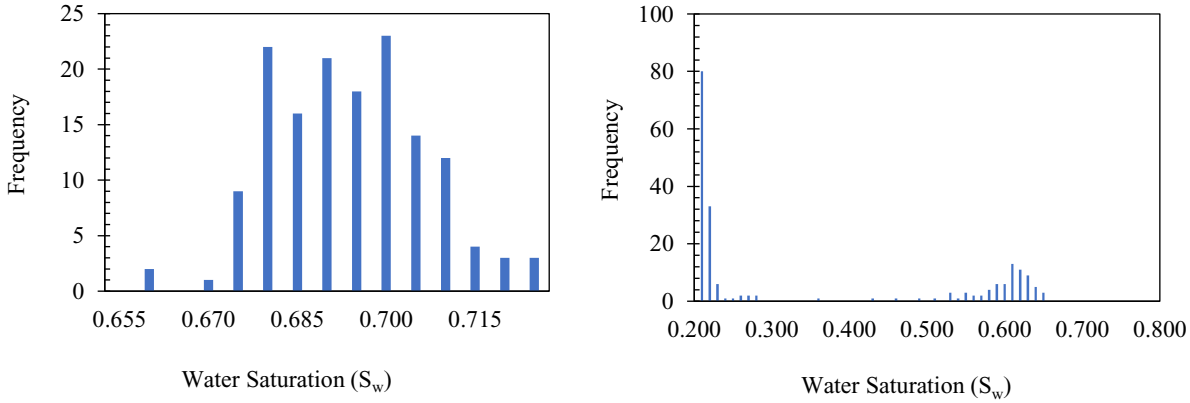

a) For grid 2

b) For grid 5

Figure 3-6: Distribution of the Water Saturation for Grid 2 and 5 after 50 Days

Figure *3-6*a depicts nearly a bell-shaped distribution ranging S_w value from 0.6 to 0.8, resulting in Gaussian distribution. On the other hand,

***Figure 3-6*b** shows a bimodal distribution ranging S_w value from 0.2 to 0.65, leading to non-Gaussian distribution. This indicates that for grid 2, waterfront of all realizations reaches after 50 days but for grid 5, a fraction of realizations still stays behind the waterfront by this time. Therefore, during data assimilation for heterogeneous reservoir case, a non-Gaussian water saturation distribution might appear in any length of the reservoir from the water injection point. For a comparison purpose, random water saturation is set for all grids with a mean of 0.2 and a standard deviation of 0.02. Then, both PF and EnKF are applied to this reservoir system. After 100 days simulation, the water saturation profile is plotted with respect to length for both cases as shown in

Figure *3-7*. It is found that the result from the PF is smoother and close to the model, whereas the result achieved from EnKF shows oscillation throughout the length (see

Figure 3-7). In addition, for some of the realizations, the assimilated S_w data drops below the critical value of S_{wc} =0.2, resulting in an unrealistic situation. It was shown previously that non-Gaussianity might appear at any length of the reservoir. Therefore, the poor performance of EnKF during data assimilation indicates that EnKF is not a good option for history matching and parameter estimation while dealing with a water flooding scenario.

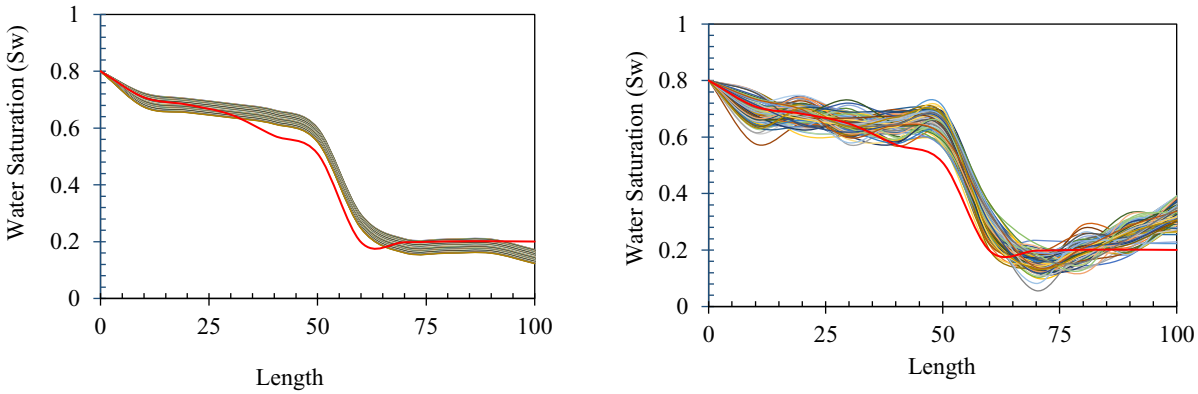

a) Updated S_w by PF

b) Updated S_w by EnKF

Figure 3-7: Water Saturation Update Obtained from PF and EnKF after 100 Days

3.5.2.2 Two-dimensional Reservoir

Based on the performance of the 1D case, the PF is applied to a case of water flooding in 2D reservoir (see **Figure 3-2**) along with EnKF. The comparative results between these two methods are discussed in this section.

Application of EnKF and PF: For the application of EnKF, a total number of 100 ensembles is applied for simulation, whereas an ensemble of 1000 uniformly distributed values for the initial state variables is generated for application of PF. A random model error is added with a standard deviation of 0.03 for pressure and 0.001 for water saturation. In addition, the random measurement error is included with a standard deviation of 0.03. The analysis starts with the pressure history matching as the wells are constrained by rates. Simulation was run for 1000 days and this time step is good for analyzing the physical phenomena happened in this reservoir.

Pressure matching: There are four production wells and one injection well in the reservoir. A constant rate is set to all wells. Therefore, the bottomhole pressure of each well is considered as the observation for history matching.

Figure *3-8* illustrates the bottomhole pressure matching of all wells after applying both PF and EnKF.

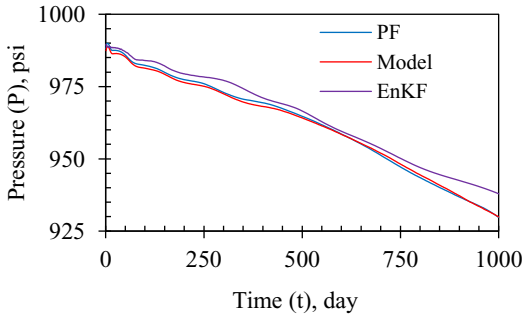

a) Production Well at (2,2)

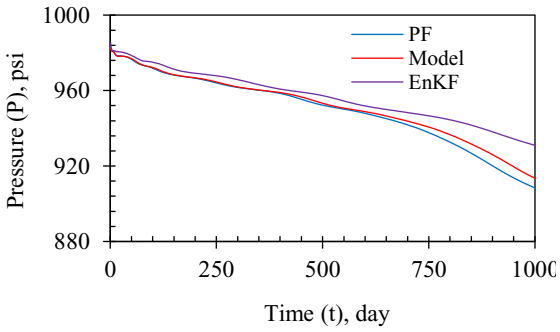

b) Production Well at (2,9)

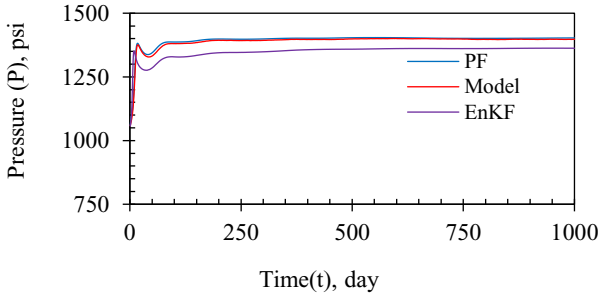

c. Injection Well at (5,5)

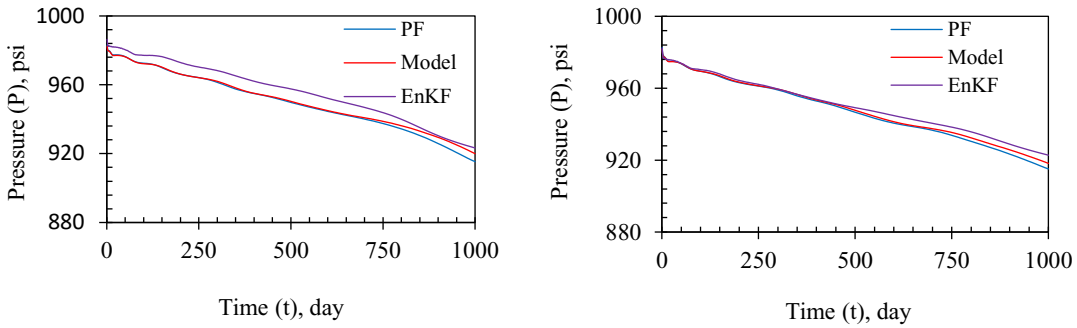

c) Production Well at (9,2)

d) Production Well at (9,9)

Figure 3-8: Bottomhole Pressure at the Production and Injection Wells

According to

Figure *3-8*, for all wells PF shows prominent matching with the model compared to the EnKF. For pressure matching, though EnKF performance is lower compared to PF, the difference between the model and EnKF is not considerable. From 1D case analysis, it is concluded that performance of EnKF in terms of water saturation is very poor. Another dynamic state variable "water saturation" matching is also investigated in this section.

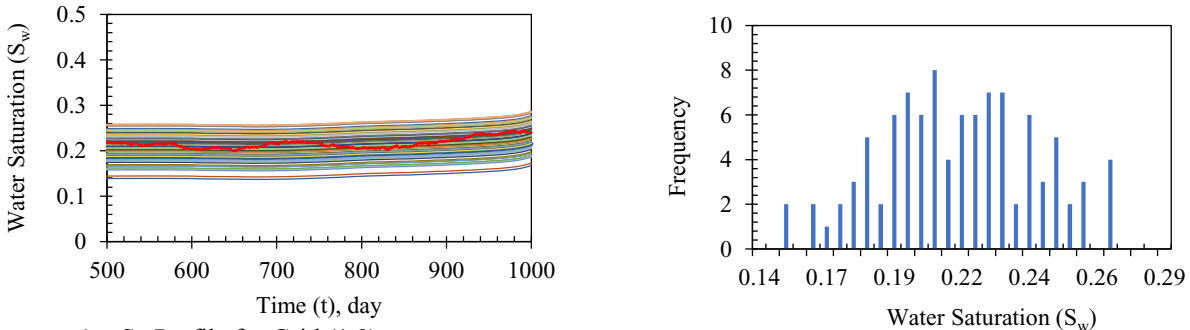

a) S_w Profile for Grid (1,9)

b) S_w Distribution for Grid (1,9)

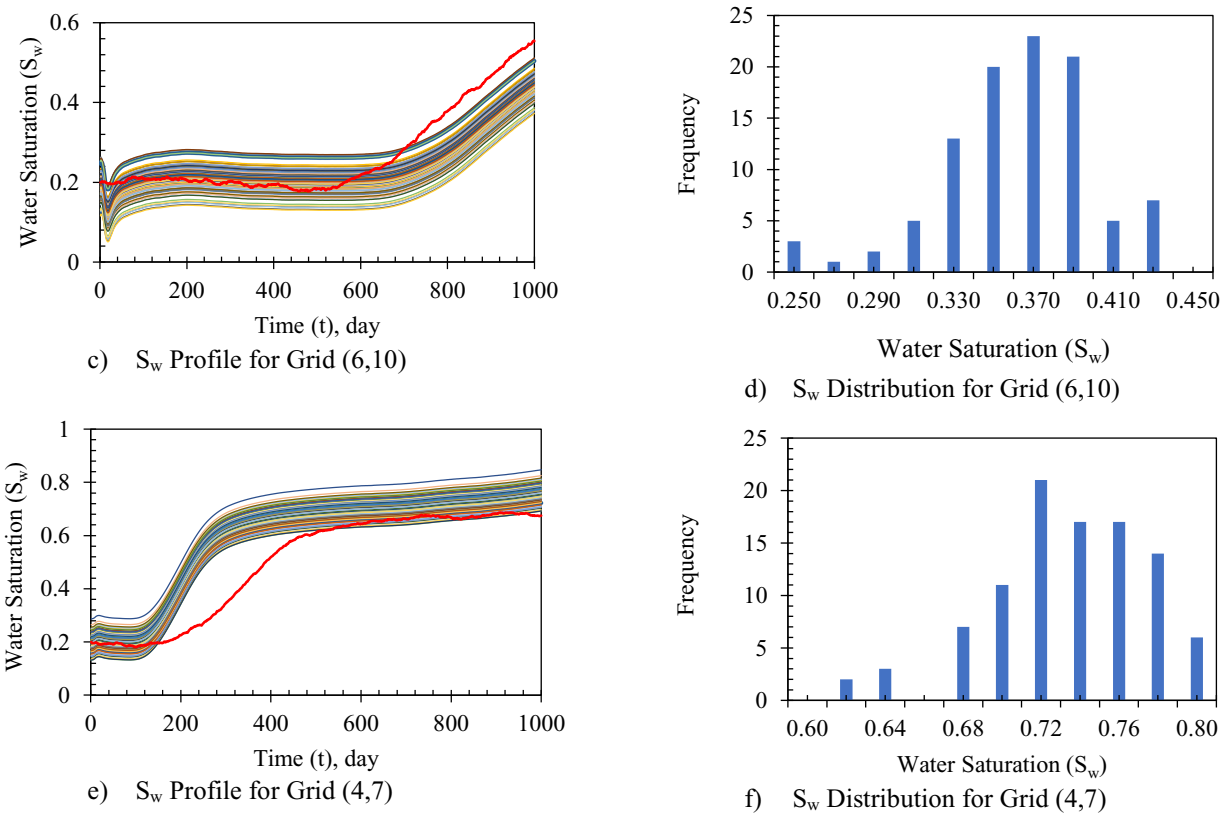

Figure 3-9: Water Saturation Profiles after Assimilation at Three Different Grid Blocks

After implementation of EnKF, water saturation versus time and frequency versus corresponding water saturation distribution are presented in

Figure *3-9*. Analyzing different situations, three observation grid blocks such as (1, 9), (6, 10), and (4, 7) are selected based on waterfront arrival. From

Figure *3-9*a, **9c**, and **9e**, it is found that grid (1, 9) is behind the waterfront area, grid (6, 10) is in the zone of high and low water saturation, and grid (4, 7) stays ahead of the waterfront. Between grids (6, 10) and (4, 7), the injected water first arrives at grid (4, 7) as it is closer to the injection well. For all cases, saturation distribution is plotted using the data taken after 873 days simulation.

It is clear from

Figure *3-9* that for grid (1, 9) the entire ensemble shows almost bell-shaped distribution. This grid is far from the injection well, and the waterfront does not reach after 873 days of simulation.

Therefore, the distribution remains almost Gaussian. However, for grid (4, 7), waterfront already arrived and is fully flooded with the injected water (see

Figure *3-9*c). Approximate Gaussian distribution is also seen for this grid. However, grid (6, 10) stays in a zone with low and high saturation. Therefore, small shifting from bell shaped is observed in water saturation distribution for this grid. It can be concluded that the bimodal distribution in this grid is responsible for this deviation.

Comparative Analysis: Based on the results obtained from PF and EnKF for the three observation grid blocks, a comparative analysis is presented in **Figure 3-10**. For all three-grid blocks, PF exhibits a better match with the model compared to EnKF throughout the entire time (see **Figure 3-10**). From

Figure *3-9*, it is concluded that the shock front does not arrive at grid (1, 9), and grid (4, 7) is fully flooded with water after 873 days of simulation. As a result, an approximate Gaussian distribution is noticed in the water saturation distribution for these two grids. Therefore, a good and consistent agreement is obtained between PF and EnKF with model for these two grids as demonstrated in **Figure 3-10**. On the other hand, grid (6, 10) is in low and high saturation zone, indicating a bimodal distribution. Therefore, after 873 days simulation, EnKF shows a deviation from the model (see **Figure 3-10b**).

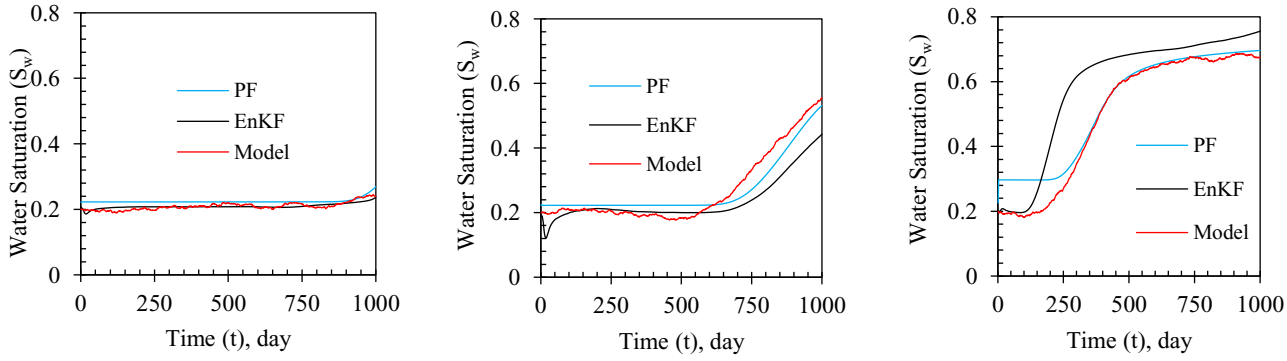

a. S_w Profile for Grid (1,9)

b. S_w Profile for Grid (6,10)

c. S_w Profile for Grid (4,7)

Figure 3-10: Performance of Water saturation Profile by EnKF and PF

For those grid blocks where complete water breakthrough occurs or shock front does not arrive, it is possible to have a good saturation assimilation in those grid blocks upon employing EnKF.

However, PF shows more accurate results according to the error values. The corresponding error analysis based on these results is presented in **Figure 3-11**.

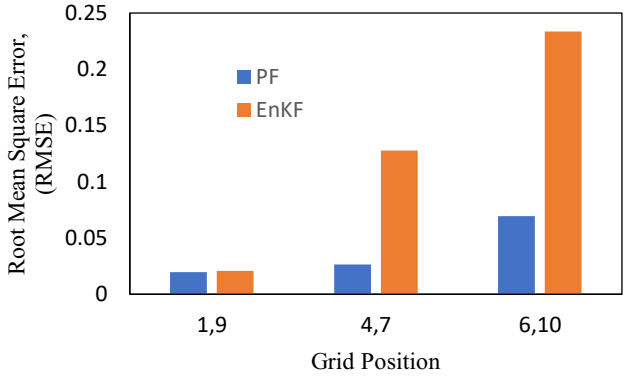

Figure 3-11: Error Analysis in History Matching for Reservoir Case.

Focusing on saturation matching, saturation profiles on the diagonal of P1-P4 and P2-P3 wells are presented in **Figure 3-12** and **Figure 3-13**. Diagonally, all three situations described above will be seen while adapting saturation data. For both diagonal cases, after 1000 days of simulation, the water breakthrough happens near the injection well (grid positions 4 to 6). The results obtained from the EnKF, and PF are in acceptable agreement with the model. This implies that the water saturation distribution is Gaussian around this zone.

In addition, after 500 days of simulation, far from the injection well (grid position 0-2 and 8-10) the waterfront does not arrive; a good match is noticed between the model and both PF and EnKF. As the grid blocks are shifted from the injection well (where there is a presence of bimodal distribution), EnKF produces more erroneous results, compared to PF.

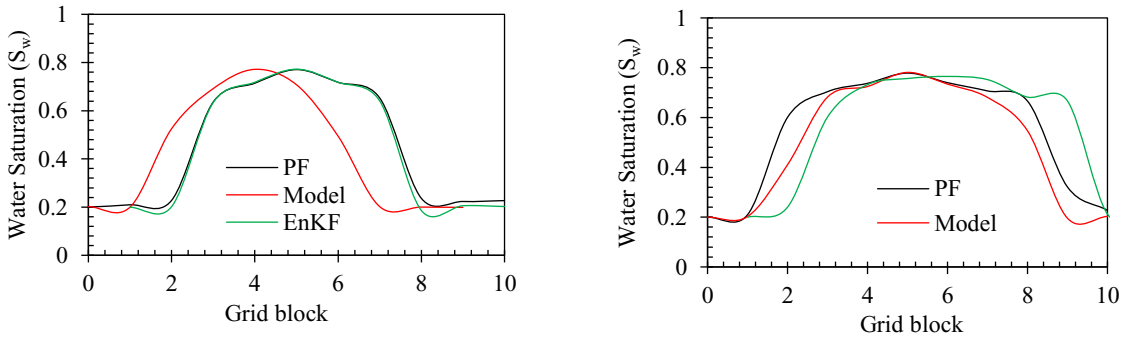

a) S_w updating after 500 days

b) S_w updating after 1000 days

Figure 3-12: Water Saturation Profile on the Diagonal of P1 and P4

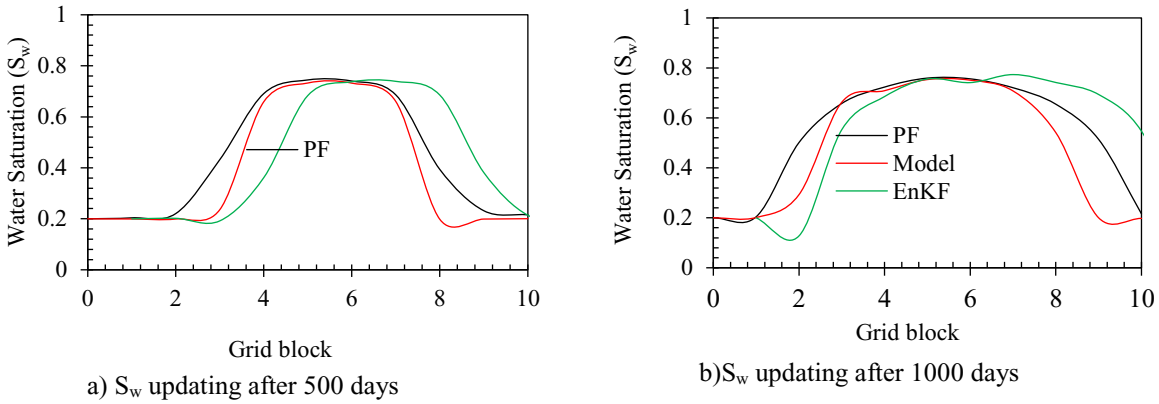

a) S_w updating after 500 days

b)S_w updating after 1000 days

Figure 3-13: Water Saturation Profile on the Diagonal of P2 and P3

Figure 3-14 demonstrates the mean of the saturation profile at the end of 1000 days of simulation.

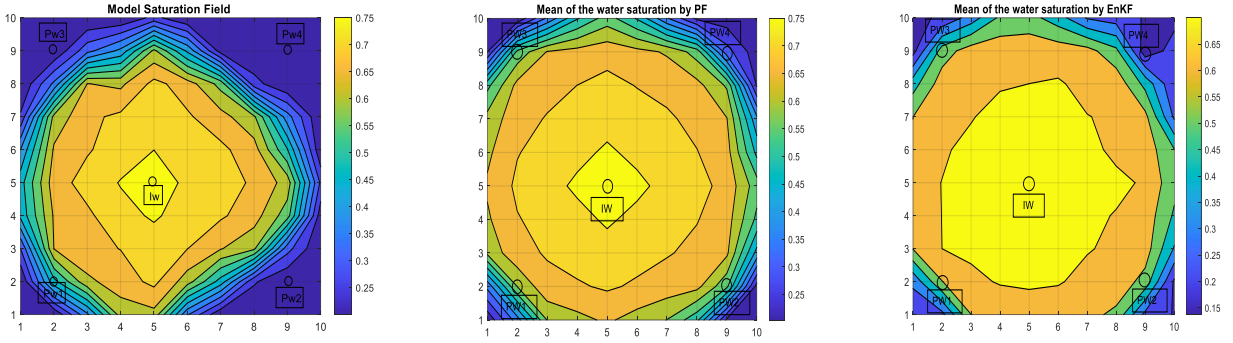

a) Saturation field for model

b) Saturation field by PF

c) Saturation field by EnKF

Figure 3-14: The Mean of the Water Saturation Updated after 1000 Days

It can be concluded that the saturation field updated by PF shows a better match with the model saturation field than EnKF.

3.5.3 Performance of Particle Perturbation

Reservoir parameters (permeability and porosity) are associated with inherent uncertainty; therefore, particle diversity is required to avoid repeated selection of highly weighted particles and thereby ensure correct estimation of these parameters. To increase particle diversity, in each time step, particle perturbation is done using ensemble covariance which is calculated from the updated state and parameter before resampling takes place. To assess the performance of ensemble covariance for particle perturbation, two cases such as "ensemble covariance" and

"randomization" are analyzed in this research work, and the corresponding comparative result is presented in **Figure 3-15**.

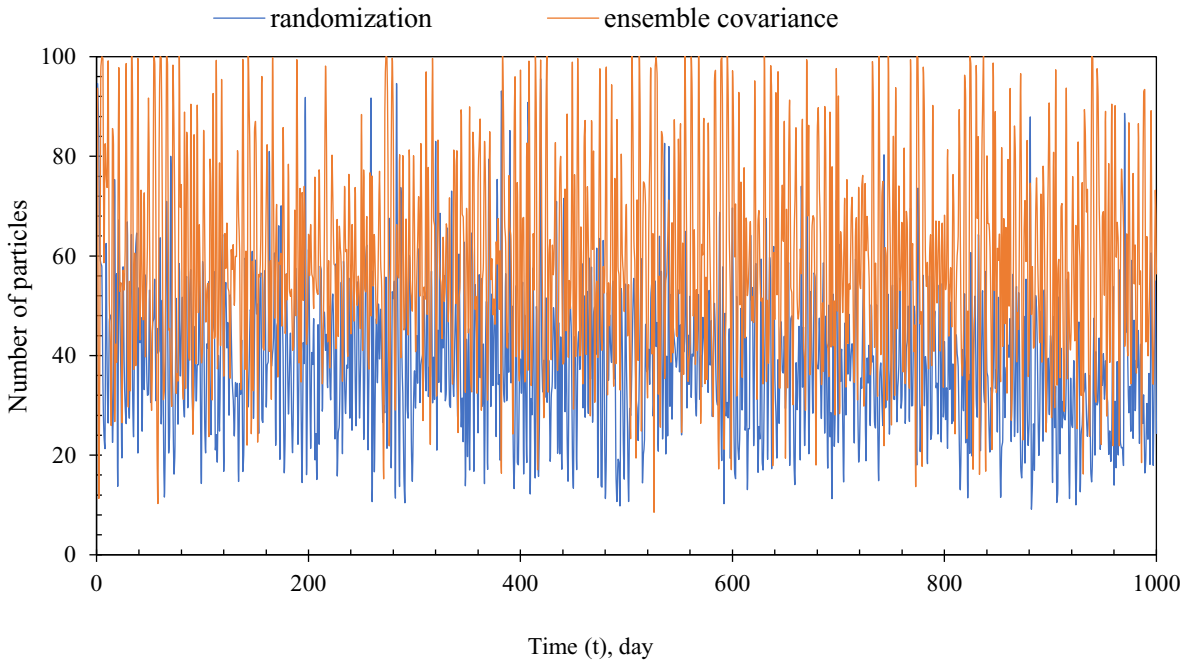

Figure 3-15: Number of Particles Resampled during Simulation

Figure 3-15 shows number of particles that participated in resampling during whole simulation time for two cases "randomization" and "ensemble covariance". It is found that for "ensemble covariance" case, number of resampled particles is higher (orange lines) compared to "randomization" case (blue lines). This indicates that addition of "ensemble covariance" ensures more particles participate in resampling and thus increases particle diversity. The similar impact can be found in parameter estimation.

Based on the analysis presented in **section 3.5.2**, grid (6, 10) shows bimodal distribution. Therefore, this grid block is selected for generating posterior distribution for permeability and porosity estimation for the above two cases.

Figure 3-16 shows the parameter (porosity and permeability) estimation after 1000 days of simulation for two cases "randomization" and "ensemble covariance". In **Figure 3-16**, orange line indicates the reference value, and high probability bar from the distribution represents the estimated value of the corresponding parameter.

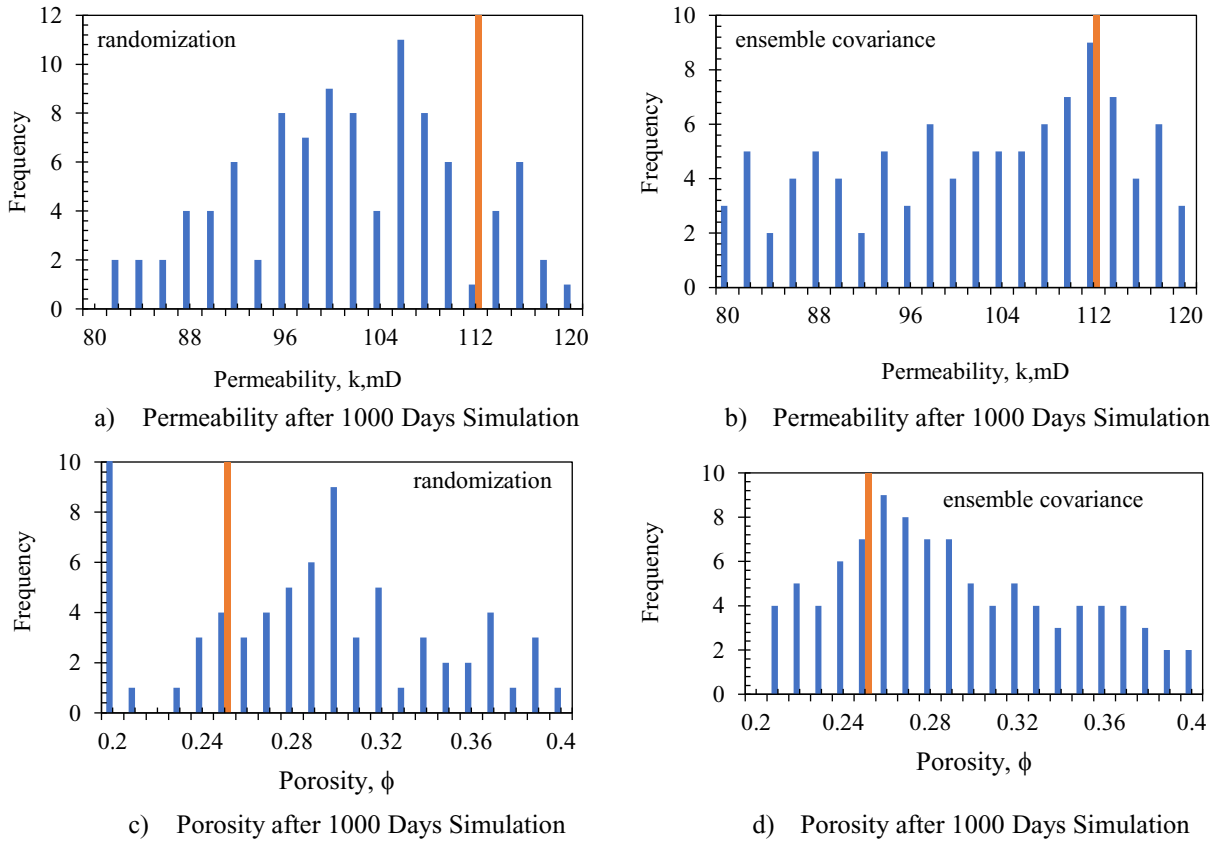

a) Permeability after 1000 Days Simulation

b) Permeability after 1000 Days Simulation

c) Porosity after 1000 Days Simulation

d) Porosity after 1000 Days Simulation

Figure 3-16: Distribution of Model Parameters

From the distribution in **Figure 3-16**, for "ensemble covariance" case the difference between the estimated value and reference value is about 0.884% and 5.76% for the permeability and porosity, respectively. On the other hand, for "randomization" case the difference is about 6.2% and 13.3%, which is higher compared to "ensemble covariance" case. It can be concluded that particle perturbation plays an important role for spreading the ensemble and correct estimation of unknown parameters. Therefore, by ensuring higher number of particles participation in resampling step, "ensemble covariance" can estimate the parameters more accurately.

3.6 Conclusions

This study focuses on the impact of non-Gaussianity in history matching for water flooding in a heterogeneous oil reservoir. Including the presence of non-Gaussianity, two approaches EnKF and PF are applied to the oil-water reservoir. Performance of these methods are compared in terms of history matching and distribution of water saturation. From the analysis, it is found that EnKF is

unable to address the non-Gaussianity and thereby provide poor history matching which leads to poor estimation of the parameter. On the other hand, PF exhibits the ability to conduct the state vector updating through resolution of non-Gaussianity.

Moreover, three observation grid blocks are considered to assess the performance of EnKF and PF. From the results, it is seen that where the non-Gaussianity is weak such as grid (1, 9), the performance of EnKF is competent with PF. However, for strong non-Gaussianity case such as grid (6, 10), EnKF shows RMSE=0.23 which is 4 times higher than PF.

For estimation of the parameters such as permeability and porosity, an approach called "ensemble covariance" is introduced for particle perturbation in the PF. Due to this approach, it is seen that higher number of particles are participating into resampling, leading to a sufficiently accurate estimation. For the representative grid block (6, 10), the error for permeability and porosity estimation is about 0.884 % and 5.76 % whereas the error is about 6.2% and 13.3% for permeability and porosity estimation in case of "randomization".

In this research work, reservoir heterogeneity is considered due to variation of porosity and permeability; however, change in other parameters such as capillary pressure, gravity, and geological facies are ignored. The analysis in this study has been done considering a synthetic oil-water reservoir. Therefore, this study can be extended to real reservoir cases.

Acknowledgements

The researchers gratefully acknowledge and thank Equinor Canada, Memorial University, Innovate NL, and the Natural Sciences and Engineering Research Council of Canada (NSERC) for providing funding for the work.

Nomenclatures

English letters

B_w	Formation volume factor of water and oil respectively res. (ft^3/std. ft^3)
B_o	Formation volume factor of water and oil respectively res. (ft^3/std. ft^3)
C_w	Water compressibility respectively (psi^{-1})
C_o	Oil compressibility respectively (psi^{-1})
C_r	Rock compressibility respectively (psi^{-1})
f_w	Water fraction
h	Thickness of the reservoir (ft)
J	Productivity Index
k	Absolute permeability (mD)
k_{rw}	Relative permeability to water
k_{ro}	Relative permeability to oil
$\vec{K}$	Permeability tensor
n	Covariance of ensemble
N_p	Particle size
P	Reservoir pressure (psi)
P_{wf}	Bottom hole flowing pressure (psi)
q_{inj}	Injection rate (ft^3/day)
q_p	Production rate (ft^3/day)
q_o'''	Flow rate per unit volume, ft^3/day/ ft^3
q_w'''	Flow rate per unit volume, ft^3/day/ ft^3
r_w	Wellbore radius (ft)
r_e	Distance between reservoir outer boundary to wellbore (ft)
r	Tuning factor for particle perturbation
S_w	Water saturation (%)
S_o	Oil saturation (%)
T	Transmissibility
V	Bulk volume (ft^3)
V_{wp}	Coefficient matrix for pressure of water phase
V_{ws}	Coefficient matrix for saturation of water phase

V_{op}	Coefficient matrix for pressure of oil phase
V_{os}	Coefficient matrix for saturation of oil phase
v	Covariance of measurement noise
w	Covariance of system noise
Δx	Grid dimension in x direction (ft)
Δy	Grid dimension in y direction (ft)

Greek symbols

μ_w	Water viscosity (cp)
μ_o	Oil viscosity (cp)
α	Unit conversion factor
ω	Particle weight

Superscripts

t	Time step index
i	Ensemble member index in algorithm
i, j	Grid number index in the reservoir model

References

1. Akter, F., Imtiaz, S., Zendehboudi, S., Hossain, K., 2021. Modified Ensemble Kalman filter for reservoir parameter and state estimation in the presence of model uncertainty. J. Pet. Sci. Eng. 199, 108323. https://doi.org/https://doi.org/10.1016/j.petrol.2020.108323
2. Chen, Y., Oliver, D.S., Zhang, D., 2009. Data assimilation for nonlinear problems by ensemble Kalman filter with reparameterization. J. Pet. Sci. Eng. 66, 1–14. https://doi.org/10.1016/j.petrol.2008.12.002
3. Gu, Y., Oliver, D.S., 2006. The ensemble Kalman filter for continuous updating of reservoir simulation models. J. Energy Resour. Technol. Trans. ASME 128, 79–87. https://doi.org/10.1115/1.2134735
4. Gu, Y., Oliver, D.S., 2005. History matching of the PUNQ-S3 reservoir model using the ensemble Kalman filter. SPE J. 10, 217–224. https://doi.org/10.2118/89942-PA
5. Imtiaz, S.A., Roy, K., Huang, B., Shah, S.L., Jampana, P., 2006. Estimation of states of nonlinear systems using a particle filter, in: 2006 IEEE International Conference on Industrial Technology. IEEE, pp. 2432–2437. https://doi.org/10.1109/ICIT.2006.372687
6. Jansen, J.D., 2013. A systems description of flow through porous media, Springer. https://doi.org/10.1007/978-3-319-00260-6.The
7. Kumar, D., Srinivasan, S., 2019. Ensemble-based assimilation of nonlinearly related dynamic data in reservoir models exhibiting non-Gaussian characteristics. Math. Geosci. 51, 75–107. https://doi.org/10.1007/s11004-018-9762-x
8. Li, L., Srinivasan, S., Zhou, H., Jaime Gomez-Hernandez, J., 2015. Two-point or multiple-point statistics? A comparison between the ensemble Kalman filtering and the ensemble pattern matching inverse methods. Adv. Water Resour. 86, 297–310. https://doi.org/10.1016/j.advwatres.2015.05.014
9. Liao, Q., Zeng, L., Chang, H., Zhang, D., 2019. Efficient history matching using the markov-chain monte carlo method by means of the transformed adaptive stochastic collocation method. SPE J. 24, 1468–1489. https://doi.org/10.2118/194488-PA
10. Lorentzen, R.J., Stordal, A.S., Luo, X., Nævdal, G., 2016. Estimation of production rates by use of transient well-flow modeling and the auxiliary particle filter: Full-scale applications. SPE Prod. Oper. 31, 163–175. https://doi.org/10.2118/176033-PA
11. Manoli, G., Rossi, M., Pasetto, D., Deiana, R., Ferraris, S., Cassiani, G., Putti, M., 2015. An iterative particle filter approach for coupled hydro-geophysical inversion of a controlled

infiltration experiment. J. Comput. Phys. 283, 37–51. https://doi.org/https://doi.org/10.1016/j.jcp.2014.11.035

12. Montzka, C., Moradkhani, H., Weihermüller, L., Franssen, H.-J.H., Canty, M., Vereecken, H., 2011. Hydraulic parameter estimation by remotely-sensed top soil moisture observations with the particle filter. J. Hydrol. 399, 410–421. https://doi.org/https://doi.org/10.1016/j.jhydrol.2011.01.020
13. Qin, J., Liang, S., Yang, K., Kaihotsu, I., Liu, R., Koike, T., 2009. Simultaneous estimation of both soil moisture and model parameters using particle filtering method through the assimilation of microwave signal. J. Geophys. Res. Atmos. 114. https://doi.org/https://doi.org/10.1029/2008JD011358
14. Schniger, A., Nowak, W., Hendricks Franssen, H.J., 2012. Parameter estimation by ensemble Kalman filters with transformed data: Approach and application to hydraulic tomography. Water Resour. Res. 48, 1–18. https://doi.org/10.1029/2011WR010462
15. Tavakoli, R., Srinivasan, S., Wheeler, M.F., 2014. Rapid updating of stochastic models by use of an ensemble-filter approach. SPE J. 19, 500–513. https://doi.org/10.2118/163673-PA
16. Xue, L., Liu, Y., Nan, T., Liu, Q., Jiang, X., 2020. An efficient automatic history matching method through the probabilistic collocation based particle filter for shale gas reservoir. J. Pet. Sci. Eng. 190, 107086. https://doi.org/10.1016/j.petrol.2020.107086
17. Yan, H., DeChant, C.M., Moradkhani, H., 2015. Improving Soil Moisture Profile Prediction With the Particle Filter-Markov Chain Monte Carlo Method. IEEE Trans. Geosci. Remote Sens. 53, 6134–6147. https://doi.org/10.1109/TGRS.2015.2432067
18. Yoon, S., 2016. Ensemble-based reservoir history matching using hyper-reduced-order models. Massachusetts Institute of Technology.
19. Zhang, H., Hendricks Franssen, H.-J., Han, X., Vrugt, J.A., Vereecken, H., 2017. State and parameter estimation of two land surface models using the ensemble Kalman filter and the particle filter. Hydrol. Earth Syst. Sci. 21, 4927–4958. https://doi.org/10.5194/hess-21-4927-2017
20. Zhou, H., Gómez-Hernández, J.J., Hendricks Franssen, H.J., Li, L., 2011. An approach to handling non-Gaussianity of parameters and state variables in ensemble Kalman filtering. Adv. Water Resour. 34, 844–864. https://doi.org/10.1016/j.advwatres.2011.04.014

Chapter 4 : An Effective Approach to Implement Asphaltene Precipitation in Reservoir Simulation

Preface

This chapter addresses an objective of this dissertation as outlined in Section 4.1 which is to analyze the formation damage due to asphaltene precipitation/deposition and its impact on reservoir parameters such as permeability and porosity. The methodology presented in this chapter aims to improve asphaltene precipitation model by introducing modifications resulting in a reduced computation time and perform reservoir simulation, as presented in Section 4.2 and Section 4.3.

I (Farhana Akter) have contributed to Conceptualization, Methodology, Formal Analysis, Investigation, Writing - Original Draft, and Writing - Review & Editing of this work, while Dr. Syed Imtiaz contributed to Conceptualization, Methodology, Formal Analysis, Writing - Review & Editing, Supervision; Dr. Sohrab Zendehboudi contributed to Writing - Review & Editing, and Supervision; Dr. Amer Aborig contributed to Writing - Review & Editing. A version of this chapter has been submitted in the Journal of Fuel.

Abstract

Formation damage due to asphaltene precipitation and deposition in petroleum reservoirs leads to low well productivity. Therefore, analyzing the asphaltene behaviors in terms of precipitation and deposition and its impact on reservoir properties is vital for predicting the production performance of reservoirs containing asphaltene. In this work, pure solid model is employed to predict asphaltene precipitation. Determination of amount of precipitated asphaltene using the solid model requires a series of flash calculations through a trial-and-error procedure. This leads to higher computational time. A modification in pure solid model is introduced for explicit estimation of the asphaltene precipitation in a single-stage flash calculation for each time step, resulting in reduction of computational time. A comparative result between the original and modified solid model at a

sample pressure 2800 psia is presented with respect to asphaltene precipitation calculation. The results show a difference of 9.945% between these two methods.

This work also discusses the simulation of wellbore region of production well in an asphaltic oil reservoir that experiences asphaltene precipitation and deposition. An analysis regarding development of asphaltene precipitation and its consequence on reservoir properties (porosity and permeability) and pressure is presented. For the simulation phase, the black oil model for four phases is developed and a detailed description on mathematical model development is presented. The results from the simulation show that around the wellbore, the asphaltene precipitation is maximum and therefore corresponding damage in permeability and porosity will be at the highest level. In addition, comparing between "asphaltene precipitation" and "no asphaltene precipitation" cases, a difference of 11.23 % in cumulative oil production is observed.

Keywords: Asphaltene Precipitation; Formation Damage; Reservoir Model; Reservoir Simulation; Oil Recovery

4.1 Introduction

The presence of asphaltene in oil reservoirs leads to a complex phenomenon around the production wells. Due to oil production, reservoir pressure declines and oil composition changes (Subramanian et al., 2016). The change in reservoir pressure and oil composition are the two key factors responsible for asphaltene precipitation. When asphaltene starts to precipitate and deposit on the rock surface, a part of formation pore space might be plugged, causing a change in the reservoir rock properties such as porosity and permeability, as well as making unfavorable impact on oil production rate (Subramanian et al., 2016). Modelling of asphaltene precipitation in the reservoir seems important to forecast the amount of precipitated (and deposited) asphaltene and its impact on oil production.

Several studies about the phase diagram of asphaltene rich oil reservoir confirm that asphaltene precipitation starts at a pressure above bubble point pressure called upper asphaltene onset pressure (UAOP) (Civan, 1992; Nghiem, 1999). Above this point, the amount of asphaltene stays in dissolved condition in oil, and the concentration of asphaltene remains steady. As the pressure declines from UAOP, the dissolved asphaltene starts to precipitate with pressure decline.

Asphaltene precipitation reaches to the maximum point at the bubble point pressure. After bubble point, precipitates tend to dissolve back into oil and thereby the amount of precipitation declines with further decrease in pressure(Nghiem, 1999). This situation continues until the reservoir pressure reaches the lower asphaltene onset pressure (LAOP). At or below LAOP, no precipitation occurs, and the amount of dissolved asphaltene reaches its original extent. The phase diagram and solubility of asphaltene are presented **Figure 4-1**.

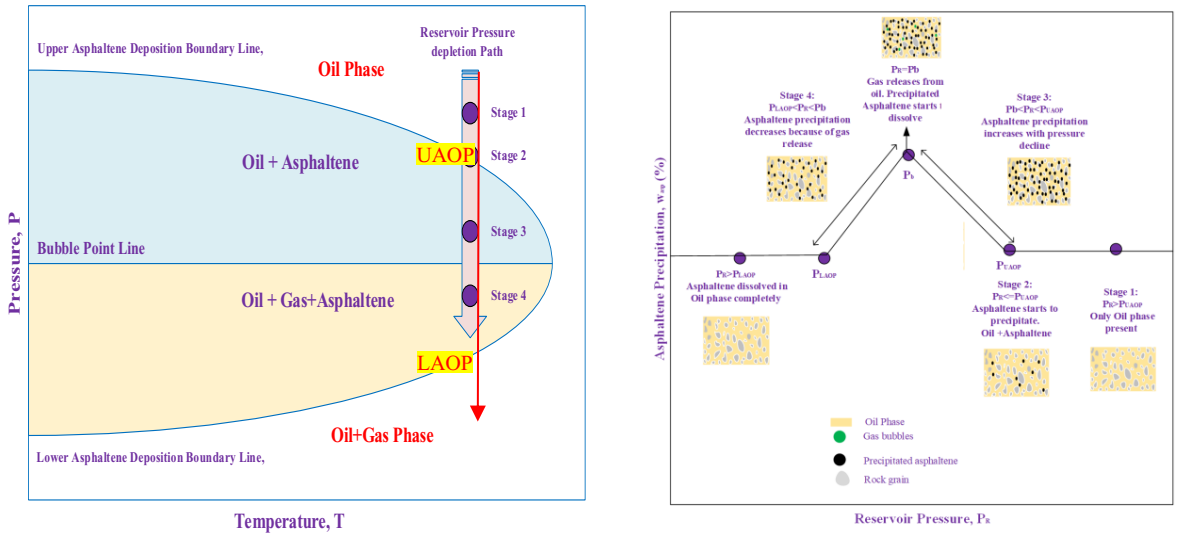

a) Phase Diagram of Asphaltene Precipitation (Gonzalez et al., 2017)

b) Precipitation of Asphaltene in the Crude Oil

Figure 4-1: Phase Diagram and Solubility of Asphaltene

Researchers have proposed various models to predict asphaltene precipitation behaviors such as solubility model, solid model, colloidal model, and micellization model (Almehaideb, 2004). In each model, the asphaltene phase is treated in a different way such as solid phase, liquid phase, and colloidal suspension. Thus, different precipitation models have been developed. All these different models about asphaltene in crude oil and asphaltene precipitation have been combined to define the phase diagram of asphaltene precipitation and asphaltene solubility (Almehaideb, 2004).

The solubility model is based on the Flory-Huggins theory, where the crude oil is split into vapor and liquid phases. In this model, vapor-liquid equilibrium calculations are performed using Soave Redlich-Kwong (SRK) equation of state (EoS). Later, the liquid phase is divided into oil rich solvent phase and asphalt phase. The amount of asphaltene precipitation is calculated from the liquid phase, assuming that the precipitated asphaltene does not change the vapor/liquid

equilibrium (Hirschberg et al., 1984; Pan and Firoozabadi, 2000; Wang and Civan, 2001). Statistical Associating Fluid Theory (SAFT) EoS is also widely used as it takes the influence of association and non-spherical chain of molecules into consideration (Mohebbinia et al., 2017). Considering modelling of asphaltene precipitation by the SAFT theory, Perturbed-Chain SAFT (PC-SAFT) has exhibited a successful performance for calculating asphaltene precipitation (Alimohammadi et al., 2019).

In the solid model, asphaltene is treated as a single component in the solid phase; the method requires calculating some empirical parameters such as molar volume of asphaltene, reference pressure, and fugacity of asphaltene at reference pressure. Those empirical parameters are determined by tuning through matching the experimental data. The amount of asphaltene precipitation is calculated by equating the fugacity of asphaltene in the solid and liquid phases (Kohse and Nghiem, 2004; Nghiem, 1999; Nghiem and Coombe, 1997).

The colloidal solution model considers asphaltene as solid particles in a colloidal suspension stabilized by adsorbed resins on asphaltene surface (Correra and Donaggio, 2000; Leontaritis and Mansoori, 1988). In the thermodynamic micellization mode, the asphaltene molecules are assumed to form a micelle core and the resin molecules adsorb onto the core surface to stabilize the micelle. The principle of the minimization of the Gibbs free energy is used to determine the micelle structure and concentration (Pan and Firoozabadi, 2000, 1998).

Apart from the methods mentioned above, researchers also have used scaling equations for rapid estimation of asphaltene precipitation. However, associated nonlinearity in the scaling equations for asphaltene precipitation calculation requires tuning of the input parameters such as pressure, molecular weight, API gravity of the crude oil, and dilution ratio. In this regard, application of smart technology makes an effort to eliminate the limitations regarding applicability of the scaling equations. Sayyad Amin et al. (2017) used a predictive tool named as response surface methodology (RSM) for accurate estimation of asphaltene precipitation. Their research work is based on finding important factors such as diluent, dilution ratio, pressure, molecular weight that have major impacts on asphaltene precipitation and corresponding interactions between the parameters. Ahmadi (2011) proposed imperialist competitive algorithm (ICA) for optimizing weights of feed forward neural network model for asphaltene precipitation prediction. Ahmadi and Shadizadeh (2012) conducted a research work on Northern Persian Gulf Oil Field for asphaltene

precipitation. In their work, a model was developed based on feed forward ANN and the model was optimized by particle swarm optimization (PSO) to predict asphaltene precipitation. A similar approach is also applied by Zendehboudi et al. (2014) to investigate the impact of parameters such as temperature, pressure, dilution ratio, and composition on asphaltene precipitation for the cases in the presence and absence of CO_2 injection. Chamkalani et al. (2014) developed a scaling equation in terms of temperature, molecular weight, and dilution ratio, and proposed a methodology based on the least square support vector machines/regression (LSSVM/LSSVR) to perform nonlinear modeling. Menshad et al. (2008) determined onset of asphaltene precipitation by applying a scaling equation (as a function of pressure) linked with genetic algorithm (GA). Sayyad Amin et al. (2010) implemented Bayesian Belief Network (BBN) as an ANN tool to analyze the impact of input parameters such as diluent, dilution ratio, pressure, molecular weight on asphaltene precipitation based on the scaling theory.

According to the solid model proposed by Nghiem et al. (1993), the heaviest component in the oil sample is divided into precipitating and non-precipitating parts, and the precipitating part is considered as a pure dense asphaltene. For calculating the fugacity of asphaltene in the solid phase, an empirical relationship called solid model is employed. Along with the solid model, an EoS is also used to model the liquid and gas phase equilibrium. At each pressure, the thermodynamic equilibrium between all phases determines whether asphaltene will precipitate or not. Thermodynamic equilibrium between all phases is established through a series of flash calculations and the stability check in each step. Once the equilibrium is established, the amount of asphaltene is calculated. Therefore, the asphaltene precipitation calculation involves both flash calculation and stability test between phases. To reach the thermodynamic equilibrium between all phases, the flash calculation and stability test are repeated several times in each time step. This approach is time-consuming and makes the calculation very slow. Furthermore, for reservoir simulation, the reservoir is split into many grid blocks and calculations are performed for individual grids. This increases computation time and requires more resources. Considering the importance of computational time for reservoir simulation, the goal of this work is to introduce a modification in the flash calculation so that it does not require repeated calculations and the amount of asphaltene can be calculated explicitly at each time step.

Through reservoir simulation studies, researchers get clear picture about the impact of precipitated asphaltene on reservoir parameters such as permeability and porosity. The detailed approach regarding reservoir modelling is presented in this work. In addition, different scenarios are shown to assess the vicinity of the wellbore and corresponding reservoir parameters (porosity/permeability). To fulfill the objective, a reservoir is modelled considering four phases (oil, water, gas, and asphaltene) and black oil model is followed. The flow equations for four phases are discretized, and a detailed numerical scheme is presented. To solve the flow equations, the equations are presented in the state-space form.

This manuscript is organized as follows: **Section 4.2** includes the theory and mathematical formulation of asphaltene precipitation. In this section, a detailed description regarding pure solid model is discussed. At the end of this section, the modification in flash calculation is presented. State space representation of reservoir model, application of asphaltene precipitation model to reservoir, and a detailed flow chart of reservoir simulation are presented in **Section 4.3**. **Section 4.4** includes results and discussion on asphaltene precipitation and model validation with experimental data, sensitivity analysis on asphaltene precipitation, and reservoir simulation involving impact of asphaltene precipitation on reservoir rock properties. Finally, **Section 4.5** introduces the main conclusions of the whole work.

4.2 Theory and Formulation of Asphaltene Precipitation

In this work, the solid model is used for asphaltene precipitation calculation. This model assumes that precipitated asphaltene is a part of the heaviest component of the oil mixture, and precipitated asphaltene is treated as a pure and immobile solid. The solid model is used to calculate the fugacity of precipitated asphaltene. In addition, gas and oil phases are modelled by an EoS. In this work, Peng-Robinson (PR) EoS is used to calculate the fugacity of oil and gas phases. In this section, a detailed description is provided regarding characterization of asphaltene and flowchart for asphaltene precipitation calculation.

4.2.1 Solid Model

The precipitated asphaltene is a pure dense phase and referred to as asphaltene phase. The fugacity of asphaltene in the asphaltene phase (f_a) is given below:

$$ln f_a = ln f_a^* + \frac{V_a(P - P^*)}{RT} \quad (4\text{-}1)$$

The accurate estimation of three parameters, such as reference pressure(P^*), fugacity of asphaltene at reference pressure (f_a^*), and molar volume of dissolved asphaltene (V_a) in Eq. (4-1) is important as they are required for calculating fugacity of precipitated asphaltene. A brief discussion regarding estimation of these three parameters is presented below.

P^* stands for the reference pressure. This parameter is calculated from the experimental data of asphaltene precipitation. Using the experimental data, the first two high-pressure points are linearly extrapolated to zero weight percentage (0%) of the precipitate, and the pressure corresponding to this point is called the reference pressure (P^*).

f_a^* introduces the fugacity at the reference pressure (P^*). The asphaltene precipitation is zero and the asphaltene stays in the oil phase in the dissolved condition. Therefore, the fugacity of the dissolved asphaltene in the oil phase is calculated using PR EoS and named as f_a^*.

V_a represents the molar volume of dissolved asphaltene in the oil phase at the reference pressure (P^*). This parameter is calculated by using PR EoS. V_a is assumed to be constant at various pressures.

4.2.2 Characterization of Asphaltene Component

In this work, asphaltene is treated as pure/single component. Since the oil sample contains dozens of components and asphaltene is present in the heaviest component (C7+), asphaltene component characterization is important for thermodynamic equilibrium calculation. The general approach is that the heaviest component is split into number of single number carbon fractions and residual component. The residual component is further divided into two components where one of the components is defined as asphaltene. The split and different features of the residual component are displayed below in **Figure 4-2**. From the figure it is shown that crude oil mixture has n_c number of components and n_c-th component is defined as the heaviest component. This heaviest component is split into two parts: precipitating and non-precipitating components. These two parts

have identical critical properties and acentric factors but have different interaction coefficients with lighter components.

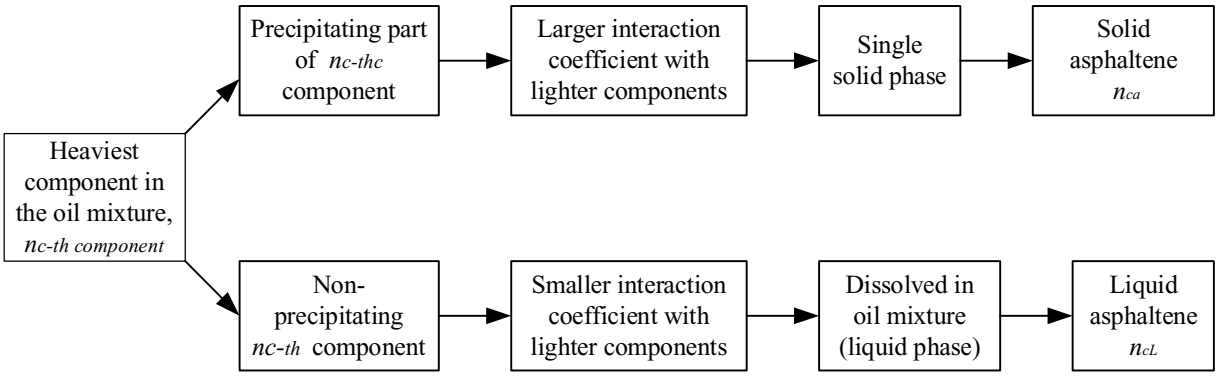

Figure 4-2: Characterization of Asphaltene Component

The precipitating component is considered as asphaltene and treated as a pure solid while non-precipitating component is considered as liquid phase. After asphaltene characterization, the components are lumped into small groups, resulting in lower number of components. Thus, this approach reduces computational time.

4.2.3 Calculation of Binary Interaction Coefficients

Binary interaction coefficients between components are determined in two steps. In the first step, the binary interactions (d_{ik}) for components starting from 1 to $(n_c - 1)$ is computed by the following equation:

$$d_{ik} = 1 - \left(\frac{2V_{ci}^{1/6} V_{ck}^{1/6}}{V_{ci}^{1/6} + V_{ck}^{1/6}} \right)^{e} \qquad (4\text{-}2)$$

Here, V_c is the critical volume of the component and e is the exponent.

In the second step, the interaction between the heaviest component and lighter components are determined through regression analysis by matching the experimental data of asphaltene precipitation (Nghiem et al., 1993).

4.2.4 Thermodynamic Equilibrium

Over production process, the reservoir pressure declines, and the reservoir oil might experience different phase changes. For oil containing asphaltene, three phases (e.g., liquid, vapor, and solid) can be found at pressure ranges.

Figure 4-1(a) shows the existence of three phases in a mixture of n_c components.

When the vapor, liquid and asphaltene phases coexist, the thermodynamic equilibrium condition is defined as follows:

$$lnf_{iv} = lnf_{il} \quad \{for\ i = 1,2 \dots \dots \dots n_c - 1\} \tag{4-3}$$

$$lnf_{n_c v} = lnf_{n_c l} = lnf_a \tag{4-4}$$

The fugacity *(f)* of each component in the liquid *(l)* and gas *(v)* phases is calculated using EoS, and the fugacity of asphaltene (f_a) can be determined using Eq. (4-1).

4.2.5 Stability Test for Asphaltene Precipitation

The stability test is performed to determine whether asphaltene will be precipitated from the liquid mixture or not. The following criterion governs the existence of the solid asphaltene phase.

$$lnf_{n_c l} > lnf_a \tag{4-5}$$

The amount of asphaltene precipitation is calculated by satisfying the following equilibrium condition:

$$lnf_{n_c l} = lnf_a \tag{4-6}$$

Using the information and equations given in sections from 4.2.1 to 4.2.5, the asphaltene precipitation model is established. The flowchart for asphaltene precipitation calculation is presented in **Figure 4-3**. It is assumed that the oil sample is taken from the reservoir at a pressure of P_R and temperature *T*. *R* and z_i are defined as the universal gas constant and composition of the oil sample, respectively.

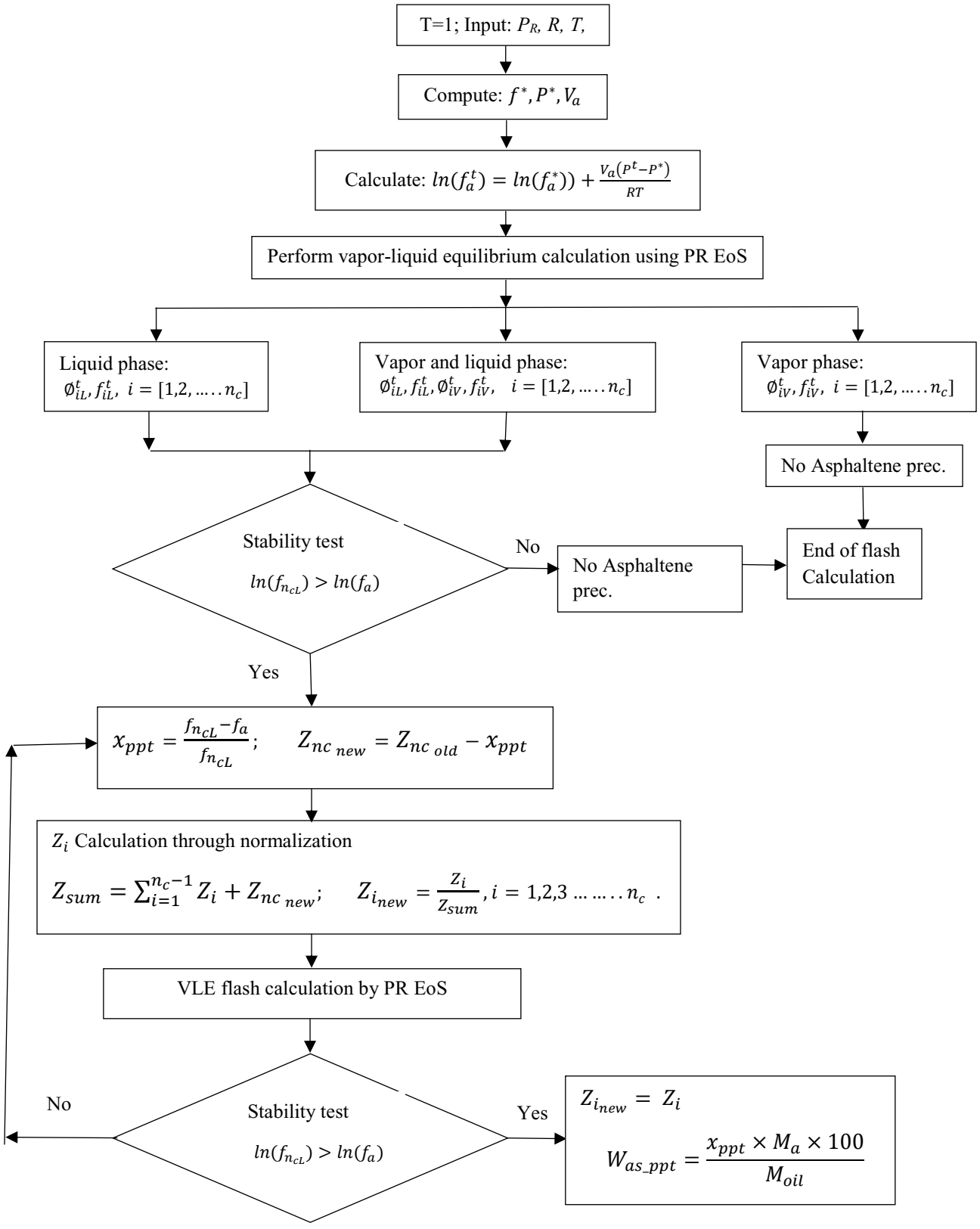

Figure 4-3: Flowchart for Asphaltene Precipitation Calculation

4.2.6 Modification in Estimation of Asphaltene Precipitation

In the solid model, asphaltene is considered as a pure solid and contains only one component. Therefore, the fugacity of asphaltene can be calculated using Eq. (4-1) at any condition directly. The equilibrium condition presented in Eq. (4- 7) can be used to equate the fugacity value between the solid and liquid phases, as shown below.

$$f_{nc_L}^{t+1} = f_{nc_L}^{t} + \Delta f_{nc_L}^{t} = f_a^{t+1} = f_a^t + \Delta f_a^t \qquad (4\text{-}7)$$

For asphaltene precipitation calculation, the equilibrium condition between the phases should be met. Therefore, we can write:

At time step t, $f_{nc_L}^{t} = f_a^t$ and at time step $t+1$, $f_{nc_L}^{t+1} = f_a^{t+1}$.

Thus, based on Eq. (4-7), $\Delta f_{nc_L}^{t} = \Delta f_a^t$.

Using Eq. (4-1), the following relationship can be written:

$$\Delta f_a^t = f^* \left(e^{\frac{V_a(P^{t+1}-P^*)}{RT}} - e^{\frac{V_a(P^{t}-P^*)}{RT}} \right) \qquad (4\text{-}8)$$

Introduction of Eq. (4-7) and (4-8) provides a way to estimate the amount of asphaltene precipitation explicitly for each time step in the single flash calculation. The brief procedure is given in **Figure 4-4**.

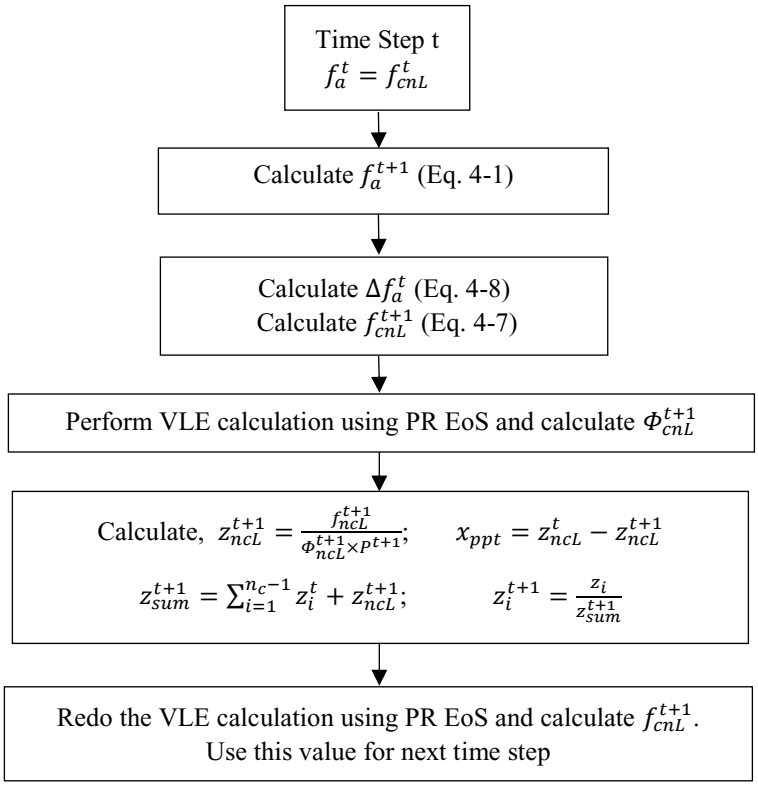

Figure 4-4: Modification in Flash Calculation

Introduction of this modification avoids the trial-and-error calculation in the flash calculation and saves considerable time in determining the asphaltene precipitation in the single flash calculation in each step.

4.3 Reservoir Model

The modified precipitation model is combined with a multiphase (e.g., oil, water, gas, and asphaltene) reservoir model to observe the effect of precipitation on reservoir rock properties and subsequently on production rate. The modeled reservoir is an asphaltene rich crude oil reservoir with a single production well.

4.3.1 Reservoir Description

A synthetic 2D reservoir model with the dimension of 100 ft ×100 ft ×50 ft and 10 × 10 × 1 grids are generated as shown in **Figure 4-5**. No flow boundary condition is considered for all sides of the reservoir. The reservoir's initial pressure is 5260 psi. There is a production well in the grid block (5, 5) in the reservoir. Production rate is set at 300 ft^3/d with a minimum bottomhole pressure

of 1000 psi. The reservoir porosity is 0.2 and the permeability is equal to 100 mD. The reservoir is assumed homogeneous in terms of porosity and permeability. Initially, the reservoir is assumed to be under saturated and filled with oil; the saturation of connate water is 0.2. When the reservoir reaches the bubble point, gas starts to evolve; the critical gas saturation is assumed to be 0.05.

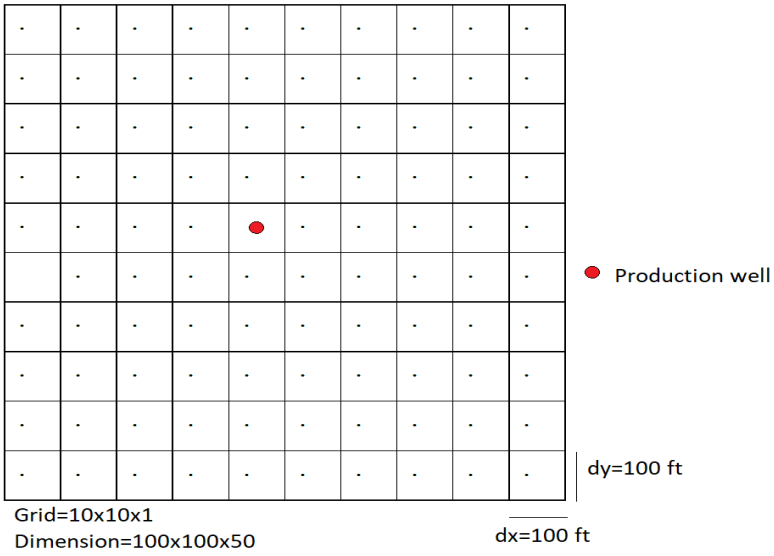

Figure 4-5: 2D Reservoir with Grid Dimension and Well Location

4.3.2 Parameterization and Mathematical Formulation

In this analysis, reservoir fluid flow equations are presented in state-space from. The augmented state vector consists of two static vectors (porosity and permeability) and four dynamic vectors namely four-phase saturation and pressure. The discretized partial differential equations of the four-phase reservoir are given below:

Water phase:

$$V\left[\frac{\emptyset S_w}{B_w}(c_w + c_r)\frac{\partial p}{\partial t} + \frac{\emptyset}{B_w}\frac{\partial s_w}{\partial t}\right]_{i,j} - (T_w)_{i-\frac{1}{2},j}p_{i-1,j} - (T_w)_{i,j-\frac{1}{2}}p_{i,j-1}$$
$$+ \left[(T_w)_{i-\frac{1}{2},j} + (T_w)_{i,j-\frac{1}{2}} + (T_w)_{i+\frac{1}{2},j} + (T_w)_{i,j+\frac{1}{2}}\right]p_{i,j} - (T_w)_{i+\frac{1}{2},j}p_{i+1,j} - (T_w)_{i,j+\frac{1}{2}}p_{i,j+1}$$
$$= [q_w]_{i,j} \qquad (4\text{-}9)$$

Oil phase:

$$V\left[\emptyset S_o\left(\frac{\partial B_o}{\partial p}+\frac{c_r}{B_o}\right)\frac{\partial p}{\partial t}-\frac{\emptyset}{B_o}\left(\frac{\partial s_w}{\partial t}+\frac{\partial s_g}{\partial t}+\frac{\partial s_a}{\partial t}\right)\right]_{i,j}-(T_o)_{i-\frac{1}{2},j}p_{i-1,j}-(T_o)_{i,j-\frac{1}{2}}p_{i,j-1}$$
$$+\left[(T_o)_{i-\frac{1}{2},j}+(T_o)_{i,j-\frac{1}{2}}+(T_o)_{i+\frac{1}{2},j}+(T_o)_{i,j+\frac{1}{2}}\right]p_{i,j}-(T_o)_{i+\frac{1}{2},j}p_{i+1,j}-(T_o)_{i,j+\frac{1}{2}}p_{i,j+1}$$
$$=[q_o]_{i,j} \quad (4\text{-}10)$$

Gas phase:

$$V\left[\left\{\emptyset S_g\left(\frac{\partial B_g}{\partial p}+\frac{c_r}{B_o}\right)+\frac{R_{so}\emptyset S_o}{5.615}\left(\frac{\partial B_o}{\partial p}+\frac{c_r}{B_o}\right)+\emptyset S_o\frac{\frac{\partial R_{so}}{\partial p}}{5.615B_o}\right\}\frac{\partial p}{\partial t}-\frac{R_{so}\emptyset}{5.615B_o}\left(\frac{\partial s_w}{\partial t}+\frac{\partial s_a}{\partial t}\right)+\left(\frac{\emptyset}{B_g}-\frac{R_{so}\emptyset}{5.615B_o}\right)\frac{\partial s_g}{\partial t}\right]_{i,j}$$
$$-\left(T_g+R_{so}T_o\right)_{i-\frac{1}{2},j}p_{i-1,j}-\left(T_g+R_{so}T_o\right)_{i,j-\frac{1}{2}}p_{i,j-1}$$
$$+\left[\left(T_g+R_{so}T_o\right)_{i-\frac{1}{2},j}+\left(T_g+R_{so}T_o\right)_{i,j-\frac{1}{2}}+\left(T_g+R_{so}T_o\right)_{i+\frac{1}{2},j}+\left(T_g+R_{so}T_o\right)_{i,j+\frac{1}{2}}\right]p_{i,j}$$
$$-\left(T_g+R_{so}T_o\right)_{i+\frac{1}{2},j}p_{i+1,j}-\left(T_g+R_{so}T_o\right)_{i,j+\frac{1}{2}}p_{i,j+1}$$
$$=\left[q_g+R_{so}q_o\right]_{i,j} \quad (4\text{-}11)$$

Asphaltene phase:

$$V\left[\left\{\emptyset S_a\frac{c_r}{B_a}+R_a\emptyset S_o\left(\frac{\partial B_o}{\partial p}+\frac{c_r}{B_o}\right)\right\}\frac{\partial p}{\partial t}-\frac{R_a\emptyset}{B_o}\left(\frac{\partial s_w}{\partial t}+\frac{\partial s_g}{\partial t}\right)+\left(\frac{\emptyset}{B_a}-\frac{R_a\emptyset}{B_o}\right)\frac{\partial s_a}{\partial t}\right]_{i,j}-(T_a+R_aT_o)_{i-\frac{1}{2},j}p_{i-1,j}$$
$$-(T_a+R_aT_o)_{i,j-\frac{1}{2}}p_{i,j-1}$$
$$+\left[(T_a+R_aT_o)_{i-\frac{1}{2},j}+(T_a+R_aT_o)_{i,j-\frac{1}{2}}+(T_a+R_aT_o)_{i+\frac{1}{2},j}+(T_a+R_aT_o)_{i,j+\frac{1}{2}}\right]p_{i,j}$$
$$-(T_a+R_aT_o)_{i+\frac{1}{2},j}p_{i+1,j}-(T_a+R_aT_o)_{i,j+\frac{1}{2}}p_{i,j+1}$$
$$=\left[\frac{S_a}{S_o}q_o+R_aq_o\right]_{i,j}+\left[\frac{1}{B_a}\frac{\partial E_a}{\partial t}\right]_{i,j} \quad (4\text{-}12)$$

Here,

$$T_{i-\frac{1}{2},j}=\frac{\Delta x\,h}{\Delta y}\lambda_{i-\frac{1}{2},j} \quad (4\text{-}13)$$

$$T_{i,j-\frac{1}{2}}=\frac{\Delta x\,h}{\Delta y}\lambda_{i,j-\frac{1}{2}} \quad (4\text{-}14)$$

$$\lambda_{i-\frac{1}{2},j}=\frac{k_rk_{i-\frac{1}{2},j}}{\mu B} \quad (4\text{-}15)$$

$$S_w+S_o+S_g+S_a=1 \quad (4\text{-}16)$$

Since asphaltene is present in the oil mixture/sample as suspension, it is assumed that the velocity of oil and asphaltene will be equal.

Therefore, the transmissibility for the oil and asphaltene is calculated as follows:

$$T_{oi-\frac{1}{2},j} = \frac{\Delta x\, h}{\Delta y} \frac{S_o}{S_a + S_o} \lambda_{oi-\frac{1}{2},j} \tag{4-17}$$

$$T_{ai-\frac{1}{2},j} = \frac{\Delta x\, h}{\Delta y} \frac{S_a}{S_a + S_o} \lambda_{ai-\frac{1}{2},j} \tag{4-18}$$

$$V = \Delta x \times \Delta y \times h \tag{4-19}$$

Assuming a constant total production, the flow rate of each phase is calculated using the following equations:

$$q_w = \frac{\lambda_w}{\lambda_w + \lambda_o + \lambda_g + \lambda_a} q_{tp} \tag{4-20}$$

$$q_g = \frac{\lambda_w}{\lambda_w + \lambda_o + \lambda_g + \lambda_a} q_{tp} + \frac{R_{so}}{5.615} q_o \tag{4-21}$$

$$q_o = \frac{\lambda_w}{\lambda_w + \lambda_o + \lambda_g + \lambda_a} q_{tp} \tag{4-22}$$

$$q_a = \frac{\lambda_w}{\lambda_w + \lambda_o + \lambda_g + \lambda_a} q_{tp} + R_a q_o \tag{4-23}$$

In Eq. (4-20) to (4-23*)*, q_{tp} refers to the total production rate of the reservoir.

The state- space formulation of the reservoir model is presented in Eq. (4-24):

$$\begin{bmatrix} \begin{bmatrix} V_{wp} & V_{wsw} \\ V_{op} & V_{osw} \end{bmatrix} & \begin{bmatrix} V_{wsg} & V_{wsa} \\ V_{osg} & V_{osa} \end{bmatrix} \\ \begin{bmatrix} V_{gp} & V_{gsw} \\ V_{ap} & V_{asw} \end{bmatrix} & \begin{bmatrix} V_{gsg} & V_{gsa} \\ V_{asg} & V_{asa} \end{bmatrix} \end{bmatrix} \times \begin{bmatrix} \frac{dp}{dt} \\ \frac{dS_w}{dt} \\ \frac{dS_g}{dt} \\ \frac{dS_a}{dt} \end{bmatrix} + \begin{bmatrix} \begin{bmatrix} T_o & 0 \\ T_w & 0 \end{bmatrix} & \begin{bmatrix} 0 & 0 \\ 0 & 0 \end{bmatrix} \\ \begin{bmatrix} T_g & 0 \\ T_a & 0 \end{bmatrix} & \begin{bmatrix} 0 & 0 \\ 0 & 0 \end{bmatrix} \end{bmatrix} \times \begin{bmatrix} p \\ S_w \\ S_g \\ S_a \end{bmatrix} = \begin{bmatrix} q_o \\ q_w \\ q_g \\ q_a \end{bmatrix} + \begin{bmatrix} 0 \\ 0 \\ 0 \\ c \end{bmatrix} \left[\frac{dE_a}{dt}\right] \tag{4-24}$$

Here,

$$p = \begin{bmatrix} p_{i,j-1} & \dots & p_{i-1,j} & p_{i,j} & p_{i+1,j} & \dots & p_{i,j+1} \end{bmatrix};\ S_w = \begin{bmatrix} S_{w_{i,j-1}} & \dots & S_{w_{i-1,j}} & S_{w_{i,j}} & S_{w_{i+1,j}} & \dots & S_{w_{i,j+1}} \end{bmatrix}$$

$$k = \begin{bmatrix} k_{i,j-1} & \dots\dots & k_{i-1,j} & k_{i,j} & k_{i+1,j} & \dots\dots & k_{i,j+1} \end{bmatrix};\ \emptyset = \begin{bmatrix} \emptyset_{\mathrm{i,j-1}} & \dots\dots & \emptyset_{\mathrm{i-1,j}} & \emptyset_{\mathrm{i,j}} & \emptyset_{\mathrm{i+1,j}} & \dots\dots & \emptyset_{\mathrm{i,j+1}} \end{bmatrix}$$

$$V_{wp} = V(c_w + c_r)[0 \quad \dots \quad \emptyset_{i,j} \times (S_w)_{i,j} \quad 0 \quad \dots \quad 0];\ V_{op} = V\left[0 \quad \dots \quad \left\{\emptyset S_o \left(\frac{\partial B_o}{\partial p} + \frac{c_r}{B_o}\right)\right\}_{i,j} \quad 0 \quad \dots \quad 0\right]$$

$$V_{gp} = V\left[0 \quad \dots \quad \left\{\emptyset S_g \left(\frac{\partial B_g}{\partial p} + \frac{c_r}{B_o}\right) + \frac{R_{so}\emptyset S_o}{5.615}\left(\frac{\partial B_o}{\partial p} + \frac{c_r}{B_o}\right) + \emptyset S_o \frac{\frac{\partial R_{so}}{\partial p}}{5.615 B_o}\right\}_{i,j} \quad 0 \quad \dots \quad 0\right]$$

$$V_{ap} = V\begin{bmatrix} 0 & \dots & \left\{\emptyset S_a \frac{c_r}{B_a} + R_a \emptyset S_o \left(\frac{\partial B_o}{\partial p} + \frac{c_r}{B_o}\right)\right\}_{i,j} & 0 & \dots & 0 \end{bmatrix}$$

$$V_{wsw} = V[0 \quad \dots \quad \emptyset_{i,j} \quad 0 \quad \dots \quad 0]; \qquad V_{wsg} = 0; \qquad V_{wsa} = 0$$

$$V_{osw} = V_{osg} = V_{osa} = -V\begin{bmatrix} 0 & \dots & \left\{\frac{\emptyset}{B_o}\right\}_{i,j} & 0 & \dots & 0 \end{bmatrix};$$

$$V_{gsw} = V_{gsa} = -V\begin{bmatrix} 0 & \dots & \left\{\frac{R_{so}\emptyset}{5.615B_o}\right\}_{i,j} & 0 & \dots & 0 \end{bmatrix}; \qquad V_{gsg} = -V\begin{bmatrix} 0 & \dots & \left\{\frac{\emptyset}{B_g} - \frac{R_{so}\emptyset}{5.615B_o}\right\}_{i,j} & 0 & \dots & 0 \end{bmatrix}$$

$$V_{asw} = V_{asg} = -V\begin{bmatrix} 0 & \dots & \left\{\frac{R_a\emptyset}{B_o}\right\}_{i,j} & 0 & \dots & 0 \end{bmatrix}; \qquad V_{asa} = -V\begin{bmatrix} 0 & \dots & \left\{\frac{\emptyset}{B_a} - \frac{R_a\emptyset}{B_o}\right\}_{i,j} & 0 & \dots & 0 \end{bmatrix}$$

$$T_w = \begin{bmatrix} -(T_w)_{i,j-\frac{1}{2}} & \dots & -(T_w)_{i-\frac{1}{2},j} & \left((T_w)_{i,j-\frac{1}{2}} + (T_w)_{i-\frac{1}{2},j} + (T_w)_{i+\frac{1}{2},j} + (T_w)_{i,j+\frac{1}{2}}\right) & -(T_w)_{i+\frac{1}{2},j} & \dots & -(T_w)_{i,j+\frac{1}{2}} \end{bmatrix}$$

$$T_o = \begin{bmatrix} -(T_o)_{i,j-\frac{1}{2}} & \dots & -(T_o)_{i-\frac{1}{2},j} & \left((T_o)_{i,j-\frac{1}{2}} + (T_o)_{i-\frac{1}{2},j} + (T_o)_{i+\frac{1}{2},j} + (T_o)_{i,j+\frac{1}{2}}\right) & -(T_o)_{i+\frac{1}{2},j} & \dots & -(T_o)_{i,j+\frac{1}{2}} \end{bmatrix}$$

$$T_g = \begin{bmatrix} -T_g + R_{so}T_{o_{i,j-\frac{1}{2}}} & \dots & -(T_g + R_{so}T_o)_{i-\frac{1}{2},j} & \left((T_g + R_{so}T_o)_{i,j-\frac{1}{2}} + (T_g + R_{so}T_o)_{i-\frac{1}{2},j} + (T_g + R_{so}T_o)_{i+\frac{1}{2},j} + (T_g + R_{so}T_o)_{i,j+\frac{1}{2}}\right) & -(T_g + R_{so}T_o)_{i+\frac{1}{2},j} & \dots & -(T_g + R_{so}T_o)_{i,j+\frac{1}{2}} \end{bmatrix}$$

$$T_a = \begin{bmatrix} -(T_a + R_aT_o)_{i,j-\frac{1}{2}} & \dots & -(T_a + R_aT_o)_{i-\frac{1}{2},j} & \left((T_a + R_aT_o)_{i,j-\frac{1}{2}} + (T_a + R_aT_o)_{i-\frac{1}{2},j} + (T_a + R_aT_o)_{i+\frac{1}{2},j} + (T_a + R_aT_o)_{i,j+\frac{1}{2}}\right) & -(T_a + R_aT_o)_{i+\frac{1}{2},j} & \dots & -(T_a + R_aT_o)_{i,j+\frac{1}{2}} \end{bmatrix}$$

$$q_w = [\dots \quad (q_w)_{i,j} \quad \dots], \qquad q_g = \begin{bmatrix} \dots & (q_g)_{i,j} & \dots \end{bmatrix}, \qquad q_o = [\dots \quad (q_o)_{i,j} \quad \dots], \qquad q_a = [\dots \quad (q_a)_{i,j} \quad \dots]$$

After simplification, Eq. (4-24) can be rewritten as follows:

$$\begin{bmatrix} p \\ S_w \\ \frac{S_g}{S_a} \end{bmatrix}_{t+1} = A_t \begin{bmatrix} p \\ S_w \\ \frac{S_g}{S_a} \end{bmatrix}_t + B_t[q_{tp}] - E_t + Q_t; \quad Q_t \sim N(0, \Sigma_t^m) \tag{4-25}$$

The corresponding equation for production well *(i,j)* to show the flow rate in terms of other parameters (e.g., fluid and reservoir characteristics) is given below:

$$q_o = \left(\frac{2 \times \pi \times k \times h \times 6.33 \times 10^{-3}}{\left[log\frac{r_e}{r_w} + S\right]}\left[\frac{k_{ro}}{B_o\,\mu_o}\frac{S_o}{S_a + S_o}\right]\right)_t \left[p_{i,j_{t+1}} - p_{prod_{t+1}}\right] = J_{p_t}\left[p_{i,j_{t+1}} - p_{prod_{t+1}}\right] \tag{4-26}$$

$$p_{prod_{t+1}} = p_{i,j_{t+1}} - \left(J_{p_t}\right)^{-1} q_{p_t}; where\ J_{p_t} = \left(\frac{2\times\pi\times k\times h\times 6.33\times10^{-3}}{\left[log\frac{r_e}{r_w}+S\right]}\left[\frac{k_{ro}}{B_o\,\mu_o}\frac{S_o}{S_a+S_o}\right]\right)_t ;$$

The state-space form of the well's flow rate equation can be rewritten as follows:

$$\left[p_{prod}\right]_{t+1} = [1 \quad 0 \quad 0 \quad 0]\begin{bmatrix} p \\ S_w \\ S_g \\ S_a \end{bmatrix}_{t+1} + \left[\left(J_{p_t}\right)^{-1}\right]\left[-q_{tp}\right]_t + R_{t+1}, \quad R_{t+1} \sim N\left(0, \Sigma^y_{t+1}\right) \tag{4-27}$$

4.3.3 Asphaltene Deposition Model

Surface deposition, entrainment, and pore throat plugging create entrapment to porous media; this is responsible for alteration of rock properties. In this study, the following model developed by Wang and Civan (2001) is used for asphaltene deposition:

$$\frac{\partial E_a}{\partial t} = \alpha_a C_a \Phi - \beta E_a\left(v_o - v_{cr,o}\right) + \gamma_i(1+\sigma E_a)u_L C_a \tag{4-28}$$

Here,

E_a = Volume fraction of deposited asphaltene on rock.
C_a = Volume fraction of precipitated asphaltene.
Φ = Porosity of the formation.
v_o, = Interstitial velocity of oil.
$v_{cr,o}$ = Critical value of v_o.
u_L = Darcy velocity of oil.

In Eq. (4-28), the first term ($\alpha_a C_a \Phi$) indicates the surface deposition; the second term $(\beta E_a(v_o - v_{cr,o}))$ reflects the entrainment; and the third term $(\gamma_i(1+\sigma E_a)u_L C_a)$ refers to the pore throat plugging. Among these three terms, surface deposition term is the dominant term (Solaimany-Nazar and Zonnouri, 2011).

After evaluating the deposition rate $(\frac{\partial E_a}{\partial t})$, the deposited asphaltene volume fraction (E_a) is calculated using Eq. (4-29), as given below (Almehaideb, 2004).

$$E_{a_{t+1}} = E_{a\_t} + \frac{\partial E_a}{\partial t}\,\Delta t \tag{4-29}$$

Eq. (4-30) and (4-31) are used to calculate the porosity and permeability at each new time step. For this case, the model developed by Wang and Civan (2001) is followed.

$$\Phi_{t+1} = \Phi_t - E_{a\_t+1} \tag{4-30}$$

$$k_{t+1} = f_p k_t \frac{\Phi_{t+1}}{\Phi_t} \quad (4\text{-}31)$$

Due to lack of experimental data regarding interstitial velocity and critical pore throat diameter, the entrainment effect is neglected. The deposition model constants which are used in this model (Eq. **4-28**) are listed in **Table 4-1**.

Table 4-1: Parameters Used in the Deposition Model (Solaimany-Nazar and Zonnouri, 2011)

Parameter	**Value**	**Parameter**	**Value**
Surface deposition rate (α_a), day^{-1}	0.085	Entrainment rate constant (β), ft^{-1}	0
Critical interstitial velocity ($v_{cr,o}$), ft/day	0	Pore throat plugging constant, (γ_i), ft^{-1}	0.07
Snowball rate constant (σ)	0.1	Coefficient for permeability modification (f_p)	1

4.3.4 Initial and Boundary Conditions

The initial and boundary conditions for the simulation are given below:

At t=0, the reservoir pressure is above upper asphaltene precipitation pressure. Therefore, no precipitated asphaltene exists in the reservoir, and the volume fraction of suspended asphaltene (C_a) and volume fraction of deposited asphaltene (E_a) will be zero in the entire reservoir. Thus, there will be no reduction in reservoir parameters (porosity and permeability).

- *Ca=0, 0<re, 0<z<h, t=0*
- $E_a = 0,\ 0 < r_e,\ 0 < z < h,\ t = 0$
- $\Phi = \Phi_0,\ 0 < r_e,\ 0 < z < h,\ t = 0$
- $k = k_0,\ 0 < r_e,\ 0 < z < h,\ t = 0$

4.3.5 Reservoir Simulation Flowchart

For the analysis of effect of asphaltene precipitation and deposition on the rock surface and corresponding damage of reservoir parameters, the reservoir simulation is conducted, assuming primary recovery process and constant well flowrate. The flowchart of the reservoir simulation linked with the asphaltene precipitation model is demonstrated in **Figure 4-6**.

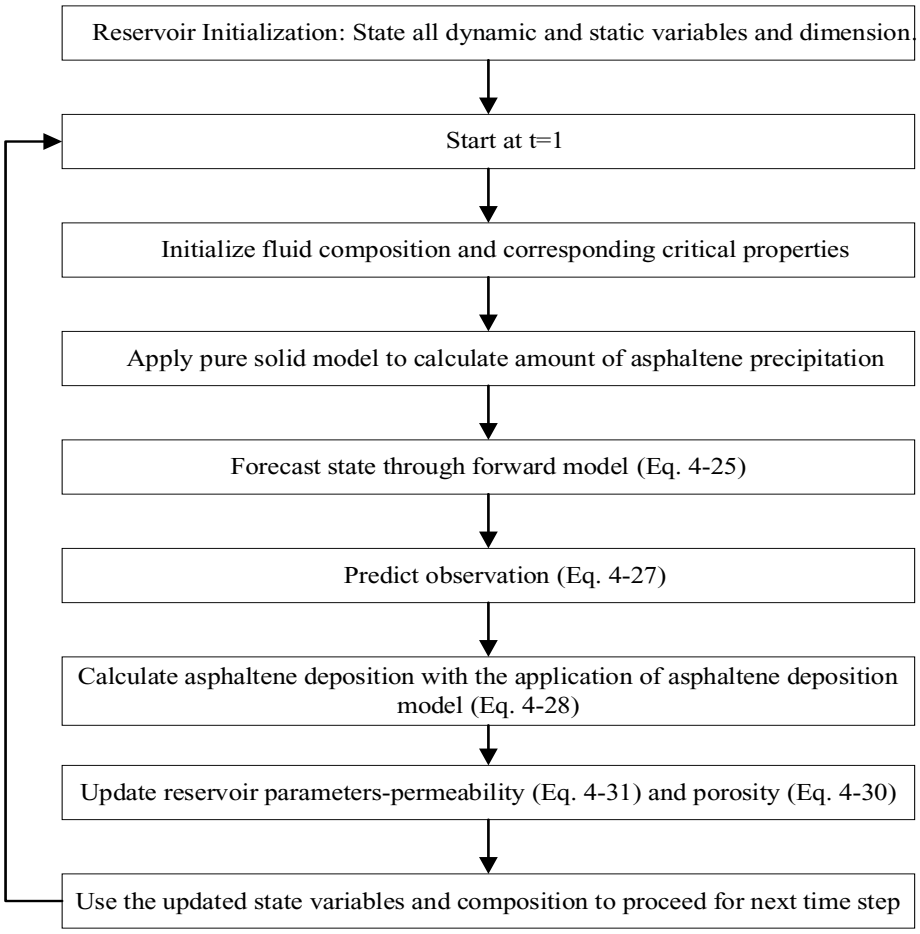

Figure 4-6: Flowchart for Reservoir Simulation.

According to **Figure 4-6**, there is a change in state variables while using forward model for state estimation in a new time step. Since the reservoir pressure (P_R) is initially higher than upper asphaltene saturation pressure (P_{UAOP}), and at this pressure asphaltene stays dissolved in the oil phase, no separate asphaltene phase is formed. Therefore, the initial state variable for asphaltene phase is defined as asphaltene pressure $(Pa = P_{UAOP})$. Later, when the reservoir pressure drops below the asphaltene saturation pressure (P_{UAOP}), asphaltene starts to precipitate from oil phase and forms separate phase called asphaltene phase (solid phase). Therefore, the state variable of asphaltene is switched from asphaltene saturation pressure $(Pa = P_{UAOP})$ to asphaltene saturation (S_a). This state variable is continued until reservoir pressure drops further below lower asphaltene saturation pressure (P_{LAOP}). From this pressure, the state variable is switched from S_a to P_a, again.

The similar type of state variable switching occurs for the gas phase. Before the bubble point, the gas stays dissolved in oil. From the bubble point, free gas starts to release from the oil and forms

a gas phase. As a result, above bubble point pressure *(P_b),* the state variable is P_b and from the bubble point pressure, the state variable is changed to S_g.

4.4 Results and Discussion

In this section, the results on asphaltene precipitation model validation and corresponding sensitivity analysis, reservoir simulation are presented.

4.4.1 Asphaltene Precipitation

This section presents the summarized results related to the asphaltene precipitation with the application of the modified methodology presented in the previous section. The specifications of the oil sample are taken from the study conducted by Burke et al. (1990). The experimental data, reservoir fluid properties, and asphaltene data are given in **Table 4-2** and **Table 4-3**.

Table 4-2: Composition and Properties of Oil Sample (Burke et al., 1990).

Component Name	**Mole (%)**	**Properties**	**Value**
Nitrogen	0.57	Molecular weight of Heptane Plus, g/gmol	329
Carbon Dioxide	2.46	Specific gravity of Heptane Plus	0.9594
Methane	36.37	Live oil molecular weight (M_{oil}), g/gmol	171.4
Ethane	3.47	API gravity of stock tank oil	19
Propane	4.05	Asphaltene content in stock tank oil (w_{asp}), wt %	16.08
iso-Butane	0.59	Reservoir temperature, ^oF	212
n-Butane	1.34	Saturation pressure, psia	2950
iso -Pentane	0.74	Initial reservoir pressure, psia	5260
n-Pentane	0.83	--	--
Hexane	1.62	--	--
Heptane Plus	47.96	--	--
Total	100	--	--

Table 4-3: Asphaltene Precipitation Data (Burke et al., 1990).

Test pressure, (psia)	Precipitates from live-oil, (wt %)	Precipitates remaining in residual stock tank oil, (wt %)	Total precipitates, (wt %)	Asphaltene solubility (Ra), (stb/stb)
LAOP=387	0	16.08	16.08	0.18736
1014.7	0.403	15.73	15.73+0.403=16.133	0.18179
2014.7	1.037	14.98	14.98+1.037=16.107	0.17318
3034.7	0.742	15.06	15.06+0.742=15.802	0.17712
4014.7	0.402	14.86	14.86+0.402=15.262	0.18179
UAOP=5173	0	16.08	16.08	0.18736
Average total precipitates (from experiment)			15.826	--

The mole fraction of heaviest component C_{7+} contains components from C_7 to C_{31+}. For calculation simplification, all oil components are lumped into seven parts as shown in **Table 4-4**. The heaviest component C_{31+} is split into non-precipitating (C_{31A+}) and precipitating (asphaltene) components. The mole fractions of these two parts are calculated as follows:

$$z_{asp} = \frac{w_{asp}}{100} \times \frac{M_{oil}}{M_{asp}} = \frac{16.08}{100} \times \frac{171.4\ g/gmol}{665.624\ g/gmol} = 0.0414$$

$$z_{C31A+} = 1 - z_{asp} - \sum_{i=1}^{30} z_i = 1 - 0.0414 - 0.8825 = 0.0761$$

Table 4-4: Recombined Oil Composition and Critical Properties (Darabi et al., 2014).

Component	P_c (psia)	T_c (^{o}R)	V_c (ft^3/lb-mol)	Molecular weight	Acentric factor	Composition, z_i
CO_2	1070.09	547.56	1.50711	44.01	0.225	0.0246
C_1-C_2	668.51	360.61	1.6431	17.417	0.0115127	0.4041
C_3-C_5	573.15	732.89	3.8098	53.516	0.179313	0.0755
C_6-C_{19}	291.41	1135.31	13.7197	164.423	0.655007	0.2719
C_{20}-C_{30}	175.41	1419.29	29.033	340.927	1.064023	0.1064
C_{31A+}	143.17	1682.93	56.5486	665.624	1.371778	0.0761
Asphaltene	143.17	1682.93	56.5486	665.624	1.371778	0.0414

For the flash calculation, PR EoS is used to model the thermodynamic behaviors of gas and oil phases. The required binary interaction coefficients (BICs) are calculated using Eq. (4-2). BIC of asphaltene with lighter components (CO_2 to C_5) is calculated with an aim to match the saturation pressure. The numerical values of BIC and solid model parameters are listed in **Table 4-5** and **Table 4-6**, respectively.

Table 4-5: BIC for the Oil Sample Used in PR EoS.

	CO_2	**C_1-C_2**	**C_3-C_5**	**C_6-C_{19}**	**C_{20}-C_{30}**	**C_{31A+}**	**Asphaltene**
CO_2	0.000	0.000	0.007	0.037	0.065	0.095	0.220
C_1-C_2	0.000	0.000	0.006	0.035	0.062	0.091	0.220
C_3-C_5	0.007	0.006	0.000	0.013	0.032	0.055	0.220
C_6-C_{19}	0.037	0.035	0.013	0.000	0.004	0.016	0.000
C_{20}-C_{30}	0.065	0.062	0.032	0.004	0.000	0.004	0.000
C_{31A+}	0.095	0.091	0.055	0.016	0.004	0.000	0.000
Asphaltene	0.220	0.220	0.220	0	0	0	0

Table 4-6: Asphaltene Precipitation Model Parameters.

Parameter	**Value**
Reference pressue, *(P^*, psia)*	5173
Asphaltene fugacity *at P^*, (f^*)*	3.95e-7
Molar volume of asphaltene, *(V_a, ft^3/lb-mol)*	10.068

Figure 4-7 represents the comparative asphaltene precipitation results obtained from the methodology presented in this chapter, original solid model, and results from Nghiem (1999) along with the corresponding experimental data.

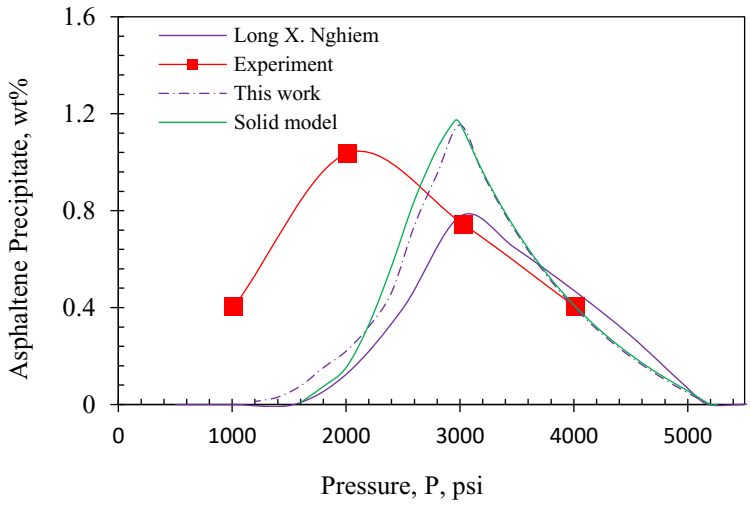

Figure 4-7: Comparison of Asphaltene Precipitation Results.

The results presented in **Figure 4-7** show that there is an agreement between this work (modified solid model), solid model (original), and the work done by Nghiem (1999) in calculating bubble point which is around 3000 psia. However, there is a big difference between the experimental value (2015 psia) and the value obtained from other works. Nghiem (1999) reported this inconsistency in their work. Typically, the bubble point pressure is the lowest pressure where the gas solubility is maximum. Below this point, gas comes out from oil reducing the gas concentration in the oil and makes asphaltene to re-dissolve in the oil mixture. Because dissolved gas is a bad solvent for asphaltene and asphaltene tends to precipitate in presence of dissolved gas (Pedersen et al., 2014). Therefore, at bubble point pressure, the maximum asphaltene precipitation is seen (Pedersen et al., 2014). From this theoretical inconsistency, it can be concluded that there might be an error in measuring the asphaltene precipitation. Since in Nghiem (1999) work, the first two initial points are matched properly, the calculated bubble point by Nghiem (1999) can be used as the reference value instead of experimental value (Gonzalez et al., 2017).

Regarding asphaltene precipitation calculation, **Figure 4-7** shows that for all cases asphaltene precipitation increases with pressure decline and reaches to its maximum value at the bubble point pressure; further decline from the bubble point, as free gas releases, a change in oil composition happens and the amount of precipitation starts to decrease. Although the trend is the same for all cases, a difference is observed in calculating the amount of asphaltene precipitation by different approaches.

At the bubble point pressure, the modified solid model shows 1.16 wt% precipitated asphaltene and from the work done by Nghiem (1999), precipitated asphaltene is about 0.804 wt%. However, according to the experimental data obtained by Burke et al. (1990), the amount of precipitated asphaltene is 1.037wt%. The deviation of the modified version and Nghiem work from the experimental data is about 10.06% and 28.09% respectively. Several influential factors (e.g., components grouping and corresponding binary interaction coefficient, molar volume of asphaltene, total asphaltene content and the empirical parameters in the solid model) are responsible to make difference in calculating asphaltene precipitation by different approaches. In addition, the type of EoS plays a role for the deviation. It should be noted that Darabi et al.(2014) and Qin et al. (2000) showed 1.1463 wt% and 1.07 wt% asphaltene precipitation at bubble point in their works.

A comparative analysis between the original solid model and modified model at the sample pressure 2800 psia is given in **Table 4-7**.

Table 4-7: Sample Calculation at *P*=2800 psia.

Model type		**Difference of asphaltene fugacity between solid and oil phases**	**Composition of precipitated asphaltene**	**Composition of asphaltene in oil phase**	**Asphaltene content in oil phase**	**Precipitated asphaltene**
		log(f_asL)-log(f_asp)	*x_asp*	$z_{\_C31B+}$	*wt%*	*wt%*
Modified solid model	Step 1	0.001063234	0.002445	0.038955	15.12256	0.957439
Original solid model	Step 1	0.017987409	0.003714	0.037686	14.63005	1.449947
	Step 2	0.011573168	0.003242	0.038158	14.81311	1.266893
	Step 3	0.007780854	0.002942	0.038458	14.92976	1.150238
	Step 4	0.003785719	0.002817	0.038583	14.97805	1.101946
	Step 5	0.00010266	0.002717	0.038683	15.01687	1.063125

Based on **Table 4-7**, the amount of precipitated asphaltene calculated by the modified solid model is 0.957439 wt% after one-step calculation, while the original solid model gives an asphaltene precipitation of 1.063125 wt% in 5 steps. The calculation shows about 9.945% difference between

two methods. Considering this iterative calculation needs to be done in all grids/cells, the reservoir simulation requires large computational time in case of using the original solid model.

4.4.2 Sensitivity Analysis

In the asphaltene precipitation calculation, three influential parameters are considered: a) total asphaltene content, b) binary interaction coefficient of asphaltene with light components, and c) molar volume of asphaltene.

Effect of amount of total precipitating component: The composition of asphaltene (z_{asp}) is calculated based on the total asphaltene content in the oil sample. Two cases are considered for this analysis. In the first case, 16.08 wt% (titration data from Burke oil sample) and in the second case, 15.823 wt% (average of the precipitated asphaltene data) are taken for the sensitivity analysis (see **Figure 4-8**). According to **Figure 4-8**, above the bubble point, the total asphaltene content does not have any impact on the precipitated asphaltene content; however, below the bubble point a minor impact is noticed. Since the difference in the total asphaltene content between two cases is low, it can be concluded the effect of total asphaltene content on asphaltene precipitation calculation is not significant.

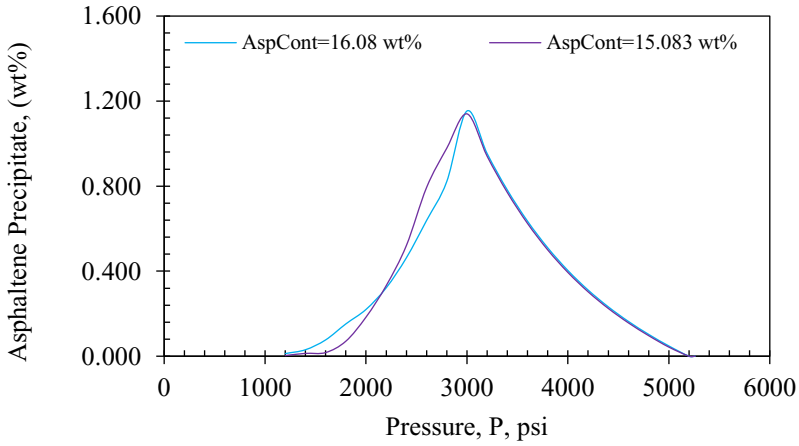

Figure 4-8: Effect of Amount of Total Precipitating Component.

Effect of binary interaction coefficient of asphaltene component: The BICs of the asphaltene part with lighter components are calculated with an aim to match the bubble point pressure. The magnitude of calculated BIC for the asphaltene with lighter components from CO_2 to C_5 is 0.22.

Using this value, the bubble point pressure is found to be 3000 psia as shown in **Figure 4-9**. *BIC*=0.215 is considered to figure out the impact of BIC on asphaltene precipitation calculation. It is found that a small change in *BIC* shifts the bubble point from 3000 psia to 2960 psia. Below the bubble point, the trend is shifted towards the right side. Note that 10% increase in the amount of asphaltene precipitation at the bubble point is noticed in the case of *BIC*=0.215.

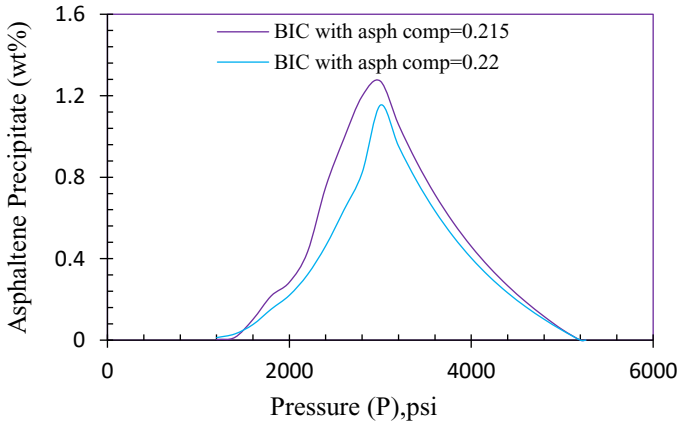

Figure 4-9: Effect of Interaction Coefficients of the Asphaltene Component.

Effect of solid molar volume of asphaltene *(V_a):* The asphaltene molar volume is calculated using PR EoS by assuming asphaltene as a pure solid component; the value of this parameter is found to be V_a = 10.068 ft^3/lb-mol. The results of this case and another case of V_a = 10.075 ft^3/lb-mol are provided in **Figure 4-10**. It is concluded that the impact of V_a on asphaltene precipitation calculation is very strong.

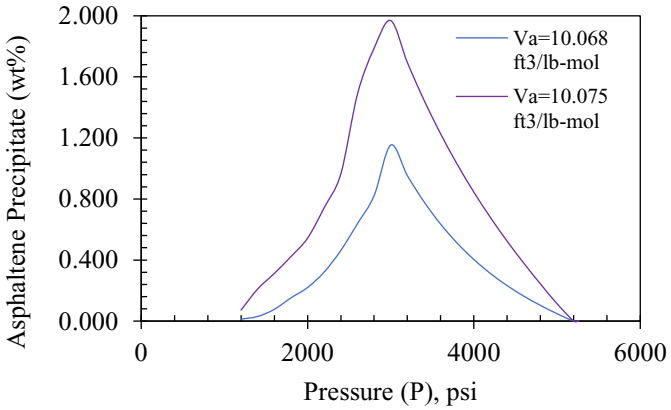

Figure 4-10: Effect of Solid Molar Volume on Asphaltene Precipitation.

4.4.3 Reservoir Simulation

This section represents the results obtained from the reservoir simulation. The reservoir is assumed homogeneous in terms of rock and fluid properties. The water present in the reservoir is assumed connate water. Therefore, water production does not have any impact on the results. The production well is constrained by constant production with a flow rate of 300 ft^3/day. The dynamic asphaltene precipitation model is incorporated into the reservoir model to capture the asphaltene precipitation for each time step and pressure drop. The simulation runs for 1000 days. This time step is good enough for analyzing the physical phenomena happened in this reservoir.

Pressure and flowrate profile of the well: When production starts, the reservoir pressure is 5260 psia. As the production continues, the reservoir pressure declines. From **Figure 4-11**, it is found that the reservoir pressure reaches to the bubble point pressure at the 842^{th} day, considering asphaltene precipitation scenario. Ignoring asphaltene precipitation, the bubble point condition is maintained at the 1020^{th} day. After reaching the bubble point pressure, a very slow pressure decline is observed for both cases because of free gas presence.

The cumulative oil production profile shows the consistency with the pressure profile as illustrated in **Figure 4-12**. Since the constant total production constrain is applied, oil production rate for both cases remains the same until bubble point condition and follows the same cumulative oil production line. When the free gas starts to evolve, the oil production rate begins to decline, and the gas production rate starts to increase. However, for the "asphaltene precipitation" case, the bubble point reaches earlier; hence, the oil production starts to decrease earlier compared to the "no asphaltene precipitation" case. Therefore, a difference of 11.23 % between these two cases is observed in terms of cumulative oil production profile after 1500 days of simulation.

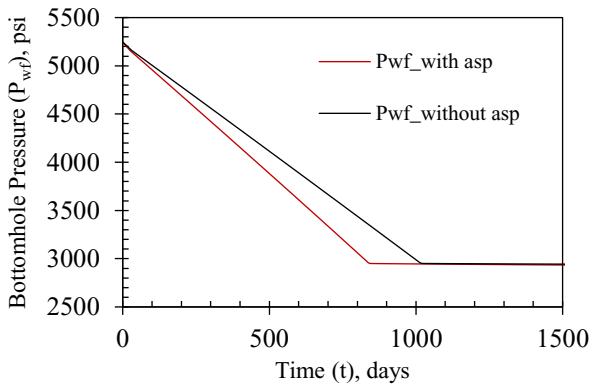

Figure 4-11: Pressure Profile of Production Well

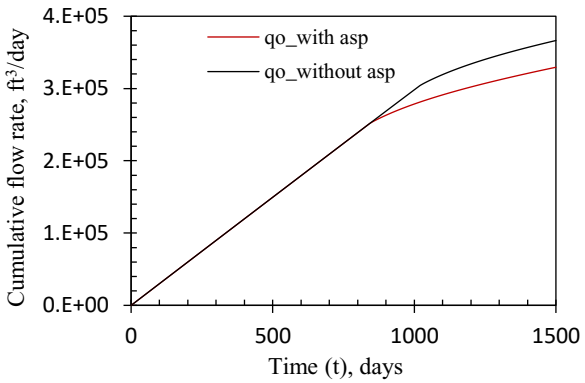

Figure 4-12: Flowrate Profile of Production Well.

Asphaltene saturation: Based on **Figure 4-13**, it is observed that the trend of precipitated asphaltene in the formation follows the asphaltene precipitation phase diagram. With pressure decline, the asphaltene starts to form and reaches to the maximum point at the bubble point pressure at the 842th day. At this point, the asphaltene saturation reaches to S_a= 0.003866. After reaching the bubble point, the free gas starts to form and precipitated asphaltene starts to dissolve again. Therefore, the amount of precipitated asphaltene is lowered.

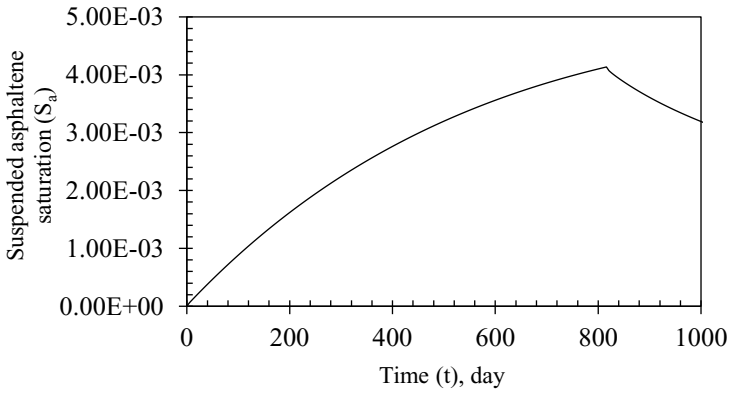

Figure 4-13: Development of Suspended Asphaltene Saturation with Time.

The variation of suspended asphaltene saturation with respect to a distance from the wellbore for different times is demonstrated in **Figure 4-14**. It is found that the development of asphaltene saturation decreases as the grid position is shifted from zero/well location. As the position is shifting from the well location, the pressure drops less which delays formation of asphaltene precipitation. **Figure 4-14** also reveals that the asphaltene saturation is maximum around the wellbore. Moreover, as time passed by, the reservoir pressure declines and therefore the asphaltene

saturation increases till the wellbore pressure *(P_{wf})* reaches bubble point pressure *(P_b)*. After reaching P_b, asphaltene saturation starts to decline as free gas evolves and results in lower asphaltene precipitation.

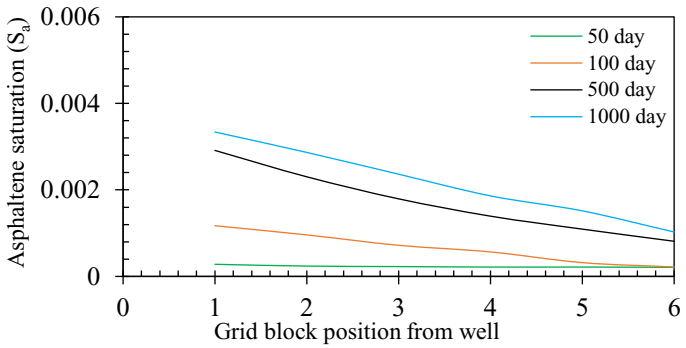

Figure 4-14: Change of Asphaltene Saturation with Grid Block Position for Different Times.

Impact on permeability and porosity: With the development of asphaltene saturation, the precipitated asphaltene deposits on the rock surface and makes changes in rock properties such as permeability and porosity. The impact of the deposited asphaltene on the permeability and porosity is illustrated in panels "a" and "b" of **Figure 4-15**. It is found that both permeability and porosity are reduced upon an increase in asphaltene saturation.

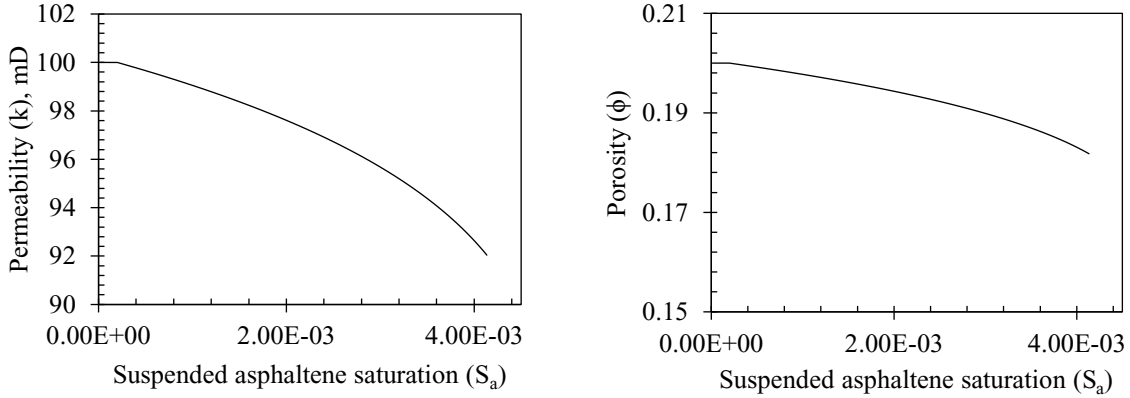

a) Change of Permeability with S_a b) Change of Porosity with S_a

Figure 4-15: Variation of Rock Properties with respect to Asphaltene Saturation.

From **Figure 4-13**, development of suspended asphaltene saturation in the wellbore region starts from day 23. Therefore, no change in the reservoir parameters is observed as shown in **Figure 4-15** until 23rd day. Afterwards, both parameters are reduced with the increase of

suspended asphaltene saturation. Bubble point is reached on 842th day and the whole simulation is run for 1000 days. Therefore, after reaching the maximum reduction in reservoir parameters (k=92.08 and ϕ=0.1818), the change in reservoir parameters is considerably low for the rest 168 days.

Figure 4-16a and **Figure 4-16b** present the change of rock properties with respect to grid position for different times. The alteration of rock properties due to deposition of precipitated asphaltene is consistent with development of asphaltene saturation.

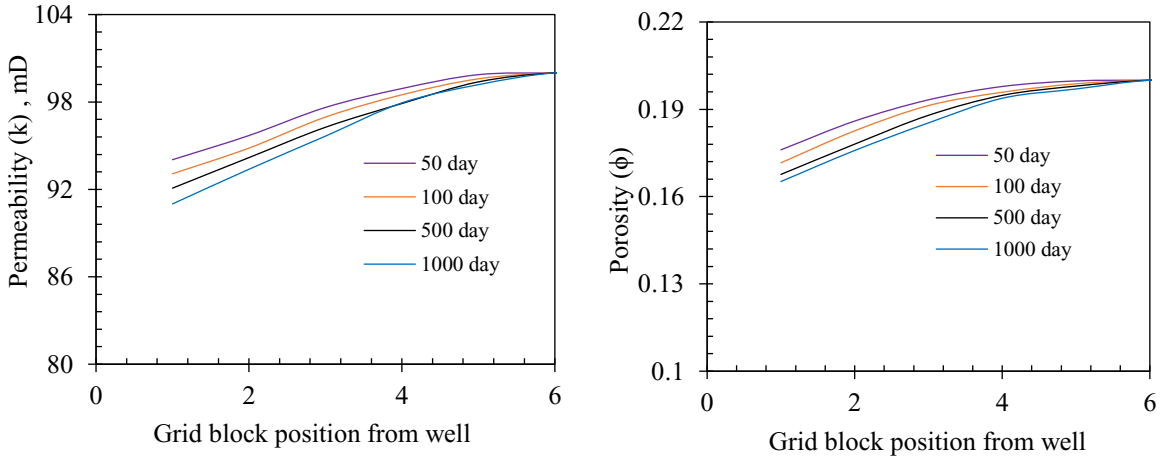

a) Change of Permeability with Distance (ft)

b) Change of Porosity with Distance (ft)

Figure 4-16: Changes in Rock Properties with Respect to Distance from the Wellbore.

From **Figure 4-16**, it is found that at the wellbore (grid position 1) the change in porosity/permeability is higher and as moving away from the wellbore, the reduction in porosity and permeability is smaller. Due to production, pressure declines faster around the wellbore compared to other grid blocks and therefore buildup of suspended asphaltene saturation increases near the wellbore. This leads to higher amount of asphaltene precipitation and deposition on the rock surface and thereby more reduction in rock properties can be seen in this zone. Moreover, the effect becomes more paramount with time till bubble point pressure, P_b, is attained.

4.5 Conclusions

In the pure solid model, repeated flash calculation is required to reach thermodynamic equilibrium at every time step, and it slows down the entire reservoir simulation process. In this regard, one of the goals of this work is to modify the asphaltene precipitation model with an aim to reduce computation time. The goal is attained by introducing a modification in the flash calculation while applying the pure solid model; thus, the repeated flash calculation can be avoided.

With the application of modified version of the solid model, the bubble point is found to be 3000 psia which is consistent with results obtained from the original solid model. However, regarding asphaltene precipitation calculation at bubble point, around 10.06 % difference is observed between the modified version and experimental work.

Based on the asphaltene precipitation calculation at sample pressure 2800 psia, only 9.945% difference is observed between the modified and original method. This small difference shows that the modified version can provide reliable results efficiently compared to the original model. However, the modified version requires one step, whereas the original version requires five steps.

A sensitivity analysis is also performed on asphaltene precipitation results. Among three parameters such as BIC of asphaltene with lighter components, molar volume of solid asphaltene, and total asphaltene content, it is found that the solid molar volume of asphaltene has the most impact on the asphaltene precipitation. Above bubble point, BIC of asphaltene with lighter components does not affect the asphaltene precipitation. However, below the bubble point it shows around 10 % change in asphaltene precipitation. The impact of total asphaltene content on asphaltene precipitation is not significant.

The modified asphaltene precipitation model is coupled with the reservoir simulation that runs for 1000 days to assess the influence of precipitated asphaltene on reservoir rock properties. The analysis reveals that around the wellbore, the suspended asphaltene saturation reaches to

its maximum value of 0.003866 and corresponding 8% and 9.1% reduction in permeability and porosity are observed respectively.

Between "asphaltene precipitation" and "no asphaltene precipitation" cases, a difference of 11.23 % in the cumulative oil production is observed. This implies that proper asphaltene precipitation modelling plays an important role to obtain a reliable prediction in terms of reservoir performance.

The current work was conducted by considering only one oil sample from Burke et al. (1990). Moreover, reservoir simulation was done assuming primary recovery, constant well flowrate, synthetic and homogeneous reservoir in terms of porosity and permeability, no capillary pressure, and no gravity effect. It is recommended to extend this work through considering more challenging tasks such as heterogeneous reservoir, secondary oil recovery process, different oil samples, and real case scenarios. Moreover, in this work only two reservoir parameters (porosity and permeability) are considered to analyze the impact of asphaltene precipitation. As a future work, the research work can be conducted to investigate other key parameters such as capillary pressure, wettability alteration due to asphaltene precipitation.

Acknowledgements

We gratefully acknowledge and thank Equinor Canada, the Natural Sciences and Engineering Research Council of Canada (NSERC), Memorial University, and Innovate NL for supporting this research study.

Nomenclatures

English letters

B_w	Formation volume factor of water res. (ft^3/std. ft^3)
B_o	Formation volume factor of oil res. (ft^3/std. ft^3)
C_w	Water compressibility (psi^{-1})

C_o	Oil compressibility (psi^{-1})
C_r	Rock compressibility (psi^{-1})
C_a	Volume ratio of suspended asphaltene in oil phase (ft^3/ft^3)
e	Exponent determined by matching the saturation pressure.
E_a	Volume fraction of deposited asphaltene
f_w	Water fraction
f_a^*	Fugacity of asphaltene at P^*
f_a	Fugacity of asphaltene at any P
h	Thickness of the reservoir (ft)
J	Productivity Index (ft^3/psi-day)
k	Absolute permeability (mD)
k_{rw}	Relative permeability to water
k_{ro}	Relative permeability to oil
$\vec{K}$	Permeability tensor
n	Covariance of ensemble
N_p	Particle size
P	Reservoir pressure (psi)
P_{UAOP}	upper asphaltene onset pressure (psi)
P_{LAOP}	Lower asphaltene onset pressure (psi)
P_b	Bubble point pressure (psi)
P_{wf}	Bottom hole flowing pressure (psi)
q_{inj}	Injection rate (ft^3/day)
q_p	Production rate (ft^3/day)
q_o'''	Oil flow rate per unit volume (ft^3/day-ft^3)
q_w'''	Water flow rate per unit volume (ft^3/day-ft^3)
r_w	Wellbore radius (ft)
r_e	Distance between reservoir outer boundary to wellbore (ft)
r	Tuning factor for particle perturbation
R	Molar gas constant (ft^3.psi. $°R^{-1}$.lb-mol^{-1})
S_w	Water saturation (fraction)

S_o	Oil saturation (fraction)
S_g	Gas saturation (fraction)
S_a	Asphaltene saturation (fraction)
T	Transmissibility
u_L	Oil phase Darcy velocity (ft^3/day)
V	Bulk volume (ft^3)
V_a	Molar volume of pure asphaltene (ft^3/lb-mol)
V_{ci}	Critical molar volume of component i (ft^3/lb-mol)
V_{wp}	Coefficient matrix for pressure of water phase
V_{ws}	Coefficient matrix for saturation of water phase
V_{op}	Coefficient matrix for pressure of oil phase
V_{os}	Coefficient matrix for saturation of oil phase
$v_{cr,o}$	Interstitial velocity of oil phase (ft^3/day)
v_o	Interstitial velocity of oil (ft^3/day)
v	Covariance of measurement noise
w	Covariance of system noise
Δx	Grid dimension in x direction (ft)
Δy	Grid dimension in y direction (ft)

Greek Symbols

ϕ	Porosity (%)
α_a	Surface deposition rate constant
μ_w	Water viscosity (cp)
μ_o	Oil viscosity (cp)
α	Unit conversion factor
ω	Particle weight

Superscripts

t	Time step index
i	Ensemble member index in algorithm
i, j	Grid number index in the reservoir model

References

1. Ahmadi, M.A., 2011. Prediction of asphaltene precipitation using artificial neural network optimized by imperialist competitive algorithm. J. Pet. Explor. Prod. Technol. 1, 99–106. https://doi.org/10.1007/s13202-011-0013-7
2. Ahmadi, M.A., Shadizadeh, S.R., 2012. New approach for prediction of asphaltene precipitation due to natural depletion by using evolutionary algorithm concept. Fuel 102, 716–723. https://doi.org/10.1016/j.fuel.2012.05.050
3. Alimohammadi, S., Zendehboudi, S., James, L., 2019. A comprehensive review of asphaltene deposition in petroleum reservoirs: Theory, challenges, and tips. Fuel 252, 753–791. https://doi.org/10.1016/j.fuel.2019.03.016
4. Almehaideb, R.A., 2004. Asphaltene precipitation and deposition in the near wellbore region: A modeling approach. J. Pet. Sci. Eng. 42, 157–170. https://doi.org/10.1016/j.petrol.2003.12.008
5. Burke, N.E., Hobbs, R.E., Kashou, S.F., 1990. Measurement and modeling of asphaltene precipitation. JPT, J. Pet. Technol. 42, 1440–1446. https://doi.org/10.2118/18273-PA
6. Chamkalani, A., Zendehboudi, S., Bahadori, A., Kharrat, R., Chamkalani, R., James, L., Chatzis, I., 2014. Integration of LSSVM technique with PSO to determine asphaltene deposition. J. Pet. Sci. Eng. 124, 243–253. https://doi.org/10.1016/j.petrol.2014.10.001
7. Civan, F., 1992. Evaluation and comparison of the formation damage models 219–236. https://doi.org/10.2523/23787-ms
8. Correra, S., Donaggio, F., 2000. OCCAM: Onset-constrained colloidal asphaltene model, in: SPE International Symposium on Asphaltene Deposition Is a Well Known Problem in Oil Formation Damage. https://doi.org/10.2118/58724-ms
9. Darabi, H., Shirdel, M., Kalaei, M.H., Sepehrnoori, K., 2014. Aspects of modeling asphaltene deposition in a compositional coupled wellbore/reservoir simulator, in: SPE Improved Oil Recovery Symposium. p. SPE-169121-MS. https://doi.org/10.2118/169121-MS
10. Gonzalez, K., Nasrabadi, H., Barrufet, M., 2017. Modeling asphaltene precipitation in a compositional reservoir simulator using three-phase equilibrium. J. Pet. Sci. Eng. 154, 602–611. https://doi.org/10.1016/j.petrol.2016.09.010

11. Hirschberg, A., DeJong, L.N.J., Schipper, B.A., Meijer, J.G., 1984. Influence of temperature and pressure on asphaltene flocculation. Soc. Pet. Eng. J. 24, 283–293. https://doi.org/10.2118/11202-PA
12. Kohse, B.F., Nghiem, L.X., 2004. Modelling asphaltene precipitation and deposition in a compositional reservoir simulator. Proc. - SPE Symp. Improv. Oil Recover. 2004-April. https://doi.org/10.2523/89437-ms
13. Leontaritis, K.J., Ali Mansoori, G., 1988. Asphaltene deposition: a survey of field experiences and research approaches. J. Pet. Sci. Eng. 1, 229–239. https://doi.org/10.1016/0920-4105(88)90013-7
14. Menshad, A.K., Mofidi, A.M., Shariatpanahi, F., Edalat, M., 2008. Developing of scaling equation with function of pressure to determine onset of asphaltene precipitation. J. Japan Pet. Inst. 51, 102–106. https://doi.org/10.1627/jpi.51.102
15. Mohebbinia, S., Sepehrnoori, K., Johns, R.T., Kazemi Nia Korrani, A., 2017. Simulation of asphaltene precipitation during gas injection using PC-SAFT EOS. J. Pet. Sci. Eng. 158, 693–706. https://doi.org/10.1016/j.petrol.2017.09.008
16. Nghiem, L.X., 1999. Phase behaviour modelling and compositional simulation of asphaltene deposition in reservoirs. University of Alberta.
17. Nghiem, L.X., Coombe, D.A., 1997. Modeling asphaltene precipitation during primary depletion. SPE J. 2, 170–176. https://doi.org/10.2118/36106-pa
18. Nghiem, L.X., Hassam, M.S., Nutakki, R., George, A.E.D., 1993. Efficient modelling of asphaltene precipitation. Proc. - SPE Annu. Tech. Conf. Exhib. Sigma, 375–384. https://doi.org/10.2118/26642-ms
19. Pan, H., Firoozabadi, A., 2000. Thermodynamic micellization model for asphaltene precipitation from reservoir crudes at high pressures and temperatures. SPE Prod. Facil. 15, 58–65. https://doi.org/10.2118/60842-PA
20. Pan, H., Firoozabadi, A., 1998. Thermodynamic micellization model for asphaltene aggregation and precipitation in petroleum fluids. SPE Prod. Facil. 13, 118–125. https://doi.org/10.2118/36741-pa
21. Pedersen, K.S., Christensen, P.L., Shaikh, J.A., 2014. Phase behavior of petroleum reservoir fluids. CRC Press. https://doi.org/10.1201/b17887
22. Qin, X., Wang, P., Sepehrnoori, K., Pope, G.A., 2000. Modeling asphaltene precipitation

in reservoir simulation. Ind. Eng. Chem. Res. 39, 2644–2654. https://doi.org/10.1021/ie990781g

23. Sayyad Amin, J., Alamdari, A., Mehranbod, N., Ayatollahi, S., Nikooee, E., 2010. Prediction of asphaltene precipitation: Learning from data at different conditions. Energy and Fuels 24, 4046–4053. https://doi.org/10.1021/ef100106r
24. Sayyad Amin, J., Nikkhah, S., Zendehboudi, S., 2017. A new experimental and modeling strategy to determine asphaltene precipitation in crude oil. Chem. Eng. Res. Des. 128, 162–173. https://doi.org/10.1016/j.cherd.2017.09.035
25. Solaimany-Nazar, A.R., Zonnouri, A., 2011. Modeling of asphaltene deposition in oil reservoirs during primary oil recovery. J. Pet. Sci. Eng. 75, 251–259. https://doi.org/https://doi.org/10.1016/j.petrol.2010.11.017
26. Subramanian, S., Simon, S., Sjöblom, J., 2016. Asphaltene Precipitation Models: A Review. J. Dispers. Sci. Technol. 37, 1027–1049. https://doi.org/10.1080/01932691.2015.1065418
27. Wang, S., Civan, F., 2001. Productivity decline of vertical and horizontal wells by asphaltene deposition in petroleum reservoirs, in: SPE International Symposium on Oilfield Chemistry. pp. 145–160. https://doi.org/10.2118/64991-ms
28. Zendehboudi, S., Shafiei, A., Bahadori, A., James, L.A., Elkamel, A., Lohi, A., 2014. Asphaltene precipitation and deposition in oil reservoirs - Technical aspects, experimental and hybrid neural network predictive tools. Chem. Eng. Res. Des. 92, 857–875. https://doi.org/10.1016/j.cherd.2013.08.001

Chapter 5 : Modelling and Parameter Estimation of Asphaltic Oil Reservoir with the Implementation of EnKF

Preface

This chapter addresses an objective of this dissertation as outlined in Section 5.1 which is to estimate the dynamic states and static parameters of the asphaltic oil reservoir by applying EnKF considering their inherent uncertainty and dynamic change due to asphaltene precipitation. The methodology presented in this chapter aims to incorporate the dynamic change of reservoir states and parameters due to production and asphaltene precipitation respectively to implement EnKF, as presented in Section 5.2 and Section 5.4.

I (Farhana Akter) have contributed to Conceptualization, Methodology, Formal Analysis, Investigation, Writing - Original Draft, and Writing - Review & Editing of this work, while Dr. Syed Imtiaz contributed to Conceptualization, Methodology, Formal Analysis, Writing - Review & Editing, Supervision; Dr. Sohrab Zendehboudi contributed to Writing - Review & Editing, and Supervision; Dr. Amer Aborig contributed to Writing - Review & Editing. A version of this chapter has been prepared for journal publication.

Abstract

Asphaltene precipitation in asphaltic oil reservoir is a complex phenomenon. Reservoir pressure drops with oil production, causing asphaltene precipitation and thereby deposition of precipitated asphaltene on the rock surface happens. This makes a change in two important reservoir parameters including porosity and permeability. The porosity and permeability change rate depends on the asphaltene deposition rate on the rock surface; therefore, porosity and permeability go through a dynamic alteration process during oil production. Moreover, these two parameters are approximately estimated from seismic or well test data and experience higher uncertainty. Therefore, alteration of 'porosity and permeability' due to asphaltene precipitation and its

associated uncertainty together cause a serious threat to reserve estimation and future projection. In this regard, proper estimation of these two key parameters 'porosity and permeability' gives a confidence to assess the impact of asphaltene precipitation/deposition on reservoir parameters.

The main objective of this work is to estimate the porosity and permeability of the asphaltic oil reservoir with the implementation of ensemble Kalman filter during reservoir simulation. The work focuses on the wellbore region of production well where alteration of porosity and permeability happens most. For the simulation, black oil model for four phase is developed and a detailed description on the mathematical model development is presented. The development of asphaltene precipitation zone and its consequence on reservoir properties 'porosity and permeability' and pressure are shown aiming to better forecast the well productivity. With EnKF application, porosity and permeability around the wellbore region are estimated. It is found that the estimation is close to the model with error values of 0.915% and 1.67% for permeability and porosity, respectively.

Keywords: Asphaltene Precipitation; Reservoir Model; History Matching; EnKF; Parameter Estimation; Formation Damage.

5.1 Introduction

Reservoir model is the key concern for field development and prediction. However, variables that are used to generate the reservoir model are comprised of considerable uncertainty. During history matching, incorporating updated information into the model provides fidelity in model and reduces the risk in future projection. The application of EnKF in petroleum industry has received considerable attention for unknown or poorly known parameters estimation and utilization of commercial reservoir simulators due to its computational efficiency, easy operation, and absence of adjoint code (Shuai et al., 2016).

In petroleum industry, Lorentzen et al. (2001) first applied EnKF to a dynamic model for two-phase flow in a well. By tuning the liquid hold up, gas fraction, slip velocity, pressure and individual fluid flow rates, the downhole pressure behavior and amount of fluid flowing out of the well during drilling operation were calculated. Later, other researchers (e.g., Brouwer et al., 2004; Gu and Oliver, 2005; Liu and Oliver, 2005; Nævdal et al., 2002; Nœvdal et al., 2005) applied

EnKF to oil reservoirs to estimate both permeability and porosity considering a water flooding case.

Besides permeability and porosity estimation, other reservoir model parameters such as fluid front (Trani et al., 2012) , absolute and relative permeability (Jahanbakhshi et al., 2015; Li et al., 2012), geothermal properties (Marquart et al., 2013), facies properties (Lorentzen et al., 2013), capillary pressure (Zhang et al., 2017) and fluid contacts (Wang et al., 2009) have been estimated with the application of EnKF.

An oil reservoir containing asphaltene experiences a complex behaviour with pressure change due to production. In the reservoir oil mixture, the asphaltene component is characterised as the heaviest fraction which is insoluble in the normal alkalines and soluble in aromatic solvents. Because of this unique feature, asphaltene passes through different phases throughout the reservoir life. Based on **Figure 5-1**, it can be noticed that while producing oil from the reservoir, a change happens in the reservoir pressure, temperature, fluid composition, and reservoir equilibrium. All these changes lead asphaltene to a change from soluble to insoluble; thereby asphaltene precipitation occurs.

According to **Figure 5-1**, at initial reservoir pressure, (P_R) asphaltene stays in the dissolved condition in oil and remains constant. When pressure drops and reaches to upper asphaltene onset pressure (P_{UAOP}), dissolved asphaltene starts to precipitate. The asphaltene precipitation increases until the reservoir pressure reaches to bubble point pressure (P_b). At this point (P_b), the asphaltene precipitation reaches to the maximum level. With further declines in the reservoir pressure, precipitation tends to dissolve back into oil and thereby amount of precipitation decreases with further pressure reduction (Krejbjerg and Pedersen, 2006). The decline in precipitation is continued until the pressure goes to lower asphaltene onset pressure (P_{LAOP}). At or below P_{LAOP}, no precipitation occurs and the amount of dissolved asphaltene reaches to its original amount.

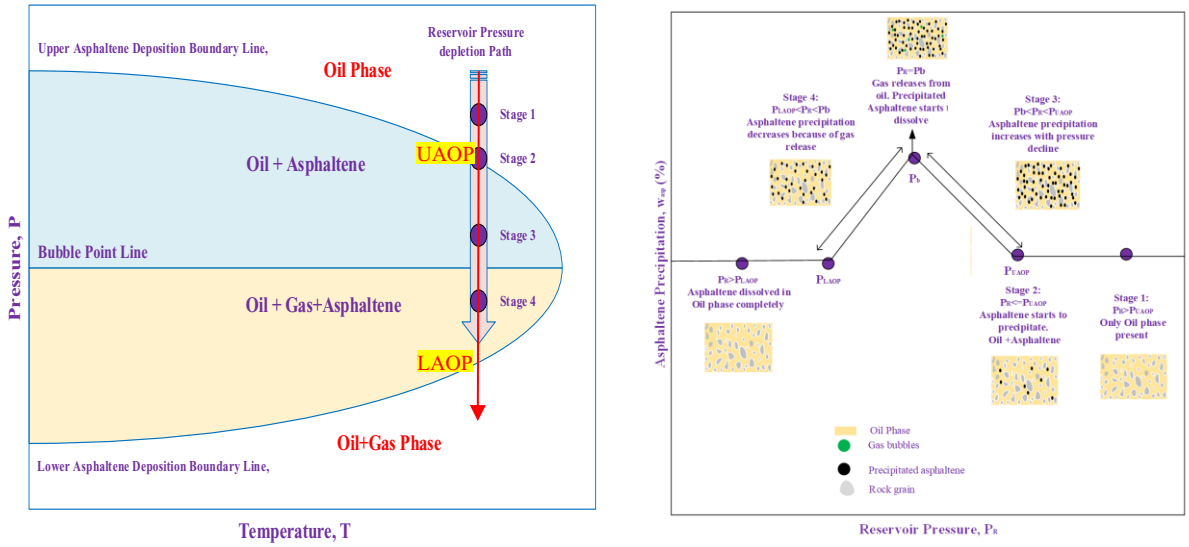

a) Phase Diagram of Asphaltene Precipitation (Gonzalez et al., 2017)

b) Precipitation of Asphaltene in the Crude Oil

Figure 5-1: Phase Diagram and Solubility of Asphaltene

To characterize the behavior of asphaltene, researchers have developed different models such as solubility model (Hirschberg et al., 1984; Pan and Firoozabadi, 2000; Wang and Civan, 2001), solid model (Kohse and Nghiem, 2004; Nghiem et al., 1998; Nghiem and Coombe, 1997; Qin et al., 2000), colloidal model(Correra and Donaggio, 2000; Leontaritis and Ali Mansoori, 1988), and micellization model (Almehaideb, 2004). In the models, asphaltene phase is defined as a solid phase, liquid phase, and colloidal suspension. Incorporation of Statistical Associating Fluid Theory or SAFT (Mohebbinia et al., 2017) into asphaltene precipitation model is also successfully implemented (Alimohammadi et al., 2019).

Advanced approaches such as response surface methodology (Sayyad Amin et al., 2017), intelligent techniques such as artificial neural network (Ahmadi, 2011), linked with particle swarm optimization (PSO) (Ahmadi and Shadizadeh, 2012; Chamkalani et al., 2014) and genetic algorithm (Menshad et al., 2008), support vector machine (Chamkalani et al., 2014), and Bayesian Belief Network as an ANN tool (Sayyad Amin et al., 2010) have been used to predict asphaltene precipitation behaviors.

From the literature it is found that the research was conducted with a special focus on the development of asphaltene precipitation model for correct estimation of precipitated asphaltene.

The reduction of the porosity and permeability in the reservoir due to precipitated asphaltene deposition on the rock surface has been discussed in the analysis. However, estimation of the porosity and permeability has not been discussed. Darabi et al. (2014) investigated the impact of gas flooding on the dynamics of asphaltene precipitation and deposition. Qin et al. (2000) studied the effect of asphaltene precipitation on reservoir flow behavior. Tabzar et al. (2018) explored the influence of asphaltene precipitation on fluid flow rate, porosity, and permeability for saturated and under saturated oil reservoir cases. Fallahnejad and Kharrat (2015) developed a fully implicit compositional simulator for modeling asphaltene deposition during natural depletion and prediction of formation damage in terms of porosity and permeability reduction. Almehaideb (2004) developed a new single-well model considering four-component (asphaltene–oil–gas–water) to simulate asphaltene 'precipitation-deposition' and plugging of oil wells during primary production that affects the well productivity.

Among reservoir parameters, porosity and permeability are the two important factors for the reservoir model as these two have influential connection to the fluid flow, reservoir pressure, and reserve estimation/prediction. These two key parameters are not measured directly in the field. In fact, they are estimated using seismic and well test data. As these two parameters contain high degree of uncertainty, therefore an analyses has been conducted to estimate the distributions of these two parameters. Thus, the reservoir model that is developed based on initial guess of the parameters lacks reliability. This inherent uncertainty in the model affects the reservoir performance. Moreover, oil production causes a change in reservoir pressure and oil composition, resulting in asphaltene precipitation phenomenon in the reservoir. This situation affects the reservoir properties (porosity and permeability) and eventually oil recovery. In this regard, correct prediction/estimation of uncertain reservoir parameters ensures the reliability of the reservoir model and provides a confidence to assess the asphaltene precipitation scenario in terms of well productivity.

The key focus of this research work is to estimate the two important reservoir properties (porosity and permeability) through the process of history matching with the implementation of ensemble Kalman filter in the asphaltic oil reservoir. Due to oil production, reservoir pressure changes and this causes a switch in the reservoir dynamic states such as from phase pressure to phase saturation for gas and asphaltene phases. This is a great challenge while applying EnKF to asphaltic oil

reservoir for parameter estimation. Therefore, to address this change in each pressure step and in each realization, a methodology is developed so that it can capture the dynamic state change for all realizations for gas and asphaltene phase, and history matching and parameter estimation can be done efficiently.

For reservoir modelling, the black oil model is followed. The flow equations for four phases such as oil-water-gas-asphaltene are discretized and a detailed numerical scheme is presented. For solving the flow equations, the equations are presented in state-space form. Asphaltene precipitation model is coupled with the reservoir simulation. Considering the computation time for reservoir simulation, the modified pure solid model is used for asphaltene precipitation calculation.

The article is organized as follows: in **Section 5.2**, theory, and formulation of ensemble Kalman filter are presented. **Section 5.3** provides a detailed description regarding asphaltene precipitation model. **Section 5.4** discusses the reservoir model development along with the implementation of EnKF for reservoir simulation. Results with corresponding discussion are presented in **Section 5.5**. Finally, **Section 5.6** highlights the conclusions.

5.2 Theory and Formulation of Ensemble Kalman Filter

In this section, we provide the theoretical background of EnKF and introduction of the tuning parameter(s) for improving EnKF estimation.

5.2.1 Ensemble Kalman Filter

EnKF is a Monte Carlo method used for data assimilation. With this technique, an ensemble of state variables of a system is generated from prior information and the system is updated through sequential data assimilation. The methodology comprises of two steps such as forecast step and update step. In the forecast step, state variables are projected forward in time. The estimated values of the states are corrected in the update step by considering the most recent observations.

Forecast step: The state variables are predicted as follows:

$$x^{i-}{}_{t+1} = f(x^{i+}{}_{t}, u_t) + Q^{i}{}_{t}, \quad Q^{i}{}_{t} \sim N(0, \Sigma_t^m) \tag{5-1}$$

Here, x is the augmented state vector, containing both states and parameters that need to be estimated.

Perturbed input, $u^i{}_t = u_t + \zeta^i{}_t \;\; ; \;\; \zeta^i{}_t \sim N(0, \Sigma_t^u)$ $(5-1a)$

Ensemble mean of the state variables, $\bar{x}_{t+1} = \frac{1}{N}\sum_{i=1}^{N} x^{i-}{}_{t+1}$

Estimated measurement, $\hat{y}^i{}_{t+1} = h(x^{i-}{}_{t+1}, u_t)$ (5-2)

Ensemble mean of estimated measurement, $\bar{y}_{t+1} = \frac{1}{N}\sum_{i=1}^{N} \hat{y}^i{}_{t+1}$

Update step: The Kalman gain is calculated by the following equation:

$K_{t+1} = \Sigma_{t+1}^{xy}\left[\Sigma_{t+1}^{yy} + R_{t+1}\right]^{-1} \quad , R_{t+1} \sim N\left(0, \Sigma_{t+1}^{y}\right)$ (5-3)

in which, Σ_{t+1}^{yy} is the forecast error covariance matrix of the prediction, and Σ_{t+1}^{xy} is the cross covariance between the state variables and predicted output. These parameters are defined as follows:

$\sum_{t+1}^{yy} = \left(\hat{y}^i{}_{t+1} - \bar{y}_{t+1}\right)\left(\hat{y}^i{}_{t+1} - \bar{y}_{t+1}\right)^T$ and $\Sigma_{t+1}^{xy} = \left(\hat{y}^i{}_{t+1} - \bar{y}_{t+1}\right)\left(x^{i-}{}_{t+1} - \bar{x}_{t+1}\right)^T$

Perturbed production data:

$y^i{}_{t+1} = y_{t+1} + \eta^i{}_{t+1}; \;\; \eta^i{}_{t+1} \sim N\left(0, \Sigma_{t+1}^{y}\right)$ (5-4)

The state is updated as follows:

$x^{i+}{}_{t+1} = x^{i-}{}_{t+1} + K_{t+1}\left(y^i{}_{t+1} - \hat{y}^i{}_{t+1}\right)$ (5-5)

5.3 Asphaltene Precipitation Model

In the oil mixture, the heaviest component (C7+) is split into several single number carbon fractions and residual components. The residual component 'n_c-th' is further divided into precipitating and non-precipitating components. Precipitating one is considered as asphaltene (n_{ca}) and treated as a pure solid. While non-precipitating component (n_{cL}) is considered as liquid phase. Modified solid model is used to calculate the fugacity of precipitated asphaltene. On the other hand, the gas and oil phases are modelled by Peng-Robinson EoS. The fugacity of asphaltene in the asphaltene phase is given below:

$$ln f_a = ln f_a^* + \frac{V_a(P - P^*)}{RT} \quad (5\text{-}6)$$

Here,

P^* = Reference pressure at which asphaltene precipitation is zero

f_a^* = Fugacity of asphaltene at reference pressure

V_a = Molar volume of dissolved asphaltene.

P = Reservoir pressure

R = Universal gas constant

T = Reservoir temperature

For components from 1 to $n_c - 1$, the binary interaction (d_{ik}) is computed by the following equation:

$$d_{ik} = 1 - \left(\frac{2V_{ci}^{1/6} V_{ck}^{1/6}}{V_{ci}^{1/6} + V_{ck}^{1/6}} \right)^e \quad (5\text{-}7)$$

Here, V_c refers to the critical volume of the component and *e* is the exponent. The interactions between the heaviest component and lighter components are determined through regression analysis by matching the experimental data of asphaltene precipitation (Nghiem et al., 1993).

Due to production, reservoir oil containing asphaltene experiences different phase changes (liquid/vapor/solid) as shown in **Figure 5-1**. In this regard, the thermodynamic equilibrium condition is defined as follows:

$$lnf_{iv} = lnf_{il} \quad \{for \ i = 1,2 \ldots \ldots . . n_c - 1\} \quad (5\text{-}8)$$

$$lnf_{n_c v} = lnf_{n_c l} = lnf_a \quad (5\text{-}9)$$

The fugacity *(f)* of each component in the liquid *(l)* and gas *(v)* phases is calculated using EoS, and the fugacity of asphaltene (f_a) can be determined using Eq. (5-6). The stability test determines whether asphaltene will be precipitated from liquid mixture or not. The following criterion governs the existence of the solid asphaltene phase.

$$lnf_{n_c l} > lnf_a \quad (5\text{-}10)$$

The amount of asphaltene precipitation is calculated by satisfying the following equilibrium condition:

$$lnf_{n_c l} = lnf_a \quad (5\text{-}11)$$

Figure 5-2 presents the explicit estimation of the amount of asphaltene precipitation for each time step in a single flash calculation.

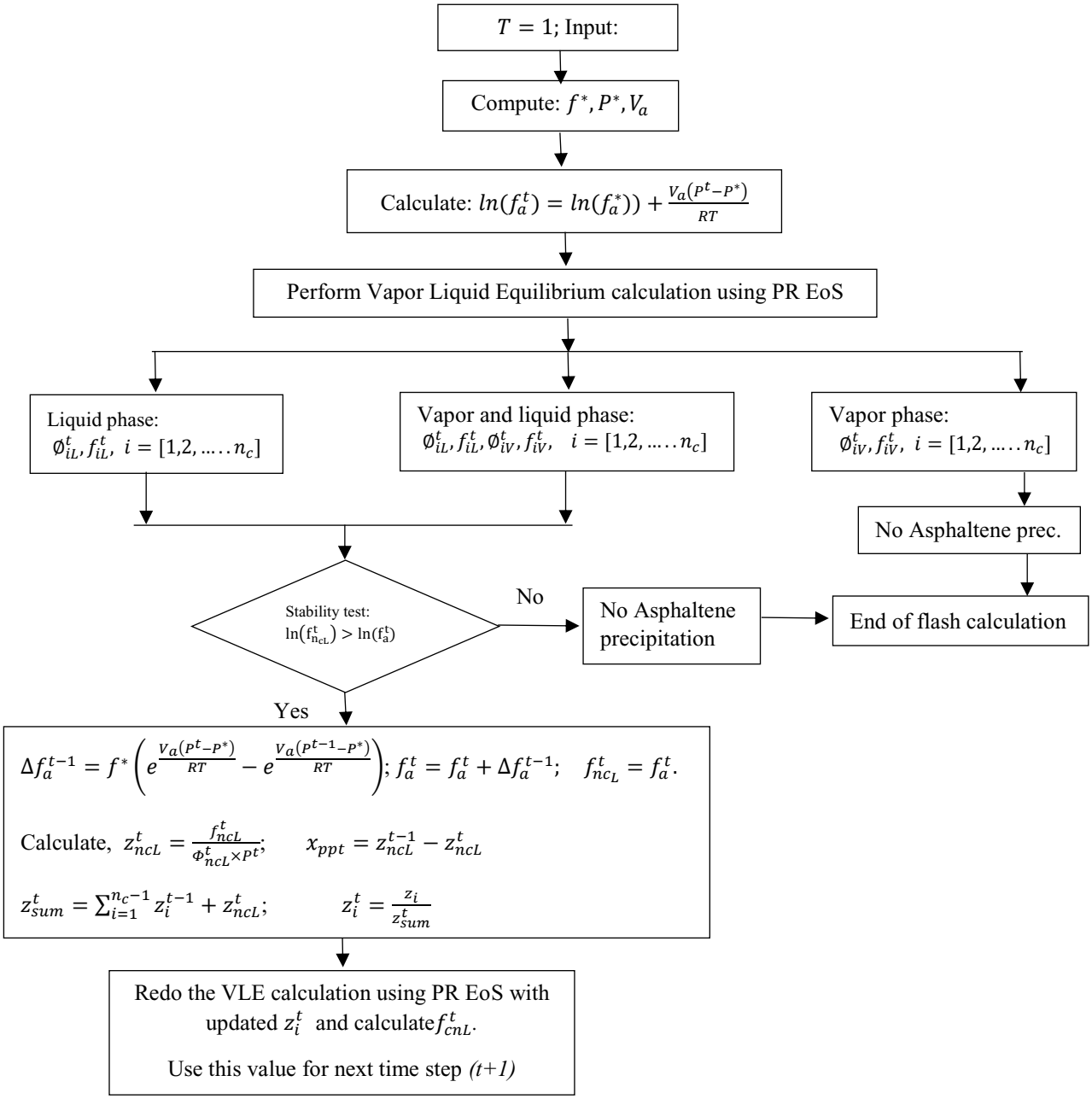

Figure 5-2: Flowchart for Asphaltene Precipitation Calculation

5.4 Reservoir Modelling with the Implementation of EnKF

5.4.1 Black Oil Model in State Space Form

For reservoir simulation, the asphaltene precipitation model is incorporated into the reservoir model to analyze the effect of precipitation on reservoir rock properties. With the implementation

of EnKF, the reservoir properties are estimated. The modeled reservoir is an asphaltene rich crude oil reservoir with a single production well.

Description of the reservoir: A synthetic 2D reservoir model with the dimension of 100 ft ×100 ft ×50 ft and 10 × 10 × 1 grids are generated as shown in **Figure 5-3**. No flow boundary condition is considered for all sides of the reservoir. The reservoir's initial pressure is 5260 psi. There is a production well in grid block (5, 5) in the reservoir. Production rate is set at 300 ft^3/d with a minimum bottom hole pressure of 1000 psi. The reservoir porosity is 0.2 and the permeability is 100 mD. The reservoir is assumed homogeneous in terms of porosity and permeability. Initially, the reservoir is assumed to be under saturated and filled with oil and connate water with saturation of 0.2. When the reservoir reaches to the bubble point, the gas starts to evolve, and critical gas saturation is assumed to be 0.05.

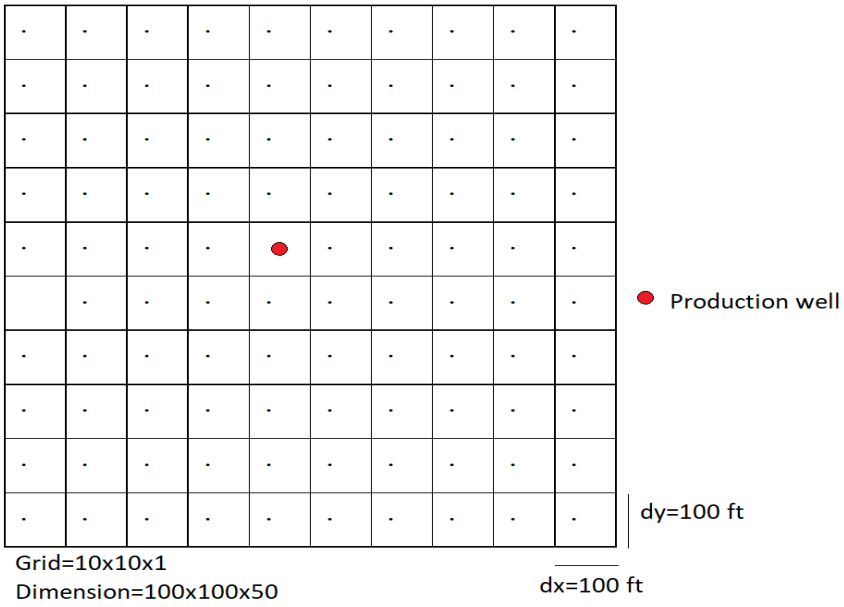

Figure 5-3: 2D Reservoir with Grid Dimension and Well Location

Parameterization and mathematical formulation: In this analysis, two static parameters (porosity and permeability) are estimated along with the dynamic states (pressure and four-phase saturation). Therefore, the augmented state vector consists of two static vectors (e.g., porosity and permeability), and four dynamic vectors namely four-phase saturation and pressure. The discretized partial differential equation of four phase (oil-gas-water-asphaltene) reservoir is given below:

Water phase:

$$V\left[\frac{\emptyset S_w}{B_w}(c_w+c_r)\frac{\partial p}{\partial t}+\frac{\emptyset}{B_w}\frac{\partial s_w}{\partial t}\right]_{i,j}-(T_w)_{i-\frac{1}{2},j}p_{i-1,j}-(T_w)_{i,j-\frac{1}{2}}p_{i,j-1}+\left[(T_w)_{i-\frac{1}{2},j}+(T_w)_{i,j-\frac{1}{2}}+(T_w)_{i+\frac{1}{2},j}+(T_w)_{i,j+\frac{1}{2}}\right]p_{i,j}$$
$$-(T_w)_{i+\frac{1}{2},j}p_{i+1,j}-(T_w)_{i,j+\frac{1}{2}}p_{i,j+1}=[q_w]_{i,j} \quad (5\text{-}12)$$

Oil phase:

$$V\left[\emptyset S_o\left(\frac{\partial B_o}{\partial p}+\frac{c_r}{B_o}\right)\frac{\partial p}{\partial t}-\frac{\emptyset}{B_o}\left(\frac{\partial s_w}{\partial t}+\frac{\partial s_g}{\partial t}+\frac{\partial s_a}{\partial t}\right)\right]_{i,j}-(T_o)_{i-\frac{1}{2},j}p_{i-1,j}-(T_o)_{i,j-\frac{1}{2}}p_{i,j-1}$$
$$+\left[(T_o)_{i-\frac{1}{2},j}+(T_o)_{i,j-\frac{1}{2}}+(T_o)_{i+\frac{1}{2},j}+(T_o)_{i,j+\frac{1}{2}}\right]p_{i,j}-(T_o)_{i+\frac{1}{2},j}p_{i+1,j}-(T_o)_{i,j+\frac{1}{2}}p_{i,j+1}=[q_o]_{i,j} \quad (5\text{-}13)$$

Gas phase:

$$V\left[\left\{\emptyset S_g\left(\frac{\partial B_g}{\partial p}+\frac{c_r}{B_o}\right)+\frac{R_{so}\emptyset S_o}{5.615}\left(\frac{\partial B_o}{\partial p}+\frac{c_r}{B_o}\right)+\emptyset S_o\frac{\frac{\partial R_{so}}{\partial p}}{5.615B_o}\right\}\frac{\partial p}{\partial t}-\frac{R_{so}\emptyset}{5.615B_o}\left(\frac{\partial s_w}{\partial t}+\frac{\partial s_a}{\partial t}\right)+\left(\frac{\emptyset}{B_g}-\frac{R_{so}\emptyset}{5.615B_o}\right)\frac{\partial s_g}{\partial t}\right]_{i,j}$$
$$-\left(T_g+R_{so}T_o\right)_{i-\frac{1}{2},j}p_{i-1,j}-\left(T_g+R_{so}T_o\right)_{i,j-\frac{1}{2}}p_{i,j-1}$$
$$+\left[\left(T_g+R_{so}T_o\right)_{i-\frac{1}{2},j}+\left(T_g+R_{so}T_o\right)_{i,j-\frac{1}{2}}+\left(T_g+R_{so}T_o\right)_{i+\frac{1}{2},j}+\left(T_g+R_{so}T_o\right)_{i,j+\frac{1}{2}}\right]p_{i,j}$$
$$-\left(T_g+R_{so}T_o\right)_{i+\frac{1}{2},j}p_{i+1,j}-\left(T_g+R_{so}T_o\right)_{i,j+\frac{1}{2}}p_{i,j+1}=\left[q_g+R_{so}q_o\right]_{i,j} \quad (5\text{-}14)$$

Asphaltene phase:

$$V\left[\left\{\emptyset S_a\frac{c_r}{B_a}+R_a\emptyset S_o\left(\frac{\partial B_o}{\partial p}+\frac{c_r}{B_o}\right)\right\}\frac{\partial p}{\partial t}-\frac{R_a\emptyset}{B_o}\left(\frac{\partial s_w}{\partial t}+\frac{\partial s_g}{\partial t}\right)+\left(\frac{\emptyset}{B_a}-\frac{R_a\emptyset}{B_o}\right)\frac{\partial s_a}{\partial t}\right]_{i,j}-\left(T_a+R_aT_o\right)_{i-\frac{1}{2},j}p_{i-1,j}$$
$$-\left(T_a+R_aT_o\right)_{i,j-\frac{1}{2}}p_{i,j-1}$$
$$+\left[\left(T_a+R_aT_o\right)_{i-\frac{1}{2},j}+\left(T_a+R_aT_o\right)_{i,j-\frac{1}{2}}+\left(T_a+R_aT_o\right)_{i+\frac{1}{2},j}+\left(T_a+R_aT_o\right)_{i,j+\frac{1}{2}}\right]p_{i,j}$$
$$-\left(T_a+R_aT_o\right)_{i+\frac{1}{2},j}p_{i+1,j}-\left(T_a+R_aT_o\right)_{i,j+\frac{1}{2}}p_{i,j+1}=\left[\frac{S_a}{S_o}q_o+R_aq_o\right]_{i,j}+\left[\frac{1}{B_a}\frac{\partial E_a}{\partial t}\right]_{i,j} \quad (5\text{-}15)$$

Here

$$T_{i-\frac{1}{2},j}=\frac{\Delta x\,h}{\Delta y}\lambda_{i-\frac{1}{2},j} \quad (5\text{-}16)$$

$$T_{i,j-\frac{1}{2}}=\frac{\Delta x\,h}{\Delta y}\lambda_{i,j-\frac{1}{2}} \quad (5\text{-}17)$$

$$\lambda_{i-\frac{1}{2},j}=\frac{k_rk_{i-\frac{1}{2},j}}{\mu B} \quad (5\text{-}18)$$

$$S_w+S_o+S_g+S_a=1 \quad (5\text{-}19)$$

Since the asphaltene is present in the oil mixture/sample as a suspension, the velocity of oil and asphaltene will be equal. Therefore, the transmissibility for oil and asphaltene will be calculated as follows:

$$T_{oi-\frac{1}{2},j} = \frac{\Delta x\, h}{\Delta y}\frac{S_o}{S_a + S_o}\lambda_{oi-\frac{1}{2},j} \tag{5-20}$$

$$T_{ai-\frac{1}{2},j} = \frac{\Delta x\, h}{\Delta y}\frac{S_a}{S_a + S_o}\lambda_{ai-\frac{1}{2},j} \tag{5-21}$$

$$V = \Delta x \times \Delta y \times h \tag{5-22}$$

Flow rate of each phase is calculated considering constant total production using the following equations:

$$q_w = \frac{\lambda_w}{\lambda_w + \lambda_o + \lambda_g + \lambda_a} q_{tp} \tag{5-23}$$

$$q_g = \frac{\lambda_w}{\lambda_w + \lambda_o + \lambda_g + \lambda_a} q_{tp} + \frac{R_{so}}{5.615} q_o \tag{5-24}$$

$$q_o = \frac{\lambda_w}{\lambda_w + \lambda_o + \lambda_g + \lambda_a} q_{tp} \tag{5-25}$$

$$q_a = \frac{\lambda_w}{\lambda_w + \lambda_o + \lambda_g + \lambda_a} q_{tp} + R_a q_o \tag{5-26}$$

In Eqs. (5-23) to (5-26), q_{tp} refers to the total production rate of the reservoir.

The state- space formulation of the reservoir model is presented below:

$$\begin{bmatrix} \begin{bmatrix} V_{wp} & V_{wsw} \\ V_{op} & V_{osw} \end{bmatrix} & \begin{bmatrix} V_{wsg} & V_{wsa} \\ V_{osg} & V_{osa} \end{bmatrix} \\ \begin{bmatrix} V_{gp} & V_{gsw} \\ V_{ap} & V_{asw} \end{bmatrix} & \begin{bmatrix} V_{gsg} & V_{gsa} \\ V_{asg} & V_{asa} \end{bmatrix} \end{bmatrix} \times \begin{bmatrix} \frac{dp}{dt} \\ \frac{dS_w}{dt} \\ \frac{dP_b}{dt} / \frac{dS_g}{dt} \\ \frac{dP_a}{dt} / \frac{dS_a}{dt} \end{bmatrix} + \begin{bmatrix} \begin{bmatrix} T_o & 0 \\ T_w & 0 \end{bmatrix} & \begin{bmatrix} 0 & 0 \\ 0 & 0 \end{bmatrix} \\ \begin{bmatrix} T_g & 0 \\ T_a & 0 \end{bmatrix} & \begin{bmatrix} 0 & 0 \\ 0 & 0 \end{bmatrix} \end{bmatrix} \times \begin{bmatrix} p \\ S_w \\ P_b/S_g \\ P_a/S_a \end{bmatrix} = \begin{bmatrix} q_o \\ q_w \\ q_g \\ q_a \end{bmatrix} + \begin{bmatrix} 0 \\ 0 \\ 0 \\ c \end{bmatrix} \left[\frac{dE_a}{dt}\right] \tag{5-27}$$

Here,

$$p = \begin{bmatrix} p_{i,j-1} & \dots & p_{i-1,j} & p_{i,j} & p_{i+1,j} & \dots & p_{i,j+1} \end{bmatrix};\ S_w = \begin{bmatrix} S_{w_{i,j-1}} & \dots & S_{w_{i-1,j}} & S_{w_{i,j}} & S_{w_{i+1,j}} & \dots & S_{w_{i,j+1}} \end{bmatrix}$$

$$k = \begin{bmatrix} k_{i,j-1} & \dots\dots & k_{i-1,j} & k_{i,j} & k_{i+1,j} & \dots\dots & k_{i,j+1} \end{bmatrix};\ \emptyset = \begin{bmatrix} \emptyset_{i,j-1} & \dots\dots & \emptyset_{i-1,j} & \emptyset_{i,j} & \emptyset_{i+1,j} & \dots\dots & \emptyset_{i,j+1} \end{bmatrix}$$

$$V_{wp} = V(c_w + c_r)[0 \quad \dots \quad \emptyset_{i,j} \times (S_w)_{i,j} \quad 0 \quad \dots \quad 0];\ V_{op} = V\left[0 \quad \dots \quad \left\{\emptyset S_o\left(\frac{\partial B_o}{\partial p} + \frac{c_r}{B_o}\right)\right\}_{i,j} \quad 0 \quad \dots \quad 0\right]$$

$$V_{gp} = V\left[0 \quad \dots \quad \left\{\emptyset S_g\left(\frac{\partial B_g}{\partial p} + \frac{c_r}{B_o}\right) + \frac{R_{so}\emptyset S_o}{5.615}\left(\frac{\partial B_o}{\partial p} + \frac{c_r}{B_o}\right) + \emptyset S_o \frac{\frac{\partial R_{so}}{\partial p}}{5.615 B_o}\right\}_{i,j} \quad 0 \quad \dots \quad 0\right]$$

$$V_{ap} = V\left[0 \quad \dots \quad \left\{\emptyset S_a \frac{c_r}{B_a} + R_a \emptyset S_o\left(\frac{\partial B_o}{\partial p} + \frac{c_r}{B_o}\right)\right\}_{i,j} \quad 0 \quad \dots \quad 0\right]$$

$$V_{wsw} = V[0 \quad \dots \quad \emptyset_{i,j} \quad 0 \quad \dots \quad 0]; \qquad V_{wsg} = 0; \qquad V_{wsa} = 0$$

$$V_{osw} = V_{osg} = V_{osa} = -V\left[0 \quad \dots \quad \left\{\frac{\emptyset}{B_o}\right\}_{i,j} \quad 0 \quad \dots \quad 0\right];$$

$$V_{gsw} = V_{gsa} = -V\left[0 \quad \dots \quad \left\{\frac{R_{so}\emptyset}{5.615B_o}\right\}_{i,j} \quad 0 \quad \dots \quad 0\right]; \qquad V_{gsg} = -V\left[0 \quad \dots \quad \left\{\frac{\emptyset}{B_g} - \frac{R_{so}\emptyset}{5.615B_o}\right\}_{i,j} \quad 0 \quad \dots \quad 0\right]$$

$$V_{asw} = V_{asg} = -V\left[0 \quad \dots \quad \left\{\frac{R_a\emptyset}{B_o}\right\}_{i,j} \quad 0 \quad \dots \quad 0\right]; \qquad V_{asa} = -V\left[0 \quad \dots \quad \left\{\frac{\emptyset}{B_a} - \frac{R_a\emptyset}{B_o}\right\}_{i,j} \quad 0 \quad \dots \quad 0\right]$$

$$T_w = \left[-(T_w)_{i,j-\frac{1}{2}} \quad \cdots \quad -(T_w)_{i-\frac{1}{2},j} \quad \left((T_w)_{i,j-\frac{1}{2}} + (T_w)_{i-\frac{1}{2},j} + (T_w)_{i+\frac{1}{2},j} + (T_w)_{i,j+\frac{1}{2}}\right) \quad -(T_w)_{i+\frac{1}{2},j} \quad \cdots \quad -(T_w)_{i,j+\frac{1}{2}}\right]$$

$$T_o = \left[-(T_o)_{i,j-\frac{1}{2}} \quad \cdots \quad -(T_o)_{i-\frac{1}{2},j} \quad \left((T_o)_{i,j-\frac{1}{2}} + (T_o)_{i-\frac{1}{2},j} + (T_o)_{i+\frac{1}{2},j} + (T_o)_{i,j+\frac{1}{2}}\right) \quad -(T_o)_{i+\frac{1}{2},j} \quad \cdots \quad -(T_o)_{i,j+\frac{1}{2}}\right]$$

$$T_g = \left[-T_g + R_{so}T_o{}_{i,j-\frac{1}{2}} \quad \cdots \quad -(T_g + R_{so}T_o)_{i-\frac{1}{2},j} \quad \left((T_g + R_{so}T_o)_{i,j-\frac{1}{2}} + (T_g + R_{so}T_o)_{i-\frac{1}{2},j} + (T_g + R_{so}T_o)_{i+\frac{1}{2},j} + (T_g + R_{so}T_o)_{i,j+\frac{1}{2}}\right) \quad -(T_g + R_{so}T_o)_{i+\frac{1}{2},j} \quad \cdots \quad -(T_g + R_{so}T_o)_{i,j+\frac{1}{2}}\right]$$

$$T_a = \left[-(T_a + R_aT_o)_{i,j-\frac{1}{2}} \quad \cdots \quad -(T_a + R_aT_o)_{i-\frac{1}{2},j} \quad \left((T_a + R_aT_o)_{i,j-\frac{1}{2}} + (T_a + R_aT_o)_{i-\frac{1}{2},j} + (T_a + R_aT_o)_{i+\frac{1}{2},j} + (T_a + R_aT_o)_{i,j+\frac{1}{2}}\right) \quad -(T_a + R_aT_o)_{i+\frac{1}{2},j} \quad \cdots \quad -(T_a + R_aT_o)_{i,j+\frac{1}{2}}\right]$$

$$q_w = [\dots \quad (q_w)_{i,j} \quad \dots], \qquad q_g = \left[\dots \quad (q_g)_{i,j} \quad \dots\right], \qquad q_o = [\dots \quad (q_o)_{i,j} \quad \dots], \qquad q_a = [\dots \quad (q_a)_{i,j} \quad \dots]$$

After simplification, Eq. (5-27) can be rewritten as follows:

$$\begin{bmatrix} p \\ S_w \\ P_b/S_g \\ P_a/S_a \end{bmatrix}_{t+1} = A_t \begin{bmatrix} p \\ S_w \\ P_b/S_g \\ P_a/S_a \end{bmatrix}_t + B_t[q_{tp}] - E_t + Q_t; \quad Q_t \sim N(0, \Sigma_t^m) \tag{5-28}$$

The corresponding equation for production well *(i,j)* to show the flow rate in terms of other parameters (e.g., fluid and reservoir characteristics) is given below:

$$q_o = \left(\frac{2 \times \pi \times k \times h \times 6.33 \times 10^{-3}}{\left[log\frac{r_e}{r_w} + S\right]}\left[\frac{k_{ro}}{B_o\,\mu_o}\frac{S_o}{S_a + S_o}\right]\right)_t \left[p_{i,j}{}_{t+1} - p_{prod}{}_{t+1}\right] = J_{p}{}_t\left[p_{i,j}{}_{t+1} - p_{prod}{}_{t+1}\right] \tag{5-29}$$

$$p_{prod_{t+1}} = p_{i,j_{t+1}} - \left(J_{p_t}\right)^{-1} q_{p_t}; where\ J_{p_t} = \left(\frac{2\times\pi\times k\times h\times 6.33\times10^{-3}}{\left[log\frac{r_e}{r_w}+S\right]}\left[\frac{k_{ro}}{B_o\,\mu_o}\frac{S_o}{S_a+S_o}\right]\right)_t ;$$

The state-space form of the well's flow rate equation can be rewritten as follows:

$$\left[p_{prod}\right]_{t+1} = [1 \quad 0 \quad 0 \quad 0]\begin{bmatrix} p \\ S_w \\ P_b/S_g \\ P_a/S_a \end{bmatrix}_{t+1} + \left[\left(J_{p_t}\right)^{-1}\right]\left[-q_{tp}\right]_t + R_{t+1}, \quad R_{t+1} \sim N\left(0, \Sigma_{t+1}^{y}\right) \tag{5-30}$$

5.4.2 Asphaltene Deposition Model and Update to Reservoir Parameters

Wang and Civan (2001) developed asphaltene deposition model (Eq. 5-33) considering surface deposition, entrainment, and pore throat plugging create entrapment to porous media which alters the reservoir rock properties. In this study, that model is used for deposition calculation.

$$\frac{\partial E_a}{\partial t} = \alpha_a C_a \varphi - \beta E_a\left(v_o - v_{cr,o}\right) + \gamma_i(1+\sigma E_a)u_L C_a \tag{5-31}$$

where,

E_a = Volume fraction of deposited asphaltene on rock.
C_a = Volume fraction of precipitated asphaltene.
Φ = Porosity of the formation.
v_o, = Interstitial velocity of oil.
$v_{cr,o}$ = Critical value of v_o.
u_L = Darcy velocity of oil.

In Eq. (5-31), the first term $(\alpha_a C_a \Phi)$ indicates the surface deposition; the second term $(\beta E_a(v_o - v_{cr,o}))$ reflects the entrainment; and the third term $(\gamma_i(1+\sigma E_a)u_L C_a)$ refers to the pore throat plugging. Among these three terms, surface deposition term is the dominant term (Solaimany-Nazar and Zonnouri, 2011).

After evaluating the deposition rate $\left(\frac{\partial E_a}{\partial t}\right)$, the deposited asphaltene volume fraction (E_a) is calculated using Eq. (5-32), as given below (Almehaideb, 2004):

$$E_a = E_a + \frac{\partial E_a}{\partial t} \times \Delta t \tag{5-32}$$

Eqs. (5-33) and (5-34) are used to calculate the porosity and permeability at the new time step. For this case, the model developed by Wang and Civan (2001) is followed, as given below:

$$\varphi_{t+1} = \varphi_t - E_a \quad (5\text{-}33)$$

$$k_{t+1} = f_p k_t \frac{\varphi_{t+1}}{\varphi_t} \quad (5\text{-}34)$$

Due to lack of experimental data regarding interstitial velocity and critical pore throat diameter, the entrainment effect is neglected. The deposition model constants which are used in this model (**Eq. 5-31**) are listed in **Table 5-1**.

Table 5-1: Parameters Used in the Deposition Model (Solaimany-Nazar and Zonnouri, 2011).

Parameter	**Value**	**Parameter**	**Value**
Surface deposition rate (α_a), day^{-1}	0.085	Entrainment rate constant (β), ft^{-1}	0
Critical interstitial velocity ($v_{cr,o}$), ft/day	0	Pore throat plugging constant (γ_i), ft^{-1}	0.07
Snowball rate constant (σ)	0.1	Coefficient for permeability modification (f_p)	1

5.4.3 Initial and Boundary Conditions

Initial reservoir pressure is above upper asphaltene precipitation pressure. Therefore, asphaltene stays dissolved in the oil mixture, and the volume fraction of suspended asphaltene (C_a) and volume fraction of deposited asphaltene (E_a) will be zero in the entire reservoir. Thus, there will be no reduction in reservoir parameters (porosity and permeability).

- $C_a = 0,\ 0 < r_e,\ 0 < z < h,\ t = 0$
- $E_a = 0,\ 0 < r_e,\ 0 < z < h,\ t = 0$
- $\Phi = \Phi_0,\ 0 < r_e,\ 0 < z < h,\ t = 0$
- $k = k_0,\ 0 < r_e,\ 0 < z < h,\ t = 0$

5.4.4 Implementation of EnKF

In this section, implementation of EnKF is described stepwise.

Steps of EnKF for the Reservoir Model:

1. Forecast of the states through forward model

$$\begin{bmatrix} p \\ S_w \\ P_b/S_g \\ P_a/S_a \\ k \\ \emptyset \end{bmatrix}_{t+1}^{i-} = A_t \begin{bmatrix} p \\ S_w \\ P_b/S_g \\ P_a/S_a \\ k \\ \emptyset \end{bmatrix}_t^{i+} + B_t \left[-q_p\right]_t^i + {Q_t}^i; \quad {Q_t}^i \sim N(0, \Sigma_t^m) \quad (5\text{-}35)$$

Forcing data perturbation, $\left[-q_p\right]^i{}_t = \left[-q_p\right]_t + \zeta^t{}_i \;\; ; \;\; \zeta^t{}_i \sim N(0, \Sigma_t^u)$ $(5-35a)$

Ensemble mean of the state variables, $\begin{bmatrix} \overline{p} \\ S_w \\ P_b/S_g \\ \frac{P_a/S_a}{k} \\ \emptyset \end{bmatrix}_{t+1} = \frac{1}{N}\sum_{i=1}^{N} \begin{bmatrix} p \\ S_w \\ \frac{P_b}{S_g} \\ \frac{P_a}{S_a} \\ \frac{k}{\emptyset} \end{bmatrix}^{i-}_{t+1}$ (5-36)

2. Prediction of the measurement

$$\left[P_{prod}\right]_{t+1} = [[1 \quad 0 \quad 0\,0 \quad 0] \quad [0 \quad 0]] \begin{bmatrix} p \\ S_w \\ P_b/S_g \\ \frac{P_a/S_a}{k} \\ \emptyset \end{bmatrix}^{i-}_{t+1} + \left[\left(J_{p_t}\right)^{-1}\right]\left[\left[-q_{tp}\right]\right]^i{}_t \quad (5\text{-}37)$$

Ensemble mean of prediction, $\left[\overline{P}_{prod}\right]_{t+1} = \frac{1}{N}\sum_{i=1}^{N}\left[\hat{P}_{prod}\right]^i{}_{t+1}$ (5-38)

Here, Σ_{t+1}^{yy} , Σ_{t+1}^{xy} are the forecast error covariance matrix of the prediction and cross covariance of the state variables and prediction. They are defined as follows:

$$\Sigma_{t+1}^{yy} = \left(\left[\hat{P}_{prod}\right]^i{}_{t+1} - \left[\overline{P}_{prod}\right]_{t+1}\right)\left(\left[\hat{P}_{prod}\right]^i{}_{t+1} - \left[\overline{P}_{prod}\right]_{t+1}\right)^T \quad (5\text{-}39)$$

$$\Sigma_{t+1}^{xy} = \left(\left[\hat{P}_{prod}\right]^i{}_{t+1} - \left[\overline{P}_{prod}\right]_{t+1}\right)\left(\begin{bmatrix} p \\ S_w \\ \frac{P_b}{S_g} \\ \frac{P_a}{S_a} \\ \frac{k}{\emptyset} \end{bmatrix}^{i-}_{t+1} - \begin{bmatrix} \overline{p} \\ S_w \\ \frac{P_b}{S_g} \\ \frac{P_a}{S_a} \\ \frac{k}{\emptyset} \end{bmatrix}_{t+1}\right)^T \quad (5\text{-}40)$$

Perturbed production data, $\left[P_{prod}\right]_{t+1}{}^i = \left[P_{prod}\right]_{t+1} + \eta^i{}_{t+1}; \;\; \eta^i{}_{t+1} \sim N\left(0, \Sigma_{t+1}^y\right)$ (5-41)

Kalman gain calculation, $K_{t+1} = \Sigma_{t+1}^{xy}\left[\;\Sigma_{t+1}^{yy} + R_{t+1}\right]^{-1}, R_{t+1} \sim N\left(0, \Sigma_{t+1}^y\right)$ (5-42)

Updated state $\begin{bmatrix} p \\ S_w \\ P_b/S_g \\ \frac{P_a/S_a}{k} \\ \emptyset \end{bmatrix}^{i+}_{t+1} = \begin{bmatrix} p \\ S_w \\ P_b/S_g \\ \frac{P_a/S_a}{k} \\ \emptyset \end{bmatrix}^{i-}_{t+1} + K_{t+1}\left(\left[P_{prod}\right]_{t+1}{}^i - \left[\hat{P}_{prod}\right]^i{}_{t+1}\right)$ (5-43)

For reservoir simulation, the execution of ensemble Kalman filter with integrated asphaltene precipitation model is presented in **Figure 5-4**. According to the flowchart as shown in **Figure 5-4**, it is noticed that forward model is used for state and parameter estimation at every new time step. However, as reservoir pressure declines, state variables for gas and asphaltene phase go through a change from 'saturation pressure' to saturation. A detailed description on this shifting is presented below.

Based on **Figure 5-1**, the initial reservoir pressure (P_R) is higher than upper asphaltene saturation pressure (P_{UAOP}) and at this pressure asphaltene stays in dissolved condition in the oil phase; no separate asphaltene phase is formed. Therefore, at the initial reservoir pressure, state variable for asphaltene phase is defined as asphaltene pressure ($P_a = P_{UAOP}$). Later, when reservoir pressure drops below asphaltene saturation pressure (P_{UAOP}), asphaltene starts to precipitate from oil phase and forms a separate phase called asphaltene phase (solid phase). Therefore, state variable of asphaltene is switched from asphaltene saturation pressure ($P_a = P_{UAOP}$) to asphaltene saturation (S_a). This state variable is continued until reservoir pressure drops further below lower asphaltene saturation pressure (P_{LAOP}). From this pressure, state variable again is switched from S_a to P_a.

The similar type of state variable switching happens for the gas phase. Before bubble point, gas stays in dissolved condition in oil and from bubble point, the free gas starts to release from oil and forms gas phase. As a result, above bubble point pressure (P_b), state variable for gas is P_b and from bubble point pressure, the state variable is changed to S_g.

While applying ensemble Kalman filter, the state variable change in the sample is directed based on reflection of majority of the samples as shown in **Figure 5-5**.

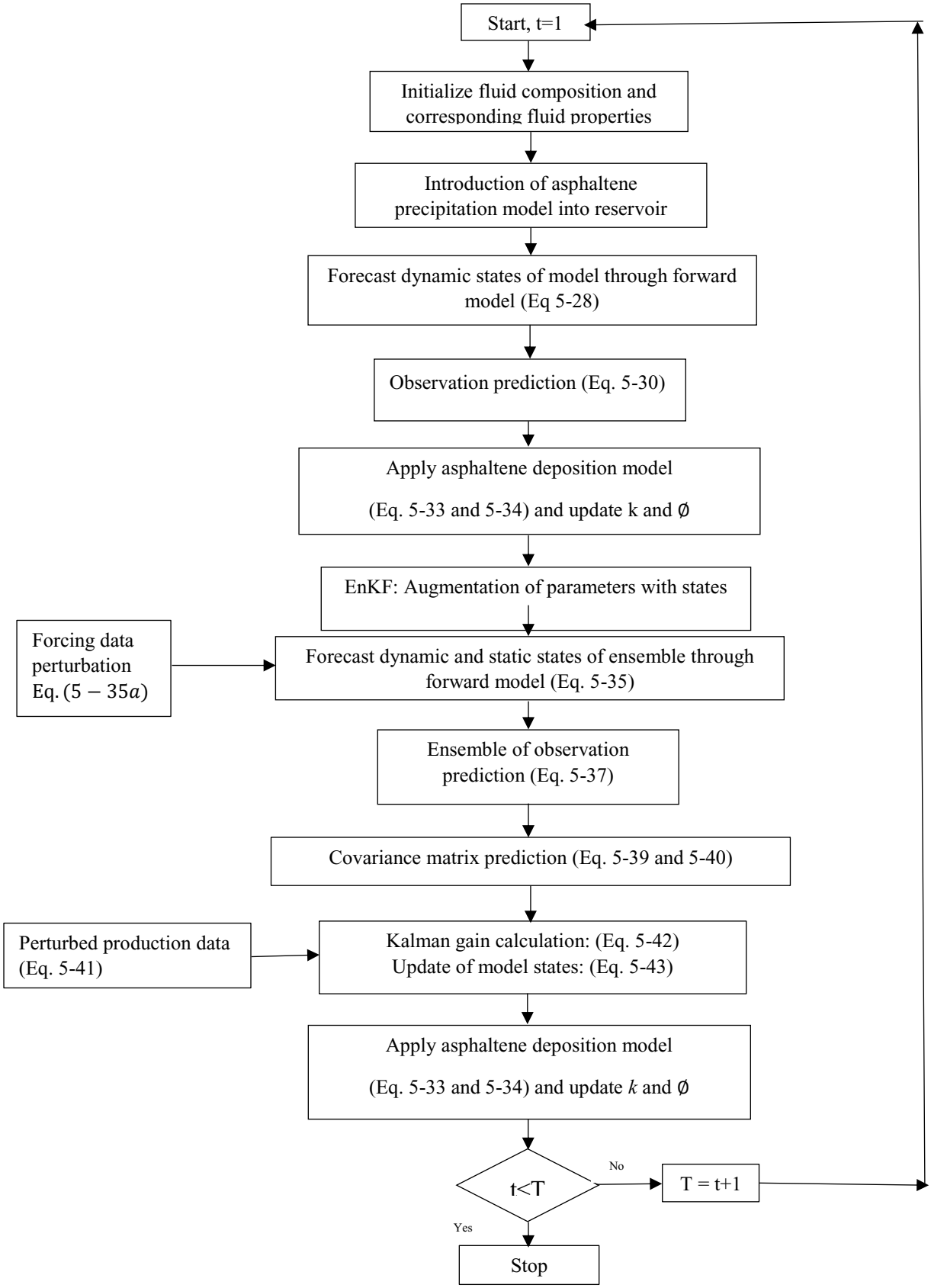

Figure 5-4: Flow Chart for Reservoir Simulation

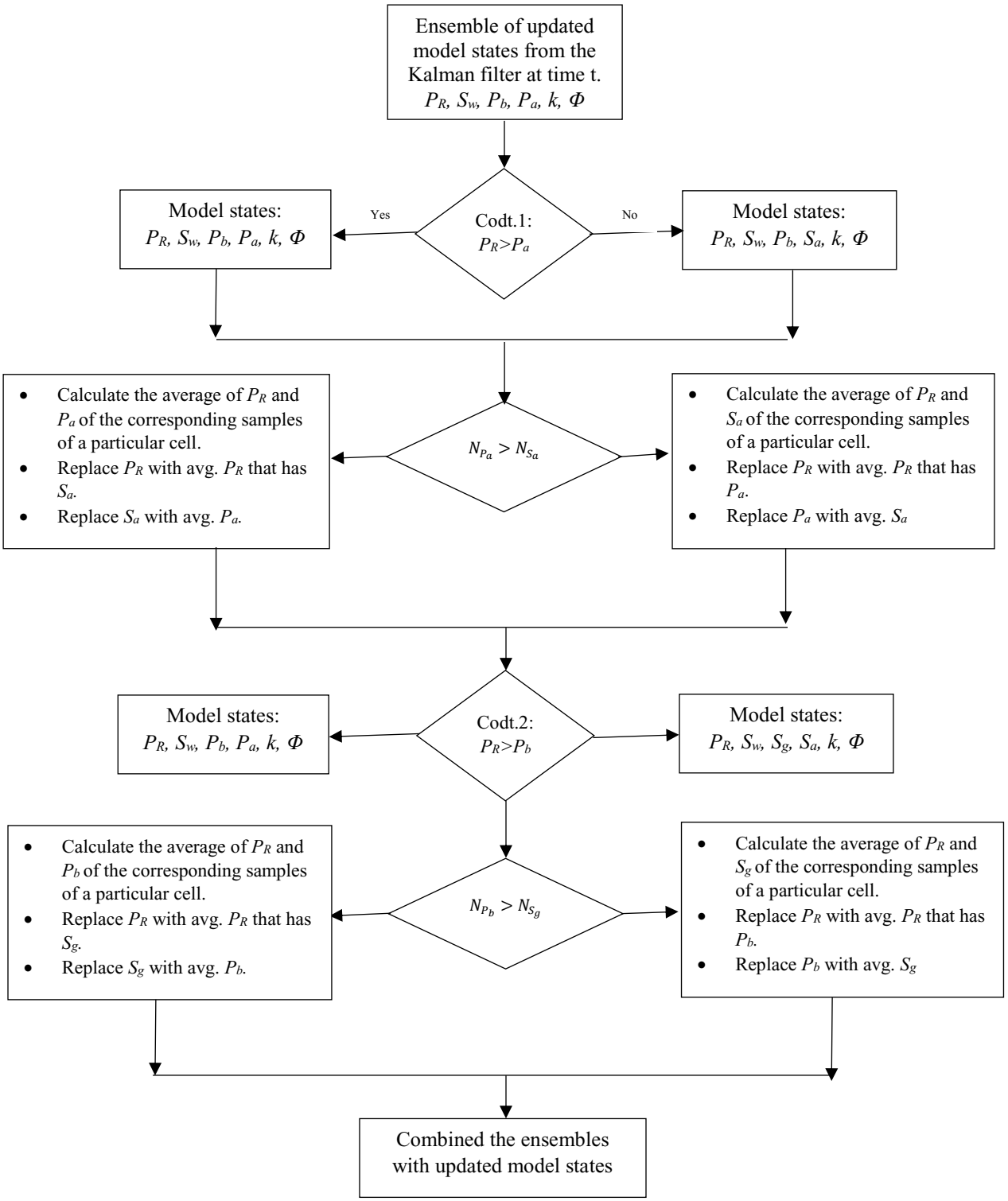

Figure 5-5: Update of Model States in Ensembles

5.5 Results and Discussion

In this section, all the results obtained from asphaltene precipitation model and reservoir simulation with the application of ensemble Kalman filter are given along with adequate discussion.

5.5.1 Asphaltene precipitation

Regarding asphaltene precipitation calculation, oil sample is taken from Burke et al.(1990), and the modified asphaltene precipitation methodology is applied. The oil characteristics are given in **Table 5-2** and **Table 5-3**.

Table 5-2: Composition and Properties of Oil Sample (Burke et al., 1990)

Component Name	**Mole (%)**	**Property**	**Value**
Nitrogen	0.57	Molecular weight of HeptanePlus	329
Carbon dioxide	2.46	Specific gravity of HeptanePlus	0.9594
Methane	36.37	Live oil molecular weight, M_{oil}	171.4
Ethane	3.47	API gravity of stock tank oil	19
Propane	4.05	Asphaltene content in stock tank oil (w_{asp}), (wt %)	16.08
iso-Butane	0.59	Reservoir temperature, (^{o}F)	212
n-Butane	1.34	Saturation pressure, (psia)	2950
iso -Pentane	0.74	Initial reservoir pressure, (psia)	5260
n-Pentane	0.83	--	--
Hexane	1.62	--	--
HeptanePlus	47.96	--	--
Total	100	--	--

Table 5-3: Asphaltene Precipitation Data (Burke et al., 1990)

Test pressure, (psia)	Precipitates from live oil (wt %)	Precipitates remaining in residual stock tank oil (wt %)	Total precipitates (wt %)	Asphaltene solubility, Ra (stb/stb)
LAOP=387	0	16.08	16.08	0.18736
1014.7	0.403	15.73	15.73+0.403=16.133	0.18179
2014.7	1.037	14.98	14.98+1.037=16.107	0.17318
3034.7	0.742	15.06	15.06+0.742=15.802	0.17712
4014.7	0.402	14.86	14.86+0.402=15.262	0.18179
UAOP=5173	0	16.08	16.08	0.18736
Average total precipitates (from experiment)			15.826	--

The mole fraction of the heaviest component C_{7+} contains components from C_7 to C_{31+}. For simplification of calculation, all oil components are lumped into seven components as shown in **Table 5-4**. The heaviest component C_{31+} is split into non-precipitating (C_{31A+}) and precipitating (asphaltene) component. The mole fraction of these two are calculated as follows:

$$z_{asp} = \frac{w_{asp}}{100} \times \frac{M_{oil}}{M_{asp}} = \frac{16.08}{100} \times \frac{171.4}{665.624} = 0.0414$$

$$z_{C31A+} = 1 - z_{asp} - \sum_{i=1}^{30} z_i = 1 - 0.0414 - 0.8825 = 0.0761$$

Table 5-4: Recombined Oil Composition and Critical Properties (Darabi et al., 2014)

Component	P_c (psia)	T_c (^{o}R)	V_c (ft^3/lb-mol)	Molecular weight	Acentric factor	Composition, z_i
CO_2	1070.09	547.56	1.50711	44.01	0.225	0.0246
C_1-C_2	668.51	360.61	1.6431	17.417	0.0115127	0.4041
C_3-C_5	573.15	732.89	3.8098	53.516	0.179313	0.0755
C_6-C_{19}	291.41	1135.31	13.7197	164.423	0.655007	0.2719
C_{20}-C_{30}	175.41	1419.29	29.033	340.927	1.064023	0.1064
C_{31A+}	143.17	1682.93	56.5486	665.624	1.371778	0.0761
Asphaltene	143.17	1682.93	56.5486	665.624	1.371778	0.0414

For flash calculation, 'PR EoS' is used to model the gas and oil phases. The required binary interaction coefficient (*BIC)* is calculated using Eq. (5-7). *BIC* of asphaltene with lighter components (CO_2 to C_5) is calculated with an aim to match the saturation pressure. The numerical values of *BIC* and solid model parameters are presented in **Table 5-5** and **Table 5-6**, respectively.

Table 5-5: BIC for the Oil Sample Used in PR EOS

	CO_2	**C_1-C_2**	**C_3-C_5**	**C_6-C_{19}**	**C_{20}-C_{30}**	**C_{31A+}**	**Asphaltene**
CO_2	0.000	0.000	0.007	0.037	0.065	0.095	0.220
C_1-C_2	0.000	0.000	0.006	0.035	0.062	0.091	0.220
C_3-C_5	0.007	0.006	0.000	0.013	0.032	0.055	0.220
C_6-C_{19}	0.037	0.035	0.013	0.000	0.004	0.016	0.000
C_{20}-C_{30}	0.065	0.062	0.032	0.004	0.000	0.004	0.000
C_{31A+}	0.095	0.091	0.055	0.016	0.004	0.000	0.000
Asphaltene	0.220	0.220	0.220	0	0	0	0

Table 5-6: Asphaltene Precipitation Model Parameters.

Parameter Name	**Value**
Reference pressure, *(P^*, psia)*	5173
Asphaltene fugacity at P^*, *(f^*, lb-mol/ft^{-3})*	3.95e-7
Molar volume of asphaltene, *(V_a, ft^3/lb-mol)*	10.068

Figure 5-6 represents the comparative asphaltene precipitation results obtained from the methodology presented in this chapter, original solid model, and results from Nghiem et al.(1999) along with the experimental data.

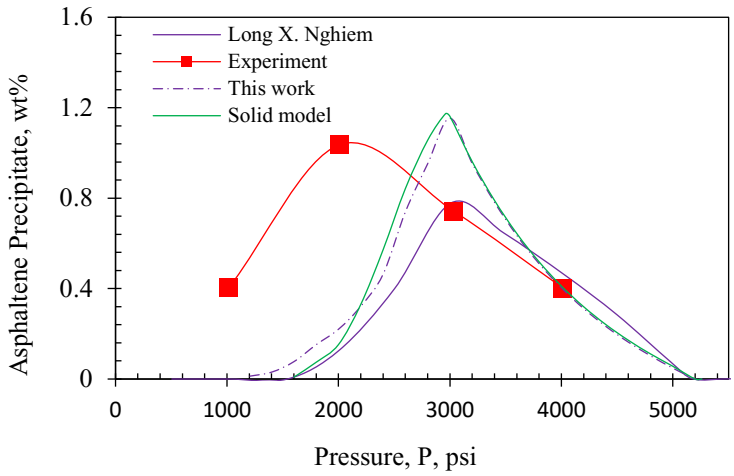

Figure 5-6: Comparison of Asphaltene Precipitation Results

Based on the proposed precipitation methodology, the calculated bubble point pressure is 3000 psia which is aligned with the result presented by solid model (original) and Nghiem et al.(1999). However, comparing with the experimental value a big deviation is observed. Nghiem et al.(1999) reported the inconsistency about the bubble point in their work. At bubble point pressure gas solubility is maximum. After this point, as gas evolves from oil and so, gas concentration is reduced in the oil. This makes asphaltene to re-dissolve in the oil mixture. Here dissolved gas acts as a bad solvent for asphaltene and asphaltene tends to precipitate in presence of dissolved gas (Pedersen et al., 2014). Therefore at bubble point pressure, the maximum asphaltene precipitation is noticed (Pedersen et al., 2014). From this theoretical aspect, it can be concluded that there might be an error in measuring the asphaltene precipitation. Since in Nghiem et al. (1999) work first two initial points are matched properly; the calculated bubble point by Nghiem et al. (1999) can be used as the reference value instead of the experimental value (Gonzalez et al., 2017).

Figure 5-6 shows that for all cases asphaltene precipitation increases with pressure decline and reaches to its maximum value at the bubble point pressure; upon further decline from the bubble point, as the free gas releases, a change in oil composition happens and the amount of precipitation starts to decline. Although the trend is the same for all cases, a difference is observed in calculating the amount of asphaltene precipitation by different approaches.

At bubble point pressure, the modified solid model shows 1.16 wt% precipitated asphaltene and from the work done by Nghiem et al. (1999), precipitated asphaltene is about 0.804 wt%. However,

according to the experimental data obtained by Burke et al. (1990), the amount of precipitated asphaltene is 1.037wt%. The deviation of the modified version and Nghiem work from the experimental data is about 10.06% and 28.09% respectively. Note that Darabi et al. (2014) and Qin et al. (2000) showed 1.1463 wt% and 1.07 wt% asphaltene precipitation at the bubble point. Several influential factors (such as components grouping and corresponding binary interaction coefficient, molar volume of asphaltene, total asphaltene content and the empirical parameters in the solid model) are responsible to make difference in calculating asphaltene precipitation by different approaches. In addition, the type of EoS plays a role for the deviation.

5.5.2 Implementation of EnKF in Reservoir Simulation

Results on parameter estimation followed by history matching is presented in this section. For this part, the ensemble Kalman filter is run for 1000 days from the first day of the production. The total number of ensembles is set 50. A random model error is added with standard deviation for pressure 0.01. In addition, random measurement error is included with standard deviation of 0.03.

The water present in the reservoir is assumed connate water. Therefore, water production does not have any impact on the result. The production well is constrained by constant production with a flow rate of 300 ft^3/day. The dynamic asphaltene precipitation model is incorporated into the reservoir model to capture the asphaltene precipitation for each time step and pressure drop. Here in the history matching section, all the red color lines represent the trend obtained from the model, green lines represent the average resulting from 50 ensembles and other lines are the estimates for all 50 ensembles.

Pressure and flow rate matching: The pressure and flow rate outcome for the production well is depicted in **Figure 5-7**. **Figure 5-7a** shows the well bottomhole pressure profile and **Figure 5-7b** shows the fluid (oil and gas) flow rate profile obtained from the model and EnKF filter. For both cases, the deviation between model and filter is represented in terms of root mean square error (RMSE). For pressure profile case, RMSE is around 11.92. On the other hand, calculated RMSE for the oil and gas are 19.56 and 24.52 respectively. The small difference for both cases shows a good agreement between the model and EnKF in terms of pressure and flow rate matching.

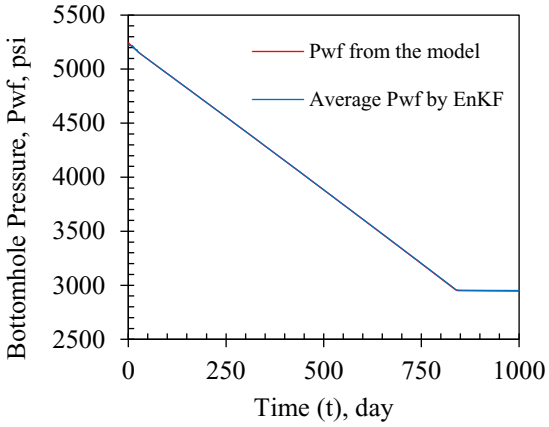

a) Well Bottomhole Pressure

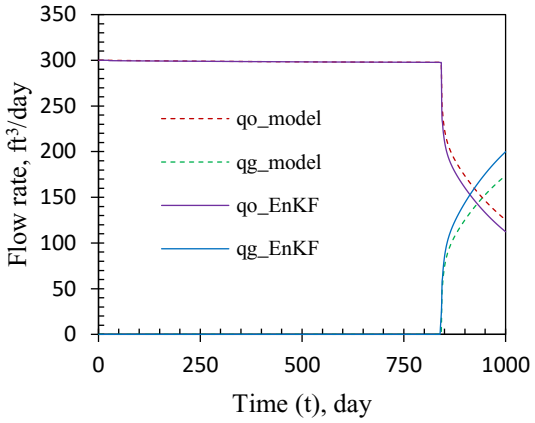

a) Well Oil and Gas Flow Rate

Figure 5-7: Well Bottomhole Pressure and Fluid Flow Rate at the Production Well

Gas saturation and asphaltene saturation matching: Figure 5-8 displays the gas and asphaltene saturation profile resulted from the model and EnKF filter. **Figure 5-8 a** shows that gas saturation starts to build up from 842th day. As the pressure keeps declining, more gas evolves and accumulates. After reaching S_g=S_{gc}=0.05, accumulated gas starts to flow. On the other hand, asphaltene starts to build up from 23th day and reaches to maximum value of S_a= 0.003866 at the bubble point. Afterwards, the saturation of suspended asphaltene starts to decline. It is clear from **Figure 5-8** that for both cases, the ensemble follows the trend of the model and shows a small deviation from the model. The small difference in gas and asphaltene saturation profiles portrays a good matching between the model and filter.

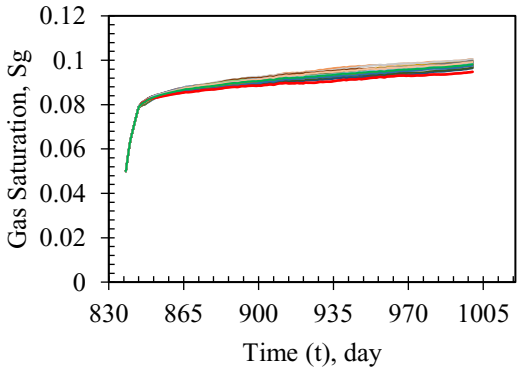

a) Gas Saturation in the Production Well

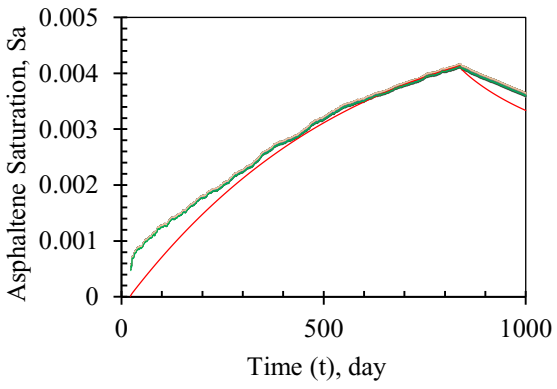

b) Asphaltene Saturation in Production Well

Figure 5-8: Gas and Asphaltene Saturation Buildup in the Production Well

Reservoir parameters estimation: After matching the bottomhole pressure, fluid flowrate, and gas and asphaltene saturation with the model, reservoir parameters 'porosity and permeability' profile are generated with respect to grid position and suspended asphaltene saturation for capturing the dynamics of the change and corresponding estimation.

Figure 5-9 represents the reservoir parameters 'permeability-porosity' change with respect to grid position where thick red line represents the data obtained from the model. Model data shows that maximum reduction of porosity and permeability happened around the grid block 1 (wellbore zone). Due to production, pressure declines faster around the wellbore compared to other grid blocks and therefore buildup of suspended asphaltene saturation happens near the wellbore earlier. This leads to higher amount of asphaltene precipitation and deposition on the rock surface in this zone. From permeability and porosity profile as shown in **Figure 5-9 a** and **b,** the similar situation happened for all the ensembles which indicates the consistency with the history matching.

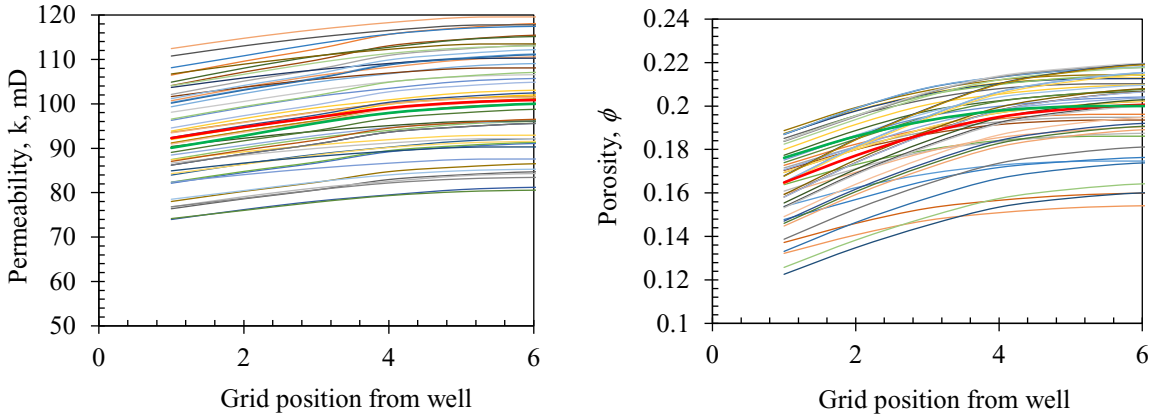

a) Permeability Change with Grid

a) Porosity Change with Grid

Figure 5-9: Parameter Change with Grid Position

Figure 5-10 represents the reservoir parameters 'permeability- porosity' change with respect to suspended asphaltene saturation build up. As shown in **Figure 5-10 a** and **b**, more reduction in porosity and permeability has been found where the suspended asphaltene saturation is higher.

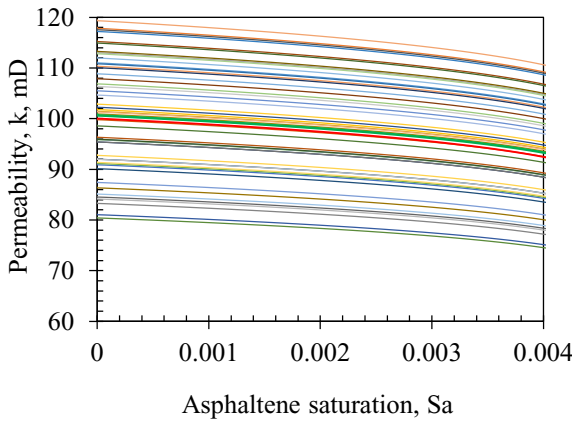

a) Permeability Change with Asphaltene Saturation

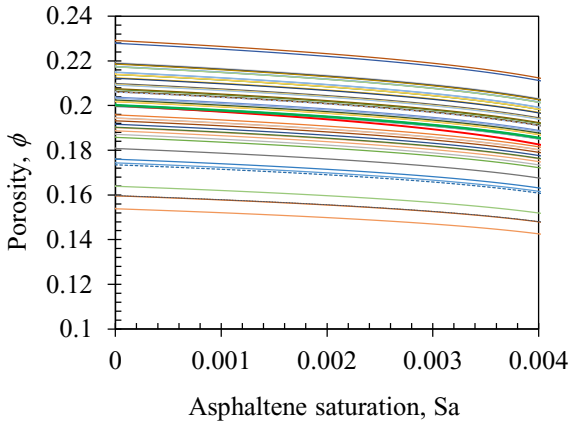

a) Porosity Change with Asphaltene Saturation

Figure 5-10: Parameter Change with Asphaltene Saturation

For both permeability and porosity profiles presented in **Figure 5-9** and **Figure 5-10**, all ensembles followed the profile obtained from the model (represented in thick red color). Moreover, the average line (thick green color) of the ensembles follows the model trend with small error. This ensures the accuracy of the estimated value of the parameters.

Following the results obtained in **Figure 5-9** and **Figure 5-10**, the distribution of permeability and porosity is presented in **Figure 5-11**.

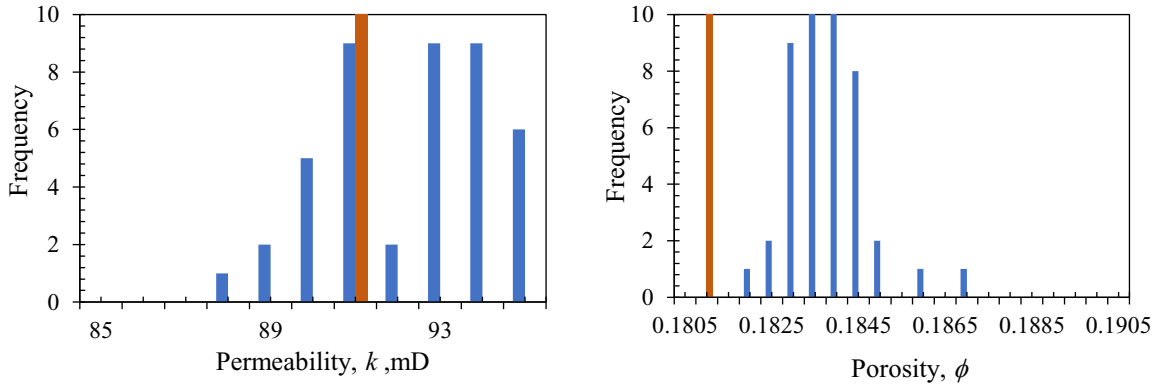

Figure 5-11: Parameter Estimation after 1000 Time Steps of Simulation.

For permeability case, the estimated permeability from the filter is about 91 mD, whereas the calculated value from the model is 91.83 mD resulting 0.91% error. On the other hand, the estimated values for porosity from the EnKF and the model are around 0.184 and 0.181, respectively and the corresponding error is about 1.657%. For both cases the error is quite small.

5.6 Conclusions

In this study, ensemble Kalman filter is applied for the estimation of the two key parameters such as permeability and porosity. For reservoir simulation, the asphaltene precipitation model is coupled with the reservoir model. In this case, modified solid model is applied for faster asphaltene precipitation calculation.

For bubble point calculation, around 10.06 % difference between the modified version and experimental work and for asphaltene calculation 9.945% difference between the modified model and original model have been observed. The small deviation in bubble point and asphaltene calculation shows a good agreement between these two approaches.

History matching has been done with respect to bottomhole pressure profile and gas/asphaltene saturation profile generation. The result obtained from the Kalman filter shows the consistency with the model in terms of profile trend and the bubble point matching. Between model and Kalman filter, small value of RMSE for pressure (11.92) validates the implementation of the EnKF to the asphaltic oil reservoir.

Regarding application of the EnKF to the asphaltic oil reservoir, the big challenge is to deal with the state variable change with pressure. Good history matching validates the proposed methodology for the application of the EnKF to this reservoir.

The simulation also shows that around the wellbore, the suspended asphaltene saturation is maximum leading to maximum asphaltene precipitation. In this zone, maximum alteration for porosity and permeability has been observed both for the model and filter. The overlap between the average value of ensemble and the model for both porosity and permeability profiles indicates the correct estimation of these two parameters. In estimation of porosity and permeability, an error of 0.91 % for permeability and 1.67% of porosity are obtained.

This work has been conducted assuming primary recovery, constant well flowrate, synthetic and homogeneous reservoir in terms of porosity and permeability, no capillary pressure, and no gravity effect. Therefore, implementation of EnKF can be extended to more challenging

cases such as heterogeneous reservoir, secondary oil recovery process (CO_2 injection), and real oil field case. In addition, other reservoir parameters such as capillary pressure, wettability, temperature can be incorporated for further investigation.

Acknowledgements

The researchers gratefully acknowledge and thank Equinor Canada, Memorial University, Innovate NL, and the Natural Sciences and Engineering Research Council of Canada (NSERC) for providing funding for the work.

Nomenclature

English letters

B_w	Formation volume factor of water res. (ft^3/std. ft^3)
B_o	Formation volume factor of oil res. (ft^3/std. ft^3)
C_w	Water compressibility (psi^{-1})
C_o	Oil compressibility (psi^{-1})
C_r	Rock compressibility (psi^{-1})
C_a	Volume ratio of suspended asphaltene in oil phase (ft^3/ft^3)
e	Exponent determined by matching the saturation pressure.
E_a	Volume fraction of deposited asphaltene
f_w	Water fraction
f_a^*	Fugacity of asphaltene at P^*
f_a	Fugacity of asphaltene at any P
h	Thickness of the reservoir (ft)
J	Productivity Index (ft^3/psi-day)
k	Absolute permeability (mD)
k_{rw}	Relative permeability to water
k_{ro}	Relative permeability to oil

$\vec{K}$	Permeability tensor
n	Covariance of ensemble
N_p	Particle size
P	Reservoir pressure (psi)
P_{UAOP}	upper asphaltene onset pressure (psi)
P_{LAOP}	Lower asphaltene onset pressure (psi)
P_b	Bubble point pressure (psi)
P_{wf}	Bottom hole flowing pressure (psi)
q_{inj}	Injection rate (ft^3/day)
q_p	Production rate (ft^3/day)
q_o'''	Oil flow rate per unit volume (ft^3/day-ft^3)
q_w'''	Water flow rate per unit volume (ft^3/day-ft^3)
r_w	Wellbore radius (ft)
r_e	Distance between reservoir outer boundary to wellbore (ft)
r	Tuning factor for particle perturbation
R	Molar gas constant (ft^3.psi. $°R^{-1}$.lb-mol^{-1})
S_w	Water saturation (fraction)
S_o	Oil saturation (fraction)
S_g	Gas saturation (fraction)
S_a	Asphaltene saturation (fraction)
T	Transmissibility
u_L	Oil phase Darcy velocity (ft^3/day)
V	Bulk volume (ft^3)
V_a	Molar volume of pure asphaltene (ft^3/lb-mol)
V_{ci}	Critical molar volume of component I (ft^3/lb-mol)
V_{wp}	Coefficient matrix for pressure of water phase
V_{ws}	Coefficient matrix for saturation of water phase
V_{op}	Coefficient matrix for pressure of oil phase
V_{os}	Coefficient matrix for saturation of oil phase
$v_{cr,o}$	Interstitial velocity of oil phase (ft^3/day)

v_o	Interstitial velocity of oil (ft^3/day)
v	Covariance of measurement noise
w	Covariance of system noise
Δx	Grid dimension in x direction (ft)
Δy	Grid dimension in y direction (ft)

Greek Symbols

ϕ	Porosity (%)
α_a	Surface deposition rate constant
μ_w	Water viscosity (cp)
μ_o	Oil viscosity (cp)
α	Unit conversion factor
ω	Particle weight

Superscripts

t	Time step index
i	Ensemble member index in algorithm
i, j	Grid number index in the reservoir model

References

1. Ahmadi, M.A., 2011. Prediction of asphaltene precipitation using artificial neural network optimized by imperialist competitive algorithm. J. Pet. Explor. Prod. Technol. 1, 99–106. https://doi.org/10.1007/s13202-011-0013-7
2. Ahmadi, M.A., Shadizadeh, S.R., 2012. New approach for prediction of asphaltene precipitation due to natural depletion by using evolutionary algorithm concept. Fuel 102, 716–723. https://doi.org/10.1016/j.fuel.2012.05.050
3. Alimohammadi, S., Zendehboudi, S., James, L., 2019. A comprehensive review of asphaltene deposition in petroleum reservoirs: Theory, challenges, and tips. Fuel 252, 753–791. https://doi.org/10.1016/j.fuel.2019.03.016
4. Almehaideb, R.A., 2004. Asphaltene precipitation and deposition in the near wellbore region: A modeling approach. J. Pet. Sci. Eng. 42, 157–170. https://doi.org/10.1016/j.petrol.2003.12.008
5. Brouwer, D.R., Nævdal, G., Jansen, J.D., Vefring, E.H., 2004. Improved reservoir management through optimal control and continuous model updating, in: Proceedings - SPE Annual Technical Conference and Exhibition. pp. 1551–1561. https://doi.org/10.2523/90149-ms
6. Burke, N.E., Hobbs, R.E., Kashou, S.F., 1990. Measurement and modeling of asphaltene precipitation. JPT, J. Pet. Technol. 42, 1440–1446. https://doi.org/10.2118/18273-PA
7. Chamkalani, A., Zendehboudi, S., Bahadori, A., Kharrat, R., Chamkalani, R., James, L., Chatzis, I., 2014. Integration of LSSVM technique with PSO to determine asphaltene deposition. J. Pet. Sci. Eng. 124, 243–253. https://doi.org/10.1016/j.petrol.2014.10.001
8. Correra, S., Donaggio, F., 2000. OCCAM: Onset-constrained colloidal asphaltene model, in: SPE International Symposium on Asphaltene Deposition Is a Well Known Problem in Oil Formation Damage. https://doi.org/10.2118/58724-ms
9. Darabi, H., Shirdel, M., Kalaei, M.H., Sepehrnoori, K., 2014. Aspects of modeling asphaltene deposition in a compositional coupled wellbore/reservoir simulator, in: SPE Improved Oil Recovery Symposium. p. SPE-169121-MS. https://doi.org/10.2118/169121-MS
10. Fallahnejad, G., Kharrat, R., 2015. Fully implicit compositional simulator for modeling of

asphaltene deposition during natural depletion. Fluid Phase Equilib. 398, 15–25. https://doi.org/10.1016/j.fluid.2015.03.045

11. Gonzalez, K., Nasrabadi, H., Barrufet, M., 2017. Modeling asphaltene precipitation in a compositional reservoir simulator using three-phase equilibrium. J. Pet. Sci. Eng. 154, 602–611. https://doi.org/10.1016/j.petrol.2016.09.010
12. Gu, Y., Oliver, D.S., 2005. History matching of the PUNQ-S3 reservoir model using the ensemble Kalman filter. SPE J. 10, 217–224. https://doi.org/10.2118/89942-PA
13. Hirschberg, A., DeJong, L.N.J., Schipper, B.A., Meijer, J.G., 1984. Influence of temperature and pressure on asphaltene flocculation. Soc. Pet. Eng. J. 24, 283–293. https://doi.org/10.2118/11202-PA
14. Jahanbakhshi, S., Pishvaie, M.R., Boozarjomehry, R.B., 2015. Joint estimation of absolute and relative permeabilities using ensemble-based Kalman filter. J. Nat. Gas Sci. Eng. 26, 1232–1245. https://doi.org/10.1016/j.jngse.2015.08.029
15. Kohse, B.F., Nghiem, L.X., 2004. Modelling asphaltene precipitation and deposition in a compositional reservoir simulator. Proc. - SPE Symp. Improv. Oil Recover. 2004-April. https://doi.org/10.2523/89437-ms
16. Krejbjerg, K., Pedersen, K.S., 2006. Controlling VLLE equilibrium with a Cubic EoS in heavy oil modeling. Can. Int. Pet. Conf. 2006, CIPC 2006 1–15. https://doi.org/10.2118/2006-052
17. Leontaritis, K.J., Ali Mansoori, G., 1988. Asphaltene deposition: a survey of field experiences and research approaches. J. Pet. Sci. Eng. 1, 229–239. https://doi.org/10.1016/0920-4105(88)90013-7
18. Li, H., Chen, S., Yang, D., Tontiwachwuthikul, P., 2012. Estimation of relative permeability by assisted history matching using the ensemble-kalman-filter method. J. Can. Pet. Technol. 51, 205–214. https://doi.org/10.2118/156027-PA
19. Liu, N., Oliver, D.S., 2005. Critical evaluation of the ensemble Kalman filter on history matching of geologic facies, in: Reservoir Simulation and Symposium. pp. 470–477. https://doi.org/10.2118/92867-pa
20. Lorentzen, R.J., Fjelde, K.K., Frøyen, J., Lage, A.C.V.M., Nævdal, G., Vefring, E.H., 2001. Underbalanced and low-head drilling operations: real time interpretation of measured data and operational support, in: SPE Annual Technical Conference and

Exhibition. pp. 591–602. https://doi.org/10.2523/71384-ms

21. Lorentzen, R.J., Ncevdal, G., Shafieirad, A., 2013. Estimating facies fields by use of the ensemble kalman filter and distance functions-applied to shallow-marine environments. SPE J. 18, 146–158. https://doi.org/10.2118/143031-pa
22. Marquart, G., Vogt, C., Klein, C., Widera, A., 2013. Estimation of geothermal reservoir properties using the ensemble Kalman filter. Energy Procedia 40, 117–126. https://doi.org/10.1016/j.egypro.2013.08.015
23. Menshad, A.K., Mofidi, A.M., Shariatpanahi, F., Edalat, M., 2008. Developing of scaling equation with function of pressure to determine onset of asphaltene precipitation. J. Japan Pet. Inst. 51, 102–106. https://doi.org/10.1627/jpi.51.102
24. Mohebbinia, S., Sepehrnoori, K., Johns, R.T., Kazemi Nia Korrani, A., 2017. Simulation of asphaltene precipitation during gas injection using PC-SAFT EOS. J. Pet. Sci. Eng. 158, 693–706. https://doi.org/10.1016/j.petrol.2017.09.008
25. Nævdal, G., Mannseth, T., Vefring, E.H., 2002. Near-well reservoir monitoring through ensemble Kalman filter, in: SPE Symposium on Improved Oil Recovery. pp. 959–967. https://doi.org/10.2523/75235-ms
26. Nghiem, L.X., Coombe, D.A., 1997. Modeling asphaltene precipitation during primary depletion. SPE J. 2, 170–176. https://doi.org/10.2118/36106-pa
27. Nghiem, L.X., Coombe, D.A., Farouq Ali, S.M., 1998. Compositional simulation of asphaltene deposition and plugging. Proc. - SPE Annu. Tech. Conf. Exhib. 1999-Septe, 129–140. https://doi.org/10.2523/48996-ms
28. Nghiem, L.X., Hassam, M.S., Nutakki, R., George, A.E.D., 1993. Efficient modelling of asphaltene precipitation. Proc. - SPE Annu. Tech. Conf. Exhib. Sigma, 375–384. https://doi.org/10.2118/26642-ms
29. Nghiem, L.X., Thesis, A., Fulfillment, P., The, O.F., For, R., Degree, T.H.E., Philosophy, D.O.F., Engineering, P., 1999. University of alberta phase behaviour modelling and compositional simulation 120.
30. Nœvdal, G., Johnsen, L.M., Aanonsen, S.I., Vefring, E.H., 2005. Reservoir monitoring and continuous model updating using ensemble Kalman Filter. SPE Repr. Ser. 66–74. https://doi.org/10.2523/84372-ms
31. Pan, H., Firoozabadi, A., 2000. Thermodynamic micellization model for asphaltene

precipitation from reservoir crudes at high pressures and temperatures. SPE Prod. Facil. 15, 58–65. https://doi.org/10.2118/60842-PA

32. Pedersen, K.S., Christensen, P.L., Shaikh, J.A., 2014. Phase behavior of petroleum reservoir fluids. CRC Press. https://doi.org/10.1201/b17887
33. Qin, X., Wang, P., Sepehrnoori, K., Pope, G.A., 2000. Modeling asphaltene precipitation in reservoir simulation. Ind. Eng. Chem. Res. 39, 2644–2654. https://doi.org/10.1021/ie990781g
34. Sayyad Amin, J., Alamdari, A., Mehranbod, N., Ayatollahi, S., Nikooee, E., 2010. Prediction of asphaltene precipitation: Learning from data at different conditions. Energy and Fuels 24, 4046–4053. https://doi.org/10.1021/ef100106r
35. Sayyad Amin, J., Nikkhah, S., Zendehboudi, S., 2017. A new experimental and modeling strategy to determine asphaltene precipitation in crude oil. Chem. Eng. Res. Des. 128, 162–173. https://doi.org/10.1016/j.cherd.2017.09.035
36. Shuai, Y., White, C., Sun, T., Feng, Y., 2016. A gathered EnKF for continuous reservoir model updating. J. Pet. Sci. Eng. 139, 205–218. https://doi.org/10.1016/j.petrol.2016.01.005
37. Solaimany-Nazar, A.R., Zonnouri, A., 2011. Modeling of asphaltene deposition in oil reservoirs during primary oil recovery. J. Pet. Sci. Eng. 75, 251–259. https://doi.org/https://doi.org/10.1016/j.petrol.2010.11.017
38. Tabzar, A., Fathinasab, M., Salehi, A., Bahrami, B., Mohammadi, A.H., 2018. Multiphase flow modeling of asphaltene precipitation and deposition. Oil Gas Sci. Technol. – Rev. d'IFP Energies Nouv. 73, 51. https://doi.org/10.2516/ogst/2018039
39. Trani, M., Arts, R., Leeuwenburgh, O., 2012. Seismic history matching of fluid fronts using the ensemble Kalman filter. SPE J. 18, 159–171. https://doi.org/10.2118/163043-PA
40. Wang, S., Civan, F., 2001. Productivity decline of vertical and horizontal wells by asphaltene deposition in petroleum reservoirs, in: SPE International Symposium on Oilfield Chemistry. pp. 145–160. https://doi.org/10.2118/64991-ms
41. Wang, Y., Li, G., Reynolds, A.C., 2009. Estimation of depths of fluid contacts by history matching using iterative ensemble kalman smoothers, in: SPE Reservoir Simulation Symposium. pp. 750–766. https://doi.org/10.2118/119056-ms
42. Zhang, Y., Yang, D., Li, H., Patil, S., 2017. Simultaneous estimation of relative

permeability and capillary pressure for PUNQ-S3 model with a damped iterative ensemble Kalman Filter technique. SPE J. 971–984. https://doi.org/10.2118/177846-ms

Chapter 6 : Conclusions and Future Recommendations

6.1 Conclusions

This research work is performed to estimate two key parameters for reservoir (porosity and permeability) for the conditions of oil production through water injection and under asphaltene precipitation. Along with estimation, the uncertainty assessment is performed. The contributions and outcomes of the thesis are summarized below:

- For the water flooding case, Ensemble Kalman Filter (EnKF) is applied to estimate porosity and permeability. Oil reservoirs lack excitation due to less change in the operating conditions. To address that excitement, a tuning parameter is introduced in the EnKF algorithm to improve the performance of history matching and thereby parameter estimation. The proposed method is first applied to an equivalent benchmark tank series system and later the methodology is applied to a reservoir case.

  In the light of the proposed modification in EnKF, the results obtained from the reservoir and tank series shows a good improvement in history matching for low ensemble size when the uncertainty in the model and measurement are high.

- The impact of non-Gaussianity around the waterfront for water flooding in a five spot heterogeneous oil reservoir is analyzed with the application of Ensemble Kalman Filter. The results show that the applicability of EnKF to address the non-Gaussianity is limited and provides poor history matching.

- For the same reservoir case, another robust filter Particle Filter (PF) is applied in the presence of non-Gaussianity and nonlinearity in terms of saturation dependent relative permeability, source term, and pressure dependent fluid properties. It was found that the performance of EnKF is comparable with PF when the non-Gaussianity is weak. On the other hand, for strong non-Gaussianity case, EnKF shows four times higher error compared to PF.

- Particle impoverishment is very common while applying PF; this leads to poor estimation of unknown parameters. To increase the number of particles participating in resampling stage of PF, an approach called "ensemble covariance" is introduced so that the particle diversification is achieved. Due to the addition of the proposed approach, the error in porosity and permeability estimation become less compared to a typical randomization approach.

- For asphaltic oil reservoir, the asphaltene precipitation model is modified with an aim to reduce computation time. First the model is validated with the experimental results and other researcher's work in terms of bubble point pressure and asphaltene precipitation at bubble point pressure. From asphaltene precipitation calculation at sample pressure, it is found that the difference between the original and modified methods is very low. This infers that the modified model can calculate asphaltene precipitation explicitly at each step while the original model requires several steps.

- The sensitivity analysis on asphaltene precipitation results shows that among three parameters (BIC, molar volume of solid asphaltene, and total asphaltene content), the molar volume of solid asphaltene has the most impact on asphaltene precipitation.

- The reservoir simulation of asphaltic oil reservoir shows that the maximum damage/reduction of porosity and permeability happens around the near wellbore region at the bubble point pressure, P_b.

- Comparing the "asphaltene precipitation" and "no asphaltene precipitation" cases, reduced oil recovery is observed due to asphaltene precipitation. This implies the necessity of reservoir parameter estimation.
- Applying EnKF to asphaltic oil reservoir, a methodology is developed in terms of switching reservoir dynamic states such as pressure to saturation for the gas and asphaltene phases with pressure decline due to oil production in each realization.

- The reservoir history matching was done in terms of bottom hole pressure, fluid production rate, development of gas saturation, and asphaltene saturation matching. Upon the application of EnKF, the results show significantly lower errors for porosity and permeability estimation, further validating the applicability of EnKF.

6.2 Recommendations for Future Work

- While building oil-water reservoir model, assumptions such as no heterogeneity, no capillary pressure, isotropic permeability-porosity, and no gravity forces are considered. Therefore, this study can be extended to a reservoir model where these assumptions will be excluded.

- To obtain more robust results, modified EnKF can be applied to more realistic cases such as heterogeneous and fractured reservoirs and/or reservoirs under different production strategies.

- While assessing non-Gaussianity in water flooding problem, reservoir heterogeneity is considered due to variation of porosity and permeability. However, changes in other parameters such as capillary pressure, gravity, and geological facies are ignored. A complete analysis can be done considering the variation in all these key parameters, too.

- Reservoir simulation in asphaltic oil reservoir is performed assuming primary recovery, constant well flowrate, synthetic and homogeneous reservoir in terms of porosity and permeability, no capillary pressure, and no gravity effect. It is recommended to extend this work taking more challenging tasks such as heterogeneous reservoir, secondary oil recovery process, incorporating effect of temperature, fluid breakthrough, and real case scenarios. Implementation of EnKF is also suggested for all these cases.

- Investigation of asphaltic oil reservoir and corresponding reservoir parameter estimation can be extended by incorporating hybrid modeling strategies that combine artificial intelligence/machine learning tools, EnKF, and commercial software packages.

- In this work, only two reservoir parameters (porosity and permeability) are taken into consideration to analyze the impact of asphaltene precipitation. As a future work, the research work can be conducted to investigate other parameters such as capillary pressure, and wettability alteration due to asphaltene precipitation.